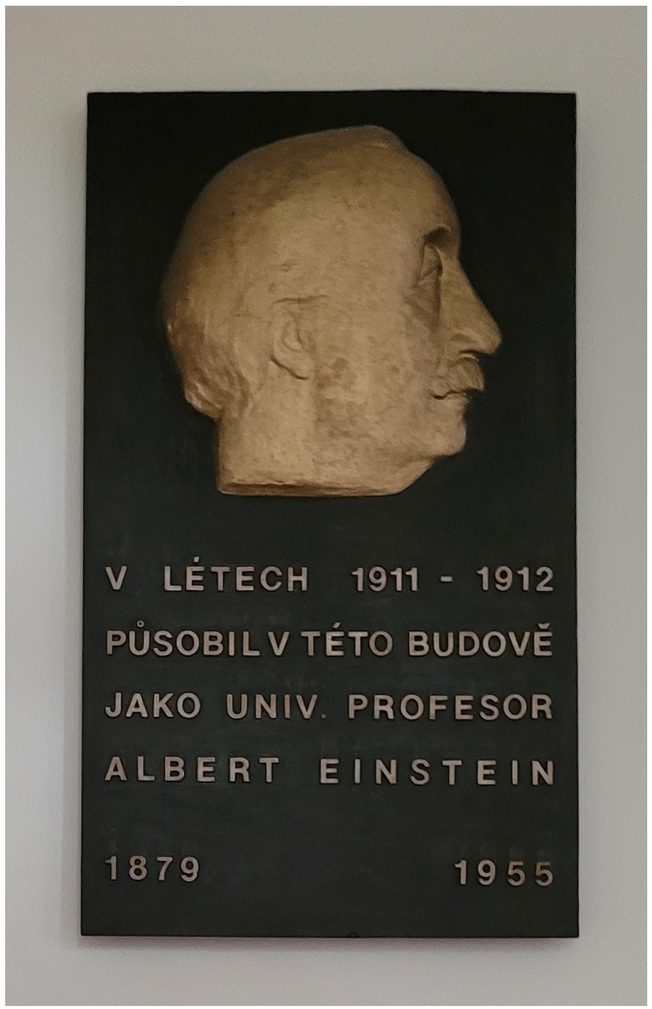

Memorial plaque of Albert Einstein
at the Faculty of Science of Charles University in Viničná street No. 7 states:
Albert Einstein was a university professor in this building from 1911 to 1912.

COSMOLOGY ON SMALL SCALES 2024

Proceedings of the International Conference

Cosmology on Small Scales 2024

Local Hubble Expansion and Other Cosmological Puzzles

Prague, September 19–21, 2024

Edited by
Michal Křížek and Yurii V. Dumin

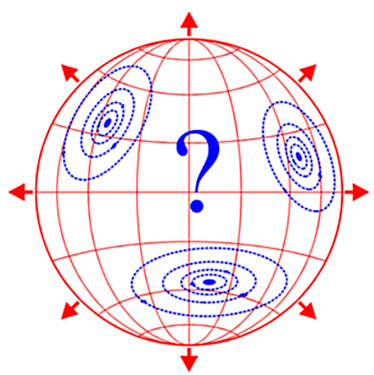

Institute of Mathematics
Czech Academy of Sciences

Proceedings of the International Conference

COSMOLOGY ON SMALL SCALES 2024

Local Hubble Expansion and Other Cosmological Puzzles

Prague, September 19–21, 2024

Edited by
Michal Křížek and Yurii V. Dumin

Institute of Mathematics
Czech Academy of Sciences
Prague 2024

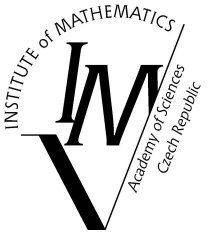

Institute of Mathematics
Czech Academy of Sciences
Prague 2024
LaTeX typesetting prepared by Hana Bílková

Dedicated to Tuomo Suntola on his 80th birthday

CONTENTS

Preface 7

K. Morawetz
Cosmological consequences of torsion 9

I. L. Zhogin
Cosmology with one extra dimension 29

M. Křížek
A few critical remarks on the special theory of relativity 47

T. Prevenslik
Cosmology and redshift in cosmic dust 57

V. I. Dokuchaev, K. Prokopev
Searching indications for dark energy in the images of black holes 61

A. Styrman
Evaluation of theories and methodologies: Relativistic Physics vs. the Dynamic Universe 75

Y.-H. Aggarwal
Solving the enigma of the origins and growth of supermassive black holes 109

Y. V. Dumin
Can the quasi-oscillatory structure of low multipoles in the CMB spectrum be associated with the domain structure of vacuum? 131

E. G. Khramova
The faint young Sun paradox 141

Y. V. Dumin
In Memory of Prof. Alexei Starobinsky (19. 4. 1948–21. 12. 2023) 153

Abstracts 159
List of participants 167
Program of the conference 173

Preface

The concept of Hubble expansion is a cornerstone of modern cosmology starting from the early days of its development in the 1920's and 30's. However, one of the crucial issues – what is the spatial scale at which the Hubble expansion begins to operate – remains unclear till now. Moreover, this question became especially important in the last 25 years in the context of dark-energy-dominated cosmology: Since the dark energy is distributed perfectly uniformly everywhere, one can expect the cosmological effects even at very small (e.g., interplanetary) scales. To address the above-mentioned issues, a series of biannual conferences "Cosmology on Small Scales" was organized since 2016. These meetings gather not only specialists in theoretical and observational cosmology, but also mathematicians, geophysicists, planetologists, etc., to discuss the problem from various points of view. The 5th conference CSS 2024 continued this tradition and was aimed at a presentation of the most recent theoretical ideas and observational findings.

The International Conference *Cosmology on Small Scales 2024: Local Hubble Expansion and Other Cosmological Puzzles* was held at the Institute of Mathematics of the Czech Academy of Sciences at Žitná 25, Prague 1, from 19 to 21 September 2024 (see `css2024.math.cas.cz`). It was a continuation of our four previous conferences; *Cosmology on Small Scales 2016: Local Hubble Expansion and Selected Controversies in Cosmology*, *Cosmology on Small Scales 2018: Dark Matter Problem and Selected Controversies in Cosmology*, *Cosmology on Small Scales 2020: Excessive Extrapolations and Selected Controversies in Cosmology Cosmology on Small Scales 2022: Dark Energy and the Local Hubble Expansion Problem.*

The main topics of the conference "Cosmology on Small Scales 2024" were:

- ▷ Local Hubble expansion – search for observational and laboratory evidence
- ▷ Cosmological effects in the localized astronomical systems
- ▷ Arguments for and against dark energy, and revisiting the foundations of physics
- ▷ Alternative models for dark matter and dark energy
- ▷ Mathematical aspects of the extrapolations used in cosmology
- ▷ Explanations of various cosmological paradoxes

Only a fraction of the presented reports in CSS2024: *Local Hubble Expansion and Other Cosmological Puzzles* is included into these proceedings; another part has been already published elsewhere. We incorporated also several abstracts and papers on "alternative cosmological theories". Although they may be questionable and the Organizing Committee is not responsible for their content, we believe that it is reasonable to present them to the wide audience.

The Organizing Committee consisted of

Prof. Michal Křížek — Chair (Czech Academy of Sciences, Czech Republic)
Assoc. Prof. Yurii Dumin — Vice-Chair (Moscow State University & Space Research Institute of RAS, Russia)
Hana Bílková (Czech Academy of Sciences, Czech Republic)

We are deeply grateful to all authors for their contributions and the support of RVO 67985840 (Institute of Mathematics of the Czech Academy of Sciences). Out sincere thanks go also to all active members of the Cosmological Section of the Czech Astronomical Society for their continual help. Finally, we are indebted to Eva Ritterová and Hana Bílková for their technical assistance in the final typesetting.

These Proceedings can be downloaded from the website:

`http://users.math.cas.cz/~krizek/list.html`

Michal Křížek and Yurii V. Dumin

Conference *Cosmology on Small Scales 2024*
Michal Křížek and Yurii Dumin (Eds.)
Institute of Mathematics CAS, Prague

COSMOLOGICAL CONSEQUENCES OF TORSION

Klaus Morawetz[1,2],

[1]Münster University of Applied Sciences
Stegerwaldstrasse 39, 48565 Steinfurt, Germany
morawetz@fh-muenster.de
[2]International Institute of Physics - UFRN
Campus Universitário Lagoa nova, 59078-970 Natal, Brazil

Abstract: The Einstein-Cartan equations, including torsion in the Weyssenhof assumption, lead to two solutions outside of matter. Besides the torsion-free Schwarzschild-Kottler solution, a new nonperturbative solution appears with a different metric. This metric can mimic dark matter and leads to space- and time-dependent acceleration parameters. As a consequence, the Hubble parameter becomes time-dependent, and fitting the Hubble parameter and deceleration parameter at present to the experimental values reveals a scenario of decreasing followed by an increasing time-dependent Hubble parameter. Large spatial structures appear, dependent on the point of light arriving, such that the present values are reproduced.

Keywords: conference, international, cosmology, torsion, solution Einstein-Cartan, Hubble tension

PACS: 98.80-k

1. Introduction and motivation

Standard cosmological models based on Friedmann equations face several challenges [30], including discrepancies in Hubble data, the dark matter problem, and the presence of giant arc structures of 3 Gpc in the universe. This paper aims to address these challenges by incorporating torsion within the Einstein-Cartan framework. In the following let us shortly describe these three problems one after another:

(i) The discrepancy of Hubble data from the early universe obtained by background radiation and data from present galaxies [51] indicating an increase Hubble constant by 5σ difference. This discrepancy is also further supported by quasars at far distance [20, 32]. Considering the time dependence of the scale parameter

$$R(t) = R_0(t_0)\left[1 + H_0(t-t_0) - \frac{q}{2}H^2(t-t_0)^2 + \dots\right] \tag{1}$$

with the Hubble and deceleration parameters

$$H = \frac{\dot{R}}{R}, \qquad q = -\frac{\ddot{R}R}{R^2} \tag{2}$$

would lead to a time change of Hubble parameter

$$\dot{H} = \frac{\ddot{R}R - \dot{R}^2}{R^2}. \tag{3}$$

Demanding $\dot{H} > 0$ means $\ddot{R}R > \dot{R}^2$ and with the help of (2) one finds the equivalence

$$\dot{H} > 0 \leftrightarrow q < -1. \tag{4}$$

The analysis of the Planck data and SHOES collaboration [9] indicate parameters

$$\begin{aligned} H_0 &= 75.35 \pm 1.68 \text{km/(sMpc)} \\ q_0 &= -1.08 \pm 0.29 \end{aligned} \tag{5}$$

at present. The theoretical challenge is how the Hubble parameter could increase with time [41, 17, 14]. We will see that this can be correctly described by including torsion [40].

(ii) The problems of dark matter [35, 29] with the help of which one tries to cure the missing masses in rotation of galaxies. A wrong time dependence of the Hubble parameter in late-time cosmology are typical for models like Lambda cold dark matter (ΛCDM). Extensions lead to models with an extra parameter [37], or e.g. investigation of unparticle cosmology [1]. If we rewrite the new metric [39] by torsion (60) into the Schwarzschild form

$$ds^2 = \left(1 - \frac{a}{r}\right) dt^2 - \frac{1}{1 - \frac{b}{r}} dr^2 - r^2 d\Omega^2 \tag{6}$$

with

$$a = r - \frac{|\Lambda|}{3} r^3, \qquad b = \left(1 - \frac{C}{3}\right) r - \frac{|\Lambda|}{3} r^3, \tag{7}$$

we can compare with the standard Schwarzschild solution with zero torsion and the extension to include the cosmological constant known as Kottler solution [13]

$$a^K = 2M - \frac{|\Lambda|}{3} r^3, \qquad b^K = 2M - \frac{|\Lambda|}{3} r^3. \tag{8}$$

We see that the new metric resulting from torsion induces a mass like term

$$M^{\text{torr}} = \frac{1}{2} \left(1 - \frac{C}{3}\right) r \tag{9}$$

which increases with larger distances. This can probably mime an additional gravitational mass modifying the outer rotation of large galaxies [23] and is therefore a candidate for dark matter [48, 4, 38]. It was also suggested to explain matter-antimatter imbalance [48]. Recent investigations for torsion leading to dark energy can be found in [5].

(iii) Large ring structures have been observed [34, 2] which seem to violate the equivalence principle. These giant arcs are stretching about 1 Gpc of proper distance in present epoch and exceed the so far largest structures of Sloan Great Wall [28] by more than a factor of 2. They are seen as filamentous and curved walls made up of galaxies and galaxy clusters [34]. The newest observation concerns big ring structures once more a factor larger: "The Big Ring on the Sky is 9.2 billion light-years from Earth. It has a diameter of about 1.3 billion light-years, and a circumference of about four billion light-years. If we could step outside and see it directly, the diameter of the Big Ring would need about 15 full Moons to cover it. It is the second ultra-large structure discovered by University of Central Lancashire (UCLan) PhD student Alexia Lopez who, two years ago, also discovered the Giant Arc on the Sky. Remarkably, the Big Ring and the Giant Arc, which is 3.3 billion light-years across, are in the same cosmological neighbourhood – they are seen at the same distance, at the same cosmic time, and are only 12 degrees apart on the sky."[33]. Here we will see that torsion leads to pronounced structures of arriving light due to a specific cosmos selected according to the present data (5).

To extend standard cosmological models, torsion has been included to modify the Einstein gravitation theory already by Cartan [11] which together with the gauge-invariance principle [58, 54] have yield a practicable classical field theory. For an overview about the development of these extensions see [26, 24] and for a modern mathematical presentation see [55, 43]. The inclusion of torsion has regained a current interest, since it promises a new direction for the search beyond the standard cosmological model [25].

Einstein-Cartan cosmologies [6] demonstrate the absence of singularities [31, 44], replacing the Big Bang with a big bounce [7, 19, 44, 47, 56]. Consequently, a black-hole cosmology ensues [45], which could potentially unify the big bounce and inflation [22, 47, 16]. Here, torsion generates a gravitational repulsion that circumvents initial singularities [49]. The emergent scenario has been investigated to find stable solutions of Einstein-Cartan equations, primarily for the closed universe [27]. By avoiding such initial singularities, it becomes feasible to study primordial fluctuations, and a finite period of cosmic inflation may be attributed to particle production due to curved spacetime [46].

In late cosmology, a non-adiabatic expansion was discovered, and the second law of thermodynamics necessitates a positive torsion term [15]. Asymptotically flat solutions have been explored in the context of gravitational lensing [12], while rotating and expanding solutions are presented in [21]. Inner stellar objects with spin and torsion are examined in [36], with mass bounds discussed in [8].

The outline of the paper is as follows. The solution of Einstein-Cartan equa-

tions are shortly reviewed in the next section II. This is largely taken from [39]. The internal consistency between torsion and gravitation is payed special attention. The section III then aplies the new metric with torsion to the problem of Hubble parameter which extends [40].

2. Einstein-Cartan theory

The Einstein-Hilbert action with the extension to torsion [11, 58, 26, 43]

$$\begin{aligned} \mathcal{L} &= -\frac{1}{2\kappa}\int \left[P - g^{ik}\left(C^{j}_{\ ij}C^{l}_{\ kl} - C^{l}_{\ im}C^{m}_{\ kl}\right)\right]\sqrt{|g|}d\Omega \\ &\quad +\mathcal{L}_m \end{aligned} \tag{10}$$

is given in terms of the Riemann curvature tensor P, the metric g and the contortion tensor C. The latter one gives the relation between affine connection Γ and the Levi-Civita connection or Christoffel symbols $\{\}$ as

$$\Gamma_{ij}^{\ k} = \begin{Bmatrix} k \\ ij \end{Bmatrix} + C^{k}_{\ ij}. \tag{11}$$

The variation of the matter part of the Lagrangian (10) defines the metric dynamical energy-momentum tensor $\mathcal{T}$ as

$$\delta\mathcal{L}_m = -\frac{1}{2}\int \mathcal{T}^{ij}\delta g_{ij}d\Omega. \tag{12}$$

The Belinfante Rosenfeld equation [3, 52] relates the dynamical metric $\mathcal{T}$ and the canonical energy-momentum T tensor by the torsion tensor S

$$\begin{aligned} \mathcal{T}_{ik} &= T_{ik} + \varepsilon Z_{ik}, \\ Z_{ik} &= -\frac{1}{2}(\nabla_l - 2S_l)(S_{ik}^{\ \ l} - S_{k\ i}^{\ l} + S^{l}_{\ ik}) \end{aligned} \tag{13}$$

where $S_i = S^{k}_{\ ik}$ and the contortion tensor in (11) is linked to the torsion tensor by

$$C_{kij} = S_{kij} + 2S_{(ij)k}. \tag{14}$$

In order to keep track of the contribution by the Belinfante-Rosenfeld equation Z_{ik}, we denote it by an auxiliary factor $\varepsilon = 1$ or $\epsilon = 0$ dependent whether we use the torsion tensor or the metric as variation variable in the variational principle.

The Einstein-Cartan equations as variation of (10) with respect to the metric tensor g firstly describe the connection of the Riemann tensor to the dynamical metric tensor

$$G_{ik} = P_{ik} - \left(\lambda + \frac{P}{2}\right)g_{ik} = \kappa T_{ik} + \kappa\varepsilon Z_{ik} + \kappa^2 U_{ik} \tag{15}$$

with $P = P_i{}^i$, the cosmological constant λ, and the additional gravitational potential due to the torsion

$$\kappa^2 U_{ik} = C^j{}_{ij} C^l{}_{kl} - C^l{}_{ij} C^j{}_{kl} - \frac{g_{ik}}{2}\left(C^{jm}{}_j C^l{}_{ml} - C^{mj}{}_l C^l{}_{jm}\right). \tag{16}$$

Secondly, by variation of (10) with respect to the contorsion, the Einstein-Cartan equations connect the torsion tensor to the spin tensor s by

$$S_{kij} = -\frac{\kappa}{2}(s_{ijk} - g_{k[j} s_{i]ll}) \tag{17}$$

which provides the relation of the contorsion tensor to the spin itself

$$C_{kij} = \frac{\kappa}{2}(2s_{k(ij)} - s_{ijk} + g_{kj} s_{ill} - g_{ij} s_{kll}). \tag{18}$$

For general classification of torsion tensors beyond spin interpretation see [10].

The additional gravitational potential becomes

$$\begin{aligned} U_{ik} = & \frac{1}{2}\left[s_i{}^j{}_j s_k{}^l{}_l - s_i{}^j{}_l s_k{}^l{}_j - s_i{}^j{}_l s_{kj}{}^l + \frac{1}{2} s^{jl}{}_i s_{jlk} \right. \\ & \left. + \frac{g_{ik}}{2}\left(\frac{1}{2} s^{jlm} s_{jlm} - s^l{}_{jm} s^{jm}{}_l - s^l{}_{jl} s^{jm}{}_m \right) \right]. \end{aligned} \tag{19}$$

The Einstein tensor as left side of (15) obeys the double contracted Bianchi identity $\nabla^{\{\}}_l G^{lk} = 0$ with respect to Levi-Civita connection which establishes the conservation law

$$\nabla^{\{\}}_l (T^{lk} + \varepsilon Z^{lk} + \kappa U^{lk}) = 0. \tag{20}$$

The equations are drastically simplified if we work with the Weyssenhoff spin liquid [42] assuming that the spin tensor takes the form $s_{ijk} = s_{ij} u_k$ with the velocity u and the remaining asymmetric spin tensor being orthogonal $s_{ij} u^j = 0$ known as Frenkel condition. Then the additional gravitational potential (19) simplifies to

$$U_{ik} = \frac{1}{2}\left[s_i{}^j s_{jk} + \sigma^2 \left(u_i u_k + \frac{g_{ik}}{2} \right) \right] \tag{21}$$

with

$$2\sigma^2 = s^m{}_l s_m{}^l. \tag{22}$$

This additional gravitational potential gives a quadratic contribution in κ to the Einstein-Cartan equation (15).

The contortion tensor (14) and torsion tensor become according to (18) and (17)

$$\begin{aligned} C_{kij} &= \frac{\kappa}{2}(s_{ki} u_j + s_{kj} u_i + s_{ji} u_k), \\ S_{kij} &= -\frac{\kappa}{2} s_{ij} u_k \end{aligned} \tag{23}$$

and $S_l = S^k{}_{ik} = 0$.

2.1. Self-consistence conditions

Since the torsion tensor (17) does not obey a dynamical equation like the Riemann tensor (15) it is sometimes considered as removeable. In the opposite, the metric determines the spin tensor and the spin tensor the metric with an intrinsic consistency mostly underestimated. In fact it leads to severe restrictions to the possible forms of metrics. We see it by considering the additional potential Z_{ik} from the Belinfante-Rosenfeld equation (13). Using (23), we obtain

$$Z_{ik} = \frac{1}{\kappa}\nabla_l C_{k\ i}^{\ l} = -\frac{1}{2}\nabla_l(s_k^{\ l}u_i + s_i^{\ l}u_k + s_{ki}u^l) \tag{24}$$

and we see from the Einstein-Cartan equation (15) that the terms should be symmetric in the indices i, k. This is visible in (21) but has to be demanded for (24). This requirement is nothing but the conservation of the spin density (see 2.4.16 of [43]). We translate the covariant derivatives with respect to Levi-Civita connections

$$Z_{ik} = \frac{1}{\kappa}\nabla_l C_{k\ i}^{\ l} = \frac{1}{\kappa}\nabla_l^{\{\}} C_{k\ i}^{\ l} + \frac{1}{\kappa}\left(-C^m_{\ kl}C_{m\ i}^{\ l} + C^l_{\ ml}C_{k\ i}^{\ m} - C^m_{\ il}C_{k\ m}^{\ l}\right). \tag{25}$$

We need

$$C_{k\ i}^{\ l} - C_{i\ k}^{\ l} = \kappa s_{ki}u^l \tag{26}$$

for the requirement

$$\begin{aligned} 0 = Z_{ik} - Z_{ki} &= \nabla_l^{\{\}}(s_{ki}u^l) + C^m_{\ il}s_{mk}u^l + C^m_{\ kl}s_{im}u^l + C^l_{\ ml}s_{ki}u^m \\ &= \nabla_l^{\{\}}(s_{ki}u^l) = \partial_l(s_{ki}u^l) - \begin{Bmatrix} m \\ kl \end{Bmatrix} s_{mi}u^l - \begin{Bmatrix} m \\ il \end{Bmatrix} s_{km}u^l + \begin{Bmatrix} l \\ ml \end{Bmatrix} s_{ki}u^m \end{aligned} \tag{27}$$

where we have used (23) and $s_{ij}u^j = 0$ as well the antisymmetry of s to see the step from the second to the third line.

We will use a coordinate system where $u^l = (u^0, 0, 0, 0)$. This implies that the asymmetric spin tensor s has a first zero column and row

$$s = \begin{pmatrix} 0 & 0 & 0 & 0 \\ 0 & 0 & c & -b \\ 0 & -c & 0 & a \\ 0 & b & -a & 0 \end{pmatrix} \tag{28}$$

and (27) translates into 6 equations for a, b, c. The first set of linear equations appear for $i = 0$

$$\begin{Bmatrix} m \\ 00 \end{Bmatrix} s_{mk} = 0 \tag{29}$$

whose solution shows that we have to have

$$a = \begin{Bmatrix} 1 \\ 00 \end{Bmatrix} d; \quad b = \begin{Bmatrix} 2 \\ 00 \end{Bmatrix} d; \quad c = \begin{Bmatrix} 3 \\ 00 \end{Bmatrix} d \tag{30}$$

with a single unknown function d. The second set of equations appear for ($i=1$, $k=2$), ($i=1$, $k=3$), ($i=2$, $k=3$) and read

$$\begin{aligned}
&\frac{1}{u^0}\partial_0(cu^0)+\left\{\begin{matrix}3\\01\end{matrix}\right\}a+\left\{\begin{matrix}3\\02\end{matrix}\right\}b+\left(\left\{\begin{matrix}0\\00\end{matrix}\right\}+\left\{\begin{matrix}3\\03\end{matrix}\right\}\right)c=0,\\
&\frac{1}{u^0}\partial_0(bu^0)+\left\{\begin{matrix}2\\01\end{matrix}\right\}a+\left(\left\{\begin{matrix}0\\00\end{matrix}\right\}+\left\{\begin{matrix}2\\02\end{matrix}\right\}\right)b+\left\{\begin{matrix}2\\03\end{matrix}\right\}c=0,\\
&\frac{1}{u^0}\partial_0(au^0)+\left(\left\{\begin{matrix}0\\00\end{matrix}\right\}+\left\{\begin{matrix}1\\01\end{matrix}\right\}\right)a+\left\{\begin{matrix}1\\02\end{matrix}\right\}b+\left\{\begin{matrix}1\\03\end{matrix}\right\}c=0.
\end{aligned}\tag{31}$$

Together with (30) these are 3 differential equations for d and the metric tensor g. Unfortunately, both constraints are mostly not respected with the presented exact solutions in the literature. It is interesting to note that the metric is obviously directly dependent on the spin content boiled down to a single function d.

2.2. Solution of Einstein-Cartan equations

Let us summarize the simplified equations by the Weyssenhoff assumption. The contribution of the Belinfante-Rosenfeld equation

$$Z_{ik}=\frac{1}{2}(Z_{ik}+Z_{ki})=\widetilde{Z}_{ik}+\kappa\widetilde{U}_{ik}\tag{32}$$

can be seen to split into

$$\widetilde{Z}_{ik}=\frac{1}{2}\nabla_l^{\{\}}(s_k{}^l u_i+s_i{}^l u_k)\tag{33}$$

and a part entering linear in κ

$$\widetilde{U}_{ik}=\frac{1}{2}(2\sigma^2 u_i u_k+s_{il}s^l{}_k).\tag{34}$$

This splitting corresponds to the two parts in (25). Summarizing, the Einstein-Cartan equations (15) take the form

$$P_{ik}=\left(\lambda+\frac{P}{2}\right)g_{ik}+\kappa(T_{ik}+\varepsilon\widetilde{Z}_{ik})+\kappa^2(U_{ik}+\varepsilon\widetilde{U}_{ik}).\tag{35}$$

The canonical energy momentum tensor is assumed to have the form

$$T_{ik}=(n+p)u_i u_k-pg_{ik}\tag{36}$$

with the mass density n and pressure p.

The torsion modifies the Einstein-Cartan equation by an additional energy-momentum tensor part $\widetilde{Z}$ of (33) and a potential quadratic in κ according to (34) and (21)

$$U_{ik}+\varepsilon\widetilde{U}_{ik}=\frac{\sigma^2}{2}\left[(2\varepsilon+1)u_i u_k+\frac{g_{ik}}{2}\right]+\frac{1+\varepsilon}{2}s_{il}s^l{}_k.\tag{37}$$

The metric and torsion are dependent on each other even outside matter which consistency results into the antisymmetric spin tensor in terms of the Weyssenhoff spin liquid parameter $2\sigma^2 = s^m{}_l s_m{}^l$ with the only nonzero components in spherical coordinates [39]

$$s_{2,3}(t,r,\theta,\phi) = -s_{3,2} = \sigma r^2 \sin\theta. \tag{38}$$

We investigate the spherically symmetric solution with a diagonal metric

$$g = \mathrm{diag}\{B(r), -A(r), -R(r), -R(r)\sin^2\theta\} \tag{39}$$

which should include the Schwarzschild solution and generally any static spherically symmetric solutions. Generally we have 10 possible functions where 4 are fixed by coordinate systems. In [39] it was proven that the spherically symmetric solution is the only one without contradictions assuming generally 6 functions. We choose freely $u^\mu = (u^0, 0, 0, 0)$ which provides with $u^\mu u_\mu = 1$ the form $u^\mu = (\sqrt{B(r)}, 0, 0, 0)$ and $u_\mu = (1/\sqrt{B(r)}, 0, 0, 0)$. Calculating the Christoffel symbols, the set of equations (30) provides $b = c = 0$ and

$$a(r) = \frac{B'(r)}{2A(r)} d(r) \sin\theta. \tag{40}$$

Since it is static it solves also (31). The θ dependence remains undetermined and we choose it here such that

$$\sigma^2(r) = \frac{B'(r)^2}{4A(r)^2 R(r)^2} d(r)^2 \tag{41}$$

becomes independent of θ, since this term appears later in the equations and we search for spherical symmetric ones. We see that the spin conservation (27) reduces the spin tensor corresponding to the assumed metric.

The contortion tensor can be easily calculated with the nonzero parts

$$\frac{a(r)\sqrt{B(r)}}{2} = C_{032} = C_{203} = C_{230} = -C_{302} = -C_{023} = -C_{320} \tag{42}$$

and wthe linear-κ contribution to the Einstein-Cartan equations $\widetilde{Z}$ according to (33) via (25) appears to be zero for this chosen metric. In other words it does not vanish due to averaging but is exactly zero.

The quadratic-κ contribution to the Einstein-Cartan equations (34) reads

$$\widetilde{U}_{ik} = \frac{\sigma^2}{2} \mathrm{diag}\{2B(r), 0, R(r), R(r)\sin^2\theta\} \tag{43}$$

and the additional gravitational potential (21) becomes

$$U_{ik} = \frac{\sigma^2}{4} \mathrm{diag}\{3B(r), -A(r), R(r), R(r)\sin^2\theta\}. \tag{44}$$

2.3. Internal Schwarzschild solution

Now we solve the Einstein-Cartan equations. It turns out that the right-hand side of (35) becomes simplified if we use an effective momentum and energy density

$$\begin{aligned} \bar{p}(r) &= p(r) + \frac{\lambda}{\kappa} - \frac{\mathrm{e}(r)^2}{4(1+\varepsilon)} \\ \bar{n}(r) &= n(r) - \frac{\lambda}{\kappa} + \frac{(3+4\varepsilon)\mathrm{e}(r)^2}{4(1+\varepsilon)}. \end{aligned} \tag{45}$$

We will use in the following

$$\mathrm{e}(r)^2 = \kappa(1+\varepsilon)\sigma^2(r) \tag{46}$$

defining $\mathrm{e}(r)$ via (41). If we do not consider $\tilde{U}_{ik}$ as in most treatments we will have to set $\varepsilon = 0$ instead of $\varepsilon = 1$.

The Riemann tensor provides 3 equations since $P_{33} = P_{22}\sin^2\theta$ on both sides. The right-hand side of (35) together with the conservation law (20) becomes then

$$\begin{aligned} P_{00} &= \frac{\kappa}{2}B(\mathrm{e}^2+\bar{n}+3\bar{p}) \\ P_{11} &= \frac{\kappa}{2}A(\bar{n}-\bar{p}-\mathrm{e}^2) \\ P_{22} &= \frac{\kappa}{2}R(\bar{n}-\bar{p}) \\ 0 &= \nabla_l[T^{lk} + \widetilde{Z}^{lk} + \kappa(U^{lk} + \widetilde{U}^{lk})] = (\bar{n}+\bar{p})\frac{B'}{2A} + \frac{\bar{p}'}{V} - \frac{\mathrm{e}^2 R'}{2AR} \end{aligned} \tag{47}$$

where all functions are r-dependent and we denote the derivative by R'. One can get rid of B combining

$$\frac{P_{00}}{2B}+\frac{P_{11}}{2A}+\frac{P_{22}}{R} = \frac{A'g'}{2A^2R}+\frac{R'^2-4RR''}{4AR^2}+\frac{1}{R} = \kappa\bar{n}. \tag{48}$$

This differential equation is solved as

$$A(r) = \frac{R'(r)^2}{4\pi R(r)}\left[1 - \kappa\frac{m(r)}{4\pi\sqrt{R(r)}}\right]^{-1} \tag{49}$$

with the total "mass" included

$$m(r) = 2\pi\int_{r_0}^{r} d\bar{r}\sqrt{R(\bar{r})}R'(\bar{r})\bar{n}(\bar{r}) + C_0. \tag{50}$$

We absorb the integration constant in $m(r)$ setting $C_0 = 0$ by assuming a proper r_0.

Next we consider

$$\frac{P_{00}}{B}+\frac{P_{11}}{A}=\frac{A'R'}{2A^2R}+\frac{B'R'}{2ABR}-\frac{2RR''-R'^2}{2AR^2}=\kappa(\bar{n}+\bar{p}). \tag{51}$$

Using the conservation (47), we have

$$\frac{B'}{B}=\frac{\mathrm{e}^2R'-2R\bar{p}'}{R(\bar{n}+\bar{p})}. \tag{52}$$

With the help of this we eliminate B in (51) and A by (49) to obtain the modified Oppenheimer-Volkov equation [8]

$$\bar{p}'=-\frac{\kappa R'(\bar{n}+\bar{p})\left(\bar{p}+\frac{m}{4\pi R^{3/2}}\right)}{4\left(1-\frac{\kappa}{4\pi\sqrt{R}}m\right)}+\mathrm{e}^2\frac{R'}{2R}. \tag{53}$$

Using this in (52), we obtain another form for B'/B

$$\frac{B'}{B}=\frac{\kappa R'}{8\pi R^{3/2}}\,\frac{m+4\pi R^{3/2}\bar{p}}{1-\frac{\kappa}{4\pi\sqrt{R}}m}. \tag{54}$$

With these solutions at hand we check that the last equation

$$\frac{P_{22}}{R}=\frac{1}{R}+\frac{A'R'}{4A^2R}-\frac{B'R'}{4ABR}-\frac{R''}{2AR}=\frac{\kappa}{2}(\bar{n}-\bar{p}) \tag{55}$$

of the Einstein-Cartan equations (47) is completed identically. The equations (54), 53) and (49) solve therefore the Einstein-Cartan equations together with the conservation law (47) and are the general solutions of the assumed spherical-symmetric and static metric (39) within the Weyssenhoff fluid. The known internal Schwarzschild solution is visible for $e\to 0$ and $\lambda\to 0$. Of course, the function $R(r)$ as prefactor of the angular parts in the metric remains undetermined dependent on the used coordinate system. A simple variable transformation $R(r)=\bar{r}^2$ would fix it in the standard form. Further treatments can be performed numerically dependent on the given momentum and density profile via the equation of state. Exact solutions for the inner region of compact objects are discussed in [12, 36, 18], for rotating stars in [21] and possible upper limits of masses of stars in [8].

An important remark we have to make. The so far undetermined torsion $\mathrm{e}(r)$ cannot be chosen arbitrarily, since (31) and the Oppenheimer-Volkov equation (53) provides with (45) an internal consistence even out of matter as we will see now.

2.4. External Schwarzschild solution

In the exterior of stars we can set $p = 0$ and $n = 0$ and should obtain the external Schwarzschild solution. The effective mass (50) and the Oppenheimer-Volkov equation (53) read then

$$\begin{aligned} m' &= \pi\sqrt{R}R'\left(-\frac{2\lambda}{\kappa}+\frac{(3+4\varepsilon)\mathrm{e}^2}{2(1+\varepsilon)}\right) \\ \frac{(\mathrm{e}^2)'}{\mathrm{e}^2} &= R'\frac{\frac{(5+6\varepsilon)\kappa m}{8\pi R^{3/3}}-\frac{2(1+\varepsilon)}{R(r)}-\frac{1+2\varepsilon}{2}\lambda-\frac{(1+2\varepsilon)}{8(1+\varepsilon)}\kappa\mathrm{e}^2(r)}{1-\frac{\kappa m(r)}{4\pi\sqrt{R(r)}}}. \end{aligned} \tag{56}$$

Note that even in the matter-free space $n = 0, p = 0$ we do not have a constant $R(r)$ and therefore $m(r)$. Due to the allowed torsion $\mathrm{e}(r)$ the function $m(r)$ is loosing its meaning as mass parameter outside the stars and is an auxiliary function of r. Not setting it constant as in the normal exterior Schwarzschild solution is only justified if it solves the Einstein-Cartan equation what we will show now.

The first equation of (56) provides $\mathrm{e} = \mathrm{e}(m')$ and inserted into the second leads to a second-order nonlinear differential equation for $m(r)$. Somewhat simplified one obtains with the transformation $R(r) = r^2$ and

$$\begin{aligned} \mathrm{e}^2(r) &= \frac{4(\varepsilon+1)}{\kappa(3+4\varepsilon)}\left(\frac{1}{r^2}+\lambda+\frac{\bar{m}'(r)}{r^2}\right) \\ m(r) &= \frac{4\pi}{\kappa}[r+\bar{m}(r)], \end{aligned} \tag{57}$$

the equation for $\bar{m}(r)$

$$\begin{aligned} r(2\varepsilon+1)\left(\bar{m}'+\lambda r^2+1\right)\left[\bar{m}'-(4\varepsilon+2)(\lambda r^2+1)\right] \\ = (4\varepsilon+3)\bar{m}\left[r\,\bar{m}''+(6\varepsilon+3)(\bar{m}'+1)+\lambda r^2(6\varepsilon+5)\right]. \end{aligned} \tag{58}$$

A series ansatz shows that this equation has two solutions

$$\bar{m}(r) = m_0\frac{\kappa}{4\pi}-r-\frac{\lambda}{3}r^3, \quad \bar{m}(r) = -r\left(\frac{\lambda}{3}r^2+\frac{1+2\varepsilon}{4+6\varepsilon}\right) \tag{59}$$

where the constant m_0 in the first solution will turn out to be the mass of a star.

One of the two solutions are the Schwarzschild-Kottler solution (8). The other one leads to the metric [39]

$$ds^2 = \hat{r}^2d\hat{t}^2-\frac{3}{C+\lambda\hat{r}^2}d\hat{r}^2-\hat{r}^2(d\theta^2+\sin^2\theta d\hat{\phi}^2) \tag{60}$$

where we abbreviate

$$C = \frac{3(1+2\varepsilon)}{2(2+3\varepsilon)} = \begin{cases} 3/4 & \text{for } \epsilon = 0 \\ 9/10 & \text{for } \epsilon = 1 \end{cases}. \tag{61}$$

A further transformation

$$\hat{r}^2 = \cos^2\tilde{t}\left[c(\tilde{r})^2\tan^2\tilde{t} - 1\right],\ \coth\hat{t} = c(\tilde{r})\tan\tilde{t} \tag{62}$$

with

$$c(\tilde{r}) = \tan\left(c + \sqrt{\frac{C}{3}}\ln\tilde{r}\right),\quad \tilde{r} = \sqrt{\frac{|\lambda|}{3}}r,\quad \tilde{t} = \sqrt{\frac{|\lambda|}{3}}t \tag{63}$$

translates the metric (60) into a Friedman-Lamaître-Robertson-Walker metric

$$ds^2 = dt^2 - a(r,t)\left(dr^2 + r^2 d\Omega^2\right). \tag{64}$$

The expansion or scale parameter becomes now space and time dependent

$$a(r,\tilde{t}) = R^2(r,t) = \frac{C\sin^2\sqrt{\frac{|\lambda|}{3}}t}{|\lambda|r^2\cos^2\left(2c + \sqrt{\frac{C}{3}}\ln\sqrt{\frac{|\lambda|}{3}}r\right)} \tag{65}$$

with an arbitrary constant c. It provides a time-like universe for $\tilde{r}^2 < \coth^2\tilde{t} - 1$ and a space-like otherwise.

The new solution are not approaching the Schwarzschild-Kottler metric with vanishing torsion parameter. This underlines the highly nonlinear character of the equations and how the torsion modifies the metric in a non-perturbative way.

3. Hubble parameter from distant light

The light we observe has passed $r = r_0 + c(t - t_0)$, indicated by the red line in Figure 1, in the spatial and time-dependent expansion parameter (65). We have to consider the Hubble parameter along this light path. One can observe oscillating behavior with respect to space and time. Interestingly, the spatial variation shows an additional maximum at large distances before it falls off rapidly.

Working in dimensionless values

$$H = \sqrt{\frac{\lambda}{3}}h,\quad \bar{r} = \sqrt{\frac{\lambda}{3c^2}}r,\quad \tau = \sqrt{\frac{\lambda}{3}}t \tag{66}$$

with the speed of light c, we obtain the time-dependent Hubble and deceleration parameters along the light path:

$$\begin{aligned} h(\tau) &= \cot\tau + \frac{\sqrt{C/3}\tan\sqrt{C/3}\ln(\bar{r}_0+\tau) - \sqrt{3}}{\bar{r}_0+\tau} \\ q(\tau) &= -1 + \frac{1}{h(\bar{r}_0+t)} + \frac{(\bar{r}_0+t)\csc^2 t - \cot t}{h^2(\bar{r}_0+t)} \\ &\quad - \frac{C\sec^2\left(\sqrt{C/3}\log(\bar{r}_0+t)\right)}{3h^2(\bar{r}_0+t)^2}. \end{aligned} \tag{67}$$

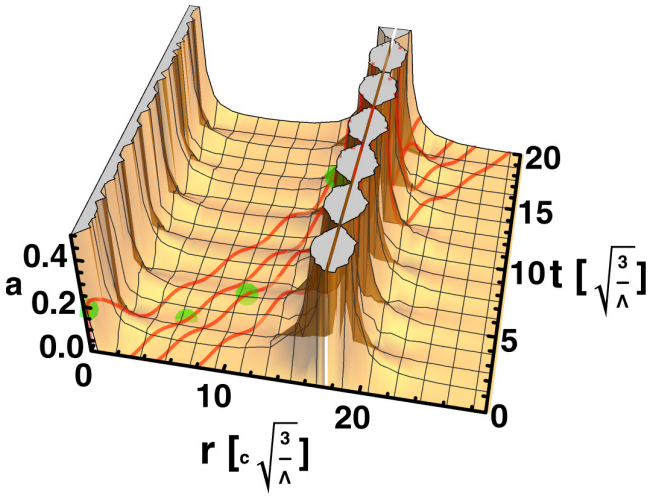

Figure 1: The time and space dependence of the expansion parameter (65) with the light path $r = r_0 + c(t - t_0)$ (red) with 4 different starting points $r_0 = 0.1, 3, 5, 8\sqrt{\lambda/3c^2}$.

Since we have q_0 and H_0 at the present time, we have two equations for the three parameter r_0, τ_0, λ. We consider r_0 as the unknown parameter of the present location of the universe and discuss possible values in the following.

There is only one window where the Hubble parameter can increase with time as observed, $\dot{H} > 0$, among the oscillating behavior shown in Figure 2, dependent on r_0. This interval is considered a possible cosmos due to observations and is indicated by the shaded area. The initial and final time of this universe window are then given by $H(t_0) = H(t_\infty) = \infty$, the present time by $H(t_p) = H_0$ by (5), and the time, where the Hubble parameter changes from falling to increasing time by $\dot{H}(t_c) = 0$. We determine the present time by reproducing the deceleration parameter (67) according to the value (5). For any parameter r_0, we can now determine these times together with the cosmological constant plotted in Figure 3.

We see that the unknown parameter $\bar{r}_0$ as the starting place in Figure 1 determines all three values of the initial time, ending time, and the cosmological constant due to the known present data (5). A larger $\bar{r}_0$ implies larger times accompanied by a larger cosmological constant. Conversely, if we know the cosmological constant by other measurements, we know $\bar{r}_0$ and the times are fixed. We have set the timescale to initially $t_0 = 0$ such that only the differences in times matter. The oscillating behavior as a big bounce instead of a big bang has been reported in [49, 44] due to torsion. Such turning points in the Hubble parameter were obtained by considering an unstable de Sitter state [41]. Depending on the parameter r_0, we can now find different ages and endings of the universe.

For a given r_0 parameter, we have the time dependence of the Hubble parameter

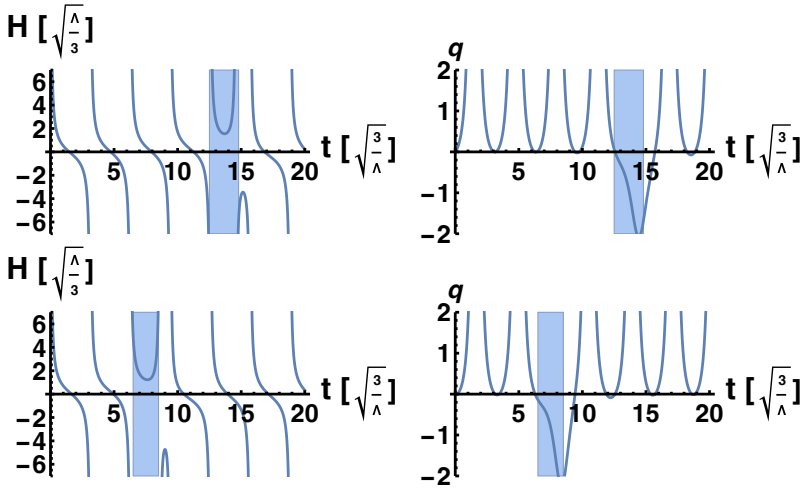

Figure 2: The dimensionless Hubble parameter (left) and deceleration parameter (right) as a function of dimensionless time assuming a present position of $r_0 = 3\sqrt{\lambda/3}/c$ (above) and $r_0 = 9\sqrt{\lambda/3}/c$ (below). The only possible windows with $\dot{h} > 0$ are indicated by the shaded areas.

and deceleration parameter in (67) fixed according to (5). Comparing with the experimental data, we have to plot them in terms of the redshift $z = -1 + R_0/R$. We have for the time dependence

$$\dot{z} = -\frac{R_0}{R}\frac{\dot{R}}{R} = (-1+z)H \tag{68}$$

and therefore with $z_0 = 0$ at the present time t_0

$$z(t) = -1 + \exp\left[-\int_{t_0}^{t} d\bar{r} H(\bar{t})\right]. \tag{69}$$

In Figure 4, the Hubble parameter versus redshift is plotted. The best choices of r_0 are indicated by dots in Figure 3 according to the experimental data in Figure 4. For further comparison of the data with present models see [1]. The resulting time where decelerating Hubble parameter changes into accelerating t_c, the present age t_p, and the end of the universe t_∞ are summarized in Table 1.

We see large scales for periodic r_0 parameters. It is suggested that these scales are the reason for the large structures observed in [2, 34].

4. Conclusion

The inclusion of torsion leads to two exact solutions of the Einstein-Cartan equations outside matter: the torsion-free Schwarzschild-Kottler solution and a new one which is nonperturbative and does not reduce to the Schwarzschild-Kottler solution

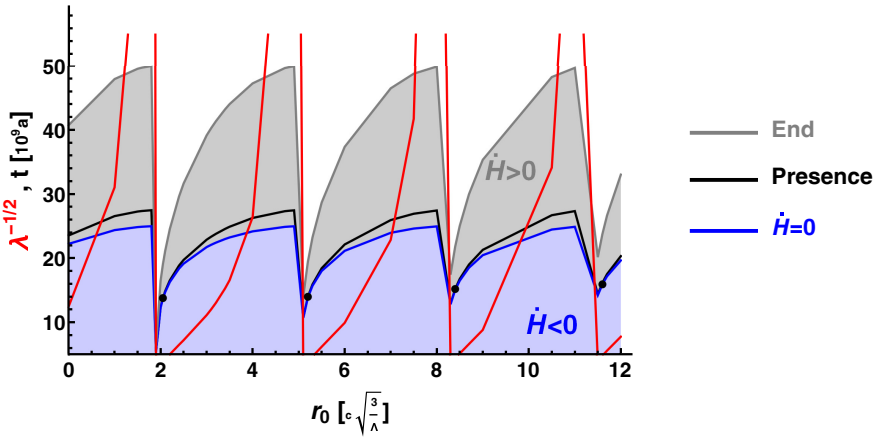

Figure 3: The age of the present universe together with the age where the Hubble parameter changes from falling into an increasing value versus the dimensionless parameter of the present location r_0. The data at presence are middle (black) lines and the corresponding cosmological constant are red lines. The best agreement with experimental data is indicated by dots.

r_0		$\lambda^{-1/2}$	t_c	t_p	t_∞
	[Gpc]	[Gyr]	[Gyr]	[Gyr]	[Gyr]
2.05	4.22	3.89	14.43	14.54	20.11
5.2	10.96	3.98	14.63	14.75	20.51
8.4	20.25	4.55	15.85	16.03	22.99
11.6	31.14	5.07	16.82	17.01	25.09

Table 1: Parameter r_0, time t_c where decelerating Hubble parameter changes into accelerating, the present age t_p, and the end of the universe t_∞ together with the cosmological constant.

when torsion vanishes. This arises from the nontrivial coupling of gravitation and torsion, which modifies the structure of the equations. It has been demonstrated that the new torsion-induced metric can mimic dark matter. A further consequence of this torsion metric is the time and space dependence of the acceleration parameter. This results in a time-dependent Hubble and deceleration parameter.

It has been shown that the evolution of the universe begins with a decreasing Hubble parameter, which switches to an increasing one within a certain evolutionary window among possible cosmological scenarios. The apparent dependence of certain times and Hubble behavior on the position parameter r_0 suggests a violation of the equivalence principle. This parameter r_0 appears as an artificial constant for large-scale structures determined by the cosmological constant. Since the Einstein-Cartan equations preserve the equivalence principle [57], or more recently [50], and since we have used an exact solution of these equations, we can conclude that locally there

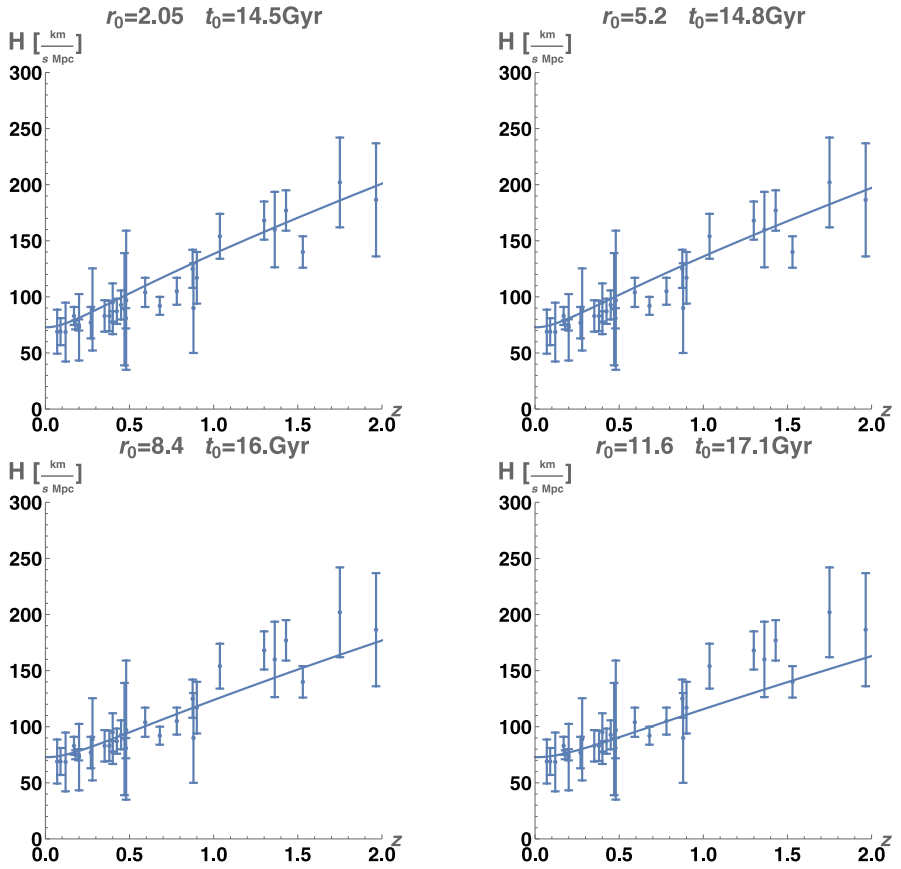

Figure 4: The Hubble parameter versus redshift together with the experimental data compilation of [53] for the best situation of Figure 3 for four different parameters r_0.

exists a transformation to a frame where the gravitational force vanishes. However, on a large scale, the time and space structure of the expansion parameter appears nonholonomic.

On a large scale, the new metric predicts the existence of gigantic spatial structures, possibly akin to recently discovered ring structures [34, 2]. Further effects of the new metric, such as wormholes, are discussed in [39].

Acknowledgements

Michal Křížek is thanked for many valuabel hints.

References

[1] Maryam Aghaei Abchouyeh and Maurice H. P. M. van Putten. Late-time universe, H_0-tension, and unparticles. *Phys. Rev. D*, 104:083511, Oct 2021.

[2] Pavan Kumar Aluri, Paolo Cea, Pravabati Chingangbam, Ming-Chung Chu, Roger G Clowes, Damien Hutsemékers, Joby P Kochappan, Alexia M Lopez,

Lang Liu, Niels C M Martens, C J A P Martins, Konstantinos Migkas, Eoin Ó Colg'ain, Pratyush Pranav, Lior Shamir, Ashok K Singal, M M Sheikh-Jabbari, Jenny Wagner, Shao-Jiang Wang, David L Wiltshire, Shek Yeung, Lu Yin, and Wen Zhao. Is the observable universe consistent with the cosmological principle? *Class. Quant. Grav.*, 40(9):094001, April 2023.

[3] F.J. Belinfante. On the current and the density of the electric charge, the energy, the linear momentum and the angular momentum of arbitrary fields. *Physica*, 7(5):449 – 474, 1940.

[4] Alexander S. Belyaev, Marc C. Thomas, and Ilya L. Shapiro. Torsion as a dark matter candidate from the higgs portal. *Phys. Rev. D*, 95:095033, May 2017.

[5] D Benisty, EI Guendelman, and H Stoecker. The dark side of the torsion: dark energy from propagating torsion. *Eur. Phys. J.*, 82(3):264, 2022.

[6] Sergio Bravo Medina, Marek Nowakowski, and Davide Batic. Einstein–cartan cosmologies. *Ann. Phys.*, 400:64 – 108, 2019.

[7] S D Brechet, M P Hobson, and A N Lasenby. Classical big-bounce cosmology: dynamical analysis of a homogeneous and irrotational weyssenhoff fluid. *Class. Quant. Grav.*, 25(24):245016, dec 2008.

[8] Piyabut Burikham, Tiberiu Harko, and Matthew J. Lake. Mass bounds for compact spherically symmetric objects in generalized gravity theories. *Phys. Rev. D*, 94:064070, Sep 2016.

[9] David Camarena and Valerio Marra. Local determination of the hubble constant and the deceleration parameter. *Phys. Rev. Research*, 2:013028, Jan 2020.

[10] S. Capozziello and C. Stornaiolo. Torsion tensor and its geometric interpretation. *Annales de la Fondation Louis de Broglie*, 32:195, 2007.

[11] Élie Cartan. Sur les variétés à connexion affine et la théorie de la relativité généralisée (première partie). *Annales scientifiques de l'École Normale Supérieure*, 3e série, 40:325–412, 1923.

[12] S. Chen, L. Zhang, and J. Jing. A new asymptotical flat and spherically symmetric solution in the generalized einstein–cartan–kibble–sciama gravity and gravitational lensing. *Eur. Phys. J. C*, 78:981, 2018.

[13] X. Chongming, W. Xuejun, and H. Zhun. A new class of spherically symmetric interior solution with cosmological constant. *Gen. Relat. Gravit.*, 19:1203, 1987.

[14] Eoin 0 Colgáin and M. M. Sheikh-Jabbari. A critique of holographic dark energy. *Classical and Quantum Gravity*, 38(17):177001, August 2021.

[15] M. Cruz, F. Izaurieta, and S. Lepe. Non-zero torsion and late cosmology. *Eur. Phys. J. C*, 80:559, 2020.

[16] Jordan L Cubero and Nikodem J Popławski. Analysis of big bounce in einstein–cartan cosmology. *Class. Quant. Grav.*, 37(2):025011, December 2019.

[17] Wei-Ming Dai, Yin-Zhe Ma, and Hong-Jian He. Reconciling Hubble constant discrepancy from holographic dark energy. *Phys. Rev. D*, 102:121302, Dec 2020.

[18] Thibault Damour and Vasilisa Nikiforova. Spherically symmetric solutions in torsion bigravity. *Phys. Rev. D*, 100:024065, Jul 2019.

[19] G de Berredo-Peixoto and E A de Freitas. On the torsion effects of a relativistic spin fluid in early cosmology. *Class. and Quant. Grav.*, 26(17):175015, August 2009.

[20] Risaliti G and E. Lusso. Cosmological constraints from the Hubble diagram of quasars at high redshifts. *Nat. Astron.*, 3:172, 2019.

[21] A.M. Galiakhmetov. Exact rotating and expanding cosmologies in einstein-cartan theory. *Gravit. Cosmol.*, 15:250, 2009.

[22] M. Gasperini. Spin-dominated inflation in the Einstein-Cartan theory. *Phys. Rev. Lett.*, 56:2873–2876, Jun 1986.

[23] Ana Luisa González-Morán, Ricardo Chávez, Elena Terlevich, Roberto Terlevich, David Fernández-Arenas, Fabio Bresolin, Manolis Plionis, Jorge Melnick, Spyros Basilakos, and Eduardo Telles. Independent cosmological constraints from high-z H II galaxies: new results from VLT-KMOS data. *Mon. Not. Roy. Astron. Soc.*, 505(1):1441–1457, 05 2021.

[24] Richard T Hammond. Torsion gravity. *Rep. Prog. Phys.*, 65(5):599–649, mar 2002.

[25] Friedrich W. Hehl, Paul von der Heyde, and G. David Kerlick. General relativity with spin and torsion and its deviations from einstein's theory. *Phys. Rev. D*, 10:1066–1069, Aug 1974.

[26] Friedrich W. Hehl, Paul von der Heyde, G. David Kerlick, and James M. Nester. General relativity with spin and torsion: Foundations and prospects. *Rev. Mod. Phys.*, 48:393–416, Jul 1976.

[27] Qihong Huang, Puxun Wu, and Hongwei Yu. Emergent scenario in the Einstein-Cartan theory. *Phys. Rev. D*, 91:103502, May 2015.

[28] J. Richard Gott III, Mario Jurić, David Schlegel, Fiona Hoyle, Michael Vogeley, Max Tegmark, Neta Bahcall, and Jon Brinkmann. A map of the universe. *The Astrophysical Journal*, 624(2):463, may 2005.

[29] Michal Křížek and Yurii V. Dumin, editors. *Dark Matter Problem and Selected Controversies in Cosmology*, Proceedings of the International Conference Cosmology on Small Scales, Prague, September 2018. Institute of Mathematics.

[30] Michal Křížek and Lawrence Somer. Exessive extrapolations of einstein equations. In Michal Křížek and Yurii V. Dumin, editors, *Exessive Extrapolations and Selected Controversies in Cosmology*, Proceedings of the International Conference Cosmology on Small Scales, page 9, Prague, September 2020. Institute of Mathematics.

[31] Bronisław Kuchowicz. Friedmann-like cosmological models without singularity. *General Relativity and Gravitation*, 9(6):511–517, Jun 1978.

[32] Xiaolei Li, Ryan E Keeley, Arman Shafieloo, Xiaogang Zheng, Shuo Cao, Marek Biesiada, and Zong-Hong Zhu. Hubble diagram at higher redshifts: model independent calibration of quasars. *Mon. Not. R. Astron. Soc.*, 507(1):919–926, 07 2021.

[33] Alexia M. Lopez. https://www.uclan.ac.uk/news/big-ring-in-the-sky.

[34] Alexia M Lopez, Roger G Clowes, and Gerard M Williger. A Giant Arc on the Sky. *Mon. Not. R. Astron. Soc.*, 516(2):1557–1572, 08 2022.

[35] M. López-Corredoira. Tests and problems of the standard model in cosmology. *Found. Phys.*, 47:711, 2017.

[36] Paulo Luz and Sante Carloni. Static compact objects in einstein-cartan theory. *Phys. Rev. D*, 100:084037, Oct 2019.

[37] Andre Maeder. An alternative to the λCDM model: The case of scale invariance. *Astrophys. J.*, 834(2):194, January 2017.

[38] Elias A S Mégier. Square-torsion gravity: a geometric candidate for dark matter. *Class. Quant. Grav.*, 36(22):225011, October 2019.

[39] Klaus Morawetz. Consistent solution of einstein–cartan equations with torsion outside matter. *Class. Quant. Grav.*, 38(20):205003, September 2021.

[40] Klaus Morawetz. Time behavior of hubble parameter by torsion. *Mod. Phys. Lett. A*, 39(03):2350192, 2024.

[41] Eoin O Colgáin, Maurice H.P.M. van Putten, and Hossein Yavartanoo. de Sitter Swampland, H0 tension & observation. *Phys. Lett. B*, 793:126–129, 2019.

[42] Y N Obukhov and V A Korotky. The Weyssenhoff fluid in Einstein-Cartan theory. *Class. Quant. Grav.*, 4(6):1633–1657, nov 1987.

[43] Nikodem Popławski. Spacetime and fields, 2009. arXiv:0911.0334v1.

[44] Nikodem Popławski. Nonsingular, big-bounce cosmology from spinor-torsion coupling. *Phys. Rev. D*, 85:107502, May 2012.

[45] Nikodem Popławski. Universe in a black hole in Einstein–Cartan gravity. *Astrophys. J.*, 832(2):96, nov 2016.

[46] Nikodem Popławski. Primordial fluctuations of scale factor in closed universe in einstein–cartan gravity. *Mod. Phys. Lett. A*, 33(40):1850236, 2018.

[47] Nikodem Popławski. The simplest origin of the big bounce and inflation. *Internat. J. Mod. Phys. D*, 27(14):1847020, 2018.

[48] Nikodem J. Popławski. Matter-antimatter asymmetry and dark matter from torsion. *Phys. Rev. D*, 83:084033, Apr 2011.

[49] Nikodem J. Popławski. Cosmology with torsion: An alternative to cosmic inflation. *Phys. Lett. B*, 694(3):181 – 185, 2010.

[50] G. Pradisi and A. Salvio. (In)equivalence of metric-affine and metric effective field theories. *Eur. Phys. J. C*, 82:840, 2022.

[51] Adam G. Riess, Wenlong Yuan, Lucas M. Macri, Dan Scolnic, Dillon Brout, Stefano Casertano, David O. Jones, Yukei Murakami, Gagandeep S. Anand, Louise Breuval, Thomas G. Brink, Alexei V. Filippenko, Samantha Hoffmann, Saurabh W. Jha, W. D'arcy Kenworthy, John Mackenty, Benjamin E. Stahl, and WeiKang Zheng. A comprehensive measurement of the local value of the Hubble constant with 1 km s^{-1} mpc^{-1} uncertainty from the Hubble space telescope and the SHOES team. *The Astrophysical Journal Letters*, 934(1):L7, July 2022.

[52] Léon Rosenfeld. *Sur le tenseur d'impulsion-énergie*. Palais des Académies (impr. de G. Thone), Bruxelles, 1940.

[53] J. Ryan, S. Doshi, and B. Ratra. *Mon. Not. R. Astron. Soc.*, 480:759, 2018.

[54] D. W. Sciama. The physical structure of general relativity. *Rev. Mod. Phys.*, 36:463–469, Jan 1964. errata 36, 1103 (1964).

[55] I.L. Shapiro. Physical aspects of the space–time torsion. *Phys. Rep.*, 357(2):113 – 213, 2002.

[56] Gabriel Unger and Nikodem Popławski. Big bounce and closed universe from spin and torsion. *Astrophys. J.*, 870(2):78, jan 2019.

[57] P. Von Der Heyde. The equivalence principle in the U4 theory of gravitation. *Lett. Nuovo Cimento*, 14:250, 1975.

[58] H. Weyl. Elektron und Gravitation I. *Z. Physik*, 56:330, 1929.

Conference *Cosmology on Small Scales 2024*
Michal Křížek and Yurii Dumin (Eds.)
Institute of Mathematics CAS, Prague

COSMOLOGY WITH ONE EXTRA DIMENSION

Ivan L. Zhogin

Institute of Solid State Chemistry and Mechanochemistry of the Siberian Branch
of the Russian Academy of Sciences, Novosibirsk, Russia
zhogin@mail.ru

Abstract: The standard cosmological model with 4D General Relativity (GR) is in no way an *island solution satisfying natural (trivial) boundary conditions*; at a negative or zero spatial curvature the number of galaxies is unlimited – that is quite strange. A 5D cosmological model, the Universe-on-the-Brane, is considered; it arises naturally in a special case of Absolute Parallelism (AP). This AP-variant, a second-order exceptional equation (EE) of the frame field $h^a{}_\mu$, does not allow singularities of solutions (if $D=5$; $D=4$ is just forbidden). That is, the equation compatibility (the regularity of its principal terms) is violated (unlike other variants, including the vacuum GR equation) when $h^a{}_\mu$ (as well as the metric) becomes one-degenerate. There are no conservation laws (CLs) in this variant, but there is a covariantly conserved stress-energy tensor (the SE-pseudotensor is trivial), and also O_4-symmetric solutions as a (longitudinal) wave running along the radius, in which, as in an optical waveguide (or a thick brane) shorter waves and quasi-particles (non-linear field configurations carrying a topological (quasi)charge) can be held. The brane thickness (in the co-moving system; $L\sim 3$–5 kau) defines the scale where the attraction $1/r^2$ transforms to slower decline $1/r$.
The Brane speed V should be a bit less than 1, because the Brane holds energy-carrying waves (3 out of 15 polarizations); the strongest three polarizations (linearly unstable and responsible for non-linear effects and quasi-particles) do not carry energy. We consider the motion of both massive bodies and massless photons in this relativistically expanding Brane.

Keywords: cosmology, 5th dimension, Hubble diagram, absolute parallelism

PACS: 98.80.-k, 98.80.Es

1. Introduction and notations

In Absolute Parallelism, the symmetry of frame field equations includes the symmetries of both special and general relativity theories. The global group (the Lorentz one is supplemented by scale transformations) acts on Latin indexes, and

(pseudo)group of coordinate diffeomorphisms – on Greek ones (all indexes run from 0 to $D-1$; $\kappa, s^a{}_b = \text{const}$):

$$h^{*a}{}_\mu(x^\nu) = \kappa s^a{}_b h^b{}_\mu(x^\nu);\ \kappa > 0,\ s^a{}_b \in \mathrm{O}(1, D-1) - \text{Lorentz group}; \tag{1}$$

$$h^{*a}{}_\mu(y) = h^a{}_\nu(x)\partial x^\nu/\partial y^\mu. \tag{2}$$

Minkowski's metric $\eta_{ab} = \mathrm{diag}(-1, 1, \ldots, 1) = \eta^{ab}$ serves to form the metric field (and deals with the Latin indexes):

$$g_{\mu\nu} = \eta_{ab} h^a{}_\mu h^b{}_\nu = h^a{}_\mu h_{a\nu}. \tag{3}$$

Equations with symmetries (1), (2) are easy to write using just partial derivatives $\partial(\cdot)/\partial x^\mu = (\cdot)_{,\mu}$, starting with the basic AP tensor (Λ-tensor, plus Λ-identity):

$$\Lambda_{a\mu\nu} = h_{a\mu,\nu} - h_{a\nu,\mu} = 2h_{a[\mu,\nu]}\,, \quad \Lambda_{a[\mu\nu,\lambda]} \equiv 0\,. \tag{4}$$

Then we switch Greek indices into Latin (scalar) ones, using $h^a{}_\mu$ and contra-frame $h_a{}^\mu$, and further differentiation becomes easy:

$$\Lambda_{abc,d} = \Lambda_{abc,\mu} h_d{}^\mu,\ \text{where, sure, } \Lambda_{abc} = \Lambda_{a\mu\nu} h_b{}^\mu h_c{}^\nu.$$

However we prefer the usual covariant derivative with symmetric connection (it is convenient when differentiating tensors with skew-symmetric indices) consistent with metric ($g_{\mu\nu;\lambda} \equiv 0$), e.g.

$$\Lambda_{a\mu\nu} = h_{a\mu;\nu} - h_{a\nu;\mu} = 2h_{a[\mu;\nu]}\,, \quad \Lambda_{a[\mu\nu;\lambda]} \equiv 0 \quad (h_a{}^\lambda \Lambda^a{}_{[\mu\nu;\lambda]} \equiv 0). \tag{5}$$

So, if we find a suitable stress-energy tensor that is covariantly conserved, this will mean that the D-momentum moves along usual Riemannian geodesics (which is necessary, together with the reproduction of Newton's approximation, to match the observations).

It is possible to define another simple tensor (of the first order), $h_{a\mu;\nu}$, but it is also skew-symmetric in two indices (and can be expressed in terms of Λ-tensor). One can simply write the Riemann curvature:

$$R_{a\mu\nu\lambda} = 2h_{a\mu;[\nu;\lambda]};\quad 2h^a{}_\mu h_{a\nu;\lambda} = -2h^a{}_\nu h_{a\mu;\lambda} = \Lambda_{\mu\nu\lambda} - \Lambda_{\nu\mu\lambda} - \Lambda_{\lambda\mu\nu}. \tag{6}$$

Einstein usually used a different covariant differentiation – with a non-symmetric connection consistent with the frame field [1] (see also [2]):

$$h^a{}_{\mu!\nu} \equiv 0 = h^a{}_{\mu,\nu} - h^a{}_\tau \Delta^\tau_{\mu\nu},\ \text{so } \Delta^\tau_{\mu\nu} = h_a{}^\tau h^a{}_{\mu,\nu};$$

at the same time, the tensor Λ, of course, was determined only through partial derivatives. It is easy to realize that $h^a{}_\mu$ and $h_a{}^\mu$ can be *carried* through such derivatives, changing the Greek indices to Latin ones; but this means that the curvature tensor for this differentiation is identically zero (while the torsion is mere Λ-tensor).

Hence, this name arose – Absolute Parallelism. Equations with this differentiation can be converted to our notations by replacing all Greek indices with Latin ones and switching to ordinary derivatives $\{\text{scalar}\}_{,\mu} h_d^{\ \mu}$ (or $\{\text{scalar}\}_{;\mu} h_d^{\ \mu}$).

Having two covariant differentiations, one can write down their linear combination, $aD^{(1)}_\mu + (1-a)D^{(2)}_\mu$ (a is any real number), and it is also a covariant thing!

We also use the following notations (see also [3, 4, 5]):

$$S_{\mu\nu\lambda} = 3\Lambda_{[\mu\nu\lambda]},\ \ \Phi_\nu = h_a^{\ \mu}\Lambda_{a\mu\nu} = \Lambda_{\mu\mu\nu},\ \ f_{\mu\nu} = 2\Phi_{[\mu;\nu]},\ \ f_{[\mu\nu;\lambda]} \equiv 0. \tag{7}$$

For better clarity, in clearly covariant expressions, we write summable (contracting) indexes at the bottom (as the others), understanding this as a kind of equivalence class – either of the two indices can be raised (matrices η^{ab} and $g^{\mu\nu}$ can be carried through covariant differentiations).

Einstein and Mayer found four classes of compatible AP equations (of the second order), including the Lagrangian two-parameter class, with Lagrangian density $h\mathcal{L}$ (the term with Λ^2 should not vanish [3, 5]):

$$h = \det h^a_{\ \mu} = \sqrt{-g},\quad \mathcal{L} = \frac{1}{4}\Lambda_{abc}\Lambda_{abc} + \frac{\gamma}{12}S_{abc}S_{abc} - \frac{\sigma}{2}\Phi_a\Phi_a. \tag{8}$$

So it was difficult to select only one equation.

Another difficulty was the lack of a suitable candidate for the electromagnetic field. In all cases, the prolonged equation for the rotor field $f_{\mu\nu}$ (looking as Maxwell's one) has a trivial current,

$$f_{\mu\nu;\nu} = J_\mu(\Lambda\Lambda') = W_{[\mu\nu]}(\Lambda^2)_{;\nu}.$$

This leads to difficulties with Coulomb-like asymptotics. Einstein and Mayer had considered the spherically symmetric static problem (preferring dimension $D = 4$) [2], p. 177, so they should see this issue.

In Section 2, we will consider a simple compatible equation (non-Lagrangian) to illustrate the application of compatibility (formal integrability) theory [6]. Then a special, exceptional variant of AP will be noted, with a special type of compatibility (the second identity does not follow automatically). The exceptional equation (EEn; non-Lagrangian too) corresponding to this case is also distinguished by the fact that, apparently, there are no singularities in solutions (if the spacetime dimension is $D=5$). Our approach extends the compatibility test to cases when the co-frame matrix $h^a_{\ \mu}$ becomes degenerate (co-singularities; the only choice is the EEn), or the contra-frame density of some weight degenerates (contra-singularities; here we have to choose $D=5$).

For EEn, we find the stress-energy (SE) tensor appearing in a prolonged fourth order equation (4^{th}-order gravity). Moreover, this equation can follow from a Lagrangian which is quadratic in field equations ($\sim$EE^2).

In Section 3, we consider the properties of 15 polarizations and start with the linear approximation. There are, among other things, three linearly unstable polarizations, the growth of which is caused by the resonant action of three rotor polarizations relating to $f_{\mu\nu}$. Also there is the longitudinal polarization (the gradient symmetry for vector Φ_μ is absent). Only f-polarizations contribute to 5-momentum, and the other 12 are *weightless*. Exact conservation laws (CLs) in this AP variant are absent (and the SE-pseudotensor is trivial).

Then the most symmetrical solutions are discussed – moving longitudinal waves, both spherically symmetric and plane.

We argue that an O_4-symmetric wave can serve as an expanding cosmological shallow waveguide for other waves (almost tangential, with shorter wavelengths). Approximate CLs can emerge on par with development of symmetries (of this cosmological waveguide) and Killing vectors.

The current thickness of the spherical shell (or Brane) in the co-moving system is perhaps $L \sim 3$–5 kau (as observed with wide binaries [7]); this length defines the scale where attraction $\sim 1/r^2$ is replaced by a slower decline $\sim 1/r$ (and Planck's length appears a composite quantity) [4, 8].

The evolution of such a Brane Universe, the growth of unstable polarizations and the birth of quasi-particles, nonlinear field configurations carrying discrete information – topological charges and (for symmetric configurations) quasi-charges, are considered. The field equations do not violate symmetries so the quasi-charges will continue too. But if the symmetry of a localized non-linear field configuration is broken by approaching another non-linear thing (quasi-particle) the quasi-charge(s) can transform somehow. We should describe also the morphisms of quasi-charge groups induced by embeddings of corresponding symmetries.

The combinatorics of quasi-particles and their phenomenology (looking as a quantum field theory) are briefly outlined; *white* quasi-particles' symmetries are subgroups of the symmetry of cosmological background, while the *color* ones (who exist in the hadron bag conditions, where the symmetry is different, larger) have some weirder symmetries [3, 9]. One should associate photons (quantized electromagnetic field) with true neutral quasi-particles possesing cylindrical symmetry plus additional discreet symmetries (including inversion of all space coordinates, i.e. CP-symmetry).

Section 4 proposes a simple cosmological 5D model of a relativistically expanding Brane Universe. A Lagrangian describing the motion of massive bodies in the Brane is proposed, and the exact solution for free motion is obtained, as well as some approximations that can be used to describe orbital motion (for example, in the Solar System). The motion of massless photons has a particularly simple appearance, and leads to a Hubble diagram consistent with the SNeIa data [10] (uniform growth of the scale factor $a \propto t$ is suggested also in the so called $R_h = ct$ cosmology [11], but there a sort of fine tuning for Dark Energy is necessary, $<w>_{(\text{all sorts})} = -1/3$).

Finally, the possibility of nonlinear (and weightless!) perturbations escaping from the Brane (during events with a large release of energy) and their subsequent Brane crossing is considering. If quasi-particles (both charged, colored, and neutral pho-

tons) occur in the intersection region, then it is possible to capture disturbances with a local violation of the Brane symmetry (and breaking the very concept of quasi-particles), leading, perhaps, to interesting effects of quasi-particle transformation/generation (LENR effects [12, 13, 14, 15]), including the growth of Earth's radius (and mass) [16, 17].

2. Compatible AP equations of second order

Let us differentiate the Lagrangian of general form (8)

$$d\mathcal{L} = \frac{1}{2}K_{abc}d\Lambda_{abc} = K_{abc}d(h_{a\nu,\lambda}h_b{}^{\nu}h_c{}^{\lambda}),\ \text{where}\ K_{abc} = \Lambda_{abc}+\gamma S_{abc}-\sigma(\eta_{ab}\Phi_c-\eta_{ac}\Phi_b).$$

Varying $h\mathcal{L}$ we write the two-parameter class of Lagrangian equations (class I_{12} in [1]) as follows (also we separate the skew-symmetric part):

$$\mathbf{B}_{a\mu} = -h^{-1}g_{\mu\nu}\frac{\delta(h\mathcal{L})}{\delta h^a{}_{\nu}} = K_{a\mu\nu;\nu} + \Lambda_{bca}K_{bc\mu} - h_{a\mu}\mathcal{L} = 0,\ \mathbf{B}_{a\mu;\mu} - \mathbf{B}_{bc}\Lambda_{bca} \equiv 0; \quad (9)$$

$$2\mathbf{B}_{[\mu\nu]} = (1+2\gamma)(S_{\mu\nu\lambda;\lambda} - \Lambda_{\mu\varepsilon\tau}\Lambda_{\varepsilon\tau\nu} + \Lambda_{\nu\varepsilon\tau}\Lambda_{\varepsilon\tau\mu}) + (1-\sigma)(f_{\mu\nu} - \Phi_\lambda\Lambda_{\lambda\mu\nu}) = 0. \quad (10)$$

We also have indicated the identity that ensures compatibility (except for a couple of 'pathological cases' [3, 5]). The case $\sigma = 1,\ \gamma = -\frac{1}{2}$ corresponds to the vacuum equation of General Relativity (the skew-symmetric part vanishes)

$$G_{\mu\nu} = R_{\mu\nu} - \frac{1}{2}g_{\mu\nu}R = 0;\ G_{\mu\nu;\nu} \equiv 0.$$

One class of non-Lagrangian equations (class II_{22112} in [1]; the term $h_{a\mu}\mathcal{L}$ is absent) looks even simpler (see Eq. (9) for tensor $K_{a\mu\nu} = K_{a[\mu\nu]}$):

$$\mathbf{A}_{a\mu} = K_{a\mu\nu;\nu} = 0,\ \mathbf{A}_{a\mu;\mu} \equiv 0; \quad (11)$$

the identity is simply obvious here.

Let us take a closer look at the simplest option, the case $\gamma = 0 = \sigma$ in (11).

2.1. A sample (and simple) compatible equation

Let us take the simple (sample) compatible AP equation (SEn; non-Lagrangian)

$$\mathbf{A}^*_{a\mu} = \Lambda_{a\mu\nu;\nu} = 0\ [\text{i.e. } (h\Lambda_a{}^{\mu\nu})_{,\nu} = 0\,],\ \ \mathbf{A}^*_{a\mu;\mu} \equiv 0\,. \quad (12)$$

After linearization, this equation looks like a D-fold Maxwell's equation, see (4),

$$h^a{}_{[\mu,\nu],\nu} = 0,\ \text{or}\ \Lambda^a{}_{\mu\nu,\nu} = 0,\ \Lambda^a{}_{[\mu\nu,\lambda]} = 0,$$

where infinitesimal diffeomorphisms serve as a set of gradient transformations. So, the number of polarisation degrees of freedom in this case (as well as for other AP equations with similar identities) is $D(D–2)$. The number of polarizations in vacuum GR (GWs) is much smaller: $D(D-3)/2$.

The compatibility theory (J. F. Pommaret, [6]) says that further identities are valid automatically. Is it really so? The other "divergence" $\mathbf{A}^{*a}{}_{\mu;\nu}h_a{}^{\nu}=0=\mathbf{A}^{*a}{}_{\mu,a}$ gives a Maxwell-like equation (contracting Λ-identity (5) one obtains $\Lambda_{abc,a}+f_{bc}\equiv 0$):

$$A^{*}_{a\mu,a}\colon\ f_{\mu\nu;\nu}-J_{\mu}(\Lambda\Lambda')=0;$$

so the next identity must be valid (automatically! current conservation): $J_{\mu;\mu}\equiv 0$.

How to check and explain this?!

Any AP equation $\mathbf{E}_{\mu\nu}(\Lambda',\Lambda^2)=0$ can be separated on the symmetric and skew-symmetric parts (for SEn, $\sigma=0$, $\tau=(1-\sigma)/(1+2\gamma)=1$; remember, $G_{\mu\nu;\nu}\equiv 0$):

$$\mathbf{E}_{[\mu\nu]}\colon\ S_{\mu\nu\lambda;\lambda}+\tau f_{\mu\nu}+V_{[\mu\nu]}(\Lambda^2)=0\,;\ \ \mathbf{E}_{(\mu\nu)}\colon\ \Lambda_{(\mu\nu)\lambda;\lambda}+\sigma(\Phi_{(\mu;\nu)}-g_{\mu\nu}\Phi_{\lambda;\lambda})+(\Lambda^2)=$$

$$=-G_{\mu\nu}+(\sigma-1)(\Phi_{(\mu;\nu)}-g_{\mu\nu}\Phi_{\lambda;\lambda})+V_{(\mu\nu)}(\Lambda^2)=0\,;$$

these parts give two Maxwell-like equations which currents should be identical – otherwise we obtain a new irregular (in the first jets) second order equation (it is the first identity necessary for compatibility; $\sigma\neq 1,\tau\neq 0$):

$$(\sigma-1)[f_{\mu\nu;\nu}-J^{(s)}_{\mu}(\Lambda\Lambda')]=0,\ \ \tau[f_{\mu\nu;\nu}-J^{(a)}_{\mu}(\Lambda\Lambda')]=0,\ \ J^{(s)}_{\mu}\equiv J^{(a)}_{\mu}\propto V_{[\mu\nu];\nu}.$$

Evidently, if $\tau\neq 0$, the current is trivial as it follows from the skew-symmetric part.

The only exception is $\tau=0$ (and $\sigma\neq 1$), with the *exceptional equation* (EEn) where the current (it is trivial too) follows only from the symmetric part. In this case the symbol G_2 [6] is not involutive, but its prolongation G_3 is involutive [3], so the second identity is sufficient for compatibility.

2.2. The exceptional equation, 5D (EEn stops singularities of solutions!)

The inevitability of singularities in solutions of GR equations (including vacuum GR) was proved only after Einstein passed away. The natural question arises about singularities in AP solutions. One can extend the compatibility analysis to cases when the co-frame becomes degenerated, $\operatorname{rank} h^{a}{}_{\mu}<D$, using the minors (of co-rank two, sometimes three; like the determinant h, they are poly-linear expressions in co-frame elements) as coefficients at the principal derivatives:

$$\begin{pmatrix}\mu & \nu\\ a & b\end{pmatrix}=\frac{\partial^2 h}{\partial h^{a}{}_{\mu}\partial h^{b}{}_{\nu}}=2!\,hh_{[a}{}^{\mu}h_{b]}{}^{\nu},\quad \begin{pmatrix}\mu & \nu & \lambda\\ a & b & c\end{pmatrix}=3!\,hh_{[a}{}^{\mu}h_{b}{}^{\nu}h_{c]}{}^{\lambda}.$$

For example, the equation (12), its principal terms, can be written as follows:

$$h^2\mathbf{A}^{*\mu}_{a}=-gg^{\alpha\mu}g^{\beta\nu}(h_{a\alpha,\beta\nu}-h_{a\beta,\alpha\nu})+(h'^2)=h_{a\alpha,\beta\nu}[\alpha\mu,\beta\nu]+(h'^2)\,. \tag{13}$$

We use the next notation for k-minors of co-metric (or co-rank-k minors):

$$[\mu_1\nu_1,\dots,\mu_k\nu_k]=\partial^k(-g)/(\partial g_{\mu_1\nu_1}\partial g_{\mu_2\nu_2}\cdots\partial g_{\mu_k\nu_k})=\frac{1}{k!}\begin{pmatrix}\mu_1 & \cdots & \mu_k\\ a_1 & \cdots & a_k\end{pmatrix}\begin{pmatrix}\nu_1 & \cdots & \nu_k\\ a_1 & \cdots & a_k\end{pmatrix}.$$

It can be shown (following the recipes of [6], see also [3]) that the symbol G_2 of Equation (13) remains involutive (and regularity holds) even if $\operatorname{rank} h^a{}_\mu = D-1$. Apparently, this indicates the possibility of co-singularities in solutions, points where some scalars (where contra-frame $h_a{}^\mu$ takes part) go to infinity. The symmetry transformations (diffeomorphisms) cannot turn a singular point into a regular one, and vice versa.

The GR vacuum equation (where only the symmetric part participates in the identity; so this time both indexes should be of the same kind) can also be represented in a similar form $2(-g)G^{\mu\nu} = [\mu\nu, \varepsilon\tau]_{,\varepsilon\tau} + t^{\mu\nu}(g'^2) = 0$ (SE pseudo-tensor), or:

$$2(-g)G^{\mu\nu} = [\mu\nu, \varepsilon\tau, \alpha\beta](g_{\alpha\beta,\varepsilon\tau} + g^{\rho\phi}\Gamma_{\rho,\varepsilon\tau}\Gamma_{\phi,\alpha\beta}) = \frac{1}{2}[\mu\nu, \varepsilon\tau, \alpha\beta]R_{\alpha\varepsilon\tau\beta} = 0. \qquad (14)$$

Divide (14) by $(-g)$ and make divergence (taking into account the Bianchi identities $R_{\mu\alpha[\nu\beta;\gamma]} \equiv 0$ and skew-symmetry of 3-minor indexes). Again, the regularity of (14) and its prolongations is preserved when $\operatorname{rank} g_{\mu\nu} = D-1$.

The only exception is the case when only the skew-symmetric part participates in the identity; this exeptional equation is unique and can be written as follows [3, 5]:

$$\mathbf{EE}_{a\mu} = L_{a\mu\nu;\nu} - \frac{1}{3}(f_{a\mu} + L_{a\mu\nu}\Phi_\nu) = 0, \quad \text{where } L_{a\mu\nu} = \Lambda_{a\mu\nu} - S_{a\mu\nu} - \frac{2}{3}h_{a[\mu}\Phi_{\nu]}. \qquad (15)$$

$$\mathbf{EE}_{[\mu\nu]}: \ S_{\mu\nu\lambda;\lambda} = 0\,; \quad \mathbf{EE}_{a\mu;\mu}: \ f_{\mu\nu;\nu} = (S_{\mu\nu\lambda}\Phi_\lambda)_{;\nu} \ (= \frac{1}{2}S_{\mu\nu\lambda}f_{\lambda\nu}); \qquad (16)$$

$$\mathbf{EE}_{(\mu\nu)}: \ G_{\mu\nu} + \frac{2}{3}(\Phi_{(\mu;\nu)} - g_{\mu\nu}\Phi_{\lambda;\lambda}) + (\Lambda^2) = 0 \ \text{ (is Stress-Energy here ?!)}. \qquad (17)$$

The EEn doesn't allow $D=4$ (we should chose $D=5$; we use $\Phi_a^2 = \Phi_a\Phi_a$, et cet.):

$$\mathbf{EE}_{\mu\mu} = E^a{}_\mu h_a{}^\mu = \frac{4-D}{3}\Phi_{\mu;\mu} - \frac{1}{2}\Lambda_{abc}^2 + \frac{1}{3}S_{abc}^2 + \frac{D-1}{9}\Phi_a^2 = 0. \qquad (18)$$

If $D=4$, the trace equation (18) becomes irregular (in the first jets).

The other kind of singularities, contra-singularities, depend on D, and their absence gives preference to the dimension $D=5$ [3, 18]. No free parameters remains in this theory.

But we have a problem with the Stress-Energy (SE) tensor, see Eq. (17) – the linear term $\Phi_{(\mu;\nu)}$ looks unappropriate for positive energy.

Pauli, noting Einstein's "inexhaustible ingenuity" (in connection with teleparallelism), also asked questions about the SE tensor and post-Newtonian effects.

The correct SE tensor appears in the prolonged 4th order equation ($\mathbf{EE}_{(\mu\nu);\tau;\tau} = 0$; the SE pseudo-tensor is trivial), which can be represented as follows [4, 19]

$$G_{\mu\nu;\tau;\tau} + G_{\varepsilon\tau}(2R_{\varepsilon\mu\tau\nu} - g_{\mu\nu}R_{\varepsilon\tau}/2) = -T_{\mu\nu} = -\frac{2}{9}T^{(f)}_{\mu\nu} + B_{[\mu\rho][\nu\tau]}(\Lambda^2)_{;\rho;\tau}\,, \qquad (19)$$

where $T^{(f)}_{\mu\nu} = f_{\mu\tau}f_{\nu\tau} - \frac{1}{4}g_{\mu\nu}f_{ab}^2$; $T_{\mu\nu;\nu} = 0$, $T^{(f)}_{00} > 0$ – the right sign for gravity wells!

This equation (19) follows also from a "quadratic Lagrangian"

$$\mathcal{L} \sim \mathbf{EE}^2_{(\mu\nu)} \sim R_{\mu\nu}G^{\mu\nu} + \frac{1}{9}f^2_{\mu\nu} + [X_\nu]_{;\nu} + (\Lambda'\Lambda^2,\, \Lambda^4). \tag{20}$$

For masses extended along the extra dimension (the scale L) one can reproduce Newton's gravity $1/r^2$ at small scales $r < L$, while for $r > L$ the asymptotic is different, $1/r$ [4, 19].

The baryonic mass of a galaxy cannot be measured as accurately as its luminosity; so the function $L_{\rm gal}(M_{\rm gal})$ can be non-linear, e.g., as it was modelled in [20],

$$L_{\rm gal} \propto M^2_{\rm gal} \text{ (for stars } \; L_{\rm st} \propto M^4_{\rm st})$$

this would support the suggested theory (but not MOND) on the ground of baryonic Tully-Fisher relation.

3. Fifteen polarizations in 5D (one need some rum to figure it out)

The compatibility theory tells how many arbitrary functions from how many variables $(5, 4, \ldots)$ determine the formal solution of general position [6]. Part of this arbitrariness relates to the coordinate choice (the gauge symmetry, diffeomorphisms). A more visual approach relates the polarizations to the number of amplitudes (related to the tensor Λ – to remove coordinate freedom) in a plane linearized wave of general type (position; the number of arbitrary phases is the same) running along some coordinate x with a wave vector k:

$$\Lambda_{\mu\nu\lambda} = a_{\mu\nu\lambda}(t)\, \mathrm{e}^{\mathrm{i}\, kx}\,.$$

An ODE system arises, and all $D(D-2)=15$ polarizations have eigenvalue $\omega^2 = k^2$.

It turns out that three of these polarizations are linearly unstable, and their amplitudes have the form

$$a(t) = (a_0 + a_1 t)\, \mathrm{e}^{\mathrm{i}\,\omega t}\,.$$

This does not break the correctness of Cauchy problem, since the ill-posedness is associated only with an exponential increase of amplitudes.

Indeed, by taking the divergence of Λ identity (5), one can obtain the evolution equation for Λ tensor (in linearized equations we use $\Box$ and $\approx$)

$$\Lambda_{\lambda\mu\nu;\tau;\tau} = -\frac{2}{3}\, f_{\mu\nu;\lambda} + (\Lambda\Lambda', \Lambda^3), \quad \text{i.e.,} \quad \Box\Lambda_{\lambda\mu\nu} \approx -\frac{2}{3}\, f_{\mu\nu,\lambda} \;\; (\Box\Lambda_{[\lambda\mu\nu]} \approx 0). \tag{21}$$

Three rotor f-polarizations cause a resonant, linear growth of three unstable polarizations. At the same time, the polarizations related to $S_{\mu\nu\lambda}, \Phi_\mu, f_{\mu\nu}$, and curvature tensor $R_{\mu\tau\nu\rho}$ (use divergence of Bianchi identity) are linearly stable:

$$\Box S_{\mu\nu\lambda} \approx 0 \approx \Box\Phi_\mu\,, \;\; \Box f_{\mu\nu} \approx 0 \approx \Box R_{\mu\tau\nu\rho}\,.$$

Even if the initial data differs very-very little from the Minkowski space in some area, $h^a{}_\mu - \delta^a_\mu \ll 1$, the solution will remain localized, but sooner or later, due to the rising waves, the solution will become nonlinear.

Polarizations can be classified into four classes, starting with the zero-class and rising waves, where the amplitudes are largest. For the following classes, with much-much smaller and smaller amplitudes, the structure of quadratic terms is important – whether the zero-class waves enter there. So, the first class includes longitudinal (no gradient symmetry for Φ_μ) and three S-polarizations:

$$\Phi_{\mu;\mu} = -\frac{3}{2}\Lambda^2_{abc} + (S^2, \Phi^2); \quad S_{[\mu\nu\lambda;\tau]} \propto \Lambda^a_{[\mu\nu}\Lambda^a{}_{\lambda\tau]}\,, \quad S_{\mu\nu\lambda;\lambda} = 0\,.$$

Note that one can introduce a pseudo-EM field $\tilde{f}_{ab} = \frac{1}{6}\,\varepsilon_{abcde}S_{cde}$ where Maxwell-like equations are valid:

$$\tilde{f}_{[\mu\nu;\lambda]} = 0\,, \quad \tilde{f}^{\mu\nu}{}_{;\nu} = \frac{1}{8}\,h^{-1}\,\varepsilon^{\mu\nu\lambda\varepsilon\tau}\Lambda_{a\nu\lambda}\Lambda_{a\varepsilon\tau}\,.$$

So, we have just three S-polarizations.

The last (f- and GW-) polarizations relate respectively to the second and third classes:

$$f_{\mu\nu;\nu} = \frac{1}{2}S_{\mu\nu\lambda}f_{\lambda\nu} \text{ (3 polarizations, second class);}$$

$$\Box R_{0i0j} \propto T_{ij}(f^2) \text{ (5 pol-ns, third class; in GR: } \Box R_{0i0j} \propto \lambda^2_{\rm Pl}\ddot{T}^*_{ij}).$$

As in GR, generation of gravitational waves in our theory is determined by the stress-energy tensor, but the natural SE scale is very different from the convention adopted in GR [4, 8].

The traditional idea (or maybe an illusion) is that space-time is populated (in addition to the metric) by many independent fields. So the interesting question – can one specify (quasi)independent fields for all polarizations, maybe in some approximation (especially since most waves have very small amplitudes).

So, for the longitudinal polarization, we can introduce an auxiliary scalar field Ψ by solving the equation, see (18):

$$\Psi_{;\mu;\mu} = -\frac{3}{2}\Lambda^2_{abc} + S^2_{abc} + \frac{4}{3}\Phi^2_a \;(= \Phi_{\mu;\mu}).$$

Now we have vector $A_\mu = \Phi_\mu - \Psi_{;\mu}$ – a conserved current, $A_{\mu;\mu} = 0$, so we can solve Maxwell-like equations for three F-polarizations that can represent the class zero waves, see (21):

$$F_{\mu\nu;\nu} = -\frac{2}{3}A_\mu,\; F_{[\mu\nu;\lambda]} = 0\,;\; F_{\mu\nu;\tau;\tau} = -\frac{2}{3}f_{\mu\nu} + (fR)\,;\; \Box(\Lambda_{\lambda\mu\nu} - F_{\mu\nu,\lambda}) \approx 0\,.$$

Thus, in some sense, we get the next set of fields (instead of $h^a{}_\mu$):

$$g_{\mu\nu} \text{ (and } R_{\mu\nu\tau\rho}),\; F_{\mu\nu},\; \Psi,\; \tilde{f}_{\mu\nu},\; f_{\mu\nu}\,.$$

3.1. Longitudinal waves – spherically-symmetric and plane

In fact, only longitudinal polarization survives (and changes the Ricci tensor) in so great symmetries. Tensor $S_{\mu\nu\lambda}$ is zero, so the current for $f_{\mu\nu}$ is zero too, and integrating equations $(hf^{\mu\nu})_{,\nu}=0$ one can find that $f_{\mu\nu}$ is zero as well.

Further integration can be performed for the spherically-symmetrical problem. As a result, we can obtain a simple system of two first-order equations [3, 5] looking like the 2D Chaplygin gas dynamics (which is characterized by the absence of gradient catastrophe in the dimension 1+1 – here they are radius and time).

The problem for a plane longitudinal wave admits a complete analytical solution (two waves traveling in opposite directions). We now consider it in more detail.

Let us change the index numbering and start it with -1, i.e., the time coordinate is $t=x^{-1}$. We direct the plane wave along the coordinate $x=x^0$ (the extra dimension). The other spatial coordinates should be isotropic (a longitudinal wave), so the frame field can be represented as follows ($\mu,\nu,\ldots=(-1,0,1,2,3)$; $i,j=(1,2,3)$; only non-zero elements are shown):

$$h^a{}_\mu(t,x)=\begin{pmatrix} a & b & & \\ c & e & & \\ & & d\,\delta^{\boldsymbol{i}}_j & \end{pmatrix},\quad h_a{}^\mu=\frac{1}{\varkappa}\begin{pmatrix} e & -c & & \\ -b & a & & \\ & & \frac{\varkappa}{d}\delta^j_{\boldsymbol{i}} & \end{pmatrix};\ \varkappa=ae-bc,\ h=\varkappa d^3. \quad (22)$$

Values of scalar indexes are denoted by bold characters: $a,b=(\boldsymbol{-1},\boldsymbol{0},\boldsymbol{1},\boldsymbol{2},\boldsymbol{3})$.

This symmetry (22) leads to $S_{\mu\nu\lambda}=0$, and allows only component $f^{-1\,0}$ for $f^{\mu\nu}$ (others should vanish). So, the equations of f-field can be integrated (taking into account the requirement of localization, trivial boundary conditions; we use notations $\dot\omega\equiv\omega_{,t}=\omega_{,-1}$, $\omega'\equiv\omega_{,x}=\omega_{,0}$):

$$(hf^{\mu\nu})_{,\nu}=0;\ \text{i.e. } (hf^{0\,-1})^{\cdot}=0,\ (hf^{-1\,0})'=0;\ \text{ so } f^{-1\,0}=0.$$

Hence $f_{\mu\nu}=0$, and we can introduce a scalar field $\psi(t,x)$ (responsible for the longitudinal polarization) as follows: $\Phi_\mu=\psi_{,\mu}/\psi$.

Now the exceptional equation (15) can be rewritten in a more compact and convenient form (for following integrations; similar to $f^{\mu i}$, $L_a{}^{\mu i}=0$)

$$\mathbf{EE}^{*\mu}_{\boldsymbol{a}}:\ \left(h\psi^{-1/3}L_{\boldsymbol{a}}{}^{\mu\nu}\right)_{,\nu}=0;\ \mathbf{EE}^{*}_{\boldsymbol{-1}}{}^{\mu}:\ \left(h\psi^{-1/3}L_{\boldsymbol{-1}}{}^{0\,-1}\right)^{\cdot}=0=\left(h\psi^{-1/3}L_{\boldsymbol{-1}}{}^{-10}\right)'; \quad (23)$$

$$\mathbf{EE}^{*\mu}_{\boldsymbol{0}}:\ \left(h\psi^{-1/3}L_{\boldsymbol{0}}{}^{0\,-1}\right)^{\cdot}=0=\left(h\psi^{-1/3}L_{\boldsymbol{0}}{}^{-10}\right)';\ \text{ hence } L_{\boldsymbol{0}}{}^{-10}=0=L^{\boldsymbol{0}}{}_{-10}=L^{\boldsymbol{-1}}{}_{-10}\,. \quad (24)$$

Two last equations can be also integrated (they admit the form of a conservation law and we introduce scalar fields τ and χ), see (15):

$$L^{\boldsymbol{-1}}{}_{-10}=0=a'-\dot b-\frac{1}{3}(a\psi'-b\dot\psi)/\psi;\quad (\psi^{-1/3}b)^{\cdot}=(\psi^{-1/3}a)'; \quad (25)$$

$$L^{\boldsymbol{0}}{}_{-10}=0=c'-\dot e-\frac{1}{3}(c\psi'-e\dot\psi)/\psi;\quad (\psi^{-1/3}e)^{\cdot}=(\psi^{-1/3}c)'; \quad (26)$$

$$\dot\tau=\psi^{-1/3}a,\ \tau'=\psi^{-1/3}b;\quad \dot\chi=\psi^{-1/3}c,\ \chi'=\psi^{-1/3}e. \quad (27)$$

Compatibility of equations for τ and χ in (27) is ensured by the conservation laws in (25) and (26) respectively. Now let us use these scalars as the new time and distance (i.e., we fix the coordinate freedom):

$$t = \tau,\ x = \chi\ \Rightarrow \psi^{-1/3}a = 1 = \psi^{-1/3}e\ (a = e = \psi^{1/3}),\ b = 0 = c.$$

We obtain that $h^a{}_\mu$ (and metric) is diagonal. Now we write out the (nonzero) components of Λ tensor and then the vector $\Phi_\mu = \psi_{,\mu}/\psi$ ($a{=}e{=}\psi^{1/3}$):

$$\Lambda^{\mathbf{-1}}{}_{-10} = a',\ \Lambda^{\mathbf{0}}{}_{0\,-1} = \dot{e},\ \Lambda^{\boldsymbol{i}}{}_{j\,-1} = \dot{d}\,\delta^{\boldsymbol{i}}_j,\ \Lambda^{\boldsymbol{i}}{}_{j0} = d'\delta^{\boldsymbol{i}}_j\,.$$

$$\Phi_{-1} = \dot{e}/e + 3\dot{d}/d = \dot{\psi}/\psi,\ \Phi_0 = a'/a + 3d'/d = \psi'/\psi\ \Rightarrow ad^3 = \psi,\ d^3 = a^2. \quad (28)$$

We need the rest components of $a^3 L_a{}^{\mu\nu}$ ($h\psi^{-1/3}{=}a^3$) to place in $\delta^{\boldsymbol{i}}_j\,\mathbf{EE}^{*j}_{\boldsymbol{i}}$, see (23):

$$a^3\delta^{\boldsymbol{i}}_j L_{\boldsymbol{i}}{}^{j\,-1} = \dot{a}/d,\ a^3\delta^{\boldsymbol{i}}_j L_{\boldsymbol{i}}{}^{j0} = -a'/d\ \Rightarrow\ \ddot{u} - u'' = 0, \quad (29)$$

where $u = a^{1/3},\ a = u^3,\ d = u^2$. Thus, the problem is reduced to the simple second-order linear equation (29), the general solution of which has the obvious form (two waves running in the opposite directions)

$$u(t,x) = A(t-x) + B(t+x)\,,\quad \text{where } A, B \text{ – quite arbitrary functions.}$$

If such a plane wave captures other short waves (serving as a wave-guide with a variable refractive index) including the second class waves, the plane wave obtains a sort of mass.

The more difficult problem is a (quasi)stationary plane longitudinal wave fill with ensembles of tangential waves belonging to different classes whose evolution would be of interest.

An even more difficult problem (but more realistic) is a longitudinal spherical wave with a filling, which, having also acquired an "effective mass", must move at a speed some lower than the speed of light.

3.2. Evolution of expanding Universe-on-the-Brane and quasi-particles

The growth of unstable polarizations (class zero) leads to appearance of strong non-linearities. Non-linear localised h-field configurations can carry digital information – topological charges and (for symmetrical configurations) quasi-charges.

One can deform $g_{\mu\nu} \to \eta_{\mu\nu}$, and, hence, $h^a{}_\mu \to s^a{}_\mu \in \mathrm{SO}(1,4)$; the topological charge group is an Abelian group under addition; it relates to the next absolute homotopy group [3, 9]:

$$\pi_4(\mathrm{SO}(1,4)) = \pi_4(\mathrm{SO}_4) = Z_2 + Z_2\ [= \Pi(1)]. \quad (30)$$

Under reflection of one or three space coordinates, P_1 or P_3, these two "fermion particles" (left and right) change one another.

The symmetry of cosmological background (in a co-moving system): $\mathrm{Sym}_0 = \mathrm{O}_3 \times \mathrm{P}_4$; *white* particles correspond to symmetries $\mathrm{Sym} \subset \mathrm{Sym}_0$, e.g. $\Pi(\mathrm{SO}_2) = Z+Z$. One should note that $\Pi(\mathrm{SO}_3) = 0$ – perhaps this means that elementary spin zero (or scalar) particles are absent. Discrete symmetries P_2 (reflection of two coordinates) can be added to rotations SO_2 in different ways [3, 9].

For simple symmetries, quasi-charge groups $\Pi(Sym)$ are reduced to relative (or diad) homotopy groups (see for example [24]); for "complex" symmetries, more general k-ad homotopy groups are necessary [3].

For *color* quasi-particles (which can exist only in very specific conditions of a hadron bag), the group SO_2 should be replaced with either self-dual or anti-self-dual one-parameter group, $\mathrm{SO}_2^+/\mathrm{SO}_2^-$, — it doubles in a sense the number of elementary color quasi-particles with respect to the white ones.

One can analyze the parameters of symmetrical framed 1-manifolds (similar to the approach of [25]) and select degenerate (spin/color) or non-degenerate prefered parameters (flavors) [3, 9].

A QM-like 4D-phenomenology emerges through averaging along the huge extra-dimension, along the length L, the width of large-scale O_4-wave in co-moving coordinates. Note, two thin lines in a 4d-space have tiny chances to intersect in a single approach.

We need auxiliary 4D-fields (quantised avatar-fields) for phenomenological description of topological (quasi)particles prone to interact; but the complete description is five-dimensional, not four!

Particles are not poker, you cannot declare them whenever you want!

It is argued that the phenomenology of quantum field theory unambiguously follows from a number of understandable principles, causality, Lorentz covariance (spin-statistics), et cet., plus one incomprehensible – the principle of superposition. In our world view, this follows as a result of averaging over the large extra dimension, taking into account the fact that weighty f-waves (interacting with which and scattering, quasi-particles acquire D-momentum) move almost tangentially in this relativistic waveguide, the Brane.

The energy associated with q-particles (topological quasi-particles) is apparently very small compared to the whole energy of ensemble of stochastic f-waves (perhaps this energy can be partly associated with the zero-point vibrations). Perhaps, the 4D GR Lagrangian for q-particles can arise as an approximation (at least for distances $x < L$) and averaging over the Brane thickness L – from the Lagrangian (20):

$$\mathcal{L}_{(\mathrm{GR})} \sim q\,R + \frac{1}{9} f^2_{\mu\nu}(\text{q-particles}) + R^2_{\mu\nu}(\text{q-particles}) + \cdots ;$$

here q represents the scalar curvature (averaged over the Brane thickness) of the cosmological (large scale, i.e. the Brane) solution; besides L it depends on the amplitude Δh of the spherical wave, $q \sim (\Delta h)^2/L^2$.

4. Cosmological 5D model – relativistically expanding Brane

We consider a model of shallow (and thick – in co-moving system) cosmological waveguide in which weak waves (from the first to the third classes), including those carrying energy, move almost tangentially (the retention angle is very small and some decrease in the velocity of waves held in the waveguide is also very small, $1-v \ll 1$). In these conditions, which differ little from Minkowski's space, it is natural to use methods of special relativity. The expansion rate of this spherical Brane (a sphere S^3 of some thickness), V, should also be slightly less than the maximum, $1-V \ll 1$, because the Brane holds the energy-carrying waves.

4.1. Massive bodies in the expanding Brane (Lagrangian description)

Let us describe the motion of a mass m in the relativistically expanding Brane using the simple relativistic Lagrangian ($c=1=\hbar$; $|t\dot{\varphi}|<1$)

$$\mathcal{L}\,dT = -m\sqrt{1-V^2-V^2T^2(d\phi/dT)^2}\,dT = -m\sqrt{1-t^2\dot{\varphi}^2}\,dt = \mathcal{L}(\dot{\varphi},t)\,dt\,, \quad (31)$$

where $\dot{\varphi}=d\varphi/dt$, $t=T/\Gamma$ ($\sim 1/H_0$) – time of observers-on-the-Brane ("at rest", i.e. the relic radiation is isotropic), $\varphi = V\Gamma\phi$ – the "stretched angle" on the cosmological sphere S^3, $\Gamma=1/\sqrt{1-V^2}$ – the Lorentz factor of the expanding Brane for the "central observer", the point O.

It turns out that the Brane radius VT_0 is much larger than the current time $t_0=1/H_0$ (by the factor Γ), and the curvature effects are negligibly small (even for the recombination era), because the angle ϕ is very small, $\phi \sim \Gamma^{-1}\ln(1+z)$. It is convenient to use the stretched angle φ and local time t. Later we will move from angular coordinates to usual ones, $x=t\varphi$, $\dot{x}=t\dot{\varphi}+x$.

We can find the exact solution for free motion. The momentum of an object with velocity $v_*=t_*\dot{\varphi}_*$ (relative to the local resting observer) at the moment t_*, $p_*=m\gamma_* v_*$, decreases (almost according to Aristotle; centrifugal force performs a work and accelerates the Brane, gravity slows it down):

$$\left(\partial\mathcal{L}/\partial\dot{\phi}\right)^{\cdot}=0,\ \text{so}\ t^2\dot{\varphi}/\sqrt{1-t^2\dot{\varphi}^2}=C\ (=\text{const}=pt/m)\,;\ p(t)=p_*t_*/t\,; \quad (32)$$

$$t\dot{\varphi}=C/\sqrt{C^2+t^2},\ \varphi(t)=\int_{t_*}^{t}\frac{C}{\sqrt{C^2+t^2}}\frac{dt}{t}\,;\ C=t_*^2\dot{\varphi}_*/\sqrt{1-t_*^2\dot{\varphi}_*{}^2}\,.$$

We can further integrate and find $\varphi(t)$ using substitution $x^2=C^2+t^2$:

$$\exp[2(\varphi-\varphi_*)]=\frac{1+t_*\dot{\varphi}_*}{1-t_*\dot{\varphi}_*}\frac{\sqrt{C^2+t^2}-C}{\sqrt{C^2+t^2}+C};$$

the maximum "extended angle" of the object displacement is ($|t_*\dot{\varphi}_*|<1$)

$$\varphi(\infty)-\varphi_*=\frac{1}{2}\ln\frac{1+t_*\dot{\varphi}_*}{1-t_*\dot{\varphi}_*}. \quad (33)$$

For massless photons the equation of motion is very simple, $t\dot{\varphi}=1$ (the velocity outside the waveguide is slightly higher), i.e. $[\varphi_*=\varphi(t_*)]$

$$\varphi(t)-\varphi_*=\ln t/t_*\,[=\ln(1+z)];$$

hence it follows the next simple Hubble diagram [10] (without curvature corrections):

$$\mu(z)=\mu_0+5\log[(1+z)\,\ln(1+z)]\,,\quad \text{where } \mu_0=-5\log(H_0 d_\star/c),\ d_\star=10\,\text{pc}\,. \tag{34}$$

When switching to coordinates $x=t\varphi$, $t\dot{\varphi}=\dot{x}-x/t$, see (31), the Lagrangian expansion into series shows that the first corrections (depending on t or $H=1/t$) form a complete derivative (so they do not work), and the dependence on t or the Hubble parameter starts with a higher order correction:

$$\mathcal{L}/m=-\sqrt{1-(\dot{x}-x/t)^2}\approx -1+\dot{x}^2/2-\dot{(x^2/t)}/2+\dot{x}^4/8-t^{-1}\dot{x}^3x/2+\cdots\,. \tag{35}$$

The orbital motion in the Solar system is quite slow (the Earth velocity is about 30 km/s, i.e. $\dot{x}\sim 10^{-4}$). However, there is still a general movement of the Solar system relative to the background of relic radiation – with the speed $v_\odot\approx 369$ km/s, see [21]. This factor can increase the effects depending on the Hubble parameter.

S-stars orbiting the very massive object Sgr-A* (supermassive "black hole") in the center of our Galaxy are moving much faster – up to $\dot{x}\sim 0.05$ or so, [22, 23].

If the body mass m depends on time (e.g. the Earth mass), the situation changes significantly – a term linear in the Hubble parameter appears, which contributes to secular growth of the Astronomical Unit:

$$\mathcal{L}+m(t)+\dot{(m\,x^2/t)}/2\approx m\dot{x}^2/2+H_0\dot{m}x^2/2+\cdots\,. \tag{36}$$

The orbital motion of bodies of variable mass has been considered for a long time, see the review [26] and references therein (see also [27]). The perturbation of Earth's orbit depends on the term $(\dot{M}_\odot+\dot{M}_\oplus)/(M_\odot+M_\oplus)$ [26].

An increase in the Earth mass about (see Figure 2) $\dot{M}_\oplus/M_\oplus\sim 10^{-8}$/yr, taking into account $M_\oplus$ and $M_\odot$, only reduces (quite significantly) the effect of decreasing Sun mass which is estimated as $\dot{M}_\odot/M_\odot\sim -9\times 10^{-14}$/yr [27].

4.2. Non-linear perturbations leave the Brane

It can be assumed that during powerful cataclysms with an incomprehensible release of energy (including Big Bang, and maybe some Small Bangs), new particles are generated, which can be supplemented by the output of nonlinear perturbations (with topological (quasi)charge, but without energy!) from the Brane.

Those perturbations that came out inside the Brane, should later cross it again, see Figure 1, causing symmetry violations (C/CP, translational symmetry along the extra dimension) and, consequently, breaking conservation laws (which are related to symmetries). If the coming perturbations interact with the Brane's quasi-particles, then some transformations of quasi-particles and generation of new ones are possible.

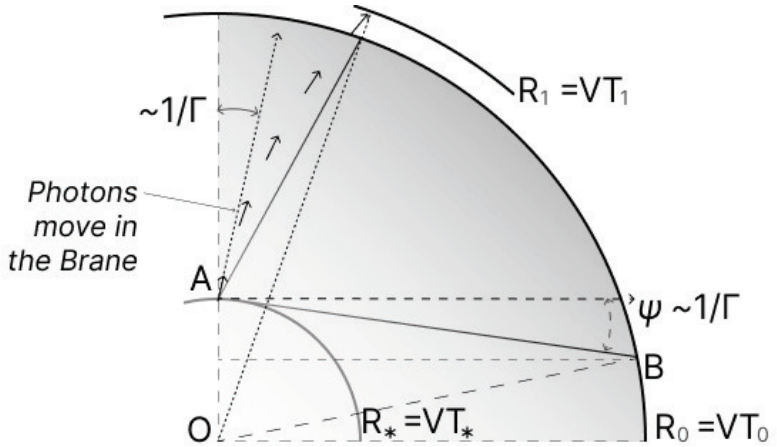

Figure 1: Extra-Brane perturbations move from A ($R_*=VT_*$) to B ($R_0=VT_0$).

The positive values of the angle ψ (see Figure 1) are limited due to the Doppler effect, $\psi \lesssim 1/\Gamma \ll 1$. Neglecting ψ, we can write the next simple equation:

$$\mathrm{AB}^2 = \mathrm{OB}^2 - \mathrm{OA}^2, \text{ or } (T_0 - T_*)^2 = V^2(T_0^2 - T_*^2).$$

Given $T_0/T_* = 1+z$, we find z for the most distant (much beyond the horizon) disturbances: $z \approx 2V^2\Gamma^2$.

The capture of nonlinear extra-Brane perturbations can produce LENR (low energy nuclear reactions) effects [12, 13, 14, 15], including the cosmological growth of the Earth [16, 17]. The ocean crust is relatively young, no older than 200 million years, see Figure 2; it grows mostly in the rift valleys of the mid-oceanic ridges

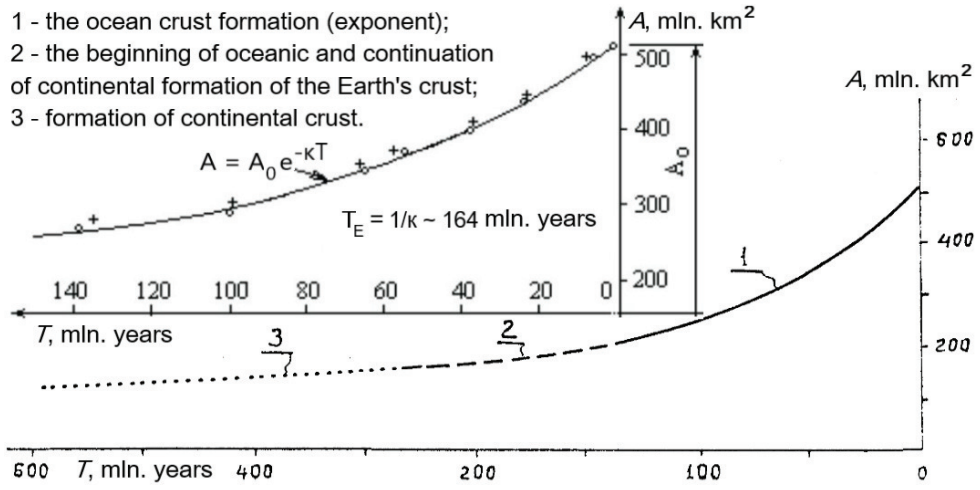

Figure 2: The main geological regularity (growth of Earth's crust) [16].

(their longitudinal growth originates due to numerous transverse/transform rifts). No sites of oceanic crust sinking under continents (subduction hypothesis) have been found [16, 17]. The Earth expansion is also indicated by the shape of paleo-tropics – a narrower band shifted to the north (oceans grow more in the southern hemisphere) [16]. The increase in Earth mass and gravity, g, is indicated by a decrease in the symmetry of younger minerals [16], and by gigantism of some dinosaurs, insects, plants (grasses) of Mesocainozoic.

In August 2023, geological hydrogen was added to the Register of Minerals (Russia). Hydrogen degassing (especially pronounced in the area of oceanic rifts, near Antarctica) destroys ozone and forms silvery clouds (height ~ 80 km, water vapor does not rise here); there are families of bacteria that feed on hydrogen. As V.N. Larin noted [17], the release of hydrogen turns the Earth into an open system, where disorder decreases and new minerals and deposits continue to form. This is even more so if new hydrogen is being formed inside the Earth (and our entire Universe-on-the-Brane turns out to be an open, evolving system where the prospects of heat death are not so relevant).

References

[1] Einstein, A., Mayer, W.: Systematische Untersuchung über kompatible Feldgleichungen, welche in einem Riemannschen Raume mit Fernparallelismus gesetzt werden können. Sitzungsber. preuss. Akad. Wiss. **K1** (1931), 257–265.

[2] Delphenich, D. H.: Selected Papers on Teleparallelism (2013; translated and edited by D. H. Delphenich).

[3] Zhogin, I.L.: *Old and new research on the Absolute Parallelism theory.* Lambert Academic Publishing, 2010. ISBN 978-3-8383-8876-2. arXiv: gr-qc/0412130.

[4] Zhogin, I.: Absolute Parallelism, modified gravity, and suppression of gravitational short waves. Proc. PIRT-2011. Moscow: BMSTU (2012), 337–346; arXiv: gr-qc/1109.1679.

[5] Zhogin, I.: Absolute Parallelism: Spherical Symmetry and Singularities. Sov. Phys. J. **34** (1992), 781; arXiv: gr-qc/0412081v3.

[6] Pommaret, J. F.: *Systems of Partial Differential Equations and Lie Pseudogroups*, Gordon and Breach, New York, 1978.

[7] Chae, K.-H.: Breakdown of the Newton–Einstein Standard Gravity at Low Acceleration in Internal Dynamics of Wide Binary Stars. ApJ **952** (2023), 128; arXiv: 2305.04613.

[8] Zhogin, I.: Extragalactic TeV photons and the zero-point vibration spectrum limit. Space, Time and Fundamental Interactions. No 3–4 (2023), 327–332; arXiv: 2308.01321.

[9] Zhogin, I.: *Topological charges and quasi-charges in Absolute Parallelism.* Preprint arXiv: gr-qc/0610076 (2006).

[10] Zhogin, I.: *One more fitting (D=5) of SNeIa redshifts.* Preprint arXiv: 0902.4513v3 (2009/2022).

[11] Melia, F., Shevchuk, A.: The $R_h = ct$ universe. Monthly Notices of the Royal Astronomical Society **419** Issue 3 (2012), 2579; arXiv:1109.5189 [astro-ph.CO].

[12] Urutskoev, L.I., Filippov, D.V., Birykov A.O. et al. The Study of Possibility of Initiating Tungsten Alpha Decay Using Electric Explosion. Applied Physics and Mathematics, No 1 (2017), 3–27 (in Russian); urleon.ru/files/article_65.

[13] Wendt, G.L., Irion, C.E.: Experimental attempts to decompose tungsten at high temperatures. Amer. Chem. Soc. **44** (1922), 1887; urleon.ru/files/lenr_1.pdf.

[14] Storms, E.: Status of cold fusion (2010). Naturwiss. **97** (2010), 861–881; lenr-canr.org - StormsEstatusofcoa.pdf.

[15] Storms, E.: *Cold Fusion Explained.* (2024).
Preprint lenr-canr.org - StormsEcoldfusioni.pdf.

[16] Blinov, V.F.: *The Growing Earth: from planets to stars.* Kyiv, 2011 (in Russian); DeepOil.ru - item178, doi: 10.13140/RG.2.2.27702.51525.

[17] Larin, V.N.: *Our Earth.* M.: Agar, 2005 (in Russian); DeepOil.ru - item55, doi: 10.13140/RG.2.2.27702.51525.

[18] Zhogin, I.L.: Trilinear generally covariant equations. Soviet Phys. J. **34**:2 (1991), 105–110; arxiv:gr-qc/0203008.

[19] Zhogin, I.L.: *On relevance of modified gravities.* Preprint arXiv: 0812.1344 [gr-qc] (2008); see also arXiv: 0704.0857 [gr-qc] (2007).

[20] Valageas, P., Schaeffer, R.: The mass and luminosity functions of galaxies and their evolution. Astron. Astrophys. **345** (1999), 329; arXiv: astro-ph/9812213.

[21] Planck Collaboration: Akrami, Y., Arroja, F., Ashdown, M., Aumont, J., Baccigalupi, C., et al.: Planck 2018 results. I. Overview and the cosmological legacy of *Planck*. Astron. Astrophys. **641** A1 (2020), 56; arXiv: 1807.06205 [astro-ph.CO].

[22] Gillessen, S. et al.: An Update on Monitoring Stellar Orbits in the Galactic Center. Astrophys. J. **837** (2017), 30; arXiv: 1611.09144 [astro-ph.GA].

[23] Lu, J. R. et al: Stellar Populations in the Central 0.5 pc of the Galaxy II: The Initial Mass Function. Astrophys. J. **764** (2013), 155; arXiv: 1301.0540 [astro-ph.SR].

[24] Dubrovin, B.A., Novikov, S.P., Fomenko, A.T.: *Modern Geometry. Methods and Applications. Part 1.* Springer-Verlag, GTM 93, 1984.

[25] Pontryagin, L.S.: Smooth Manifolds and Their Applications to Homotopy Theory. Am. Math. Soc. Trans. Ser. 2 **11** (1959), 1–114; [2d/3rd ed., M.: Nauka, 1976/1985 (Russian)].

[26] Veras, D.: Post-main-sequence planetary system evolution. R. Soc. Open Sci. **3** (2016), 150571; DOI: 10.1098/rsos.150571.

[27] Iorio, L.: Orbital effects of Sun's mass loss and the Earth's fate. Nat. Sci. **2** (2010), 329–337; arXiv: gr-qc/0511138v2.

Conference *Cosmology on Small Scales 2024*
Michal Křížek and Yurii Dumin (Eds.)
Institute of Mathematics CAS, Prague

A FEW CRITICAL REMARKS ON THE SPECIAL THEORY OF RELATIVITY

Michal Křížek
Institute of Mathematics, Czech Academy of Sciences
Žitná 25, 115 67 Prague 1, Czech Republic
e-mail: krizek@math.cas.cz

Abstract: According to the special theory of relativity (STR), time passes more slowly in uniformly moving inertial frames than at rest. This phenomenon is called time dilation and it based on Einstein's principle of relativity. We show why this principle does not apply in the real physical universe. Then we illustrate why the Hafele-Keating experiment for testing the validity of STR is questionable. We finish with several other critical remarks on STR.

Keywords: Lorentz transformation, inertial systems, time dilatation, length contraction, clock paradox

PACS: 03.30.+p

1. Introduction

According to Newton's first law of inertia, a body is at rest or in a uniform rectilinear motion unless acted upon by an external force. This basic principle is used to introduce the so-called inertial frames in special relativity (STR).

Consider a fixed coordinate frame (system) S with orthogonal x, y, z axes, in which there is a stationary system of hypothetical synchronized clocks that define the time coordinate t. Let S' be a system with orthogonal x', y', z' axes that are parallel to x, y, z and at rest all axes have the same scale. The time t' is introduced in S' in a similar way to S by a system of synchronized clocks in S'. Let the origin of the system S' move along the x-axis at a constant speed $v \in (-c, c)$, where c is the speed of light in vacuum. Thus, the systems S and S' move in a uniform rectilinear motion relative to each other and we will call them *inertial* (see Figure 1).

STR is based on two basic postulates (assumptions) that Albert Einstein [10, p. 895] thought were a good description of reality:

P1. The laws of nature have the same mathematical expression in all inertial systems.

P2. The speed of light c is the same in all inertial systems.

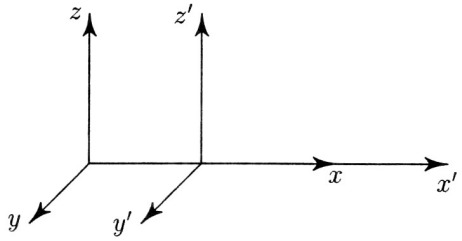

Figure 1: The inertial system S' is moving with velocity $v \in (-c, c)$ relative to the system S.

Let the instant when the origin of the systems S and S' pass each other define the beginning of the countdown of time, i.e., $t = 0$ in S and $t' = 0$ in S'. From here Einstein derived (see [10, p. 902]) that

$$\begin{aligned} x' &= \gamma(x - vt), && (1)\\ y' &= y,\\ z' &= z,\\ t' &= \gamma\Big(t - \frac{vx}{c^2}\Big), && (2) \end{aligned}$$

where $x, y, z, t \in (-\infty, \infty)$ and

$$\gamma = \frac{1}{\sqrt{1 - \frac{v^2}{c^2}}} \geq 1. \tag{3}$$

The relations (1)–(2) are called the *Lorentz transformation*. The inverse Lorentz transformation is of the form (see e.g. [18])

$$x = \gamma(x' + vt'), \tag{4}$$

$$t = \gamma\Big(t' + \frac{vx'}{c^2}\Big). \tag{5}$$

To see this, we multiply (2) and (5) by c and set $\beta = v/c$. Then omitting $y = y'$ and $z = z'$, we get by (1)–(5) that

$$\begin{pmatrix} \gamma & -\beta\gamma \\ -\beta\gamma & \gamma \end{pmatrix} \begin{pmatrix} \gamma & \beta\gamma \\ \beta\gamma & \gamma \end{pmatrix} = \begin{pmatrix} \gamma^2 - \beta^2\gamma^2 & 0 \\ 0 & \gamma^2 - \beta^2\gamma^2 \end{pmatrix} = \begin{pmatrix} 1 & 0 \\ 0 & 1 \end{pmatrix},$$

where the reciprocal value of γ fulfills the equation for the unit circle

$$\beta^2 + (1/\gamma)^2 = 1.$$

Hence, the composition of the Lorentz transformation with its inverse yields the unit matrix.

From (5) for $x' = 0$ we can easily derive the well-known formula for *time dilation*

$$\Delta t' = \gamma^{-1} \Delta t, \tag{6}$$

where Δt and $\Delta t'$ are the corresponding intervals of proper (elapsed) time in the systems S and S', respectively. Thus, according to (5), the clock ticks fastest at rest.

2. The principle of relativity does not hold for relativistic velocities

Einstein derived the Lorentz transformation (1)–(2) from the assumptions P1 and P2, which are unfortunately questionable. For example, a fast-moving traveler will see the spectrum of galaxies on one half of the celestial sphere shifted to blue colors and on the opposite half to red colors, i.e., the principle of relativity P1 does not hold in the physical universe. This is not a null hypothesis, because it can be easily verified e.g. by observing the spectral line Hα in all directions. By P1, all inertial systems should be indistinguishable, i.e. equivalent. Another counterexample is the ubiquitous cosmic microwave background radiation (CMB). The Sun is moving with respect to the CMB at 370 km/s. A third such system can be associated with intergalactic gas (or dust) between galaxies. Thus, there exist several prefered reference system.

Of course, Einstein could not have known in 1905 about the existence of other galaxies, which were only confirmed in the 1920s. However, he could have guessed that a fast-moving traveler in the Milky Way would see the spectrum of stars in one half of the celestial sphere shifted to blue colors and in the other half to red colors, as immediately apparent from the Doppler effect which was well known in 1905, see [10, p. 910]. Hence, we can find easily that the assumption P1 is not satisfied in the physical universe for any $v \geq 0.05c$. At such high velocities we would observe significant anisotropy.

Notice also that the Doppler effect is not included in the Lorentz transformation. However, in the real physical universe this effect cannot be eliminated in any case. We must not forget that STR is only a very simple mathematical model.

As for the assumption P2 of the constancy of the speed of light in all inertial frames, this is now bypassed by defining $c = 299\,792\,458$ km/s to be satisfied exactly. More precisely, one meter is defined as the length of the path traveled by light in vacuum during a time interval of $1/299\,792\,458$ of a second, where the second is defined by a hyperfine transition frequency of cesium.

3. Testing the validity of STR by the Hafele-Keating experiment

The Hafele-Keating experiment [12, 13] with two portable cesium atomic clocks (eastward and westward) in commercial airplanes and one on the Earth is not too credible, since none of the corresponding three systems was inertial. The reason is that the Earth rotates and orbits the Sun which produces centrifugal forces.

Moreover, since the speed of airplanes is $v \sim 10^{-6}c$, by (3) we obtain

$$\gamma \cong \frac{1}{\sqrt{1-10^{-12}}} \cong \frac{1}{0.999\,999\,999\,9995} \cong 1 + 5 \cdot 10^{-13}.$$

There are $24 \cdot 3600 = 86\,400$ seconds per day. The pure total travel time lasted about 2 days and we set $\Delta t = 2 \cdot 86\,400 = 172\,800$ s. Therefore by (5), the time delay should be approximately

$$\Delta t - \Delta t' = \Big(1 - \frac{1}{\gamma}\Big)\Delta t \cong (\gamma - 1)\Delta t = 5 \cdot 10^{-13} \cdot 172\,800 = 86.4 \cdot 10^{-9} \text{ s}$$

provided airplanes were to be in inertial systems. Unfortunately, the corresponding zigzag trajectory is not specified in [12] and thus, this experiment cannot be independently verified.

The predicted calculated delay (including the gravitational redshift) was 40 ns during the eastward trip and 275 ns during the westward trip, see [12]. The observed delay was 59 ns and 273 ns, respectively, see [13]. However, vibrations of airplanes producing non-negligible accelerations and several other effects were not taken into account, too.

Another well-known experiment by Michelson and Morley [17] for testing the validity of STR was performed in air[1] and with a fixed distance between the light source and the interferometric detector. So their proof of the non-existence of the ether is not very credible as well (see [24, 26]) even though some papers claim opposite (see [25]). It seems that experiments with relativistic cosmic muons (see [11]) are also no so precise as STR would require.

4. The clock paradox

Now we will revisit the well-known clock paradox (called also the twin paradox in popular relativistic literature), because there are still many misunderstandings about it. For simplicity, we choose

$$v = 0.8c$$

so that anyone can recalculate the whole example for this particular value of velocity. Then by (5)

$$\gamma = \frac{1}{\sqrt{1-0.64}} = \frac{1}{0.6} = \frac{5}{3}. \tag{7}$$

Consider now spacetime travelers Adam and Bob (they do not have to be twins or brothers). Assume that Adam is always at the origin of the stationary system S far from all gravitational sources and that Bob flies at velocity v to a star 4 light years away, i.e., Bob will be at the origin of the system S' for the entire duration of his flight.

[1]The speed of light essentially depends on the environment in which the light is moving.

To avoid non-zero accelerations at Bob's launch, we will assume that Bob just flies past Adam at a constant velocity v and at the moment of meeting at the origin O, they reset their clocks to $t = t' = 0$. After $\Delta t = 5$ years of Adam's proper time, Bob will be at a distance of $\Delta x = v\Delta t = 4$ light years, and according to relations (6) and (7), Bob's clock will show only $\Delta t' = \frac{3}{5}\cdot 5 = 3$ years. At the target star, Bob again just passes the information about his proper time to another traveler Charles who is flying from Bob towards Adam in the opposite direction at a constant velocity $(-v)$ in S. I.e. Charles will be at the origin $x'' = 0$ of the third system S'' all the way to Adam. From the relation $\Delta t'' = \gamma^{-1}\Delta t$ (cf. (6)) we easily find that at the time of Charles' meeting with Adam, Charles' clock will counter-intuitively show only $3 + 3 = 6$ years, while Adam's clock will show $2\Delta t = 10$ years, see Figure 2. This is called the *clock paradox*. We denote the event when Adam's clock will show 10 years by the symbol A. The event when Bob gives Charles information about the length of his flight is denoted by B, see Figure 2. The whole situation is symmetric with respect to the horizontal line passing through point B.

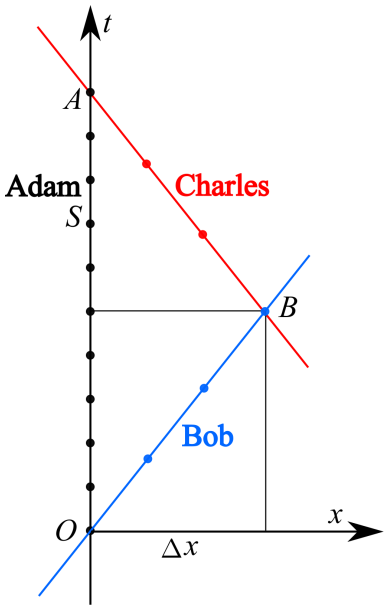

Figure 2: Worldlines of Adam, Bob and Charles from the view of the S system for $c = 1$ (light year)/year. In this case, the angle AOB is less than 45°. One-year clock ticks of proper time (i.e., special exceptional events) are marked with bullets on the individual worldlines.

Now let us look at the whole situation from the point of view of Bob, who is at rest at the origin of the system S'. Again, we will assume the validity of the time dilation formula, but the systems S and S' just switch their roles. It is often claimed that this situation is symmetric. However, this is not true, since the star is fixed in S, while in S' it moves. Bob's clock at the target star will also show only 3 years,

because the star 4 light years away was approaching him at a speed of 0.8c and we must take into account the well-known relation

$$\Delta x' = \gamma^{-1}\Delta x \tag{8}$$

for *length contraction* which follows from (4). In particular,

$$\Delta x' = \frac{3}{5}\cdot 4 = \frac{12}{5} = 2.4 = 0.8 + 0.8 + 0.8 \quad \text{light years.}$$

Therefore, Bob tells to the passing Charles that his clock shows 3 years.

From Einstein's relation for composition of relativistic velocities [10, p. 905] it can be deduced that Charles will have a velocity

$$w = -\frac{2v}{1+\frac{4}{5}\cdot\frac{4}{5}} = -\frac{1.6c}{\frac{41}{25}} = -\frac{40}{41}c$$

in the system S'. His worldline is therefore given by the line

$$t' = -\frac{41}{40}x' + 3.$$

The sides of the triangle AOB in the systems S and S' are formed two same triples $(10, 3, 3)$ considered in proper years.

Finally, let us show that the angle of the line AB with the t' axis is less than 45° in Figure 3 for $c = 1$ (light year)/year. The distances between the dots on Adam's and Bob's worldlines are just swapped in Figures 2 and 3. Thus, the event A in S' has a horizontal spatial coordinate of $x'_A = -\frac{40}{3} = 13.\overline{333}$ light years, which can be easily found from the ratio $x'_A/(-4) = 10/3$, see Figure 3. Substituting x'_A to Adam's world line

$$t' = -\frac{5}{4}x',$$

for the vertical time coordinate of the event A we get

$$t'_A = \frac{50}{3} = 3 + 13.\overline{666} = 16.\overline{666} \quad \text{years.}$$

Hence, the angle between the straight line segment AB with the t' axis is less than 45°.

Apparently, a similar argument can be made for infinitely many velocities $v \neq 0.8c$. For this, it is enough to consider only three clocks located in the inertial systems S, S' and S'', i.e., we do not need any synchronization of all clocks in any of these systems.

In [16], we assume that Adam stays at rest on Earth feeling a constant acceleration g. Bob flies in a rocket and feels the same acceleration g along the axis x. His world line is hyperbolic intersecting Adam's world line twice. Using time dilation and the clock paradox, we prove that Bob's clock runs slower than Adam's clock. This contradicts Einstein's equivalence principle. Hence, the principle of relativity is not consistent with the equivalence principle, since STR predicts time dilation.

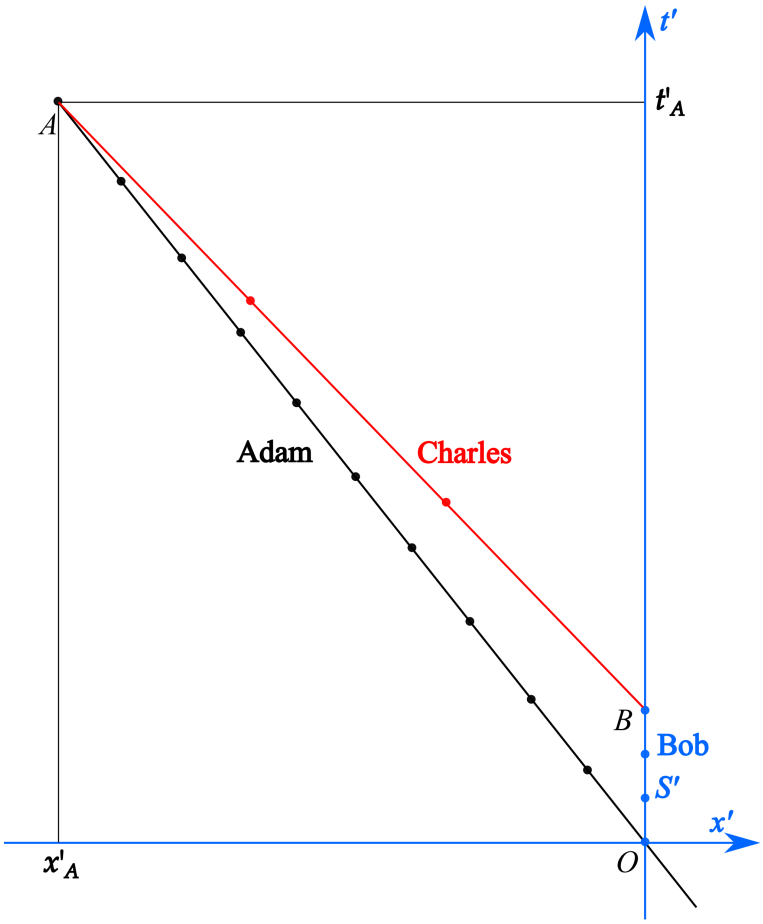

Figure 3: Worldlines of Adam, Bob and Charles from the view of the system S' for $c = 1$ (light-year)/year. One-year clock ticks of proper time are again marked with bullets.

5. The reversed triangle inequality

The time lengths of the three straight lines segments between the events A, B, O satisfy the so-called *reversed triangle inequality*

$$OB + BA < OA, \tag{9}$$

see [19, p. 421]. These segments represent the unique longest path between particular events in S and S', respectively, see Figures 2 and 3. The proposed reversed triangular inequality (9) for time intervals in Figure 2 is of the form $3 + 3 < 10$.

From (1)–(2) we find that $(ct')^2 - (x')^2 = (ct)^2 - x^2$. Hence, this difference is thus invariant with respect to the Lorentz transformation.

By time dilation and the reversed triangle inequality we obtain, in fact, a very counter-intuitive statement which is a basic property of STR: *"The longer the composite world line of Bob and Charles, the less proper flight time they need,"* see rows 3 and 4 of the next table:

$\beta = v/c$	0	0.6	0.8	0.917	0.980	0.995
γ	1	5/4	5/3	5/2	5	10
total travel time [yr]	10	8	6	4	2	1
maximum distance [ly]	0	3	4	4.583	4.899	4.975

Is this really true in the physical universe?

6. Concluding remarks

As far as we know, there are no scholarly articles that criticize number theory, group theory, graph theory, probability theory, matrix theory, etc. On the other hand, there are dozens of papers criticizing STR (see e.g. [1, 2, 3, 4, 5, 6, 7, 8, 9, 15, 20, 21, 22, 23, 27]) and many researchers do not accept various paradoxical phenomena proposed by STR. How is it possible? The main reason is probably that the current mainstream relativistic community is not willing to admit that Einstein's assumptions P1 and P2 could have some problems. Einstein himself did not perform any physical experiments with STR, but restricted himself only to theoretical speculations which have nothing to do with reality, see Section 2. Moreover, he stated: *No amount of experimentation can ever prove me right, a single experiment can prove me wrong.*

The STR resembles the situation of article with the title *Lemma* 1, see [14], which can be characterized as follows:

Assume that Lemma 1 *implies Lemma* 2*, from which we further derive Lemma* 3*. These auxiliary results lead to a new fascinating and beautiful theory*[2] *such as the STR. But after some time we find that Lemma 1 is wrong, and therefore the theory need not describe reality well.*

In contemporary special theory of relativity such a hypothesis as Lemma 1 is the statement that the **principle of relativity P1** describes the physical universe very well. This hidden wrong assumption is considered to be obvious. However, from Section 2 we know that P1 obviously does not hold for **relativistic velocities** $v \geq 0.05c$. The postulate P1 is at the very beginning of Einstein's 1905 paper [10]. This error permeates the whole theory of relativity for more than one century, because STR is also the basis of general relativity.

Acknowledgments. The author is indebted to Jan Brandts and Václav Vavryčuk for useful suggestions and to Hana Bílková for drawing all figures. Supported by the Czech Academy of Sciences (RVO 67985840) and the Czech Science Foundation (Grant no. 24-10586S).

[2]For example, the Lorentz transformation (1)–(2) does not allow superluminal velocities. Another beautiful statement states that the Lorentz transformations form an Abelian group for all $v \in (-c, c)$, see [15, p. 26] for the proof.

References

[1] Ashby, N.: Relativity in the Global Positioning System, Living Rev. Relativity 6, Article no. 1, 42 pp. (2003).

[2] Boughn, S. P.: The case of the identically accelerated twins, Am. J. Phys. 57 (1989), 791–793.

[3] Brown, W. S.: Is the Special Theory of Relativity wrong?: The underlying physics of the Lorentz transformation. Nature 219 (1968), 791–793.

[4] Debs, T. A., Redhead, M. L. G.: The twin "paradox" and the conventionality of simultaneity. Am. J. Phys. 64 (1996), 384–392.

[5] Dingle, H.: Relativity and space travel. Nature 177 (1956), 782–784.

[6] Dingle, H.: Special Theory of Relativity. Nature 195 (1962), 985–986.

[7] Dingle, H.: The case against special relativity. Nature 216 (1967), 119–122.

[8] Dingle, H.: Is the Special Theory right or wrong?: The case against the Special Theory of Relativity. Nature 217 (1968), 19–20.

[9] Dingle, H.: Science at the crossroad. Martin Brian & O'Keeffe, London, 1972.

[10] Einstein, A.: Zur Elektrodynamik bewegter Körper. Ann. der Phys. 322 (10) (1905), 891–921.

[11] Frisch, D. H., Smith, J. H.: Measurement of the relativistic time dilation using μ-mesons. Amer. J. Phys. 31 (1963), 342–355.

[12] Hafele, J. C., Keating, R. E.: Around-the-world atomic clocks: Predicted relativistic time gains. Science 177 (1972), 166–168.

[13] Hafele, J. C., Keating, R. E.: Around-the-world atomic clocks: Observed relativistic time gains. Science 177 (1972), 168–170.

[14] Königsdorf, H.: Lemma 1. In Meine ungehörigen Träume, Geschichten, Berlin, Aufbau-Verlag, Edition Neue Texte, 1978; also Pokroky Mat. Fyz. Astronom. 27 (1982), 101–106.

[15] Křížek, M., Somer, L.: Mathematical aspects of paradoxes in cosmology. Can mathematics explain the contemporary cosmological crisis? Springer, Cham, 2023.

[16] Křížek, M., Vavryčuk, V.: Twin paradox in accelerated systems and the Equivalence Principle. Submitted to J. Phys. Conf. Ser. in 2024, 1–9.

[17] Michelson, A. A., Morley, E. W.: On the relative motion of the Earth and the luminiferous ether. Amer. J. Sci. 34 (1887), 333–345.

[18] Pauli, W.: Theory of relativity. Dover Publ., Inc., New York, 1981.

[19] Penrose, R.: The road to reality. Vintage Books, London, 2005.

[20] Pesic, P.: Einstein and the twin paradox. Eur. J. Phys. 24 (2003), 585–590.

[21] Suntola, T.: The dynamic universe. Toward a unified picture of physical reality. Phys. Foundation Soc., The Finnish Soc. Natur. Phil., 2018.

[22] Theofilos, G.: Einstein's Special Theory of Relativity is absolutely wrong. Amer. Phys. Soc., New England Section Fall Meeting, November 10–11, 2000.

[23] Vavryčuk, V.: Cosmological consequences of the Lorentz and Doppler transformations. To appear in Mod. Phys. Lett. A (2024), 1–9.

[24] Wang, R., Zheng, Y., Yao, A., Langley, D.: Modified Sagnac experiment for measuring travel-time difference between counter-propagating light beams in a uniformly moving fiber. Phys. Lett. A 312 (2003), 7–10.

[25] Will, C. M.: The confrontation between General Relativity and experiment. Living Rev. Relativity 17 (2014), 4.

[26] Yuan, T.: Why the Michelson-Morley experiment cannot observe the movement of interference fringe. Preprint Beihang Univ., 2021, 1–11.

[27] Ziefle, R. G.: Einstein's bias blind spot: It is evident that the longitudinal Doppler effect contradicts the constancy of the velocity of light c in reference frames. Phys. Essays 35 (2022), 287–293.

Conference *Cosmology on Small Scales 2024*
Michal Křížek and Yurii Dumin (Eds.)
Institute of Mathematics CAS, Prague

COSMOLOGY AND REDSHIFT IN COSMIC DUST

Thomas Prevenslik†

QED Radiations
Berlin, Germany
thomas@nanoqed.org

Abstract: Based on the Planck law of quantum mechanics, cosmic dust cannot conserve galaxy light by a temperature increase because the quantum size of the dust requires the heat capacity of the constituent atoms to vanish. Conservation of galaxy light absorbed in dust therefore proceeds by the re-emission of galaxy light, but redshifted beyond that given by the actual recession redshift thereby overstating velocities to the extent that to hold the galaxies together dark matter is thought to exist. Because of the ubiquity of cosmic dust in the Universe all astronomical velocity measurements based on redshift are highly overstated, the consequences of which are of great importance in cosmology. Cosmic dust is shown to explain the at galaxy rotation curves of spiral galaxies without dark matter and negate an accelerating Universe based on redshift showing the fartherist known supernovae brighter than expected. Recently, the discovery of the transparent Ghost galaxy absent cosmic dust showing a falling rotation curve and the absence of dark matter affirms cosmic dust, and not dark matter is the source of the long-standing at rotation curves.

Keywords: cosmology, dark matter, cosmic dust redshift

PACS: 98.80.Bp, 98.80.Es, 98.62.Py

1. Introduction

Since the 1970's, dark matter was thought to exist because the rotational velocities found [1] in Andromeda M31 and other low-redshift galaxies ($z < 0.001$) were characterized by at rotation curves having higher velocities than expected from the falling curves given by Newtonian mechanics, suggesting dark matter was present to hold the galaxies together. The M31 rotation velocities were inferred from the redshift of the nitrogen NII line, the consequence of which was that at rotation curves became the signature of the existence of dark matter.

However, high-redshift ($0.6 < z < 2.6$) galaxies in the distant Universe were recently found [2] to have falling rotation curves suggesting the absence of dark matter. Similarly, the recently discovered DF2 galaxy was found [3] to have a falling

rotation curve suggesting the absence of dark matter. DF2 is called the Ghost galaxy because it is transparent suggesting dark matter is not present because of the absence of cosmic dust. What this means is modern cosmology faces a dilemma as dark matter should not depend on the transparency of a galaxy or whether a galaxy is in the local or distant Universe.

Unlike the data for the M31 galaxy that shows at rotation curves out to 24 kpc, the criticism of the falling rotation curves in the high-redshift galaxies [2] is the data was only taken out to about 10 kpc – not long enough to verify the curve is indeed falling. Since extended data can be resolved by future work, the emphasis in this paper is placed on the critique of at rotation curves in M31 and specifically, to the unanswered question posed by Rubin and Ford in [1] as to what causes the decrease in intensity of the nitrogen NII line with increasing distance from the galaxy nucleus. However, the dependence of dark matter on absence of cosmic dust in the Ghost galaxy is also discussed.

2. Proposal

In the spiral M31 galaxy, the redshift of the NII line used to infer rotation velocities occurs upon absorption in cosmic dust distributed throughout the galaxy, the submicron dust particles concentrated in the outermost spiral arms. For clarity, only three dust particles are illustrated in Figure 1.

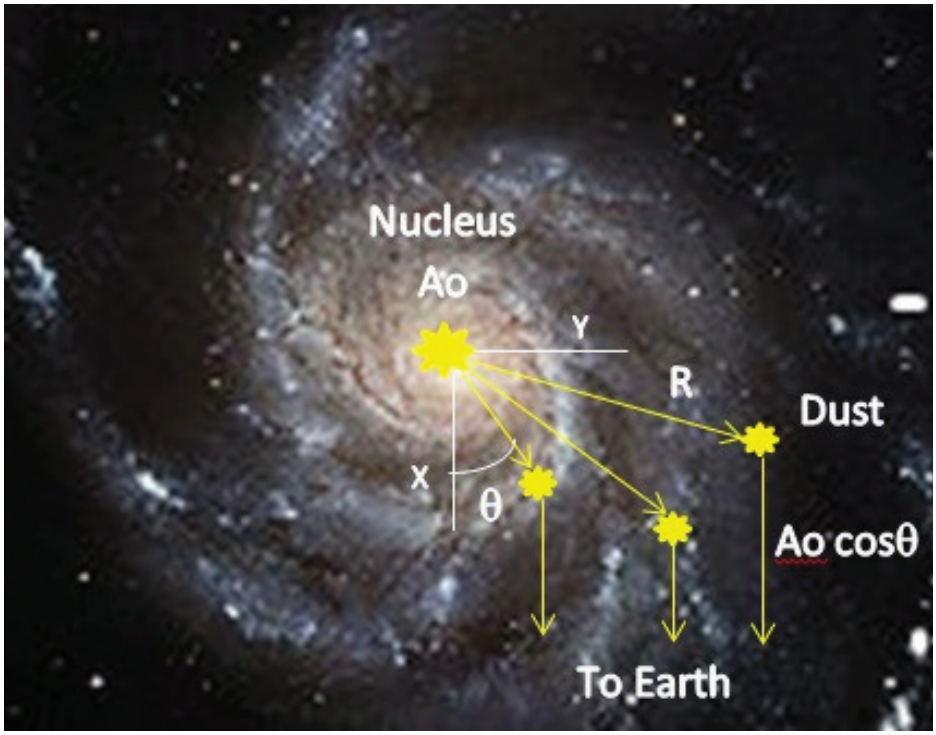

Figure 1: Flat rotation curves from cosmic dust particles in spiral galaxy.

The cosmic dust particles are located relative to the x-axis with origin at the galaxy nucleus oriented in the direction of the observer on Earth by radius R and angular position θ. The distance y from the nucleus to the dust particles is

$$y = R$$

$\sin\theta$. Ultraviolet radiation from stars within the nucleus is assumed to produce an intensity A_O of ionized NII nitrogen at 658.3 nm moving spherically outward from the nucleus shown by arrows until absorption by a dust particle. The redshifted NII line is re-emitted in the direction of the incident NII line momentum. Hence, the line intensity of the redshifted NII line to the Earth decreases by $A_O \cos\theta$. Consistent with [1] observation, the velocity V of the rotation curve is determined from the redshift z of NII which is nearly uniform across the galaxy while the NII line intensity decreases with distance y from the nucleus and vanishes as θ approaches 90 degrees.

3. Background

The redshift in cosmic dust went unnoticed for almost a century because the light-matter interaction of galaxy light including the NII line was assumed to follow classical physics allowing the heat capacity of the atoms in nanoscopic dust particles to conserve the galaxy photon by an increase in temperature. But the heat capacity of the atom given by the Planck law of QM is not scale invariant being finite at the macroscale while vanishing at the nanoscale. QM stands for quantum mechanics. Conservation of the galaxy photon is therefore only possible by a non-thermal mechanism proposed here to be simple QED.

4. Simple QED

Simple QED relies on the high S/V ratios of cosmic dust whereby the NII photon of wavelength λ is absorbed almost entirely in the dust surface placing constituent atoms under the high EM confinement necessary in the Planck law for heat capacity to vanish. S/V stands for surface to volume. A non-thermal EM standing photon having half-wavelength $\lambda/2 = d$ is then created as the NII photon adjusts to the EM confinement bounded by the dust surface. The speed of light c corrected for the refractive index n of the dust gives the Planck energy E of the redshift NII photon, $E = h(c/n)/\lambda$. On Earth, the NII line is observed to have wavelength $2nd$ with redshift $z = (2nd - \lambda)/\lambda$, where $\lambda = 658.3\,\text{nm}$. Once the Planck energy of NII absorbed in the dust surface is expended in forming the redshifted NII, the EM confinement vanishes and the redshifted NII is then free to travel to the Earth. See diverse simple QED applications in nanostructures at `http://www.nanoqed.org/`, 2010–2018.

5. Discussion

The shape of the galaxy rotation velocity V curve depends on the redshift z of the NII line in the absorption at each dust particle throughout the galaxy located at

distance y from the nucleus is, $V(y) = cz$. But z depends on the refractive index n of the dust, typically silicates while the diameter d of cosmic dust varies, $d < 500\,\text{nm}$. Hence, the velocity $V(y)$ may significantly fluctuate from dust throughout the galaxy, and not produce the at rotation curves observed.

However, this is not a problem in practice because the range on the measurement of redshift z is limited, e.g., the redshift measured [1] with the NII line at 658.3 nm in M31 was small $z < 0.001$. For silicates having $n = 1.3$, the corresponding dust diameter d is, $d = 253.2\,\text{nm}$ giving the same velocity V for the same dust diameter d anywhere in the galaxy. Hence, all dust diameters near 253.2 nm in the galaxy have the same dust redshift giving the at rotation velocity curve. For single photon absorption, blueshift from smaller dust $d < 253.2\,\text{nm}$ is precluded by conservation of energy. Redshift at $z > 0.001$ and $d > 253.2\,\text{nm}$ does occur in the NIR and FIR, but was not reported in M31 because emphasis [1] was placed on NII detection near 658.3 nm.

Similar to dark matter as redshift in cosmic dust of M31, accelerated Universe expansion [4] from the observation that Supernovae based on brightness were found closer than expected based on redshift is an illusion because the redshift of cosmic dust does indeed make the Supernovae appear farther away. If Supernovae observations are corrected for cosmic dust, the Universe is not expanding consistent with the static and dynamic Universe once proposed by Einstein.

6. Conclusions

The low-redshift M31 spiral galaxy having a at rotation curve is the consequence of redshift of the NII line in cosmic dust which requires the intensity of the NII line to decrease with the distance from the nucleus.

High-redshift galaxies showing falling rotation curves are more compact than The M31 galaxy, but otherwise like the Ghost galaxy are mostly transparent and void of cosmic dust.

Flat galaxy rotation curves depend solely on cosmic dust having nothing to do with dark matter allowing galaxy dynamics at both low and high redshift to be governed by Newtonian mechanics.

References

[1] Rubin V. and Ford W.: Rotation of the Andromeda Nebula from a Spectroscopic Survey of Emission Regions. Astrophys. J., 159, 379, 1970.

[2] Genzel, R., et al.: Strongly Baryon-Dominated Disk Galaxies at the Peak of Galaxy Formation Ten Billion Years Ago. Nature, 543, 397–401, 2017.

[3] van Dokkum, P., et al.: A galaxy lacking dark matter, Nature, 555, 629, 2018.

[4] Riess A. G. et al.: The Farthest Known Supernova: Support for an Accelerating Universe and a Glimpse of the Epoch of Deceleration, Astrophys. J., 560, 49–71, 2001.

Conference *Cosmology on Small Scales 2024*
Michal Křížek and Yurii Dumin (Eds.)
Institute of Mathematics CAS, Prague

SEARCHING INDICATIONS FOR DARK ENERGY IN THE IMAGES OF BLACK HOLES

Vyacheslav Dokuchaev[1], Konstantin Prokopev[1]

[1]Institute for Nuclear Research of the Russian Academy of Sciences
117312, prospekt 60-letiya Oktyabrya 7a, Moscow, Russia
dokuchaev@inr.ac.ru, k.prokopev@minus.inr.ac.ru

Abstract: The form of black hole image, viewed by a distant observer (or telescope) in the cosmologically local Universe provides indications for the presence of dark energy. The specific feature of black hole image is the dark spot, viewed on the celestial sphere, projected inside the position of classical black hole shadow. The form of this black spot depends, in particular, on the presence of dark energy. In the nearest future it would be possible to search indications for dark energy at the images of supermassive black holes SgrA* and M87* by observations with the projected Space Observatory Millimetron.

Keywords: conference, international, cosmology, black holes

PACS: 04.20.Fy, 04.20.Jb, 04.50.Kd, 04.60.Bc, 04.70.Bw

1. Introduction

How does a black hole look like? This is a standard question of both scientific experts and general public. In this paper, the black hole images are calculated based on general relativity and equations of motion in the classical Kerr–Newman metric [1, 2, 3, 4, 5, 6], describing the rotating and electrically charged black hole (see Appendix A, B and C for details). These images are gravitationally lensed images of black hole event horizon.

Numerical supercomputer simulations of general relativistic hydro-magnetic accretion onto black holes (see, e. g., [7, 8, 9, 10, 11, 12, 13]) affirm the Blandford-Znajek mechanism [14] of energy extraction from fast rotating Kerr black holes. The crucial feature of this mechanism is an electric current flowing through the black hole immersed into external poloidal magnetic field. This electric current heats the accreting plasma up to the nearest outskirts of the black hole event horizon. Very high luminosity of this hot accreting plasma will spoil some parts of the black spots at the astrophysical black hole images.

Images of astrophysical black holes may be viewed as black spots on the celestial sphere, projected inside the possible positions of classical black hole shadows. See Figures 1 and 2 for some examples of the classical black hole shadows.

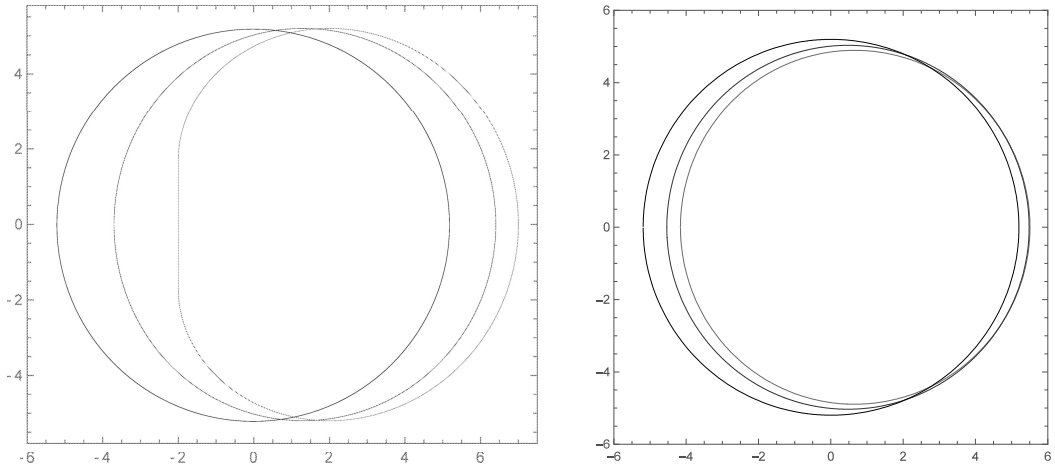

Figure 1: Some examples of classical black hole shadows are shown for the cases of supermassive black holes SgrA* and M87*.
Left panel: the shadows of SgrA* (with a possible inclinations of rotation axes with respect to the polar angle θ_0) in the spherically symmetric Schwarzschild case ($a = 0$) is black circle with a radius $r_{\rm sh} = 3\sqrt{3} \simeq 5.196$. The closed curves are the shadows of extremely fast rotating black hole ($a = 1$) and ($a = 0.65$), respectively. Note, that the vertical sizes of shadows in the case of SgrA* are independent on the values of spin a.
Right panel: The corresponding forms of shadows in the case of M87* (with a possible inclinations of rotation axes with respect to the polar angle $\theta_0 = 163^\circ$) for spin values $a = 1$ (largest closed curve), $a = 0.75$, and $a = 0$ (circle) of radius $r_{\rm sh} = 3\sqrt{3}$.

The apparent shape of the black hole shadow, as seen by a distant observer in the equatorial plane, is determined parametrically, $(\lambda, q) = (\lambda(r), q(r))$, from simultaneous solution of equations $V_r(r) = 0$ and $[rV_r(r)]' = 0$ (see e.g., [6, 17, 18]):

$$\lambda = \frac{-r^3 + 3r^2 - a^2(r+1)}{a(r-1)}, \quad q^2 = \frac{r^3[4a^2 - r(r-3)^2]}{a^2(r-1)^2}. \tag{1}$$

It must be stressed that the forms of discussed dark spots are independent on the distribution and emission of the accreting plasma. Instead of, the corresponding forms of dark spots are completely defined by the properties of black hole gravitational field and black hole parameters like black hole mass M and spin a. (Throughout this paper we use the standard dimensionless units with $GM/c^2 = 1$, where G – Newtonian gravitational constant, c – velocity of light).

See Figure 3 for an example of reconstruction of the spherically symmetric Shwarzschild black hole event horizon silhouette using $3D$ numerically calculated trajectories of photons, which start very near the black hole event horizon and are registered by a distant observer (by a distant telescope). Correspondingly, Figure 4 shows the example of reconstruction of the extremely fast rotating Kerr black hole with spin $a = 1$.

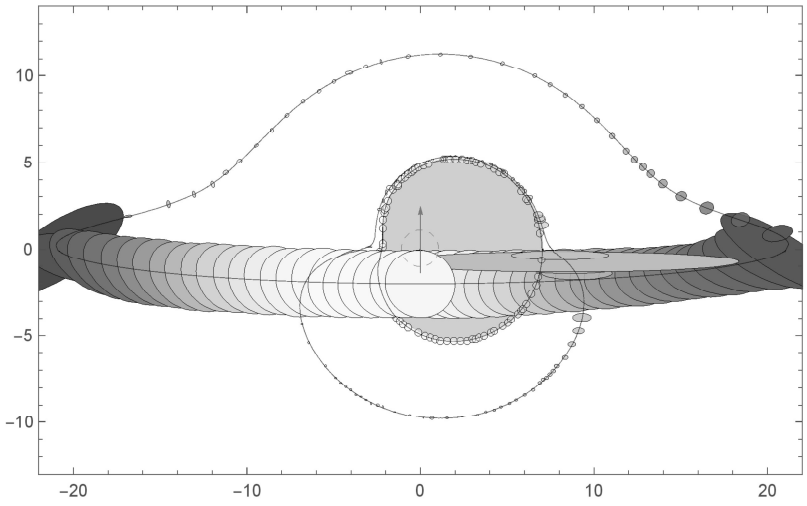

Figure 2: The numerical simulation of compact spherical probe (neutron star or spaceship) orbiting around a fast-rotating black hole ($a = 0.9982$) at a circular orbit with a dimensionless radius $r = 20$. One orbital period in discrete time intervals is shown. A distant observer is placed a little bit above the black hole equatorial plane. It is shown the direct image and the first and second light echoes. The central gray region is the classical black hole shadow. The images second light echo is concentrated at the outskirts of shadow. It is also considered the gravitational lensing of spherical probe in the black hole gravitational field (in the ellipsoidal approximation), viewed by distant observer as deformation of the probe. For details see [15].

The trajectories of photons at all figures of this paper are calculated numerically by using test particle equations of motion in the Kerr metric (see Appendix B and C). The event horizon silhouette (dark spot) always projects at the celestial sphere within the classical black hole shadow.

2. Classical black hole shadow

Some examples of the classical black hole shadows are shown in Figure 1 for the cases of supermassive black holes M87* at the center of galaxy M87 and SgrA* at the center of our native Milky Way galaxy. Left panel: the shadows of SgrA* (with a possible inclinations of rotation axes with respect to the polar angle θ_0) in the spherically symmetric Schwarzschild case ($a = 0$) is black circle with a radius $r_{\rm sh} = 3\sqrt{3} \simeq 5.196$. The closed large curve is the shadow of extremely fast rotating black hole ($a = 1$) and the closed smaller curve corresponds to the shadow of moderately fast rotating black hole ($a = 0.65$), respectively. Note, that the vertical sizes of shadows in the case of SgrA* are independent on the values of spin a. Right pane: The corresponding forms of shadows in the case of M87* (with a possible inclinations of rotation axes with respect to the polar angle $\theta_0 = 163^\circ$) for spin values $a = 1$, $a = 0.75$, and $a = 0$ of radius (or vertical size) $r_{\rm sh} = 3\sqrt{3}$.

See Figure 2 for the numerical simulation of compact spherical probe (neutron star or spaceship) orbiting around a fast-rotating black hole ($a = 0.9982$) at a circular orbit with a dimensionless radius $r = 20$. It is shown one orbital period in discrete time intervals. A distant observer is placed a little bit above the black hole equatorial plane. It is shown the direct image and the first and the second light echoes. The gray region is the classical black hole shadow. The images second light echo is concentrated at the outskirts of the shadow. It is also considered the gravitational lensing of spherical probe in the black hole gravitational field (in the ellipsoidal approximation), viewed by a distant observer as deformation of the probe. For details of numerical calculations see [15].

3. Dark spots at black hole images

The form of a dark spot at the astrophysical black hole image, which is viewed by a distant telescope (observer) at the black hole equatorial plane, may be calculated by using Brandon Carter [4] integral equation of motion in the Kerr metric

$$\int_2^\infty \frac{dr}{\sqrt{V_r}} = 2\int_{\theta_{\min}}^{\pi/2} \frac{d\theta}{\sqrt{V_\theta}}. \tag{2}$$

where $\theta_{\min}$ is a turning point of the photon trajectory for direct image in the polar direction (for details, see [19, 20]).

In the Schwarzschild case a turning point is at polar angle

$$\theta_{\min} = \arccos \frac{q}{\sqrt{q^2+\lambda^2}}, \tag{3}$$

where q and λ are parameters of photon trajectories from equation (12). Respectively, from the right-hand-side integral in (2) is $\pi/\sqrt{q^2+\lambda^2}$. The resulting numerical solution of integral equation (2) provides the radius of event horizon image $r_{\rm eh} = \sqrt{q^2+\lambda^2} = 4.457$.

The nearest hemisphere of the event horizon is projected into the disk with radius $r_{\rm EW} \simeq 2.848$. The farthest hemisphere is projected into the hollow dark disk with radius $r_{\rm eh} \simeq 4.457$. It is a radius of the gravitationally lensed event horizon image.

Figures 3 and 4 show the corresponding numerical solutions for the gravitationally lensed event horizon images in the Schwarzschild ($a = 0$) and extremely fast Kerr rotation case ($a = 1$) for the rotation axes orientation of the supermassive black hole SgrA*. The near hemisphere of the event horizon is projected by the lensing photons into the central dark region. Respectively the far hemisphere is projected into the hollow light colored region. The closed curves at the event horizon globe are the corresponding reconstructed parallels and meridians.

The event horizon globe of the Kerr black hole ($e = 0$, $a \neq 0$) according to general equation (9) is rotating with an angular velocity as a solid body

$$\Omega_{\rm h} = \frac{a}{2(1+\sqrt{1-a^2})}. \tag{4}$$

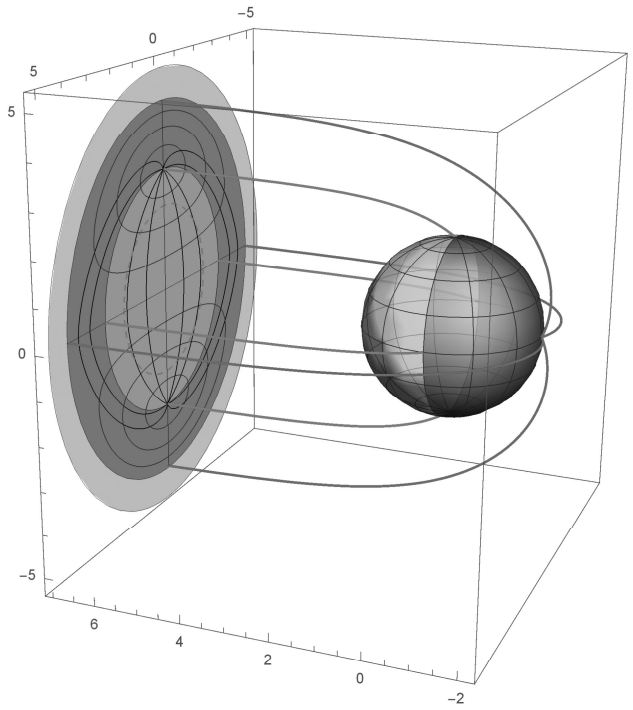

Figure 3: Reconstruction of the Shwarzschild black hole event horizon silhouette using $3D$ trajectories of photons (numerically calculated by using equations of motion in the Kerr metric), which start very near the black hole event horizon and are registered by a distant observer (by a distant telescope). The event horizon silhouette always projects at the celestial sphere within the classical black hole shadow with a radius $3\sqrt{3}$. Meanwhile, the corresponding radius of event horizon silhouette is $r_{\rm h} \simeq 4.457$, see [21, 22].

Figure 5 shows a $3D$ picture of the supermassive black hole M87* with a supposed spin parameter $a = 1$ surrounded by a thin accretion disk, which is supposed to be nontransparent. An inclination angle of M87* rotation axis with respect to a distant observer is supposed to be near 17°. The arrows indicate direction of the black hole rotation axis. The smallest black closed curve is the outer boundary of the dark spot which may be viewed by a distant observer at the celestial sphere. Two numerically calculated photon trajectories are started from the inner boundary of the accretion disk (in the vicinity of black hole event horizon equator) and finished far from black hole at the position of a distant observer. The largest closed curve at this $3D$ picture is an outer boundary of the classical black hole shadow. We remind that black spots on the images of astrophysical black holes are always projected inside the possible positions of the black hole shadows. The dashed circle is a projection on the celestial sphere of the imaginary sphere with unit radius in the absence of gravity (i. e. in the Euclidean space). The southern hemisphere of the gravitationally lensed event horizon globe may be viewed by a distant observer in the case of M87*.

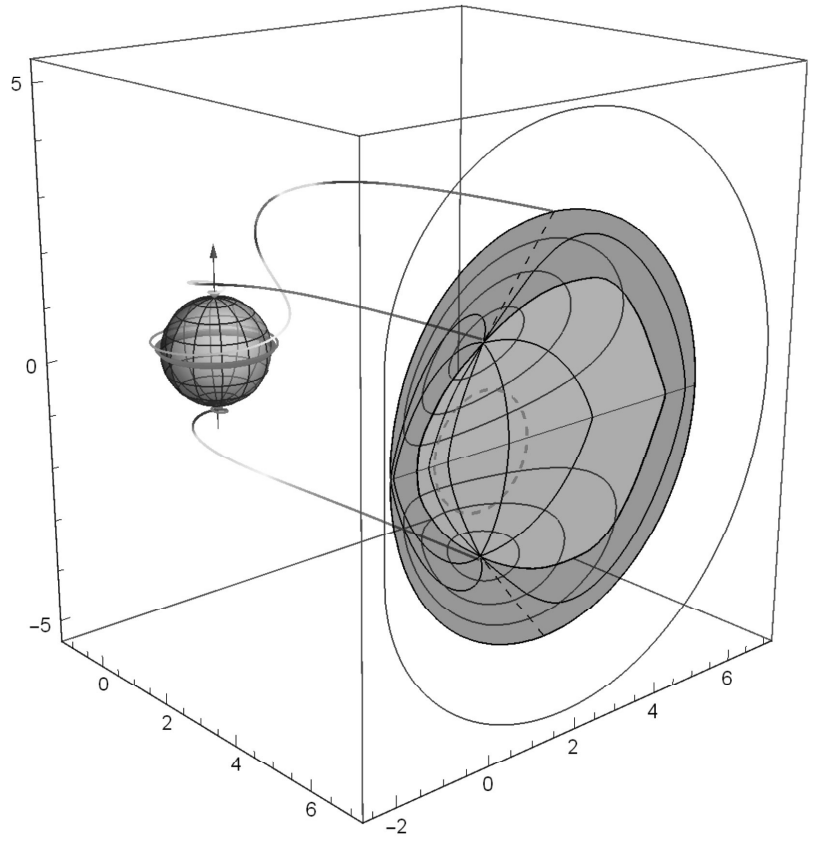

Figure 4: Reconstruction of extremely fast Kerr black hole ($a = 1$) event horizon silhouette for the rotation axes orientation of the supermassive black hole SgrA*. It is used $3D$ trajectories of photons (numerically calculated curves), which start very near the black hole event horizon and are registered by a distant observer (by a distant telescope). The nearest hemisphere of the event horizon is projected into (light colored) disk with radius $r_{\rm EW} \simeq 2.848$. The farthest hemisphere is projected into the hollow (dark disk with radius $r_{\rm eh} \simeq 4.457$. It is a radius of the gravitationally lensed event horizon image. The reconstructed curves are the corresponding parallels and meridians at the gravitationally lensed image of the event horizon globe.

Figures 6 and 7 show the compositions of the Event Horizon Telescope image of supermassive black hole SgrA* and M87*, respectively.

See at Figure 8 the gravitationally lensed images in discrete time intervals of small probe (neutron star or cosmic ship) with a zero angular momentum ($\lambda = 0$) and zero Carter constant ($q = 0$), which is plunging into a fast-rotating black hole. A distant observer is placed a little bit above the black hole equatorial plane. The small probe is winding around the black hole equator of the event horizon globe. It is shown one circle of this winding. The escaping signals from this prob are exponentially fading in time. For numerical animation see [16].

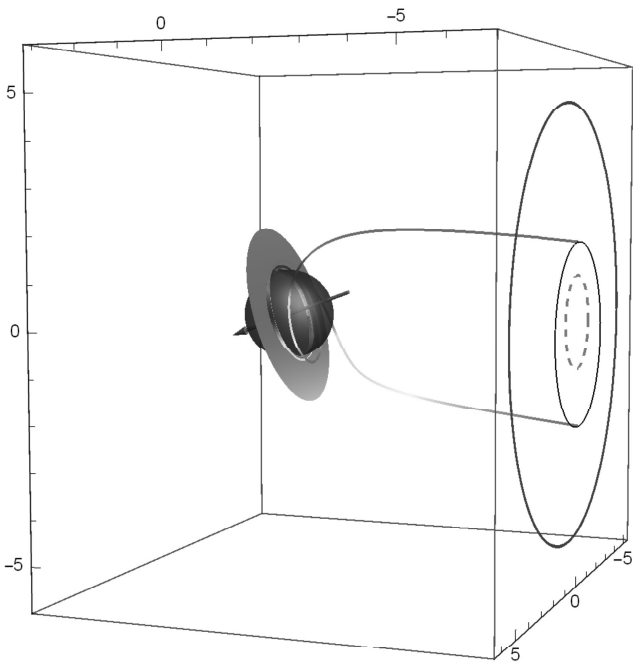

Figure 5: $3D$ picture of the supermassive black hole M87* with a supposed spin parameter $a = 1$ surrounded by thin accretion disk, which is supposed to be non-transparent. The largest closed curve is an outer boundary of the classical black hole shadow, viewed by a distant observer (telescope) at the celestial sky. Two numerically calculated photon trajectories are started from the inner boundary of the accretion disk (in the vicinity of black hole event horizon equator) and finished far from black hole at the position of a distant observer.

4. Discussions and conclusions

In this paper, possible forms of black hole images, viewed by a distant observer, are calculated based on general relativity and equations of motion in the Kerr-Newman metric. Black hole image is a gravitationally lensed image of the black hole event horizon. It may be viewed as a black spot on the celestial sphere, projected inside the position of classical black hole shadow. The event horizon silhouette (dark spot) always projects at the celestial sphere within the classical black hole shadow.

Images of astrophysical black holes may be viewed as black spots on the celestial sphere, projected inside the possible positions of classical black hole shadows. Very high luminosity of hot accreting plasma will spoil some parts of the black spots at the astrophysical black hole images.

It must be stressed that the forms of discussed dark spots are independent on the distribution and emission of the accreting plasma. Instead of, the corresponding forms of dark spots are completely defined by the properties of black hole gravitational field and black hole parameters like black hole mass M and spin a.

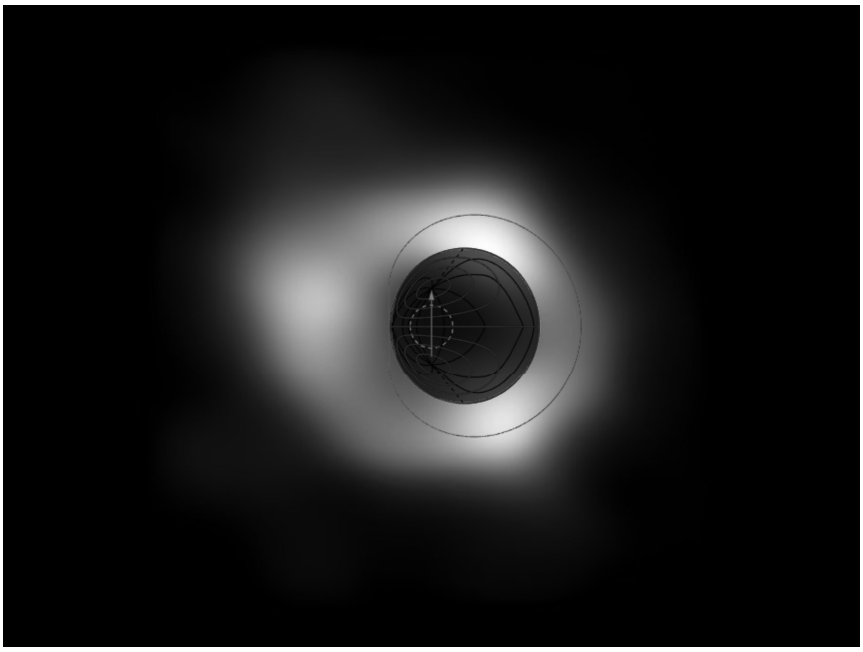

Figure 6: A composition of the Event Horizon Telescope image of supermassive black hole SgrA* [23, 24, 25, 26, 27, 28, 29] with the numerically modeled dark spot, corresponding to the gravitationally lensed image of the event horizon globe with spin $a = 1$. The closed purple curve is the outline of classical black hole shadow. The magenta arrow is the direction of black hole rotation axis. The magenta dashed circle is a position of the black hole event horizon with radius $r_{\rm h} = 1$ in the Euclidean space without gravity.

In the nearest future it would be possible to verify modified gravity theories by observations of astrophysical black hole with international Millimetron Space Observatory [39, 40, 41, 42].

A. Kerr–Newman metric

The line element of the classical Kerr–Newman metric [1, 2, 3, 4, 5, 6], describing in particular the rotating ($a \neq 0$) and electrically charged ($e \neq 0$) black hole, is

$$ds^2 = -e^{2\nu}dt^2 + e^{2\psi}(d\phi - \omega dt)^2 + e^{2\mu_1}dr^2 + e^{2\mu_2}d\theta^2, \tag{5}$$

where

$$e^{2\nu} = \frac{\Sigma\Delta}{A}, \quad e^{2\psi} = \frac{A\sin^2\theta}{\Sigma}, \quad e^{2\mu_1} = \frac{\Sigma}{\Delta}, \quad e^{2\mu_2} = \Sigma, \quad \omega = \frac{2Mar}{A}, \tag{6}$$

$$\Delta = r^2 - 2Mr + a^2 + e^2, \quad \Sigma = r^2 + a^2\cos^2\theta, \quad A = (r^2 + a^2)^2 - a^2\Delta\sin^2\theta, \tag{7}$$

where M is black hole mass, $a = J/M$ is black hole specific angular momentum (spin), e is black hole electric charge, ω is frame-dragging angular velocity.

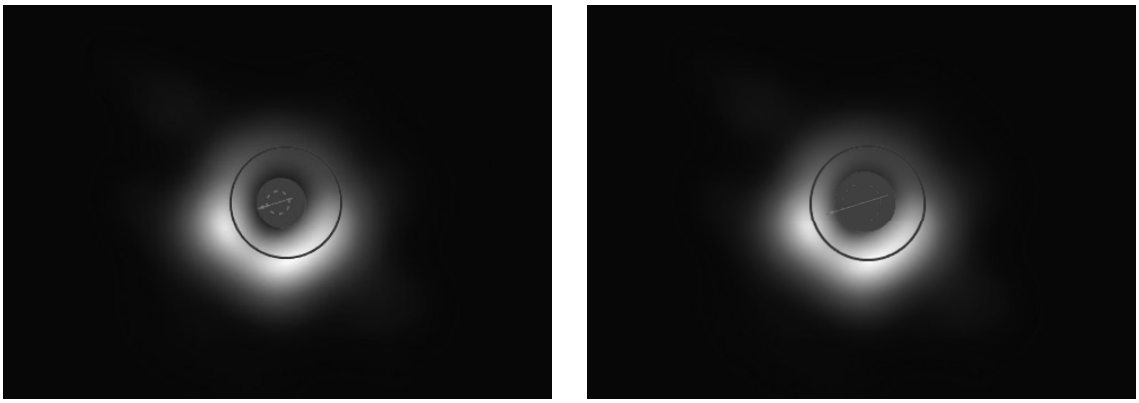

Figure 7: Superposition of the modeled dark spot with the Event Horizon Telescope image of supermassive black hole M87*:
Left panel, $a = 1$;
Right panel $a = 0.75$.
A 17° inclination angle of the black hole rotation axis at the celestial sphere is supposed. Note that the size of dark spot in the case of rotation axis orientation of this black hole weakly dependent on the value of spin parameter a.

Roots of equation $\Delta = 0$ define the black hole event horizon radius r_+ and the Cauchy radius r_-:

$$r_\pm = 1 \pm \sqrt{1 - a^2 - q^2}. \tag{8}$$

The event horizon of the Kerr-Newman black hole rotates as a solid body (i. e., independent of the polar angle θ) with angular velocity

$$\omega_+ = \frac{2Mar_+}{(r_+^2 + a^2)^2} \tag{9}$$

According to Brandon Carter equations of motion [4] there are the following integrals of motion: μ is particle mass, E is particle total energy, L is particle azimuth angular momentum and Q is the specific Carter constant, defining the non-equatorial motion. The corresponding radial potential $R(r)$ is

$$R(r) = P^2 - \Delta[\mu^2 r^2 + (L - aE)^2 + Q], \tag{10}$$

where $P = E(r^2 + a^2) - aL$. The polar potential $\Theta(\theta)$ is

$$\Theta(\theta) = Q - \cos^2\theta[a^2(\mu^2 - E^2) + L^2 \sin^{-2}\theta]. \tag{11}$$

Particle trajectories depend in general on three parameters

$$\gamma = \frac{E}{\mu}, \quad \lambda = \frac{L}{\mu}, \quad q = \frac{\sqrt{Q}}{E}. \tag{12}$$

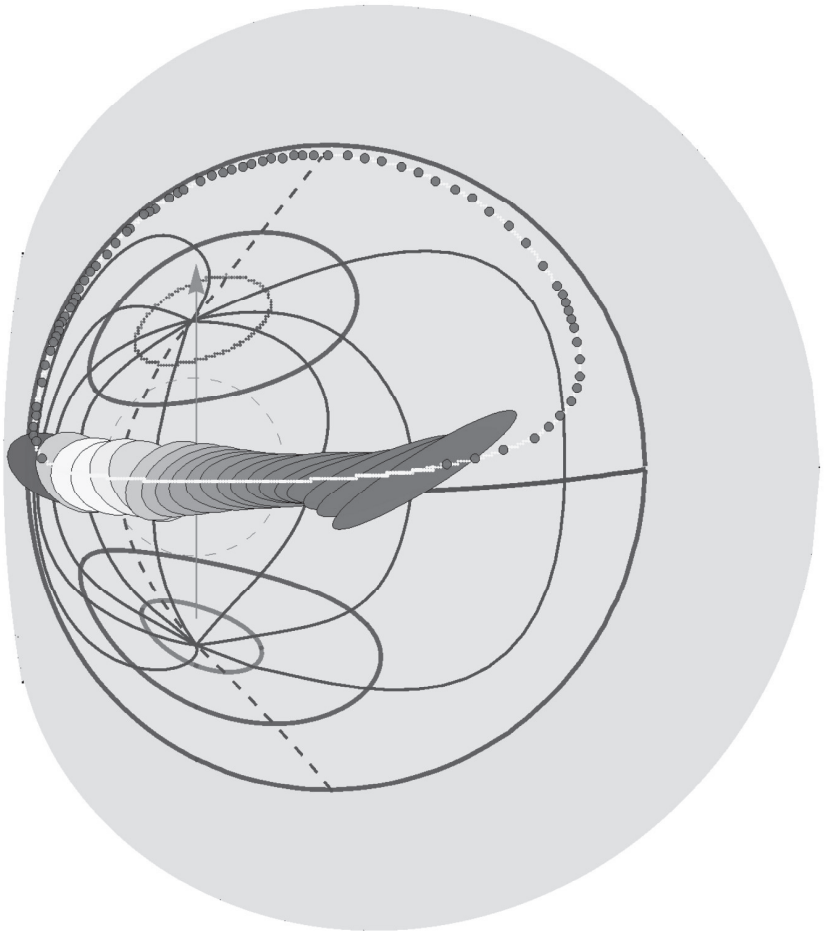

Figure 8: Gravitationally lensed images in discrete time intervals of small probe (neutron star or cosmic ship) with a zero angular momentum ($\lambda = 0$) and zero Carter constant ($q = 0$), which is plunging into a fast-rotating black hole. A distant observer is placed a little bit above the black hole equatorial plane. The small probe is winding around the black hole equator of the event horizon globe. It is shown one circle of this winding. The escaping signals from this probe are exponentially fading in time. For details of numerical calculations and for animation see [30, 31, 32, 33, 34, 35].

For massless particles like photons there are two parameters: λ and q. The corresponding horizontal and vertical impact parameters, α and β, which are viewed on the celestial sphere by a distant observer, placed at the polar angle θ_0 are [17, 19, 20]):

$$\alpha = -\frac{\lambda}{\sin\theta_0}, \quad \beta = \pm\sqrt{\Theta(\theta_0)}. \tag{13}$$

From astrophysical point of view (see, e. g., [36, 37, 38]) the most probable are the cases of fast-rotating supermassive black holes with spin values close to the maximum value, $a_{\max} = 1$.

B. Equations of motion for test particles

The first order differential equations of motion in the Kerr-Newman metric, derived by Brandon Carter [4], are

$$\Sigma\frac{dr}{d\tau} = \pm\sqrt{R(r)}, \tag{14}$$

$$\Sigma\frac{d\theta}{d\tau} = \pm\sqrt{\Theta(\theta)}, \tag{15}$$

$$\Sigma\frac{d\phi}{d\tau} = L\sin^{-2}\theta + a(\Delta^{-1}P - E), \tag{16}$$

$$\Sigma\frac{dt}{d\tau} = a(L - aE\sin^2\theta) + (r^2+a^2)\Delta^{-1}P, \tag{17}$$

where τ — a proper time of the massive ($\mu \neq 0$) particle or an affine parameter of massless ($\mu = 0$) particle like photons.

C. Integral equations for test particle motion

The integral equations of motion (14)–(17) are very useful for the following numerical calculations

$$\int\frac{dr}{\sqrt{R(r)}} = \int\frac{d\theta}{\sqrt{\Theta(\theta)}}, \tag{18}$$

$$\tau = \int\frac{r^2}{\sqrt{R(r)}}\,dr + \int\frac{a^2\cos^2\theta}{\sqrt{\Theta(\theta)}}\,d\theta, \tag{19}$$

$$\phi = \int\frac{aP}{\Delta\sqrt{R(r)}}\,dr + \int\frac{L - aE\sin^2\theta}{\sin^2\theta\sqrt{\Theta(\theta)}}\,d\theta, \tag{20}$$

$$t = \int\frac{(r^2+a^2)P}{\Delta\sqrt{R(r)}}\,dr + \int\frac{(L - aE\sin^2\theta)a}{\sqrt{\Theta(\theta)}}\,d\theta. \tag{21}$$

The integrals in equations (18)–(21) monotonically grow along the particle trajectory and change sign at both the radial and polar turning points:

$$\int_{r_0}^{r_s}\frac{dr}{\sqrt{R(r)}} = \int_{\theta_0}^{\theta_s}\frac{d\theta}{\sqrt{\Theta(\theta)}}, \tag{22}$$

where r_s and θ_s are, respectively the initial and polar particle coordinates, and $r_0 \gg r_{\rm h}$ and θ_0 are the corresponding final particle coordinates. The more complicated case is with the one turning point in the latitude (or polar) direction, $\theta_{\rm min}(\lambda, q)$, which is a solution of the equation $\Theta(\theta) = 0$. The corresponding ordinary integrals in equation (18) are written as

$$\int_{r_s}^{r_0}\frac{dr}{\sqrt{R(r)}} = \int_{\theta_{\rm min}}^{\theta_s}\frac{d\theta}{\sqrt{\Theta(\theta)}} + \int_{\theta_{\rm min}}^{\theta_0}\frac{d\theta}{\sqrt{\Theta(\theta)}}. \tag{23}$$

We use these equations in our numerical calculations of photon trajectories, starting in the vicinity of Kerr-Newman black hole and finishing at the position of a distant observer very far from black hole.

Acknowledgments

Authors are grateful to E. O. Babichev, V. A. Berezin, Yu. N. Eroshenko, N. O. Nazarova and A. L. Smirnov for stimulating discussions.

References

[1] Kerr, R. P.: Gravitational Field of a Spinning Mass as an Example of Algebraically Special Metrics, PRL 11, 237 (1989).

[2] Newman, E., Janis, A.: Note on the Kerr spinning-particle metric. Commun. in Math. Phys. **6** (1965), 915.

[3] Newman, E., Couch, E., Chinnapared, K., Exton, A., Prakash, A, Torrence, R.: Metric of a rotating, charged mass. Commun. in Math. Phys. **6** (1965), 918.

[4] Carter, B.: Global structure of the Kerr family of gravitational fields. Phys. Rev. **174** (1968), 1559.

[5] Misner, C. W., Thorne, R. S., Wheeler, J. A.: Gravitation (W. H. Freeman and Company, San Francisco) (1973) Chapter 34.

[6] Chandrasekhar, S.: The mathematical theory of black holes (Oxford University Press, Oxford) (1983) Chapters 5 and 7.

[7] Tchekhovskoy, A., Narayan, R., McKinney, J. C.: Efficient generation of jets from magnetically arrested accretion on a rapidly spinning black hole. MNRAS 418, L79 (2011).

[8] Tchekhovskoy, A., McKinney, J. C., Narayan, R.: General relativistic modeling of magnetized jets from accreting black holes. Journal of Physics Conference Series **372** (2012), 012040.

[9] McKinney, J. C., Tchekhovskoy, A, Blandford, R. D.: General relativistic magnetohydrodynamic simulations of magnetically choked accretion flows around black holes. MNRAS 423 (2012), 3083.

[10] Ressler, S. M., Tchekhovskoy, A., Quataert, E., Chandra, M., Gammie, C. F.: Electron thermodynamics in GRMHD simulations of low-luminosity black hole accretion. MNRAS **454** (2015) 1848.

[11] Ressler, S. M., Tchekhovskoy, A., Quataert, E., Gammie, C. F.: Electron thermodynamics in GRMHD simulations of low-luminosity black hole accretion. MNRAS 467 (2017), 3604.

[12] Foucart, F., Chandra, M., Gammie, C. F., Quataert, E, Tchekhovskoy, A.: Electron thermodynamics in GRMHD simulations of low-luminosity black hole accretion. MNRAS 470 (2017), 2240.

[13] Ryan, B. R., Ressler, S. M., Dolence, J. C., Gammie, C. F., Quataert, E.: Two-temperature GRRMHD Simulations of M87. Astrophys. J. **864** (2018), 126.

[14] Blandford, R. D., Znajek, R. L.: Electromagnetic extraction of energy from Kerr black holes. MNRAS 179 (1977), 433.

[15] Dokuchaev, V. I., Nazarova, N. O.: Star motion around rotating black hole. `https://youtu.be/P6DneV0vk7U` (2018).

[16] Dokuchaev, V. I., Nazarova, N. O.: Infall of the star into rotating black hole viewed by a distant observer. `https://youtu.be/fps-3frL0AM` (2018).

[17] Bardeen, J. M.: Black Holes; DeWitt, C., DeWitt, B. S., Eds. (Gordon and Breach Science Publishers: New York, NY, USA) (1973) pp. 215.

[18] Bisnovatyi-Koganand, G. S., Tsupko, O. Yu.: Shadow of a black hole at cosmological distances. Phys. Rev. D **98** (2018), 084020.

[19] Cunningham, C. T., Bardeen, J. M.: The optical appearance of a star orbiting an extreme Kerr black hole. Astrophys. J. **173** (1972), L137.

[20] Cunningham, C. T., Bardeen, J. M.: The optical appearance of a star orbiting an extreme Kerr black hole. Astrophys. J. **183** (1972), 237.

[21] V. I. Dokuchaev and N. O. Nazarova, "Event horizon image within black hole shadow", Exp. Theor. Phys. 128, 578 (2019).

[22] Dokuchaev, V. I., Nazarova, N. O.: Silhouettes of invisible black holes. Physics-Uspekhi **63** (2019), 583.

[23] The Event Horizon Telescope Collaboration: First M87 Event Horizon Telescope Results. I. The Shadow of the Supermassive Black Hole. Astrophys. J. **875** (2019).

[24] The Event Horizon Telescope Collaboration: First M87 Event Horizon Telescope Results. II. Array and Instrumentation. Astrophys. J. **875** (2019), L2.

[25] The Event Horizon Telescope Collaboration. M87 Event Horizon Telescope Results. III. Data Processing and Calibration. Astrophys. J. **875** (2019), L3.

[26] The Event Horizon Telescope Collaboration. First M87 Event Horizon Telescope Results. IV. Imaging the Central Supermassive Black Hole. Astrophys. J. **875** (2019), L4.

[27] The Event Horizon Telescope Collaboration. First M87 Event Horizon Telescope Results. V. Physical Origin of the Asymmetric Ring. Astrophys. J. **875** (2019), L5.

[28] The Event Horizon Telescope Collaboration. First M87 Event Horizon Telescope Results. VI. The Shadow and Mass of the Central Black Hole. Astrophys. J. **875** (2019), L6.

[29] Event Horizon Telescope Collaboration, "First Sagittarius A* Event Horizon Telescope Results. I. The Shadow of the Supermassive Black Hole in the Center of the Milky Way", Astrophys. J. 930, L12 (2022).

[30] Dokuchaev, V. I.: Spin and mass of the nearest supermassive black hole. GRG **46** (2014), 1832.

[31] Dokuchaev, V. I.: To see invisible: image of the event horizon within the black hole shadow. IJMPD **28** (2019), 1941005.

[32] Dokuchaev, V. I., Nazarova, N. O.: The brightest point in accretion disk and black hole spin: implication to the image of black hole M87*. Universe **5** (2019), 183.

[33] Dokuchaev, V. I., Nazarova, N. O.: Modeling the motion of a bright spot in jets from black holes M87*and SgrA*. GRG **53** (2021), 83.

[34] V. I. Dokuchaev and N. O. Nazarova and V. P. Smirnov, "Event horizon silhouette: implications to supermassive black holes M87* and SgrA*", GRG 51, 81 (2019).

[35] Dokuchaev, V. I.: Physical origin of the dark spot in the first image of supermassive black hole SgrA*. Astronomy **1**(2) (2022), 93.

[36] Reynolds, C. S.: Observing black holes spin. Nature Astronomy **3** (2019), 41.

[37] Nokhrina, E. E., Gurvits, L. I., Beskin, V. S., Nakamura, M., Asada K., Hada, K.: M87 black hole mass and spin estimate through the position of the jet boundary shape break. MNRAS **489** (2019), 1197.

[38] Ayzenberg, D., et al.: Fundamental physics opportunities with the next-generation event horizon telescope. arXiv:2312.02130 [astro-ph.HE] (2023).

[39] Kardashev, N. S., Novikov, I. D., Lukash, V. N., Pilipenko, S. V., Mikheeva, E. V., Bisikalo, D. V., Wiebe, D. S., Doroshkevich, A. G., Zasov, A. V., Zinchenko, I. I.: Review of scientific topics for the Millimetron space observatory. Phys. Usp. **57** (2014), 1199.

[40] Rudnitskiy, A. G., Mzhelskiy, P. V., Shchurov, M. A., Syachina, T. A., Zapevalin, P. R.: Analysis of orbital configurations for Millimetron space observatory. Acta Astronautica **196** (2014), 29.

[41] Likhachev, S. E., Rudnitskiy, A. G., Shchurov, M. A., Andrianov, A. S., Baryshev, A. M., Chernov, S. V., Kostenko, V. I.: High-resolution imaging of a black hole shadow with Millimetron orbit around lagrange point l2. MNRAS **511** (2022), 668.

[42] Ivanov, P. B., Mikheeva, E. V., Lukash, V. N., Malinovsky, A. M., Chernov, S. V., Andrianov, A. S., Kostenko V. I., Likhachev, S. F.: Interferometric observations of supermassive black holes in the millimeter wave band. Phys.-Usp. **62** (2022), 423.

Conference *Cosmology on Small Scales 2024*
Michal Křížek and Yurii Dumin (Eds.)
Institute of Mathematics CAS, Prague

EVALUATION OF THEORIES AND METHODOLOGIES: RELATIVISTIC PHYSICS VS. THE DYNAMIC UNIVERSE

Avril Styrman[1]

[1] University of Helsinki, PL 24, Unioninkatu 40, 00014, Finland
avril.styrman@helsinki.fi

Abstract: In the classical ideal, a physical theory provides understandable dynamic explanations and yields novel predictions of phenomena. Relativistic Physics (RP), namely the special and general theories of relativity and relativistic cosmology, does not meet this ideal. This discrepancy has been addressed by transforming the classical ideal into a 'relativistic methodology', where it is accepted that nature is not fully understandable, predictions are prioritized over dynamic explanations, new phenomena may be accommodated in an orderly fashion with the aid of additional hypotheses, and anomalous data may be disregarded. Relativistic methodology and the enduring confidence in RP stem from tradition, where physicists who have learned to conceptualize reality through RP see it as the only alternative. Thomas Kuhn and Paul Feyerabend have taught us that to fully understand a theory's weaknesses, it must be juxtaposed with an alternate theory, and that its replacement requires a superior theory. Here, RP is confronted with Tuomo Suntola's Dynamic Universe (DU). Suntola claims that DU matches or surpasses RP's predictive accuracy for several central phenomena from the terrestrial to the largest cosmological scales, while adhering to the classical ideal and cohering with quantum mechanics. If this claim withstands scrutiny, DU deserves further attention from physicists, philosophers and funding institutions.

Keywords: theory evaluation, theoretical virtues, unification, cosmology, general relativity, the dynamic universe

PACS: 98.80.-k, 04.50.+h

1. Introduction

This work evaluates the fitness of Relativistic Physics (RP) —comprising Special and General Relativity (SR & GR) and GR-based Standard Cosmology (SC), whose contemporary version is often called ΛCDM— against Tuomo Suntola's Dynamic Universe (DU), and the methodologies underlying the theories.[1] It is notable that RP

[1] DU is documented in Suntola [76], outlined in [78, 74, 73] and placed in a historical context in [77].

has been developed by hundreds of physicists for more than 100 years, whereas DU has been developed primarily by a single person for 25 years. It is understandable that thus far DU has been developed to explain only the very central phenomena. Therefore, the pressing question is not whether DU currently explains everything that RP does, but whether DU is currently good enough to deserve funding for further development. The argument is that DU's current track record indeed signals that its fruitfulness as a research program exceeds that of RP.

RP was built to explain phenomena that Newtonian mechanics failed to explain. The shift from Newtonian mechanics to RP marked a shift from the classical ideal, where a scientific theory provides understandable dynamic explanations and yields novel predictions of phenomena, to 'relativistic methodology,' where it is accepted that nature is not fully understandable, predictions are prioritized over dynamic explanations, new phenomena may be accommodated in an orderly fashion with the aid of additional hypotheses, and anomalous data may be disregarded. The enduring confidence in RP and the associated methodological choices are rooted in a tradition where physicists, immersed in the practice of conceptualizing reality through RP, regard it as the true or the only correct explanation for phenomena in its scope. Quine [56, p. 40] noted this social phenomenon: "Any statement can be held true come what may, if we make drastic enough adjustments elsewhere in the system." Gower [21, pp. 244–5] makes a related remark: "The choices scientists make are conventional rather than rational, and relate, allegedly, to the prevailing cultural, political and ideological values of the society supporting their investigations." Yet, due to its increasing tension with the classical ideal, a growing number of physicists find RP deficient, proposing alternatives that address its issues. The creation of alternatives to better comprehend and address the defects of a paradigm is a phase in the Kuhnian [35, p. 77] evolution of theories, which "involves the comparison of both paradigms with nature and with each other" and where *the invention of alternatives to the view at the center of discussion constitutes an essential part of the empirical method* (Feyerabend [14, p. 41]).

DU provides a comprehensive point for comparison with RP, addressing what, from the classical perspective, are its shortcomings, based on entirely different fundamental law hypotheses than those of RP. DU replaces RP's metric explanation, where the units of time and distance vary locally and energy conservation is open, with a holistic and dynamic explanation where the velocity of light and rest energy vary locally, and energy is conserved globally. Suntola maintains that DU's predictions are at least as accurate as those of RP for many of the central phenomena within RP's scope, and that unlike RP, DU aligns well with the classical ideal. Namely, DU's fairly simple basic structure provides a dynamic and causal-mechanical explanation that yields an understandable picture of reality; it is unified as it explains a wide range of heterogeneous phenomena, produces novel predictions and reduces reliance on additional hypotheses, and encounters less anomalous data. Furthermore, Suntola maintains that DU and quantum mechanics (QM) are intrinsically unified at the level of postulates, and that therefore, DU provides an alternative to the project of

unifying QM and GR by constructing an additional structure such as string theory or quantum gravity on top of them. In the following, it is assumed that Suntola's central claims are correct, which, I believe, is the case. I encourage everyone to challenge Suntola's claims and the conclusions I've drawn from them.

Apparently, a judgment of the relative fitness of RP and DU hinges on the chosen methodology. A critical reader may assess which methodology, relativistic or classical, appears to yield a faster rate of progress in science in general and more viable physics in particular. A methodology may be stated in terms of the criteria it accepts. Criteria that conform to the classical ideal, and which are referred to as classical criteria here, are formulated in §2. The historical succession that gave rise to RP and its methodology is reviewed in §3. The basic structures and central predictions of RP and DU are contrasted in §4. It is suggested in §5 that transparent criteria could tackle contemporary dogmatism as well as excessive theory proliferation in physics. The concluding remarks are given in §6.

2. Classical criteria

Systematization of the evaluation criteria for scientific theories, or theoretical virtues, in the philosophy of science since Kuhn [34] and McMullin [45] has been largely aligned with the classical ideal, though this alignment is often not explicitly acknowledged. The proposed systematization, which includes a taxonomy and a priority order of virtues, particularly aims to encapsulate the essence of the classical ideal.[2] The primary focus is on explanatory virtues. In the top-level classification of ethical, explanatory, and pragmatic virtues, ethical virtues are essential for a reliable evaluation of the explanatory virtues, and the explanatory virtues are prioritized over the pragmatic virtues. Within the explanatory virtues, evidential virtues have the highest priority, and ontological weight has the second highest priority. Unifying power is defined as the ratio of T's total evidentiality to its ontological weight, and T's diachronic virtuousness is defined in terms of the evolution of its unifying power over time. First, the subject of evaluation, a scientific theory, is defined following Lakatos [36] and Schurz [63, ch. 5.6] as a basic structure complemented by a periphery.

- **The basic structure** of a scientific theory or its hard core is the set of its fundamental assumptions, primary principles, premises, postulates, axioms, or hypotheses of universal laws of nature, such as Newton's law of gravitation and his three laws of motion. Law hypotheses of a physical theory are often formulated applying primitive concepts such as mass, distance, time and electric charge, and exactified by mathematics. The basic structure gives a theory its identity and remains unaltered, whereas its periphery may change over time.

[2]The given formulation of evidential virtues modifies Keas' formulation [27]. Contextual virtues conform to McMullin [44] and various coherentists (cf. Mackonis [40]). The formulation of unifying power follows Kaila [26, pp. 77–83] and Niiniluoto [48, pp. 158–159]. The distinction between ontological and syntactic simplicity aligns with Niiniluoto [48, p. 149] and Mackonis [40, p. 987].

- **The periphery** of a scientific theory consists of propositions derived from its basic structure, and of its auxiliaries, which are theoretical elements added on top of its basic structure so that the theory could explain phenomena. Auxiliaries include hypothetical entities and properties, such as Neptune in Newtonian mechanics and the hypothesis that gas molecules have positive sizes in the ideal gas theory, from their postulation until their discovery. Empirical parameters such as primitive mathematical descriptions of perceptions, and empirically measured constants needed for fine-tuning a theory are also its auxiliaries. For instance, mass, electric charge and magnetic moment of electron and proton are empirical parameters of the standard model of particle physics.

- **Ethical virtues** aim to capture methodological honesty, openness and integrity. Data ought not to be modified; anomalous data ought to be acknowledged; applied formulas ought to be derived from the basic structure of T or considered as primitive ontological commitments.

- **Explanatory virtues**.

  - *Evidential virtues, aka empirical virtues.*

    * *Accuracy*: the closer T's predictions are to the empirical data about phenomenon p, the more accurate T is with regard to p.
    * *Explanatory depth*: The greater T's depth for phenomenon p, the wider the range of conditions where its explanations remain valid, and the longer the chain of backward-directed causes of p that T can trace. The greater T's depth, the more likely it is that T yields novel predictions.
    * *Consistency*: The components of T's basic structure and its auxiliaries, its predictions and its explanations do not contradict one another. T's inconsistency decreases its depth, and at least potentially its accuracy.
    * *Total evidentiality*: T's total evidentiality $E(T) = \sum_{i=1}^{n} E(T, p_i)$ is the sum of T's evidentialities for phenomena $p_1 \dots p_n$ in T's scope. $E(T_1) = E(T_2)$ when T_1 and T_2 have the same accuracy and depth for $p_1 \dots p_n$. In a simple setting, $E(T, p_i) = 1$ if T's accuracy and depth meet some threshold, and 0 if not, equating $E(T)$ with T's factual scope or the number of phenomena T explains. In a nuanced setting, the value of $E(T, p_i)$ may be any real number in the interval [0 1].

  - *Ontological weight* $O(T)$, aka T's ontological simplicity and simplicity of T's content, is the sum of weights of ontological commitments in T's basic structure and periphery.

  - *Unifying power*, aka relative simplicity, the principle of economy, parsimony and Ockham's razor, $UP(T)$ is the ratio $E(T)/O(T)$ of T's evidentiality $E(T)$ to its ontological weight $O(T)$. $UP(T)$ is great when T gives accurate and deep explanations for several heterogeneous phenomena, with a simple and consistent basic structure and periphery.

- *Diachronic virtues*, aka fruitfulness, fertility, consilience and fecundity. When T is diachronically virtuous, $UP(T)$ grows over time as its basic structure, alone or with non-ad hoc auxiliaries, survives testing, produces novel predictions and explanations, and guides research that yields technological innovations.
- *Contextual virtues*, aka external or universal coherence, congruence, consonance, and fit with background knowledge or other virtuous theories $\mathbb{T}$: T is consistent with $\mathbb{T}$, and there are strong explanatory relations between T and $\mathbb{T}$. T's external consistency may be analyzed in terms of its effect to $E(T\&\mathbb{T})$, and the strength of explanatory relations between T and $\mathbb{T}$ may be analyzed in terms of their effect to $O(T\&\mathbb{T})$.

- **Pragmatic virtues**, aka applicability and intelligibility. T is labor-saving or convenient for human action: easy to use, easy to test and easy to understand. Simplicity of T's form or T's syntactic or numeric simplicity is considered a pragmatic virtue.

3. A short history of celestial mechanics

The evolution of celestial mechanics can be divided into geocentric, heliocentric-Newtonian (classical), and relativistic (modern) stages.[3] The geocentric theory is the epitome of the observed-oriented and local approach. It postulates the Earth as the stationary center of the Universe, with the observer at rest. The geocentric method was to give mathematical descriptions of perceptions from the viewpoint of a static observer. Geocentricity resulted in a very complex and intricate system, with the number of applied circles increasing from Eudoxus' 27 to Ptolemy's 80. In Kuhn's [35, p. 68] words "astronomy's complexity was increasing far more rapidly than its accuracy and ... a discrepancy corrected in one place was likely to show up in another".

The transition from geocentricism to heliocentricism was a shift from an observer-oriented to a system-oriented theory, where it is recognized that the observer on Earth orbits the Sun. Newton's version of the heliocentric theory surpassed Ptolemy's geocentric theory in the central classical virtues: accuracy, simplicity, understandability, and usability. The success of Newtonian mechanics in the 18th and the early 19th centuries created a sense of finality around it, which lasted until the rise of electromagnetism in the mid-19th century. Maxwell's equations, which describe electric and magnetic fields and their interactions, transcended Newtonian mechanics and revolutionized our understanding of light as an electromagnetic wave.

The rise of electromagnetism led to the decline of mechanical philosophy, which demanded that a physical theory provides a *causal-mechanical explanation*, namely, an "*explanation-how*, that implies the description of the *processes* underlying the phenomenon to be explained and of the *entities* that engage in such processes" (Felline [13]). Mechanistic models — which tried to represent the behavior of

[3]See Suntola [77] and Shioyama [65] for the transition from classical to modern physics.

molecules and the electromagnetic aether in terms of rods, wheels, weights, and springs— became too complex and intricate, and Maxwell opted for law-based explanations of electromagnetic phenomena, namely, mathematical descriptions of laws that govern electromagnetic fields. The general shift away from mechanicism, and towards law-based explanations and mathematical descriptions, contributed to a broader acceptance of a more abstract understandings of natural phenomena. This shift softened the path for the metric explanation of SR.

The 1887 Michelson-Morley experiment prompted the transition from Newtonian mechanics to SR. The experiment aimed to confirm the existence of the luminiferous aether or Newtonian absolute space, within which light was expected to obey Galilean transformations, i.e., its velocity was thought to add linearly to the velocity of its reference frame (rotating Earth). Instead, the experiment was interpreted to show that the velocity of light is independent of the motion of its frame. This led to the rejection of the Galilean transformations and initiated a search for new kinds of coordinate transformations that describe how velocities sum up, given the constancy of the speed of light. Woldemar Voigt, George FitzGerald, Joseph Larmor and Hendrik Lorentz were the central contributors to the process of creating the coordinate transformations, in the context of absolute time and space. Walter Kaufmann's 1902 experiments directly falsified Newton's laws of motion by showing that a constant force does not produce constant acceleration in an electron as it approaches the speed of light. By 1904, Lorentz had finalized the coordinate transformations now known as *Lorentz transformations*, that accommodate Kaufmann's findings. Lorentz transformations enhanced Galilean *kinematics* with *metrics*, by letting the units of time and distance vary within the inertial frame of an object moving relative to an observer's rest frame.

Kinematics describes the motion of an object in terms of its position, velocity, and acceleration without considering the cause of its motion, whereas *dynamics* explains the cause of motion based on the laws of motion, incorporating force or energy transactions. Thus, a dynamic explanation of motion is a causal explanation of motion, albeit one that does not have to adhere to classical mechanicism. Galilean transformations are kinematic —they sum up velocities linearly without integrating the cause of motion. Newtonian mechanics adopted the linear summation of velocities from Galilean transformations but shifted from kinematics to dynamics by introducing the laws of motion. The Lorentz transformations introduced a relativistic correction to the linear summation of velocities in Galilean transformations. However, they reverted to kinematics by leaving the cause of motion unspecified, and to an observer-oriented approach by describing the coordinate transformations of an inertial (non-accelerating) frame of reference in motion relative to an observer at rest.

In 1905, SR regularized the observer-oriented and kinematic approaches of the Lorentz transformations by providing them ontological foundations: the constancy of the speed of light and the relativity principle. The relativity principle, which posits that the laws of nature are the same in all inertial frames of reference, allows any observer to be considered the state of rest and the perspective from which motion

is analyzed. The relativity principle, together with the constancy of the speed of light, allowed for the derivation of the Lorentz transformations. SR also regularized relativistic mass increase, which had been suggested earlier by Lorentz. While SR's explanations of time dilation and length contraction are entirely metric, SR includes a dynamic aspect in the sense that it can be viewed as a relativistic correction of Newton's laws of motion. In 1908, Hermann Minkowski further expanded SR by introducing spacetime geometry, which intertwines the three spatial dimensions with the time dimension.

In 1915, SR was extended to GR by postulating the equivalence principle, which equates gravitational and inertial acceleration and allows describing motion in accelerating frames of reference. The equivalence principle was not directly inherited from Newtonian mechanics but is congenial with it. The Equivalence Principle and SR were applied to derive GR field equations, which describe gravitational interactions in terms of spacetime curvature caused by mass and energy density. The first solution to the field equations was the Schwarzschild metric in 1916, which refined the prediction of Mercury's perihelion advance and predicted the gravitational bending of light, confirmed by the 1919 Eddington experiment. While SR is purely observer-oriented, GR is partially system-oriented. In Schwarzschild metric, the observer is situated 'far' from the mass center being analyzed, and near Earth the non-rotating Earth-centered inertial (ECI) frame is often considered the state of rest. GR also introduced the mechanism where gravity can be seen as a consequence of mass and energy that curve spacetime. Alexander Friedmann's 1919–22 solutions to GR field equations, where the whole universe is considered a single mass center, laid the foundation for GR-based cosmology.

The transition from Newtonian mechanics to RP and QM meant a profound transformation in both the scientific worldview and the methodology of physics. Newton's *Mathematical Principles of Natural Philosophy* initiated mathematical physics. However, the task that led to *Principia* was driven by ontology: it aimed to identify the force behind Keplerian elliptical orbits, a force that was described mathematically. While Newton's mathematics was confined to the context of the well-understood Keplerian heliocentric system, in modern physics the order was reversed: mathematics took over, and the resulting worldview has been sought by exploring the implications of mathematical formulations of contemporary theories. Contemporary theoretical physics emphasizes mathematical descriptions of phenomena, often without relying on an intuitive worldview behind the observed behavior of nature. Concerning RP, history has repeated itself: the observer-oriented SR has led to an increasingly complex and intricate overall system. Suntola suggests that once again, we should replace an observer-oriented theory with a simpler, unified and dynamic theory, whose genuinely holistic or system-oriented causal-mechanical basic structure integrates the observer's perspective and enables a more comprehensive understanding of the universe as a whole. DU is a proposal for such a theory. Consequently, if DU indeed achieves what it claims, the relation between RP and DU parallels the relation between geocentrism and heliocentrism.

4. The evaluation

Some properties of the basic structures of DU and RP are contrasted first, after which several of their central predictions and explanations are analyzed in Examples 1–16.

In a nutshell, the three relativistic theories, SR, GR and SC, are metric-dynamic hybrids that accommodate phenomena and make nature incomprehensible. SR and GR leave open the conservation of energy, whereas SC violates it and does not provide a definite geometry of space. In contrast, DU is a single fully dynamic theory that builds on the conservation of energy and a definite geometry of space, produces novel predictions, and yields an understandable scientific worldview.

RP is a cumulative structure of the postulates of SR, GR and SC. SR, as a metric correction of Newtonian mechanics, is an observer-oriented hybrid of the metric and dynamic approaches. On one hand, SR inherits dynamics from Newtonian mechanics that it corrects. On the other hand, the observer is given a privileged status in the SR metric. GR is a hybrid of the metric and dynamic approaches, as well as a hybrid of the observer-oriented and system-oriented approaches. Like in SR, GR's observer-orientedness is implicit in its metrics, but it is partially system-oriented in the sense that the Schwarzschild metric identifies a local mass center. Yet, GR is not genuinely holistic as it is limited to a local frame of reference. GR introduces a mechanism where the energy-momentum tensor causes the curvature of spacetime, which in turn determines how objects move along geodesics, resulting in what we perceive as gravitational effects. However, GR has not provided viable dynamic explanations and instead relies on metric explanations e.g., for the effect of motion and gravitation on atomic clocks (Ex.4) and orbits near black holes (Ex.5).

Relativistic metric, where the units of time and distance and relativistic mass vary locally while the velocity of light and rest energy remain constant, has made the conceptions of time and space, and the overall scientific worldview along with them, incomprehensible. Relativistic metric is an exception in physics and in empirical science in general, as most theories in physics —such as electrodynamics, thermodynamics and quantum mechanics— and theories in geology, meteorology, chemistry and biology provide dynamic explanations. While classical rod-and-wheel-type mechanical explanations may not suffice for contemporary physical theories, causal-dynamic explanations remain desirable. According to Salmon [61, p. 259] and Douglas [10, pp. 461, 457], a theory that encompasses both laws and causal explanations is more likely to yield understanding and produce novel predictions than a theory with laws alone. RP conforms to their remarks, albeit in a negative sense. The basic structures of SR, GR and SC do not encompass causal explanations. The examples below show that in various cases, instead of producing novel predictions, the relativistic theories must accommodate phenomena with the help of additional hypotheses, which appear ad hoc as they lack independent support, and their only function is to save the theories from falsification.

DU's basic structure is the zero-energy balance of the energies of motion and grav-

itation in spherically closed space. In DU, all four dimensions are metric, and space is the three-dimensional surface of a four-dimensional sphere, aka 3-sphere, whose radius is the fourth dimension. In contrast, RP adopts a space-time geometry where the three spatial dimensions are intertwined with the time dimension. However, SC does not specify whether space is flat, spherically closed, or hyperbolically open.

DU's basic structure was formulated by the end of the 1990's to remedy the relativistic spacetime geometry that distorts time and distance. Since then, it has provided novel predictions for, inter alia, all phenomena discussed in the examples below. In contrast to relativistic metric, DU begins with a holistic dynamic mechanism and applies it consistently across different scales of phenomena. DU allows the velocity of light and rest mass to vary locally while keeping the units of time and distance constant; by explaining relativistic phenomena without distorting time and distance, DU preserves an understandable scientific worldview (Ex. 1–2). As a single fully dynamic, system-oriented and holistic theory, which serves as a predictive tool and also provides a basis for an understandable scientific worldview, DU serves as a comprehensive alternative to the three relativistic theories. DU is also an alternative to the approach of rectifying the issues of the relativistic theories by making minor adjustments, while sustaining their basic postulates.[4]

The zero-energy principle implemented in DU is a conservation law of energy. Such laws assert that the total energy of a closed system is conserved: the sum of kinetic energy and potential energy in its various forms. In respecting the conservation of energy, DU aligns e.g., with thermodynamics, electromagnetism, QM and high-energy physics, where conservation laws are central.[5] Furthermore, DU introduces a system of nested energy frames (Ex. 1) that links local motion with global motion, or local frames with the whole space. Thus, DU substantially develops the Leibnizian approach of describing motion, where energy is the fundamental conserved quantity, namely, the sum of living force (vis viva) and dead force (vis mortua) of stellar objects is conserved. In the force-based approach adapted by RP, energy [kg m^2/s^2] is derived as the distance [m] over which a force [kg m/s^2] accelerates mass [kg], whereas the energy-based approach starts with a system or an energy frame with total mass and total potential energy, and derives force as the gradient of potential energy. While in RP mass is a form of energy, in DU mass is a substance for the expression of the energy of motion and potential energy. DU honors dimensional analysis which requires that mass is measured in kilograms [kg], and energy in joules [kg m^2/s^2].

DU conforms to the Aristotelian concept of *entelechia*, where motion is the actu-

[4]For example, Modified Newtonian Dynamics modifies the gravitational law but leaves GR otherwise intact, and therefore, with the exception to providing an explanation of gravitational phenomena from the scale of outer regions of galaxies to galaxy clusters without dark matter (Ex. 8), it inherits all problems of RP, such as those discussed in this work.

[5]Although Newtonian mechanics is a force-based theory, Laplace used energy conservation, which he inherited from Leibniz, to explain anomalous orbits of the Moon, Jupiter, and Saturn in the context of Newtonian mechanics (Suntola [77, p. 50]).

alization of potentiality and all mass objects strive toward their minimum potential energy; an apple senses the gradient of the local potential field and instantaneously actualizes motion toward the minimum potential energy. DU's explanation —where interactions are instantaneous and do not require a medium, where motion is actualization of potentiality, and where energy bookkeeping is central— contrasts with the standard explanation adapted in RP where interactions propagate at the speed of light by means of gauge bosons or force carriers (such as gluons for the strong force, bosons for the weak force, and gravitons for gravity), where the motion of an object is caused by a force acting on it, and where energy bookkeeping plays no role.

In contrast to DU, SR and GR inherit force as the fundamental quantity from Newtonian mechanics. As hybrids of metric and force-dynamics, SR and GR leave open questions regarding energy bookkeeping and the relationship between local and global motion. Furthermore, SC is at odds with energy conservation First, creation ex nihilo in the big bang and cosmological inflation violate energy conservation (Ex. 7). Second, dark energy complicates energy conservation (Ex. 8). Third, the standard interpretation of the Planck equation as an intrinsic property of radiation implies that the redshifting of cosmic background radiation results in a loss of energy (Ex. 10). Finally, the RP convention that local systems do not expand appears to result from the absence of an energy bookkeeping system that would interconnect local motion with global motion. Without such a system, the expansion of planetary orbits would violate energy conservation; to uphold the no-local-expansion hypothesis, RP faces explanatory anomalies and requires additional hypotheses to resolve them (Ex. 13–16).

1. *The search for a rest frame.* A state of rest is needed as the perspective for analyzing motion. The relativity principle of SR and GR asserts that the laws of physics have the same form in all frames of reference. Thus, no absolute state of rest exists, but any observer can in principle be chosen as the state of rest. In SR, from the perspective of an observer A in a rest frame, time appears to run slower for an inertially moving (non-accelerating) observer B, and distances in B's frame appear contracted in the direction of B's motion; these phenonena are called *time dilation* and *length contraction*, respectively. SR is viable e.g., in the context of particle accelerators, where the accelerator functions as the perceiver at a state of rest, and where the accelerator and the accelerated particles remain at a constant gravitational potential. The SR explanation where the unit of time varies locally violates absolute simultaneity. This has practically destroyed an understandable conception of time and an understandable scientific worldview along with it (Ex. 2).

   In GR, an object at a greater distance from a mass center, i.e., at a greater gravitational potential, experiences faster flow of time or is subject to *gravitational blueshift*, whereas an object at a smaller gravitational potential experiences slower flow of time or is subject to *gravitational redshift*. The Schwarzschild solution of GR field equations fixes the state of rest to a single mass center in otherwise

empty space. For instance, in atomic clock tests, the mass center is typically the Earth-centered inertial (ECI) frame. This means that the SR interpretation of the relativity principle, where the state of rest can be chosen freely, may be dropped in Schwarzschild space. From the viewpoint of a critic, this appears as internal inconsistency. The choice between SR and GR and the selection of an appropriate rest frame for each scenario has proven challenging. First, the vast quantity of literature about the Twin Paradox highlights the difficulty of deciding the correct way to apply SR in specific tests or thought experiments, or whether GR should be applied instead. For instance, Křížek and Somer [33, §2.5 & §2.6] identify a number of false arguments concerning the Twin Paradox, and their own solution. Yet, the 100+ years of debate about the paradox shows that people regularly 'misunderstand' SR. Second, in the 1971 Hafele-Keating experiment, atomic clocks on airplanes circling the Earth showed time dilation, matching Hafele's GR prediction with the ECI frame as the rest frame: the eastward clock lost time and the westward clock gained time relative to the ground station (Hafele [23]). Prior to the test, Schlegel [62] argued for using the ground station as the rest frame, which would predict identical readings on the airborne clocks. See also Ex. 3.

DU (§1.2.4 & §5.2) gives equally accurate predictions as SR and GR of the effect of motion and gravitation to atomic clocks, and provides a unique explanation for them (Ex. 4), without suffering from the difficulty of figuring out how SR should be applied or from choosing between SR and GR. DU respects absolute simultaneity and yields an understandable worldview, relying on exactly one conception of time that holds from the largest cosmological scale to the scale of elementary particles, and does not suffer from other relativistic dilemmas (Ex. 2). In DU, the center of the universe, i.e., the center of the 3-sphere, is ontologically speaking the sole state of absolute rest. However, the practical state of absolute rest is *hypothetical homogeneous space*, where all matter is uniformly distributed in space. Figure 1 illustrates the nested energy frames: an ion moves in an accelerator's frame, which moves in the ECI frame, which moves in the Solar System frame, which moves in the Milky Way frame, which moves in the frame of a galaxy cluster, and so on, until a frame moves with respect to the state of rest in hypothetical homogeneous space.

The first-level equation, $E_{rest(Ion\in A,v)} = E_{rest(Ion\in A,0)}\sqrt{1-\beta_{Ion}^2}$, has the following meaning. $E_{rest(Ion\in A,v)}$, the rest energy of an ion moving at velocity v in the accelerator A's frame, is the product of the rest energy of the ion when stationary with in frame A, denoted as $E_{rest(Ion\in A,0)}$, and the velocity factor $\sqrt{1-\beta_{Ion}^2}$, that incorporates the effect of the Ion's velocity v relative to A. In the second-level equation

$$E_{rest(Ion\in A,v\in ECI,v')} = E_{rest(Ion\in A,0\in ECI,0)}(1-\delta_A)\sqrt{1-\beta_A^2}\sqrt{1-\beta_{Ion}^2}$$

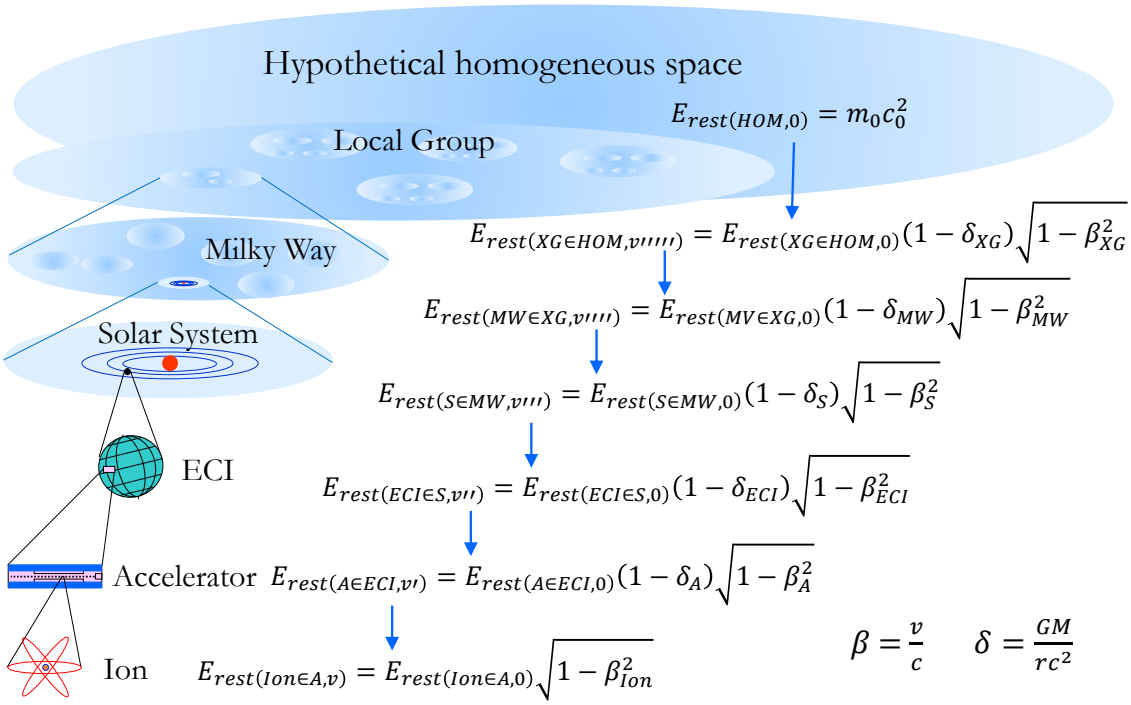

Figure 1: The system of nested energy frames.

the effect of the ECI frame is written out. Here, $E_{rest(Ion\in A,v\in ECI,v')}$ denotes the rest energy of the ion moving at velocity v in A, which moves at velocity v' in the ECI frame. $E_{rest(Ion\in A,0\in ECI,0)}$ denotes the rest energy of the ion stationary relative to A, which is stationary relative to the ECI frame. The gravitational factor $(1-\delta_A)$ incorporates the effect of A's distance from the barycenter of the ECI frame, while the velocity factor $\sqrt{1-\beta_A^2}$ incorporates the effect of A's velocity v' relative to the ECI frame. The velocity factor $\sqrt{1-\beta_{Ion}^2}$ incorporates the effect of the ion's velocity v relative to A, exactly as in the first-level equation.

In the third-level equation, $E_{rest(Ion\in A,v\in ECI,v'\in S,v'')}$ denotes the rest energy of the ion moving at velocity v in A, which moves at velocity v' in the ECI frame, which moves at velocity v'' in the Solar System frame S. This equation adds the effect of the ECI frame's distance from and velocity relative to the barycenter of the Solar System frame S, while sustaining the first-level and the second-level terms. And so on, up to hypothetical homogeneous space.

2. *Philosophers' dilemmas.* The task of finalizing the relativistic conception of time has been delegated to philosophers, whose 100+ year investigation has not resulted in consensus about key questions: Does time pass? Is entropy a viable anchor for the direction of time? Is the present all that exists or do the past and/or future exit too? What is meant by the present moment, and how can RP be made compatible with basic human cognition and common use of language?

Robb [58, pp. v–vi] and Geach [19, p. 312] contemplate the last problem: implicitly, we apply absolute simultaneity in our conceptualizations and speak about common objects such as persons, the Earth, and the universe at the present moment; however, SR and GR imply that such objects have parts that do not exist at the same time. Tooley [80, §11] and others have tried to reconcile SR with absolute simultaneity by adding a privileged reference frame. But for SR it is as an additional hypothesis, and it violates the relativity principle. *Cosmic time* allows us to talk about temporal states of the universe as wholes. Cosmic time is founded on the cosmological principle, according to which the universe is homogeneous and isotropic on large scales. But since the universe is not homogeneous and isotropic locally, cosmic time does not save the functionality of absolute simultaneity. Furthermore, cosmic time raises the question of how can we talk about a totality at time t, without denoting its parts at t? It appears that non-understandability of nature must be accepted as a part of the relativistic worldview. In contrast, DU does not clash with basic human cognition, as it is compatible with presentism, it commits to absolute simultaneity, and entails forward-directed passage of time, independently of entropy (cf. Styrman [71]).

3. *The 1976 Gravity Probe A experiment* is one of the most frequently cited GR tests. The Scout-D rocket carried an atomic clock (Gravity Probe A) to an altitude of 10,000 km, that transmitted a signal to the ground station during its journey. The test was supposed to confirm the 1970 GR prediction by Kleppner et al. [31] with the ECI frame as the state of rest. In 1980, Vessot et al. [81] reported that the effect of gravitation conforms to the 1970 GR prediction, whereas the effect of motion conforms to SR with the ground station as the state of rest, i.e., two theories and two states of rest were applied in explaining the same phenomenon. Furthermore, Vessot et al. [81, p. 2082] apply the SR term $|\overrightarrow{v_e} - \overrightarrow{v_s}|^2/(2c^2)$ for motion, referring to Kleppner et al. [31] who apply the GR term $(v_s^2 - v_e^2)/(2c^2)$ for motion.

   This, and the four-year delay between the 1976 test and the 1980 report made Dr. Suntola suspicious (Suntola [72, pp. 52–3]). In 1999 Dr. Vessot sent him the analysis of the test, where the derivation of the prediction had reached a dead end due to approximations made in an early stage. The SR-like term $|\overrightarrow{v_e} - \overrightarrow{v_s}|^2/(2c^2)$ was not derived, but applied as it produced a match with the data. Suntola [75] analyzed the experiment and discovered that Vessot et al. did not take into account the displacement of the ground station due to Earth's rotation affecting the two-way Doppler cancellation signal used in the experiment. With this factor, the GR velocity term transforms into $|\overrightarrow{v_e} - \overrightarrow{v_s}|^2/(2c^2)$. Thus, when the test is correctly analyzed, GR with the ECI frame suffices as an explanation. Suntola sent his analysis to Vessot, but the final report was not corrected. This example signals the difficulty of choosing the rest frame in the context of SR and GR, the complexity of their formalism, the accommodation of the test data, and unaddressed ethical issues: an unannounced jump in a derivation appears

as misconduct of individual scientists, and a missing erratum as misconduct of a journal. DU (eq. 1.2.4:16) gives the correct prediction with the ECI frame at the state of rest, without the relativistic dilemmas.

4. *Causal explanation for atomic clocks.* The GR prediction —that a clock at a higher gravitational potential or altitude will show a greater accumulated reading than a clock at a lower altitude— has been tested around a millimetre difference in altitudes (Bothwell et al. [3]). Yet, there is no standard GR explanation for the phenomenon. Okorokov [51, p. 400] contemplates two explanations:

   4.1. *The clock frequency varies as a function of its altitude.* The task is to explain the physical processes that entail the variance. The key factors appear in the quantum mechanical formula for the characteristic frequency of atomic oscillators

$$f = \frac{m_e c^2}{h} F(\alpha, \Delta[n, j]),$$

   where m_e is the rest mass of electron e, c is the velocity of light, $m_e c^2$ is the electron's rest energy, h is the Planck constant, and F is a function of the fine structure constant α and the difference $\Delta[n, j]$ of the electron's quantum numbers n and j, which characterize the states between which the electron oscillates. SR and GR make m_e and c and thus $m_e c^2$ constant, i.e., something else in the clock should vary. What might it be? Okorokov [51, p. 400] and Okun' and Selivanov [52] agree in that an atom's energy level or the distance between its nuclear levels depends on its altitude. However, the mechanism of how this variance affects an atomic oscillator remains open.

   In DU the frequency of an atomic clock is determined by its state of motion and gravitation. DU makes the units of time and distance constant and lets m_e and c vary locally, namely, m_e varies as a function of the clock's state of motion, and c varies as a function of its state of gravitation. Specifically, in DU the formula for atomic oscillators is $f = \frac{m_e c}{h_0} F(\alpha, \Delta[n, j])$, where c is the local velocity of light and h_0 is the intrinsic Planck constant, where the velocity of the expansion of space c_0 is removed. The greater is the clock's altitude, the higher is the local velocity of light c and the greater is the ticking frequency of a clock. Intuitively, the greater is the altitude and distance from the mass center, the less is space bent toward the fourth dimension, the greater is c, and the more momentum the electron has for oscillating. The greater is the clock's velocity, the greater is the electron's momentum in space and the smaller is its rest momentum or momentum in the fourth dimension. Intuitively, the more the electron uses its momentum in a space direction, the less momentum is available for the fourth dimension, i.e., the less rest momentum the electron has for oscillation. (DU §1.2.3–4, 2.1.4, 4.1.2,4,5, 5.1.1).

   4.2. *The clock frequency is independent of its altitude.* The test setting is depicted in Figure 2, where clock A at a higher altitude is assumed to show the

same accumulated reading as clock B (500). A sends electromagnetic radiation to B at the frequency of A. The task is to explain why B receives a greater number of transmitted cycles per second than its own frequency. In Malykin's [41] characterization "the clocks run identically at different altitudes, but at the same time, the ascending photons undergo a redshift since they lose energy, while the descending photons, correspondingly, undergo a blueshift since they acquire energy". In other words, the explanation is that the frequency of descending radiation increases as it acquires energy, whereas the frequency of ascending radiation decreases as it loses energy. In the first place, it is hard to believe that the clock frequencies are the same, as we can clearly see in a laboratory that A shows a greater accumulated reading. Furthermore, the mechanism that increases/decreases the number of radiation cycles during their journey remains open. The basic relativistic metric explanation sustains invariance of the clock frequencies: from the aspect of B, the unit of time in the frame of A is smaller, i.e., A experiences a faster flow of time. This conforms to Schutz [64, p. 113]: "gravitational redshift implies that time itself runs slightly faster at the higher altitude than it does on the Earth".

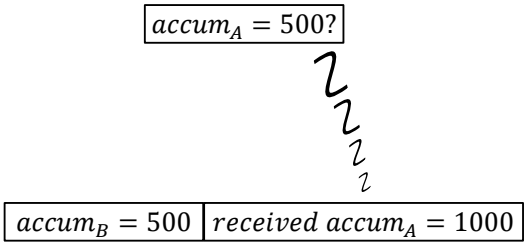

Figure 2: How does the frequency of cycles change during the journey?

5. *Unstable orbits.* Schwarzschild metric predicts that the innermost stable circular orbit radius (ISCO) for a non-rotating black hole is 3 times the Schwarzschild critical radius (SCR) aka event horizon or the border of a black hole (Misner, Thorne and Wheeler [47, p. 911]). Below ISCO, the orbital velocity of a test mass exceeds its escape velocity, making it depart the orbit. When Schwarzschild metric is applied to the black hole Sagittarius A* (Sgr A*) in the center of the Milky Way, the minimum orbital period at 3×SCR is about 27 minutes. This is at odds with the observed 16.8 ± 2 minute orbital periods. Thus, Schwarzschild metric is falsified near black holes (Genzel et al. [20]). Kerr's 1963 solution of GR field equations, aka Kerr metric, allows a black hole and space around it to rotate. For rotating black holes ISCO is 1.5×SCR. For Sgr A* the minimal orbital period at 1.5×SCR is 9.5 minutes, which is less than the observed 16.8 ± 2 minute periods. In sum, Kerr metric saves phenomena by applying rotational velocity of Sgr A* as a hypothetical property.

   In DU the critical radius is 0.5×SCR and the minimum period around Sgr A*

is 14.8 minutes. The minimum period is at SCR, for DU predicts that orbital velocities slow down from SCR to 0.5×SCR. The DU solution is not only stable down to 0.5×SCR but also suggests that slow orbits maintain the mass of a black hole. Thus, according to DU there need be nothing inside a black hole, but its mass may be situated at its orbit. The DU explanation takes into account energy conservation and the effect of the rest of space to local systems, and suggests that Schwarzschild metric fails e.g., because it does not take these elements into account (DU §1.2.6).

GR's escape problem can also be seen near the Sun. Schwarzschild metric correctly predicts Mercury's c. 575 arc seconds/century perihelion shift, but it also increases Mercury's main axis. For a single period, the increase is small and omitted as a second order effect by Weber [82, pp. 64–67], Berry [7, p. 83] and Foster and Nightingale [16, ch. 4.5]. However, in their solutions expansion of the main axis entails Mercury's escape in less than 400.000 years. Proponents of GR have great difficulties in accepting this result, for the prediction for Mercury's perihelion shift was Einstein's central goal in the construction of GR and its important early victory (Janssen and Renn [25]). In personal communication, a proponent of GR argued that solutions which entail Mercury's escape are surely meant only as approximations. But why is there a different approximation in each book? Where is the correct approximation, and is it derived from Schwarzschild metric? The analysis of Křížek and Somer [33, §4 & §5] indicates that due to its mathematical complexity, no exact GR solution is available, but only approximations can be given. DU's (§1.2.6) unique solution, which does not contain cumulative terms, predicts Mercury's perihelion shift and a stable orbit. In general, DU is syntactically or mathematically much simpler than GR.

Cosmology: Expansion of the universe

Since the late 1920s, it has been widely accepted that the universe is expanding from a singularity. Explaining its cause is the first task for cosmology. SC suggests the big bang. In the classical presentist conception where time goes forward, SC seems to entail creation from nothing. Brane cosmology and quantum fluctuations have been proposed as causes of the big bang, which in turn raise the question about their own origins. In the context of spacetime eternalism where past, present and future coexist, one may also suggest that the big bang does not require a further explanation. DU suggests a preceding contraction as the cause of the singularity. This aligns well with presentism and the Aristotelian eternal universe, that was never born and will never vanish (*On the Heavens*, bk. 1, part 10).

SC and DU agree that the current expansion rate, the Hubble constant $H_0 \approx 70\,(\mathrm{km/s})/\mathrm{Mpc}$, when calculated based on nearby stars where 1 Mpc $\approx 31 \times 10^{12}$ km. In SC the expansion rate depends on the density parameter (Ex. 8) whose value has changed over time. The expansion started from the big bang, continued by inflatory expansion (Ex. 7), after which the dark energy -driven basic SC expansion

took over (Ex. 8). DU's contraction-expansion cycle behaves like a pendulum that sustains the zero-sum of the energies of motion and gravitation: the contraction was accelerating until the singularity, and the expansion has been decelerating since the singularity. The concept of redshift is applied in most of the examples. Redshift $z = (\lambda_{obs} - \lambda_{em})/\lambda_{em}$, is defined in terms of the wavelengts of light at the time of emission (λ_{em}) and observation (λ_{obs}). Redshift denotes how much the wavelength of the observed light has lengthened along with the expansion of the universe. The more the wavelength has lengthened (the more redshifted the light is), the longer the light has been traveling through expanding space, and hence, the farther away and the further back in time the emitting object was.

6. *Antimatter and baryogenesis.* To conserve energy and the charge, parity, and time reversal symmetry, the matter that came into existence in the big bang had to be compensated by an equal amount of antimatter. But today everything we see is made almost entirely of matter. Therefore, SC must deal with *matter-antimatter asymmetry* or *C asymmetry*, namely, asymmetry of the number of particles and antiparticles. Sakharov's [60] 1967 work gave rise to baryogenesis, the research program that aims to explain how the hypothesized initial C symmetry was transformed to the current C asymmetry. There is no consensual explanation for the transformation, but baryogenesis has been subdivided in several different theories (Riotto and Trodden [57]). DU does not require the hypothesis of initial C symmetry nor baryogenesis. In DU (§3.3.5) the expansion of the universe was preceded by contraction, where the release of gravitational energy created the current energy of motion, which appears primarily as rest energy.

7. *Cosmological inflation*, the hypothesis of a brief period of very rapid expansion of space shortly after the big bang, was established in the 1980s as a solution to problems of pre-inflationary SC. According to Stuchlík [70, p. 141], inflation occurred between 10^{-36} s and 10^{-32} s after the big bang, during which the universe grew about $e^{100} \approx 10^{43}$ times. According to Liddle [37, pp. 108–9], the universe grew e^{100} times between 10^{-36} s and 10^{-34} s. When the speculative nature of the focal magnitudes is accepted, inflation explains (1) why the geometry of space appears very close to flat, resolving the *flatness problem*, and (2) why the cosmic microwave background radiation (CMB) is remarkably isotropic even though regions of the universe separated by vast distances should not have had sufficient time to yield the isotropy, resolving the *horizon problem.* Inflation resolves (3) the *problem of structure formation* by enabling the formation of large-scale structures in the universe after the inflation, (4) *the magnetic monopole problem* by diluting the number of magnetic monopoles per unit volume, and (5) *the problem of cosmic strings* by suppressing their formation and density. Problems (1–2) are based on empirical evidence only, whereas (3–5) are based on what models of particle physics, beyond the standard model of particle physics, predict about the contents of the early universe (Lyth and Liddle [39, §18 & 21], Liddle [37, §13]).

Inflation yields the "difficulty in finding a smooth ending to the period of exponential expansion" (Guth [22, p. 353]) or the *graceful exit* problem, whose one component is the *reheating problem* or the question of in which kind of a process the energy stored in the inflationary field is transferred e.g., into radiation and matter, leading to a hot and dense early universe. Several hypotheses have been proposed to resolve the reheating problem.

DU resolves problem (1), for in SC flatness means Friedmann's critical mass density, which in DU means zero-energy balance implicit in DU's basic structure. DU implies that the velocity of expansion and the velocity of light —and thus all motion and processes in space— were at their fastest immediately after the singularity and have been steadily decelerating ever since. Consequently, it seems that DU offers the basis of explaining what inflation does in terms of the velocity of expansion. Given that the initial state of CMB conforms to the SC hypothesis, then DU expansion is compatible with its homogeneity, resolving problem (2). If the hypothetical mechanisms for the formation of structures are similar to those applied with SC, then DU provides sufficiently energy for rapid formation of structures, diluting magnetic monopoles, and suppression of cosmic strings, resolving problems (3–5). Finally, as DU entails a smooth expansion, it has no graceful exit problem. For instance, in DU at $t = 10^{-36}$ s, the radius of the universe $R_4 \approx 2.9899 \times 10^{-10}$ m, and at $t = 10^{-32}$ s, $R_4 \approx 1.3878 \times 10^{-7}$ m (DU eq. 3.3.3:7).

8. *The density parameter, dark matter and dark energy.* In SC's density parameter $\Omega = \Omega_m + \Omega_\Lambda$, Ω_m denotes the total mass of visible or normal matter including planets, stars, nebulae and yet unperceived but gravitationally attractive *dark matter*, [6] and Ω_Λ denotes gravitationally repulsive dark energy. Currently it is assumed that roughly 68% of the universe is composed of dark energy, 27% of dark matter, and less than 5% of normal baryonic matter. Dark energy, unlike other forms of matter, works against gravitation, and it complicates energy conservation due to the uncertain variation of its quantity over time. Since 1998, dark energy has been applied in aligning the SC prediction of the magnitude-redshift relation of Ia supernovae with observations, whereas DU (§1.3.3) gives a precise prediction by its basic structure, as illustrated in Figure 3. The treatment of dark energy as an empirical fact awaiting discovery signals overwhelming

[6] Dark matter is needed by SC and DU to explain why fast moving stars do not depart their galaxies. In RP there is no theoretical description of dark matter but it is identified through its gravitational effect alone. In DU dark matter is unstructured matter, which is the initial and the basic form of matter; it is assumed that a certain share of unstructured matter has been transformed into visible, structured matter (DU §7.3). While SC's cosmological principle (Ex. 2) characterizes the current space, DU's hypothetical homogeneous space (HHS) is the hypothesized initial state of the Universe, where all matter is structureless and there is no motion in space. DU is compatible with the cosmological principle in the sense that DU accepts that in the cosmological scale mass is uniformly distributed in space, which together with the spherical symmetry makes space look essentially the same at any location.

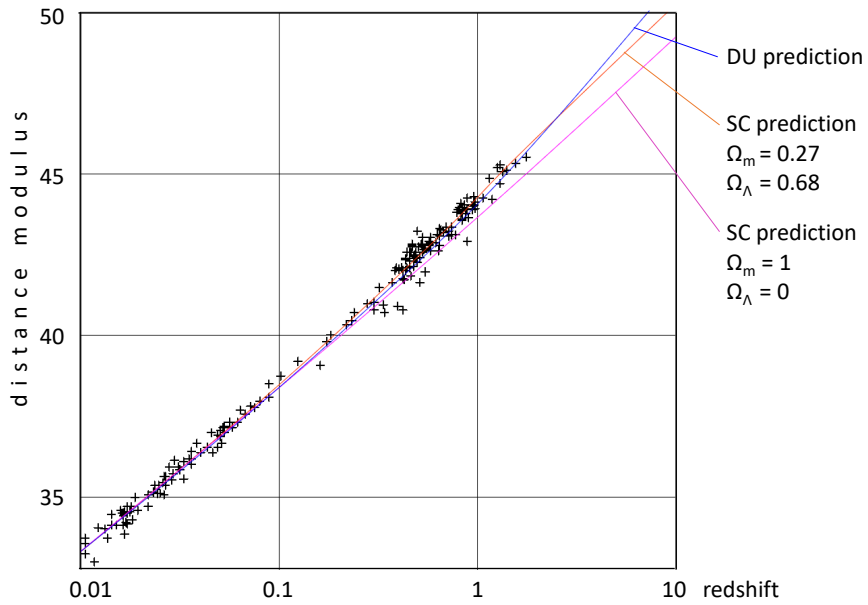

Figure 3: Riess et al. [1] dataset of Ia supernovae (crosses). Distance modulus $\mu = m - M$, where m is the apparent magnitude or the observed brightness and M is the absolute or actual magnitude. The K-corrected SC predictions are obtained by giving the density parameter the value $\Omega_m = 1$ for the lower curve, and $\Omega_m = 0.27$ and $\Omega_\Lambda = 0.73$ for the higher curve.

confidence in SC. First, the survey of Frieman et al. [18] indicates that significant amounts of money have been invested in attempts to detect dark energy. Second, one half of the 2011 Nobel Prize in Physics was awarded for Ia supernova measurements, and the other half for deducing the hypothesis of dark energy and the resulting prediction that the expansion of the Universe is accelerating. However, the general attitude has been changing, partly due to the findings of the James Webb Space Telescope. For instance, Particle Data Group [54, p. 440] states that "it may be that the phenomenon of dark energy is entirely illusory".

9. *K-correction.* In SC, in bandpass photometry measurements, direct observations are K-corrected, meaning filter mismatch correction and their conversion to the 'emitter's rest frame' (Kim et al. [28]). In the case of Ia supernovae (Ex. 8) the measured bolometric peak magnitudes are converted to the rest frame of the supernovae, by multiplying the observed magnitudes by the energy dilution factor $\sim (1 + z)^2$ in the K-correction. The DU prediction (§6.3.1–4) matches the measured bolometric peak magnitudes of normal Ia supernovae (Tonry [2, p. 14, Table 7]) with only the filter mismatch correction, i.e., without a conversion to emitter's rest frame. Thus, from the DU aspect, the SC conversion to emitter's rest frame appears as data modification, one that was probably made unknowingly, while being immersed in the SC reality. DU re-

veals the reason for the extra $(1+z)^2$ for energy dilution in the SC conversion. First, Tolman [79] applied comoving distance, namely the current distance of the perceiver and the emitter, as the basis for areal dilution. In SC, in the redshift range [1 2] relevant to Ia supernova observations, the use of co-moving distance results approximately in an extra $1+z$ power dilution. DU gets by without the extra $1+z$ by applying light travel distance or optical distance, namely the distance that light has traveled since the emission (DU eq. 6.2.2:2). Second, Tolman applied double redshift dilution $(1+z)^2$, motivated both by the Doppler effect (which was the original interpretation of redshift) and the Planck equation, whereas a single redshift dilution $(1+z)$ suffices for DU where the Planck equation describes the emission/absorption event (DU §5.1.1).

10. *Conservation of CMB energy.* In SC the cosmic microwave background radiation (CMB) energy density [J/m^3] decreases by the factor $(1+z)^{-4}$ due to the expansion of space, while the volume of space increases by the factor $(1+z)^3$. Given that the redshift of CMB is 1090, the current energy of the CMB is $(1+z)^3/(1+z)^4 = 1/(1+z) = 1/1091$ of its energy at the time of emission, i.e., less than 0.1% of the original CMB energy. This conforms to Tolman's [79, §6] law for radiation energy dilution. In DU, the rate of CMB energy density dilution, $(1+z)^{-3}$, and the rate at which the volume of space increases, $1/(1+z)^3$, cancel each other out, i.e., the expansion of space does not lose energy. This difference originates from interpretation of the Planck equation $E = hf$. Conventionally it describes the energy of radiation, whereas in DU it describes the event of emission or absorption of one cycle or one quantum of radiation. CMB frequency (f) decreases as its wavelength (λ) increases over time, as indicated by $f = c/\lambda$. In DU the time in which one cycle of a wave is detected increases and thus the power [J/s] of CMB is reduced, but the energy carried by each cycle is conserved (DU §6.4.1). Adopting the DU interpretation of the Planck equation in SC would require reworking cosmological distance definitions, which would have profound implications.

11. *Formation of galaxies.* Data from the James Webb Space Telescope reveals that galaxies formed much earlier than anticipated based on SC. Frank and Gleiser [17] suggest that resolving this discrepancy may involve a new type of 'dark' element or a radical departure from SC. DU appears to align with the data, as it entails that all processes were faster in the past, up to four times at $z = 15$ and ten times at $z = 100$.

12. *Angular size of galaxies.* SC predicts that when $z > 1$, the greater is z, the greater is the apparent angular size of an object, i.e., the greater the object appears to us (Etherington [12]). The SC prediction does not match the data from Nilsson et al. [49], which demonstrates that the apparent angular size of a galaxy and a quasar decreases in direct proportion to its redshift, as shown in Figure 4. According to López-Corredoira [8, p. 4–12] several tests reveal the discrepancy with

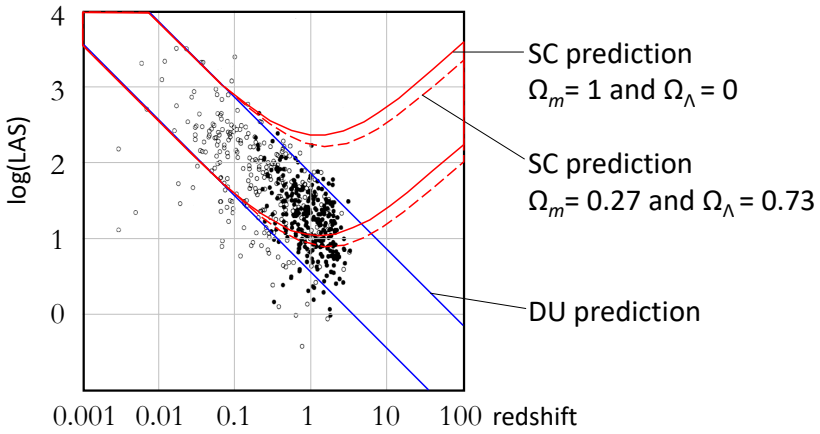

Figure 4: Nilsson et al. [49] dataset of quasars (filled circles) and galaxies (open circles) in the redshift range $0.001 < z < 3$. LAS = Largest Apparent Angular Size.

the SC prediction. DU predicts that the apparent size of an object whose parts are gravitationally bound decreases in direct proportion to the increase of z. The central explanatory factor here is that, unlike GR, DU does not require a reciprocity assumption, and in DU gravitationally bound objects like galaxies and planetary systems expand in direct proportion to the expansion of space, as in Ex. 13–16. (DU §1.3.2–3, eq. 6.2.1:2, §6.2.3, eq. 6.2.3:2, Suntola [77, pp. 92–93]).

Expansion of the Solar System

De Sitter [68] established the standard view that local gravitationally bound systems, such as planetary systems and galaxies, do not expand with the expansion of space, but only the space between galaxies expands. The *no-local-expansion hypothesis* likely stems from the aim of energy conservation: non-expanding local systems conserve energy, whereas expanding ones would necessitate energy bookkeeping not found in GR. Examples 13–16 show that a substantial amount of evidence has accumulated since 1930's that challenges the no-local-expansion hypothesis. However, since expansion of local systems would undermine GR, physicists have proposed various additional hypotheses to sustain the no-local-expansion hypothesis. In DU's *uniform expansion hypothesis* all gravitationally bound systems expand in direct proportion to the expansion of space, whereas compact objects such as planets and atoms, that are also bound by stronger interactions, do not expand. DU's energy bookkeeping ensures the conservation of total energy during the expansion (DU §6.2.2). According to Sipilä [66] the uniform expansion hypothesis "does not *add* complexity to cosmology or to physics in general, but makes it more uniform, for it merely *removes* the special convention that gravitationally bound systems do not expand, while the Universe as a whole does expand".

13. *The Earth-Sun Distance.* According to Krasinsky and Brumberg [32] measurements of interplanetary distances suggest an increase in the Earth-Sun distance, aka the astronomical unit (au), by 15±4 m per sidereal year, which is at odds with the no-local-expansion hypothesis. According to Iorio [24] "the alleged anomaly motivated many researchers to find viable explanations in terms of various either conventional or unconventional physical mechanism". Krasinsky and Brumberg [32, p. 275] suggest that the *Einstein effect* eliminates the increase of au: "This effect is caused by the rate clock difference between the observer's atomic time scale and the time scale of the equations of motion". Iorio [24] suggests that the measured increase of au is no longer a problem because the International Astronomical Union defined au as a constant in 2012.

    In DU, the focal measurements directly show the extended distances. If the Solar System were to expand at the Hubble constant rate of ≈ 70 (km/s)/Mpc, the astronomical unit (au) would increase annually by about 10.65 m, which is quite close to 15 ± 4 m.[7] King and Sipilä [29] argue that the uniform expansion also holds for gravitationally bound subsystems of the Solar System. For instance, the measured annual recession of Titan from Saturn is 11 cm. Based solely on $H_0 \approx 70$ (km/s)/Mpc, the rate of Titan's annual recession would be 8.6 cm. This leaves only 2.4 cm to be explained by tidal friction, which is proportional to the tidal friction in the recession of the Moon (Ex. 16).

14. *The Faint Young Sun paradox.* Solar luminosity or the radiation efficiency of the Sun has been increasing approximately 7% in a billion years (Bahcall et al. [5]). This implies that the Sun was $\sim$ 25–30% less luminous 3.8 billion years ago (Gya).[8] Together the faint young Sun and the no-local-expansion hypothesis suggest that Earth would have been globally glaciated 3.8–2.5 Gya. However, geological evidence suggests the presence of liquid water on Earth's surface during this period. Initially, Sagan and Mullen [59] proposed a massive greenhouse effect as an explanation for the discrepancy. Other solutions have been proposed later. For instance, Spalding and Woodward [69, p. 28] argue that Earth's earlier faster spin rate enables a warm equator while preserving cold poles. DU predicts that the Earth was closer to the Sun 3.8 Gya, which allows existence of liquid water and higher mean temperature, even with $25 - 30\%$ smaller solar luminosity.

    Together the faint young Sun and the no-local-expansion hypothesis suggest that Mars was much colder 3.8 Gya than currently ($\sim -63\,^\circ$C). But there is

[7] First, the Hubble constant ≈ 70 (km/s)/Mpc, and the number of seconds in a year $\approx 365 \times 24 \times 60 \times 60$. We get $365 \times 24 \times 60 \times 60$ s $\times$ 70 (km/s)/Mpc = 220 752 000 0 km/Mpc, i.e., a stretch of 1 Mpc expands 220 752 000 0 km per year. The current Earth-Sun distance $\approx 149 \times 10^6$ km, and 1 Mpc $\approx 3.086 \times 10^{19}$ km. Thus, the annual increase of the Earth-Sun distance should be 220 752 000 0 km $\times$ (149 $\times 10^6$ km / 3.086 $\times 10^{19}$ km) ≈ 10.65 m. In DU the corresponding annual increase of Earth's orbital period is 3.4×10^{-3} s (DU §5.6.2).

[8] In DU '3.8 Gya' is translated as 'when the 4-radius of the Universe was 3.8 billion light years shorter', which makes up 3.52 billion years, based on current International Atomic Time seconds.

evidence of liquid water on Mars back then. Various mechanisms, such as greenhouse effects, impact-induced melting, volcanic activity and hydrothermal systems have been proposed to explain the discrepancy (Ojha et al. [50] and Batalha et al. [6, p. 7]). The findings of NASA Curiosity Rover indicate that there was not enough CO_2 to maintain surficial water (Bristow et al. [4, p. 2166]). As a remedy, Kite et al. [30] suggest that a non-CO_2 gas is needed to warm early Mars, and Batalha et al. [6, p. 7] suggest a geophysical mechanism where the "greenhouse effect is enhanced by substantial amounts of H_2 outgassed from Mars' reduced crust and mantle". DU predicts that Mars was closer to the Sun in the past, at a distance where liquid water was possible even with the smaller Solar luminosity at least around the equator of Mars (Sipilä [66, §2], DU §1.3.1). As the Solar System expanded, Mars moved farther, its temperature decreased and its water turned into ice.

15. *Variation in the number of days in a year.* Coral fossil data indicates that the number of days in a year has decreased steadily for hundreds of millions of years, as illustrated in Figure 5 (Eicher [11, p. 117]). The standard explanation in the context of the no-local-expansion hypothesis is based solely on the decrease of the spin rate of Earth due to tidal friction. Mathews and Lambert's [42] prediction that tidal friction slows down the day 2.5 ms per 100 y does not match the coral fossil data. The discrepancy remains unexplained. The DU prediction combines the effect of tidal friction on the length of a day, with the effect of the expansion of the Solar System on the length of a year —as Earth's orbit expands, its orbital velocity decreases and the year gets longer (Sipilä [66, §3], DU §5.6.3). A perfect match with the coral fossil data is obtained with $H_0 = 70$ (km/s)/Mpc. And vice versa, the coral fossil data provides a basis for estimating the Hubble constant as $H_0 = 70\pm\ 2$ (km/s)/Mpc independently of cosmological observations.

16. *Increase of the Earth-Moon distance.* The present average Earth-Moon distance is 384400 km, and the length of a sidereal month is 27.322 days, which corresponds to $365.242374/27.322 \approx 13.368$ sidereal months in a year. Williams [83] maintains that 635 million years ago (Mya) there were 14.1 ± 0.1 sidereal months in a year.[9] The task is to explain the 0.732 difference in sidereal months in a year.

    Given the no-local-expansion hypothesis, the length of a year is constant. Thus, the explanation for the 0.732 sidereal months difference is that the orbital period of the Moon has been shorter in the past, which follows from a shorter orbit and a faster orbital velocity, which follow from a shorter Earth-Moon distance in the past. Thus, the task is to explain the annual Moon retreat or why the Earth-Moon distance has been increasing in just the way that yields 14.1 ± 0.1 sidereal months in a year 635 Mya. Given that the length of a year is constant, 635 Mya

[9] Williams [83] studied a 620 My old sandstone deposit. In private communication with Sipilä he revised the dating to 635 My (Sipilä [66]).

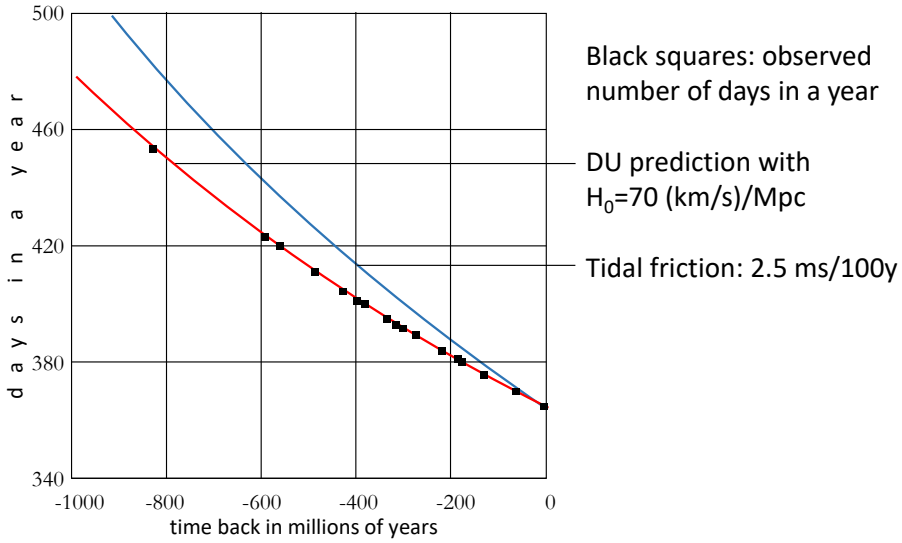

Figure 5: Variation in the number of days in a year.

there were 365.2422/14.1 ≈ 25.9 current days in one sideral month. Therefore, the sidereal month was 25.9/27.322 ≈ 0.948 times the present sidereal month. Therefore, based on Kepler's 3rd law the Earth-Moon distance was $0.948^{2/3} \times 384\,400 = 370\,956$ km, which is 384 400 km – 370 956 km = 13 444 km less than the current Earth-Moon distance. This gives 13 444 km / 635 My ≈ 2.1 cm/y as the average annual Moon retreat, which is substantially less than today's 3.82 cm/y. Given today's 3.82 cm/y and the average 2.1 cm/y since 635 My, if the rate has been linearly increasing, the rate at −635 My was 0.38 cm/a, and the rate at −705 My was 0 cm/y. These calculations are very approximate, but the average 2.1 cm/y since 635 My is a clear anomaly. As a remedy, Williams [83, p. 55] suggests that the "present high rate of lunar recession may reflect the near resonance of oceanic free modes and tidal frequencies". This hypothesis is at odds with Mathews and Lambert's [42] result that there are no jumps in the effect of tidal friction to length of the day (Ex. 15).

Van Flandern [15] noticed already in 1975 that tidal friction explains only about 55% of today's 3.82 cm/y Moon retreat (cf. Křížek and Somer [33, p. 186]). The uniform expansion hypothesis, with the Hubble constant 70 (km/s)/Mpc, entails that 2.75 cm of the annual Moon retreat results from the expansion of space, and only 3.82 cm – 2.75 cm = 1.07 cm needs to be explained by tidal effects. The uniform expansion hypothesis also entails that the length of a year 635 Mya was 349 current days. Therefore, the length of a sidereal month was 349/14.1 = 24.8 current days. Therefore, the sidereal month 635 Mya was 24.8/27.3 ≈ 0.9084 times the present sidereal month. Applying Kepler's 3rd law, the Earth-Moon distance was $0.9084^{2/3} \times 384\,400 = 360\,552$ km, i.e., the distance has increased

$384\,400 - 360\,552 = 23\,848$ km in 635 My. This gives 23 848 km / 635 My ≈ 3.755 cm/y as the average Moon retreat rate, which is close to today's 3.82 cm/y. (DU §5.6, Sipilä [67] [66, ch. 4]).

5. Criteria, dogmatism and theory proliferation

The previous section indicates that classical criteria favor DU over RP as an explanation for many central phenomena. This raises the question of whether it is still optimal for physics and for society in general to prioritize consistency and familiarity with RP over classical criteria. Currently, an influential class of physicists regards relativistic theories as the sole correct options, while disregarding the merits of rival theories. Public review policies signal fair evaluation, but in practice the peer review system functions as a method of censorship that upholds established theories, and rejects alternative theories by an editorial decision when inconsistency with the established theory is found in the title or in the abstract (López-Córredoira [8, §8.3.4], [38, pp. 8, 72], Panarella [53, p. 3]). López-Corredoira [8, §8.3.7] and Dawid [9, p. 24] recognize *groupthink* as one reason behind the social phenomenon: "the members of a group may be forced into the unreflected adoption of the group's standard positions by a mix of intellectual group pressure, admiration for the group's leading figures and the understanding that fundamental dissent would harm career perspectives. An all too positive and uncritical self-assessment of the group is the natural consequence".

López-Corredoira [38, pp. 188–190] advocates for a system that could remedy unfair peer review decisions and transform natural science into "an open space belonging to all those restless minds who want to think about how nature is, rather than a feud between a few owners who want to defend their status." On the other hand, physics journals receive numerous heterogeneous submissions, and understanding the mechanisms of a fundamentally different alternative theory can be challenging and time-consuming, even for those willing to try. Transparent criteria could tackle both dogmatism and the excessive proliferation of theories in physics. Journals could openly articulate their evaluation criteria, subject them to scrutiny by physicists and philosophers, and seriously consider any violations or adherence. This suggestion is in line with Maxwell's [43] *aim-oriented empiricism*, where joint efforts of physicists and philosophers of science would generate positive feedback between improving physical theories and the aims and methods of physics. Under the proposed criteria, inconsistency with the standard theory would not be among the reasons why a rival theory could be justifiably rejected, but the criteria would be so strict that only good candidates would pass the evaluation: a reviewer should assess whether a rival theory adheres to ethical, explanatory, and pragmatic virtues.

Relativistic dogmatism has a long history. In 1931, Hjalmar Mellin [46] declared that science is no longer free as "the most influential positions in universities and colleges and the most widely circulated scientific journals are held by Einsteinians, who try to prevent their opponents from entering similar positions and presenting

their anti-Einstein opinions".[10] Suntola [72, p. 54] points out that peer reviewers are often those who have the best command of current theories and who are the most committed to them. This echoes Planck's [55, pp. 33–34] notion that a "new scientific truth does not triumph by convincing its opponents and making them see the light, but rather because its opponents eventually die and a new generation grows up that is familiar with it". But new generations do not get familiar with new truths, as they are taught standard theories as the only available *physics* at universities. Feyerabend [14, pp. 42–45] identifies the cycle of dogmatism: the only genuine way to scrutinize the all-embracing principles of a standard theory is to compare them with equally comprehensive principles of an alternative theory, but the consistency criterion precludes this process right from the start.

One cannot avoid the feeling of social injustice whenever the proponents of RP embrace its correctness, with no second thoughts about relativistic methodology, where anomalous data may be dismissed by accommodating it with additional hypotheses, disregarding it, or even modifying it. To make genuine dialogue possible, philosophy of science should be strongly integrated into physics education —or into all education, from kindergarten to universities. If physicists generally understood the cornerstones of the philosophy of science —such as that observations are often theory-laden, that they are not being taught absolute truths but provisional theories likely to be replaced in the future, that there are other immensely important criteria in addition to the accuracy of predictions, and that these help to separate, for example, legitimate and illegitimate ways to produce a prediction— they would inevitably be more open to alternatives and more willing to engage in dialogue.

6. Conclusions

Within the scope of the given examples, the Dynamic Universe meets the classical criteria much better than Relativistic Physics.

First, RP violates some ethical virtues, that are respected by DU. The *conversion to emitter's rest frame* in the K-correction appears a modification of anomalous data to make it match the SC prediction (Ex. 9). The Scout-D experiment was accommodated using a non-derived formula (Ex. 3). GR's missing explanation for the development of the number of days in a year appears as disregard of anomalous data (Ex. 15). That GR's textbook approximations yield Mercury's escape appears as an unrecognized predictive failure (Ex. 5).

Second, when DU and RP are assigned the scope of the given examples, and their basic structures are considered to have equal ontological weight, DU has a much

[10]For the record, while acting on the board of The Finnish Society for Natural Philosophy, I found that the attitudes of Finnish physics professors (a-e) toward DU are uncompromisingly dogmatic: (a) DU is wrong because it is not physics; DU is not physics because it is wrong. (b) Science is open to new workable ideas; if DU were workable, it would already have been accepted; as DU has not been accepted, it is not workable. (c) Suntola is dangerous because he knows mathematics so well. (d) Suntola's ideas do not rise above the threshold that I would spend time on them. (e) Before I comment on DU, it must explain the polarization of the cosmic background radiation spectrum.

smaller total ontological weight and therefore a much greater unifying power. For, RP deploys a considerable amount of additional hypotheses not required by DU, including baryogenesis to explain matter-antimatter asymmetry (Ex. 6), theories of inflation and graceful exit (Ex. 7), dark energy for explaining supernova perceptions (Ex. 8), frameworks for unifying GR and QM (Ex. 4), rotational velocity of a black hole in Kerr metric (Ex. 5), and hypotheses for defending the no-local-expansion hypothesis, in the context of evolution of the Earth-Sun distance (Ex. 13), evolution of the Earth-Moon distance (Ex. 16) and the Faint young Sun paradox (Ex. 14). Furthermore, RP's explanatory failures such as the incorrect prediction of the angular size of galaxies (Ex. 4), the unrecognized data modification in the K-correction (Ex. 9), the missing explanation for the development of the number of days in a year (Ex. 15), the unrecognized problem of Mercury's escape (Ex. 5) and the missing consensual dynamic explanation for atomic clocks (Ex. 4) decrease RP's scope. Then again, if these problems will be remedied with the help of additional hypotheses, such as a hypothetical mechanism for GR's dynamic explanation for atomic clocks, they will increase RP's ontological weight. The ad hoc accommodation is so common to the relativistic thoeries that is deserves to be recognized as the gold standard of the relativistic method. Of course, this feature is naturally coupled with the belief that actually none of the auxiliaries are ad hoc. Perhaps this belief can be legitimized by formulating a convenient definition of ad hocness, echoing Quine's insight that a belief may be sustained come what may, by making changes elsewhere in the system.

Third, DU appears pragmatically more virtuous than RP. As a single theory with a definite geometry of space DU is easier to learn and to understand than SR, GR and SC, where SC leaves geometry of the whole space open. RP especially makes nature non-understandable, whereas DU yields an in principle understandable picture or reality (Ex. 2). Notably, I am not arguing that DU is *easy* to understand. On the contrary, one we look behind to hood of the 3-sphere geometry and the zero-energy principle, sufficient comprehension of DU's basic structure requires a deep study into the foundations. However, once it is properly understood, it can be seen how DU's basic dynamic explanation yields various unique novel predictions. In contrast, in RP there have been difficulties in choosing whether to apply SR or GR, the relativity principle is upheld in SR but contravened in GR (Ex. 1 & 3), there are different metrics for different situations, and GR's syntactic complexity exceeds DU's syntactic complexity (Ex. 5).

These results have bearings for the fitness of DU and RP as alternative research programs. Thus far, the work of a single person with DU has yielded outstanding results, such as providing novel predictions of phenomena that hundreds of physicists have investigated for over 100 years in the context of RP, resulting in their orderly ad hoc accommodation. According to classical criteria, this suggests that RP is in a stage of decline. After its initial triumphs, its problems have escalated. The general public is becoming increasingly aware of the problems of standard cosmology, although it is not yet widely recognized that the roots of these problems lie in SR

and GR. Meanwhile, an increasing number of physicists have lost confidence in RP as a whole and have begun to search for fundamentally different theories that could overcome its main challenges. If RP were replaced, its development would perfectly match the Kuhnian model. Relativistic methodology hinders this transition, as it characteristically tries to conceal the fallacies of RP, primarily by legitimizing the orderly accommodating data with the help of additional hypotheses, and secondarily by ignoring anomalous data and even by modifying it. Given these tools and the manifest image of a flawless theory, it is natural to supress all competition in the education system and in the peer review processes of journals and funding institutions. In light of the present evaluation, it is evident that contemporary dogmatism is seriously impeding the progress of physics.

Suppose that DU were allocated, say, for period of 10 years, 1‰ or even 0.1‰ of the funding currently allocated to RP. Given DU's current track record, such funding would likely lead to further achievements and solidify DU's position as a viable research program. One could take these funds, for instance, from cosmological research projects, which DU renders obsolete, such as baryogenesis, inflationary cosmology, and large-scale projects aimed at detecting dark energy. However, due to contemporary dogmatism in physics, it seems that this scenario will remain a mere dream in the near future. As a long-term remedy, I propose two actions: (1) journals should adopt transparent evaluation criteria, subject them to scrutiny by scientists and philosophers, and ensure they are respected by peer reviewers; (2) the philosophy of science should be comprehensively integrated into educational programs.

Acknowledgements

I thank Tuomo Suntola, Heikki Sipilä and Michal Křížek and for comments.

References

[1] A. G. R. et al. "Type Ia Supernova Discoveries at z > 1 from the Hubble Space Telescope: Evidence for Past Deceleration and Constraints on Dark Energy Evolution". In: *The Astrophysical Journal* 607.2 (Apr. 2004), pp. 665–687. DOI: 10.1086/383612.

[2] J. L. T. et al. "Cosmological Results from High-z Supernovae". In: *Astrophysical Journal* 594.1 (Sept. 2003), pp. 1–24. DOI: 10.1086/376865.

[3] T. B. et al. "Resolving the gravitational redshift across a millimetre-scale atomic sample". In: *Nature* 602 (7897 2022), pp. 420–424. DOI: 10.1038/s41586-021-04349-7.

[4] T. F. B. et al. "Low Hesperian P_{CO2} constrained from in situ mineralogical analysis at Gale Crater, Mars". In: *PNAS* 114.9 (Feb. 2017), pp. 2166–2170.

[5] J. N. Bahcall, M. Pinsonneault, and S. Basu. "Solar Models: Current Epoch and Time Dependences,Neutrinos, and Helioseismological Properties". In: *The Astrophysical Journal* 555.2 (Apr. 2001), pp. 990–1012. DOI: 10.1086/321493.

[6] N. E. Batalha et al. “Climate cycling on early Mars caused by the carbonate-silicate cycle”. In: *Earth and Planetary Science Letters* 455 (2016), pp. 7–13. DOI: 10.1016/j.epsl.2016.08.044.

[7] M. Berry. *Principles of cosmology and gravitation*. Cambridge University Press, 1989.

[8] M. L. Corredoira. *Fundamental Ideas in Cosmology: Scientific, philosophical and sociological critical perspectives*. Bristol, UK: IOP Publishing, 2022.

[9] R. Dawid. *String Theory and the Scientific Method*. Cambridge University Press, 2013.

[10] H. E. Douglas. “Reintroducing Prediction to Explanation”. In: *Philosophy of Science* 76.4 (2009), pp. 444–463.

[11] D. L. Eicher. *Geologic time*. London: Prentice/Hall International Inc., 1976.

[12] I. M. Etherington. “LX. On the definition of distance in general relativity”. In: *The London, Edinburgh, and Dublin Philosophical Magazine and Journal of Science* 15.100 (1933), pp. 761–773. DOI: 10.1080/14786443309462220.

[13] L. Felline. “Mechanistic Explanation in Physics”. In: *The Routledge Companion for Philosophy of Physics*. Ed. by E. Knox and A. Wilson. Routledge, 2021. Chap. 33, pp. 476–486.

[14] P. K. Feyerabend. *Against Method: Outline of an Anarchistic Theory of Knowledge*. 3rd ed. London: Verso, 1993.

[15] T. C. V. Flandern. “A Determination of the Rate of Change of G”. In: *Mon. Not. R. astr. Soc.* 170 (1975), pp. 333–342.

[16] J. Foster and J. Nightingale. *A Short Course in General Relativity*. 2nd ed. Springer, 2001.

[17] A. Frank and M. Gleiser. “The Story of Our Universe May Be Starting to Unravel”. In: *The New York Times* (Sept. 2023). DOI: https://www.nytimes.com/2023/09/02/opinion/cosmology-crisis-webb-telescope.html.

[18] J. A. Frieman, M. S. Turner, and D. Huterer. “Dark Energy and the Accelerating Universe”. In: *Annual Review of Astronomy and Astrophysics* 46.1 (2008), pp. 385–432. DOI: 10.1146/annurev.astro.46.060407.145243.

[19] P. Geach. *Logic Matters*. Oxford: Oxford University Press, 1972.

[20] R. Genzel et al. “Near-infrared flares from accreting gas around the supermassive black hole at the Galactic Centre”. In: *Nature* 425.6961 (Oct. 2003), pp. 934–937. DOI: 10.1038/nature02065.

[21] B. Gower. *Scientific Method: A Historical and Philosophical Introduction*. New York: Routledge, 1996.

[22] A. H. Guth. "The Inflationary Universe: A Possible Solution to the Horizon and Flatness Problems". In: *Physical Review D* 23 (1981), pp. 347–356. DOI: 10.1103/PhysRevD.23.347.

[23] J. Hafele and R. Keating. "Around-the-World Atomic Clocks: Predicted Relativistic Time Gains". In: *Science* 177 (4044 1972), pp. 166–8.

[24] L. Iorio. "Gravitational anomalies in the solar system?" In: *International Journal of Modern Physics D* 24.06 (2015), p. 1530015.

[25] M. Janssen and J. Renn. *How Einstein Found His Field Equations: Sources and Interpretation*. Springer International Publishing, 2022.

[26] E. Kaila. *Human Knowledge: A Classic Statement of Logical Empiricism*. Translated by Anssi Korhonen. Edited by Juha Manninen, Ilkka Niiniluoto and George A. Reisch. Originally published in 1939 as *Inhimillinen Tieto: Mitä se on ja mitä se ei ole*. Chicago, Illinois: Open Court, 2014.

[27] M. N. Keas. "Systematizing the Theoretical Virtues". In: *Synthese* 195.6 (2018), pp. 2761–2793.

[28] A. Kim, A. Goobar, and S. Perlmutter. "A Generalized K Correction for Type IA Supernovae: Comparing R-band Photometry beyond z=0.2 with B, V, and R-band Nearby Photometry". In: *Publications of the Astronomical Society of the Pacific* 108 (Feb. 1996), pp. 190–201.

[29] L. A. King and H. Sipilä. "Cosmological expansion in the Solar System". In: *Physics Essays* 35.2 (2022), pp. 139–142. DOI: 10.4006/0836-1398-35.2.139.

[30] E. S. Kite et al. "Changing spatial distribution of water flow charts major change in Mars's greenhouse effect". In: *Science Advances* 8.21 (2022), eabo5894. DOI: 10.1126/sciadv.abo5894.

[31] D. Kleppner, R. F. Vessot, and N. F. Ramsey. "An orbiting clock experiment to determine the gravitational red shift". In: *Astrophysics and Space Science* 6 (1 Jan. 1970), pp. 13–32. DOI: 10.1007/BF00653616.

[32] G. A Krasinsky and V. A. Brumberg. "Secular increase of astronomical unit from analysis of the major planet motions, and its interpretation". In: *Celestial Mechanics and Dynamical Astronomy* 90 (3 2004), pp. 267–288. DOI: 10.1007/s10569-004-0633-z.

[33] M. Křížek and L. Somer. *Mathematical Aspects of Paradoxes in Cosmology*. Springer Cham, 2023. DOI: 10.1007/978-3-031-31768-2.

[34] T. Kuhn. "Objectivity, Value Judgment, and Theory Choice". In: *The Essential Tension*. University of Chicago Press, 1977, pp. 320–39.

[35] T. Kuhn. *The Structure of Scientific Revolutions*. 2nd ed. Chicago: University of Chicago Press, 1970.

[36] I. Lakatos. "Falsification and the Methodology of Scientific Research Programmes". In: *Criticism and the Growth of Knowledge: Proceedings of the International Colloquium in the Philosophy of Science, London, 1965*. Ed. by I. Lakatos and A. Musgrave. Cambridge University Press, 1970, pp. 170–196.

[37] A. Liddle. *An Introduction to Modern Cosmology*. 3rd ed. John Wiley & Sons, 2015.

[38] M. López-Corredoira. *The Twilight of the Scientific Age*. BrownWalker Press: Boca Raton, Florida, 2013.

[39] D. H. Lyth and A. R. Liddle. *The Primordial Density Perturbation: Cosmology, Inflation and the Origin of Structure*. Cambridge University Press, 2009. DOI: 10.1017/CBO9780511819209.

[40] A. Mackonis. "Inference to the Best Explanation, Coherence and Other Explanatory Virtues". In: *Synthese* 190.6 (2013), pp. 975–995.

[41] G. B. Malykin. "Method for Experimental Verification of the Effect of Gravitational Time Dilation by Using an Active Hydrogen Maser". In: *Radiophysics and Quantum Electronics* 58 (4 2015), pp. 290–295. DOI: 10.1007/s11141-015-9603-4.

[42] Mathews, P. M. and Lambert, S. B. "Effect of mantle and ocean tides on the Earth's rotation rate". In: *Astronomy & Astrophysics* 493.1 (2009), pp. 325–330. DOI: 10.1051/0004-6361:200810343.

[43] N. Maxwell. "Unification and Revolution: A Paradigm for Paradigms". In: *Journal for General Philosophy of Science* 45.1 (2014), pp. 133–149. DOI: 10.1007/s10838-013-9225-5.

[44] E. McMullin. "The Virtues of a Good Theory". In: *The Routledge companion to philosophy of science*. Ed. by M. Curd and S. Psillos. New York: Routledge, 2014, pp. 561–571.

[45] E. McMullin. "Values in Science". In: *Proceedings of the Biennial Meeting of the Philosophy of Science Association*. Ed. by P. D. Asquith and T. Nickles. Vol. 1. Philosophy of Science Association, 1982, pp. 3–28.

[46] H. Mellin. "Einsteinin teorian mahdottomuus". In: *Suomalainen tiedeakatemia: esitelmät ja pöytäkirjat 1931*. Ed. by G. Komppa. Teksti 10.10.1931 esitelmästä. Helsinki: Suomalainen tiedeakatemia, 1932, pp. 67–74.

[47] C. W. Misner, K. S. Thorne, and J. A. Wheeler. *Gravitation*. New York: W.H. Freeman, 1973.

[48] I. Niiniluoto. *Descriptive and Inductive Simplicity,* in W. Salmon and G. Wolters (eds.), *Logic, Language, and the Structure of Theories, Proceedings of the Carnap-Reichenbach Centennial, University of Konstanz, 21.-24. May 1991,* pp. 147-70. Pittsburgh: University of Pittsburgh Press/Universitätsverlag Konstanz, 1994.

[49] K. Nilsson et al. “On the Redshift–Apparent Size Diagram of Double Radio Sources”. In: *The Astrophysical Journal* 413 (Aug. 1993), pp. 453–476. DOI: 10.1086/173016.

[50] L. Ojha et al. “Amagmatic hydrothermal systems on Mars from radiogenic heat”. In: *Nature Communications* 12 (1 Mar. 2021), p. 1754. DOI: 10.1038/s41467-021-21762-8.

[51] V. V. Okorokov. “On a Discrepancy of Experiments Supporting Certain Conclusions of General Relativity”. In: *Doklady Physics* 46.6 (2001), pp. 400–402. DOI: 10.1134/1.1384934.

[52] L. Okun’ and K. Selivanov. “On the consistency of experiments supporting general relativity”. In: *Doklady Physics* 47.6 (2002), p. 461. DOI: 10.1134/1.1493388.

[53] E. Panarella. “Editorial: Fifteen Years Later”. In: *Physics Essays* 16.1 (2003), p. 3.

[54] R. L. W. et al (Particle Data Group). “Review of Particle Physics”. In: *Progress of Theoretical and Experimental Physics* 2022 (2022), p. 083C01. DOI: 10.1093/ptep/ptac097.

[55] M. Planck. *Scientific Autobiography and Other Papers*. New York: Philosophical Library, 1949.

[56] W. V. O. Quine. “Two Dogmas of Empiricism”. In: *The Philosophical Review* 60.1 (1951), pp. 20–43.

[57] A. Riotto and M. Trodden. “Recent Progress in Baryogenesis”. In: *Annual Review of Nuclear and Particle Science* 49.1 (1999), pp. 35–75. DOI: 10.1146/annurev.nucl.49.1.35.

[58] A. A. Robb. *The Absolute Relations of Time and Space*. Cambridge: Cambridge University Press, 1921.

[59] C. Sagan and G. Mullen. “Earth and Mars: Evolution of Atmospheres and Surface Temperatures”. In: *Science* 177.4043 (1972), pp. 52–56. DOI: 10.1126/science.177.4043.52.

[60] A. D. Sakharov. “Violation of CP invariance, C asymmetry, and baryon asymmetry of the universe”. In: *Soviet Physics Uspekhi* 34.5 (1991), pp. 392–393. DOI: 10.1070/PU1991v034n05ABEH002497.

[61] W. C. Salmon. *Scientific Explanation and the Causal Structure of the World*. Princeton University Press, 1984.

[62] R. Schlegel. “Relativistic East-West Effect on Airborne Clocks”. In: *Nature Physical Science* 229 (8 Feb. 1971), pp. 237–238. DOI: 10.1038/physci229237a0.

[63] G. Schurz. *Philosophy of Science: A Unified Approach*. Routledge, 2013.

[64] B. Schutz. *A First Course in General Relativity*. 3rd ed. Cambridge University Press, 2022.

[65] T. Shioyama. *Newton, Faraday, Einstein: From Classical Physics To Modern Physics*. Singapore: World Scientific Publishing Company, 2021.

[66] H. Sipilä. "Is the Solar System expanding?" In: *Unification in Physics and Philosophy 9-11 May 2019, Porvoo and Helsinki, Finland*. Ed. by A. Styrman. Vol. 1466. IOP Publishing, Feb. 2020, p. 012004. DOI: 10.1088/1742-6596/1466/1/012004.

[67] H. Sipilä. "Recalculation of the Moon Retreat Velocity Supports Expansion of Gravitationally Bound Local Systems". In: *Proceedings of the International Conference Cosmology on Small Scales 2022: Dark Energy and the Local Hubble Expansion Problem. Prague, September 21-24, 2022*. Ed. by M. Křížek and Y. V. Dumin. https://css2022.math.cas.cz/proceedingsCSS2022.pdf. Prague: Institute of Mathematics, Czech Academy of Sciences, 2022, pp. 30–32.

[68] W. de Sitter. "Do the galaxies expand with the universe?" In: *Bulletin of the Astronomical Institutes of the Netherlands* 6.223 (1931), p. 146.

[69] C. Spalding and W. W. Fischer. "A shorter Archean day-length biases interpretations of the early Earth's climate". In: *Earth and Planetary Science Letters* 514 (2019), pp. 28–36. DOI: 10.1016/j.epsl.2019.02.032.

[70] Z. Stuchlík. "Inflationary Paradigm". In: *Proceedings of the 29th Conference on Variable Star Research. 7th - 9th November 1997. Brno, Czech Republic*. Ed. by J. Dusek and M. Zejda. 1998, pp. 129–146.

[71] A. Styrman. "The Passage of Time as Causal Succession of Events". In: *The Journal of Philosophy* 120 (12 Dec. 2023), pp. 681–697. DOI: https://doi.org/10.5840/jphil20231201237.

[72] T. Suntola. "Ääri-ilmiöistä rakentavaan vuorovaikutukseen (From extreme polarisation to constructive interaction)". In: *Tieteessä tapahtuu* 32.1 (2014), pp. 49–54.

[73] T. Suntola. "In a holistic perspective, everything in space is interconnected". In: *Proceedings of the International Conference Cosmology on Small Scales 2022: Dark Energy and the Local Hubble Expansion Problem. Prague, September 21-24, 2022*. Ed. by M. Křížek and Y. V. Dumin. https://css2022.math.cas.cz/proceedingsCSS2022.pdf. Prague: Institute of Mathematics, Czech Academy of Sciences, 2022, pp. 66–84.

[74] T. Suntola. "In a holistic perspective, time is absolute and relativity a direct consequence of the conservation of total energy". In: *Physics Essays* 34.4 (2021). http://dx.doi.org/10.4006/0836-1398-34.4.486, pp. 486–501.

[75] T. Suntola. “Re-evaluation of the Scout D experiment as a Test of Relativity Theory”. In: *Galilean Electrodynamics* 14.4 (July–Aug. 2003), pp. 71–77.

[76] T. Suntola. *The Dynamic Universe: Toward a Unified Picture of Physical Reality*. 4th ed. Espoo & Helsinki: Physics Foundations Society & The Finnish Society for Natural Philosophy, 2018.

[77] T. Suntola. *The Short History of Science — or the long path to the union of metaphysics and science*. Espoo: Physics Foundations Society; Helsinki: The Finnish Society for Natural Philosophy, 2018.

[78] T. Suntola et al. “Fundamental concepts — from force to energy”. In: *International Journal of Astrophysics and Space Science. Special Issue: Quantum Vacuum, Fundamental Arena of the Universe: Models, Applications and Perspectives* 2.6-1 (2014), pp. 46–56. DOI: 10.11648/j.ijass.s.2014020601.16.

[79] R. C. Tolman. “On the Estimation of Distances in a Curved Universe with a Non-Static Line Element”. In: *Proceedings of the National Academy of Sciences of the United States of America* 16.7 (June 1930), pp. 511–520.

[80] M. Tooley. *Time, Tense and Causation*. Oxford: Oxford University Press, 1997.

[81] R. F. C. Vessot et al. “Test of Relativistic Gravitation with a Space-Borne Hydrogen Maser”. In: *Phys. Rev. Lett.* 45 (26 Dec. 1980), pp. 2081–2084. DOI: 10.1103/PhysRevLett.45.2081. URL: https://link.aps.org/doi/10.1103/PhysRevLett.45.2081.

[82] J. Weber. *General relativity and Gravitational Waves*. New York: Interscience Publishers, 1961.

[83] G. E. Williams. “Geological constraints on the Precambrian history of Earth’s rotation and the Moon’s orbit”. In: *Reviews of Geophysics* 38.1 (2000), pp. 37–59. DOI: 10.1029/1999RG900016.

Conference *Cosmology on Small Scales 2024*
Michal Křížek and Yurii Dumin (Eds.)
Institute of Mathematics CAS, Prague

SOLVING THE ENIGMA OF THE ORIGINS AND GROWTH OF SUPERMASSIVE BLACK HOLES

Yash Aggarwal

Lamont-Doherty Earth Observatory of Columbia University
Palisades, NY 10965, USA
haggarwal@hotmail.com

Abstract: We found a theoretically supported empirical relation from which the seed mass Ms of a supermassive black hole (SMBH) is ascertained. Based on theoretical considerations and observed mass M_{BH} versus age t distribution of 93 high-z (> 5.6) SMBHs, we get $M_{BH} = Ms\exp[14.6(t-100)/t]$ with age t in million years, It is applied to 132,446 SMBHs at $z < 2.4$ cataloged by Kozlowski. This relation and its derivatives are tested. The results indicate the following. Seeds $\sim 5\,M_\odot - (3\pm1)\times10^4\,M_\odot$ (solar masses) assembled at $z \sim 30$, of which 90% have $4 < 1500\,M_\odot$, account for the masses of the smallest to the largest SMBH. In particular, GNz11, CEERS_1019, and UHZ1, the recently-discovered ultra high-z AGNs require seeds $\sim 20-420\,M_\odot$. Classifying the seed population, $\sim 58\%$ are deemed light ($< 400\,M_\odot$) or Pop III remnants; $\sim 39\%$ as intermediate size ($400-3000\,M_\odot$) formed by hierarchical growth via runaway merger of BHs; and the rest $< 3\%$ as heavier seeds ($3\times10^3 - 3\times10^4\,M_\odot$) that too could have formed by mergers of BHs. Apparently, the DCBH mechanism is not required. The BH accretion rate increases exponentially reaching a broad plateau at $z \sim 8.5-6$, after which it decreases monotonically. During the first ~ 150 Myr, SMBHs may have experienced super-Eddington accretion or the radiative efficiency may have been < 0.1. The Eddington ratio and radiative efficiency are found to be functions of redshift, with the former decreasing and the latter increasing as z decreases. The maximum mass a seed can accrete via luminous accretion is $\sim 2.2\times10^6$Ms.

Keywords: black holes, redshift, Eddington ratio

PACS: 04.70.Bw, 04.50.Kd

1. Introduction

The recent discovery of GNz11, an active galactic nucleus (AGN) with an estimated mass $M_{BH} \sim 1.5\times10^6\,M_\odot$ (solar masses) at $z = 10.6$ (see e.g. [22]), implies that supermassive black holes (SMBHs) were already in place in the universe when it was only ~ 434 million years (Myr) old. The existence of such a high-z AGN and

SMBHs $> 10^{10}\,M_\odot$ less than a billion years old (see e.g. [35]) has defied comprehension of how these black holes (BHs), starting from progenitor seeds formed at earlier epochs, became so massive in such short times. Finding an answer to this dilemma requires knowledge of their size distribution and inception times. Mechanisms by which seeds may have formed have been extensively reviewed, among others, by [18] and [33] and can broadly be divided into 3 categories depending on the size of the seeds. Formation of light seeds with a typical mass of $\sim 100\,M_\odot$ resulting from the collapse of massive metal-free first stars (see [21], [14]) dubbed as Pop III remnants. Formation of heavy seeds $10^4\,M_\odot - 10^6\,M_\odot$ from the collapse of pristine gas clouds in massive dark matter halos (see [2], [6], [19], [30]) dubbed as DCBHs, or by hierarchical growth of BHs in dense stellar clusters, see [9]. And the formation of intermediate-size ($\sim 10^3\,M_\odot$) seeds via runaway collisions of stars in dense stellar clusters (see [11], [23], [28],) or by hierarchical merger of BHs in stellar clusters, see [9], [20]. Simulations attempting to understand the properties of the seeds formed by such mechanisms, drawbacks, and conditions necessary for their formation have also been extensively reviewed, see [18], [33]. It is safe to conclude that there is no consensus as to which of the proposed mechanisms may have played a dominant role and presumably cannot be ascertained without knowing the size distribution of the seeds formed.

It is now generally accepted that BH seeds formed at $z > 20$ and likely at $z \sim 30$ (see e.g. [21], [25], [37]), and the recent discovery of GNz11 at $z = 10.6$ supports such an assumption. However, how the seeds grew by many orders of magnitude in less than a billion years remains an enigma. This dilemma is best illustrated by the following case studies of 3 recently discovered SMBHs at $z > 8.6$. Larson et al. in [17] concluded that CEERS$_{-1019}$ at z ~ 8.7 and $M_{BH} \sim 9 \times 10^6\,M_\odot$ requires super-Eddington accretion from stellar-sized seeds or Eddington accretion from massive BHs seeds. Schneider [29] and Maiolino et al. in [22] concluded that GNz11 at $z = 10.6$ and $M_{BH} \sim 1.5 \times 10^6\,M_\odot$ is accreting at super-Eddington rates. And, Natrajan et al. in [24] concluded that the AGN in the galaxy UHZ1 at $z = 10.1$ with an estimated $M_{BH} \sim 4 \times 10^7\,M_\odot$ grew from a heavy seed that is probably a DCBH. While studies of individual AGNs provide valuable insights into the properties of that BH and may support a particular theory of formation or growth of BH seeds, they cannot rule out other theories or channels of seed formation, see [33]. Presumably, solving the dual interrelated enigma of the origins and growth of SMBHs requires insights and constraints derived from large sets of observational data. Hopefully, the James Web Space Telescope will provide such data in years to come. Meanwhile, a large corpus of publicly available data exists, consisting of known properties (redshift, mass M_{BH}, Eddington ratio) of over a hundred thousand AGN at various redshifts that we use to resolve the dual enigma. Specifically, this corpus consists of 93 high-z AGN at $z > 5.6$ ranging in mass over 4 orders of magnitude and ~ 600 Myr in age compiled by us, and 132,446 lower-z AGN at $z < 2.4$ with $M_{BH} > 10^7\,M_\odot$ determined using MgII lines by [16].

We begin by deconstructing and analyzing the well-known theoretical formula

for spherical accretion or the so-called Salpeter relation. Besides age t and its seed mass Ms and inception time ts, the M_{BH} of a BH depends upon a dimensionless parameter $\mathcal{V}$ that is a function of δ the duty cycle, λ the Eddington ratio, and radiative efficiency ε. We show that $\mathcal{V}$ must be an inverse function of age t such that $\mathcal{V} = \beta 45/t$, where β is a dimensionless proportionality constant; and the key to solving the equation and determining a BH's seed mass Ms knowing its M_{BH} and z is to find the value of β and seed inception time ts. Prompted by this insight, we analyze the mass versus age distribution of the 93 high-z SMBHs. The distribution reveals that a group of 60 BHs have masses within a factor of 2 despite marked differences in their ages; which leads to the formulation of 60 equations with 3 common parameters (Ms, ts, and β). Simultaneously solving these equations and subsets, we get the optimum values of β and ts. The empirical relation thus derived is first applied to the 93 high-z BHs. Conclusions drawn from an analysis of the resulting distribution of seed sizes are then tested and validated against the predicted distribution of seed sizes for the 132,446 low-z AGNs. More importantly, comparative analyses of the resultant seed mass distribution and mass functions of BHs derived from simulations reported in the literature help classify the seeds into 3 categories depending on their size and likely formation mechanism. After that, the derivates of the principal relation are analyzed to garner insights into a BH's accretion rate, the Eddington ratio, and the radiative efficiency as functions of z and find the role if any super-Eddington accretion plays in the growth of SMBHs. We end with a summary of the principal conclusions.

2. Theoretical basis

In conventional Astrophysics, the growth of a BH via spherically symmetrical accretion is expressed by Eq. (1) or the so-called Salpeter relation, where M_{BH} is a BH's mass, t its age, Ms the mass and ts the inception time of its seed, and $\mathcal{V}$ a dimensionless parameter defined by Eq. (2)

$$M_{BH}(t) = \mathrm{Ms}\exp[\mathcal{V}(t - ts)/45(\mathrm{Myr})], \tag{1}$$

$$\mathcal{V} = (0.1/0.9)\delta\lambda(1-\varepsilon)/\varepsilon \sim 0.11\delta\lambda(1-\varepsilon)/\varepsilon. \tag{2}$$

In Eq. (2), ε is the radiative efficiency, δ the duty cycle, and λ the Eddington ratio, all rolled into one parameter $\mathcal{V}$ dubbed "growth efficiency" by [37] averaged over a BH's lifespan. For $\delta = 1$, $\varepsilon = 0.1$, and $\lambda = 1$, $\mathcal{V} = 1$ and Eq. (1) reduces to the conventional Salpeter relation for a BH accreting at the Eddington limit. The parameter $\mathcal{V}$, however, cannot be a constant because a BH of say $10^{10}\,M_{\odot}$ at say $t = 10^9$ years would grow by ~ 100 orders of magnitude by $t = 10^{10}$ years. This is not the case, either observationally or theoretically, see [15]. On the contrary, evidence shows that δ decreases as z decreases (Shankar et al., 2010) and so do λ and $(1-\varepsilon)/\varepsilon$, see [1]. Hence, $\mathcal{V}$ must decrease with z or be an inverse function of t. And since $\mathcal{V}$ is nondimensional, we can simply define $\mathcal{V} = \beta 45/t$, where β is a nondimensional

proportionality constant and t in Myr. Thus, Eq. (1) reduces to Eq. (3)

$$\mathrm{M_{BH}}(t) = \mathrm{Ms}\exp[\beta(t - ts)/t]. \tag{3}$$

Seed inception time ts is often assumed to be $\sim$ 100Myr or $z \sim 30$ and a BH's mass $\mathrm{M_{BH}}$ and age t are known from observational data. Hence, a BH's seed mass Ms can be determined using Eq. (3) if the value of β were known. In the next section, we determine the optimum value of β and seek constraints on inception time ts using publicly available data for SMBHs younger than a billion years.

3. Observational database

We searched the literature for BHs younger than a billion years at $z > 5.65$ whose masses are known. Two previous studies facilitated the research. Chon in [7] lists the z and $\mathrm{M_{BH}}$ of 38 such BHs discovered until the end of 2017. We updated the $\mathrm{M_{BH}}$ listed in Chon with more recent determinations where available. In addition, we found data for 21 SMBHs discovered until the end of 2022. Table 1 (Supplement) lists the 59 SMBHs with references for the sources of data. The average reported 1σ uncertainty in the mass of the 59 BHs is $\sim$ 0.11dex. Shen et al. in [31] list 50 such BHs within a narrow z range straddling $z = 6$, the $\mathrm{M_{BH}}$ of 12 which are not well constrained and 6 are duplicates of those in Table 1 The remaining 32 BHs extracted from their Table 3 are identified in the Supplement. In addition, there are 2 more recently discovered BHs at $z > 8.6$. These are GNz112 at $z = 10.6$ with MBH $\sim 1.5 \times 10^6\,\mathrm{M_\odot}$ and CEERS_101911 at $z \sim 8.7$ with $\mathrm{M_{BH}} \sim 9 \times 10^6\,\mathrm{M_\odot}$ for a total of 93. At lower redshifts, Kozlowski in [16] lists $\sim$ 280,000 AGN at $z < 2.4$ and $\mathrm{M_{BH}} > 10^7\,\mathrm{M_\odot}$, of which $\sim$ 132,446 AGN have $\mathrm{M_{BH}}$ determined using the more reliable MgII lines and Eddington ratios based on a weighted average of bolometric luminosities derived using 2 or more AGN luminosities. The uncertainty in the determination of $\mathrm{M_{BH}}$ is, however, not known in most cases. We note that the high-z sample of 93 AGN is skewed in favor of the larger BHs since $\sim$ 75% have $\mathrm{M_{BH}} > 10^9\,\mathrm{M_\odot}$; whereas the lower-$z$ sample of $\sim$ 132,446 has $\sim$ 63% in the $10^8 - 10^9\,\mathrm{M_\odot}$ range, $\sim 27\% > 10^9\,\mathrm{M_\odot}$, and the rest $\sim 10\% < 10^8\,\mathrm{M_\odot}$.

Note that z is converted into t using the Hubble constant ($H_\odot = 67.4$ km/s/Mpc) and matter density parameter ($\Omega_m = 0.315$) from [27]. An SMBH is defined as $\geq 10^6\,\mathrm{M_\odot}$. Throughout this paper, $\mathrm{M_{BH}}$ and Ms are in solar masses ($\mathrm{M_\odot}$) and age t in Myr. AGN at $z > 5.6$ are designated high z and those at $z < 2.4$ as lower-z AGN.

4. Empirical relations

Figure 1 shows the mass $\mathrm{M_{BH}}$ versus age t distribution of 91 of the 93 SMBHs with density contours. The two recently discovered at $t < 600$ Myr fall outside the bounds of Fig. 1. The 91 BHs range $\sim$ 2.5 orders of magnitude in $\mathrm{M_{BH}}$ and $\sim$ 325Myr in age. For each of the 91 BHs, we can write an Eq. (3) expressing $\mathrm{M_{BH}}$ as a function of its unknown seed mass Ms, known age t, and 2 unknown constants (β and ts). Equation (3) shows that a BH's $\mathrm{M_{BH}}$ is directly proportional to its seed mass Ms

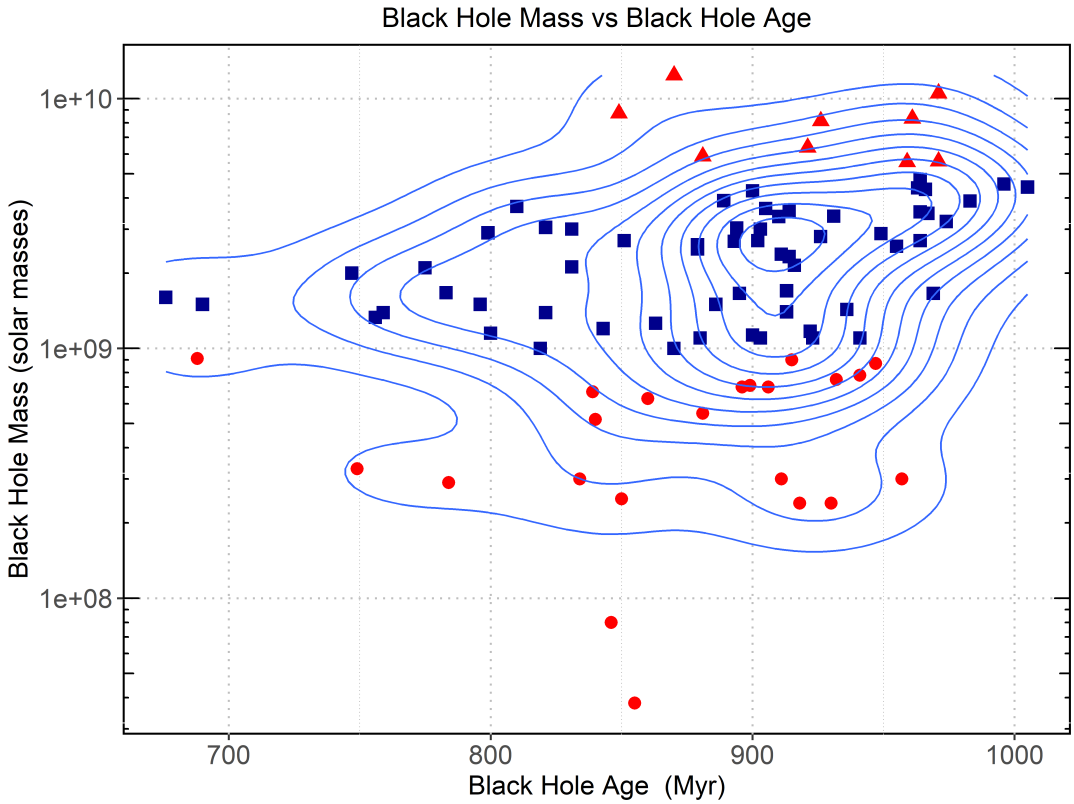

Figure 1: Mass M_{BH} versus age t for 91 SMBHS listed in the Supplement. Density contours are shown. The average reported 1σ uncertainty in M_{BH} is $\sim$ 0.11dex. Their M_{BH} range over > 2.5 orders of magnitude and their ages span $\sim$ 320 Myr of cosmic time. Note that $\sim$ 60 BHs denoted by blue squares have M_{BH} within a factor of ~ 2 of $2.5 \times 10^9\,M_\odot$ and others have higher (red triangles) or lower (red circles) masses.

and increases with age t. The following analysis, however, illustrates that within this age range, a BH's mass depends predominantly on its seed mass Ms and relatively little on its age t. The term $(t - ts)/t$ in the exponent in Eq. (3) for the 91 BHs varies by $< 6\%$ for $ts = 100$Myr. And assuming that the seed of the largest BH (#31, Table 1) in Fig. 1 was a heavy seed $\geq 10^4\,M_\odot$, we get an upper limit of 15.85 for the likely value of β. Hence, the maximum variation in the value of the exponent in Eq. (3) for the 91 BHs is a factor of ~ 2 compared to a 2.5 order of magnitude difference in M_{BH}. The 91 equations cannot be solved simultaneously because Ms varies and is not a constant.

Examining Fig. 1 reveals that a large body of BHs (60) identified by blue squares have strikingly similar masses within a factor of 2 of $2.5 \times 10^9\,M_\odot$ but ages that differ spanning $\sim$ 325Myr of cosmic time. The obvious conclusion is that this group of BHs had seeds with similar Ms even though their ages varied. Thus, for each of these

60 BHs, we can write Eq. (3) with one variable (t) and 3 free parameters (Ms, ts, β) that are constants or nearly so. We used the "SANN" method (see [3]) with 10 million iterations to simultaneously solve the equations and optimize parameter values. Several sets of values for the parameters were generated using all 60 equations and subsets, allowing all three parameters to be free, assuming ts to be 100,150, and 200 Myr, and varying the time window within which the BHs had similar masses; the motivation being to obtain the most likely optimum value for β. Computations with $ts = 150$ and 200 gave the largest RMS residuals and were rejected. A covariance was noted between ts and β, in that an earlier ts gave a somewhat lower β and vice versa. As suspected, subsets comprising BHs with masses within a narrower range of the mean value of $2.5 \times 10^9\,\mathrm{M}_\odot$ produced lower residuals. The ensemble of the solutions indicated that the most likely value for ts was neither much less nor much more than 100 Myr. Finally, $ts = 100$ Myr ($z \sim 30$) and the corresponding $\beta \cong 14.6$ were adopted as the most likely optimum values.

Substituting these values of β and ts in Eq. (3), we get Eq. (4A) where t is in Myr and $\mathrm{M_{BH}}$ and Ms in solar masses.

$$\mathrm{M_{BH}} = \mathrm{Ms}\exp[14.6(t-100)/t] \tag{4A}$$

And using the approximation $1/t \propto (1+z)3/2$ for high z (see [4], we can rewrite Eq. (4A) expressing a BH's $\mathrm{M_{BH}}$ as a function of its redshift z as in Eq. (4B)

$$\mathrm{M_{BH}} = \mathrm{Ms}\exp 14.6[1-(1+z)^{3/2}/(1+30)^{3/2}] \tag{4B}$$

Note that Eq. (4A) and (4B) may yield slightly different results because of the approximation. Note also that Eq. (4) does not depend on any material assumption or data selection.

5. Application to high-z SMBHs: Limits on seed size and growth

Figure 2 shows the seed mass Ms versus age t distribution for the 91 BHs in Fig. 1 predicted using Eq. (4) Figures 1&2 share identical $\mathrm{M_{BH}}$ symbols. Remarkably, the predicted Ms distribution in Fig. 2 closely mimics the observed $\mathrm{M_{BH}}$ distribution in Fig. 1. The 60 blue squares having similar $\mathrm{M_{BH}}$ have markedly similar Ms; the red circles having smaller $\mathrm{M_{BH}}$ have correspondingly smaller Ms; the red triangles with the largest $\mathrm{M_{BH}}$ have the largest Ms; and the BHs range in $\mathrm{M_{BH}}$ over 2.5 orders of magnitude and so do their Ms. Furthermore, the density contours in the two Figs. are almost identical.

Figure 3 shows the predicted seed mass Ms versus BH mass $\mathrm{M_{BH}}$ for all 93 BHs including GNz11 and CEERS_1019, the 2 red dots in the lower left corner of the figure. The symbols are the same as those in Figs. 1&2. The largest BH in Fig.3 (#31 in Table 1) requires a seed mass $\mathrm{Ms} = (3 \pm 1) \times 10^4\,\mathrm{M}_\odot$ for a $\sim 2\sigma$ uncertainty in its mass. Of the 93 BHs, GNz11 and CEERS_1019 are the smallest requiring Ms $\sim 20\,\mathrm{M}_\odot$ and $\sim 53\,\mathrm{M}_\odot$ respectively, or a few to several tens of solar masses. We did

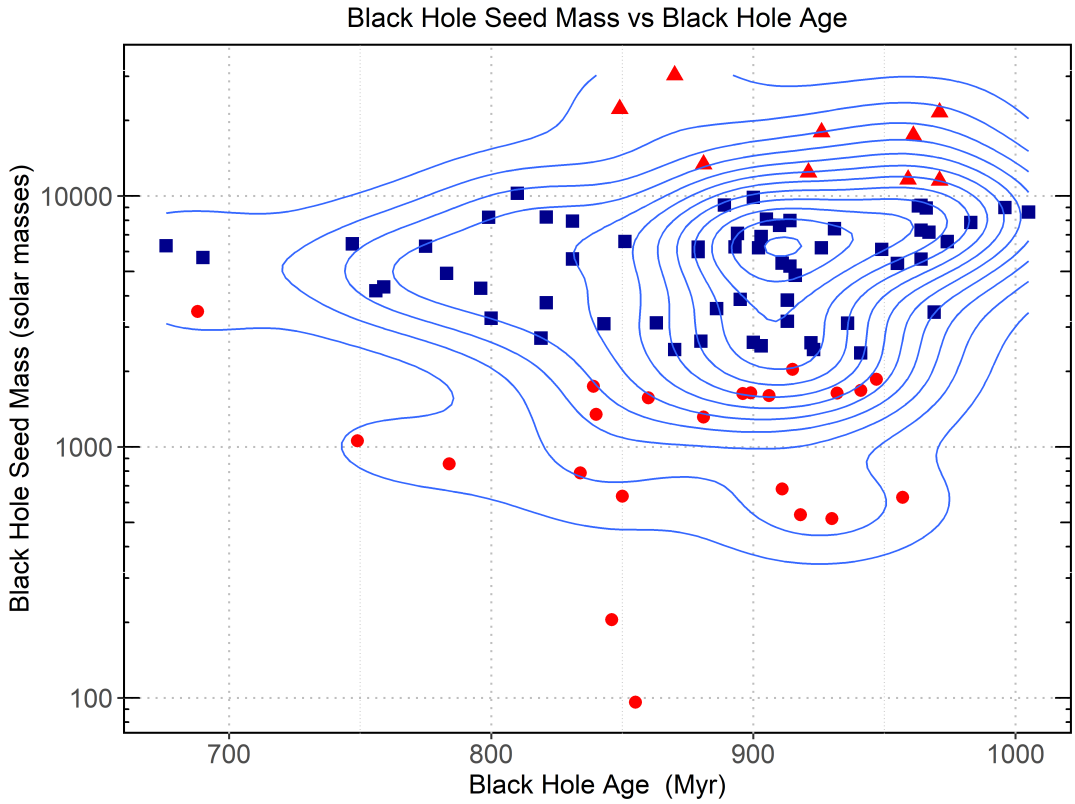

Figure 2: Black hole seed mass Ms versus age t predicted by Eq. 4. The symbols are the same as in Fig.1 differentiating BH mass M_{BH}. The distribution of Ms mimics the distribution of M_{BH} in Fig. 1 and so do the density contours.

not plot the predicted Ms for the third recently discovered AGN, UHZ1 at $z = 10.1$, because its mass is based on the assumption that its Eddington ratio $\lambda = 1$, see [24]. Nevertheless, taking their estimate ($4 \times 10^7\,M_\odot$) at face value, Eq. (5) predicts a seed mass Ms $\sim 418\,M_\odot$ well below the mass expected if it were a DCBH as postulated by [24]. We conclude that none of the 3 recently discovered AGN at $z > 8.6$ require heavy seeds. Instead, their masses are accounted for with seeds formed at $z = 30$ ranging in mass from a few tens to a few hundred solar masses.

Furthermore, we can place upper and lower limits on the size of seeds that formed at $z \sim 30$. The largest high-z BH (#31) was discovered ~ 10 years ago and the second largest (#59) more than 2 decades ago. It is highly probable that they represent an upper limit on the size of SMBHs in the early universe. If so, we can conclude that the largest seeds formed at $z \sim 30$ did not exceed $\sim (3 \pm 1) \times 10^4\,M_\odot$, the seed mass required for the largest of the 93 SMBHs. Conversely, while we cannot place a strict lower limit on the size of seeds formed at $z = 30$, we can conclude that it has to be $< 20\,M_\odot$ based on the Ms required for GNz11 the smallest of the 93 high-z SMBHs. Lastly, we note that Eq. (4A) predicts that the maximum size a BH can achieve

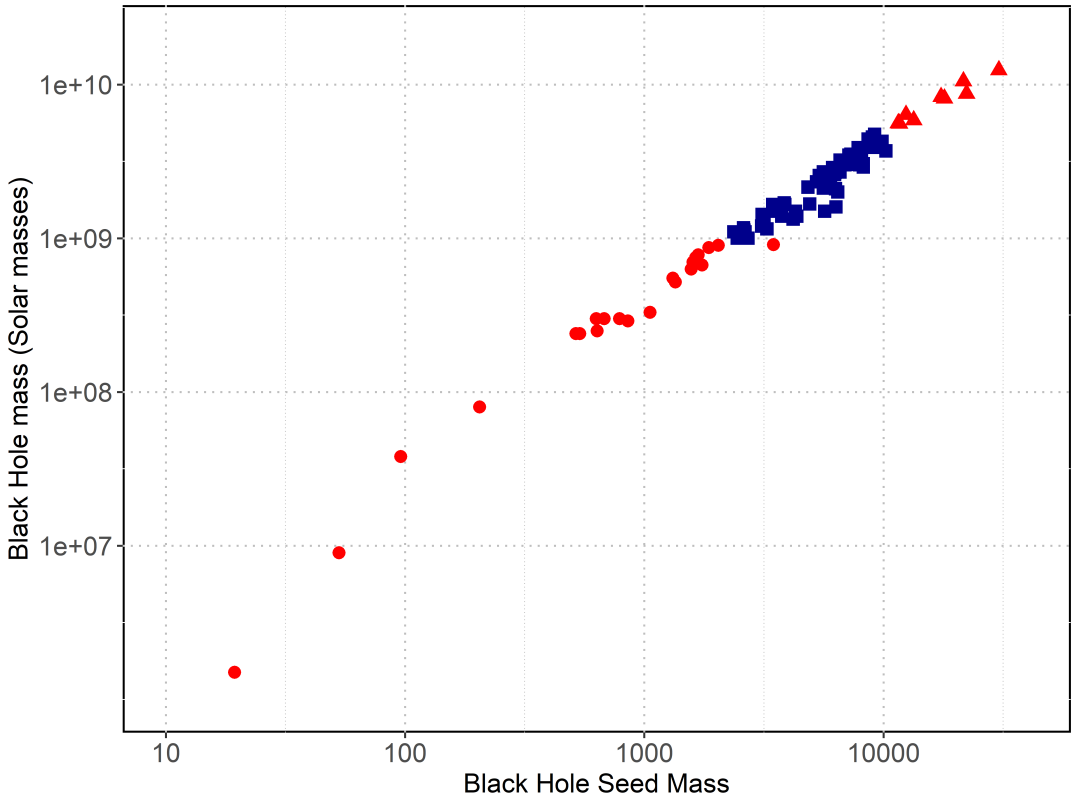

Figure 3: Black hole seed mass Ms versus BH mass M_{BH} on a log-log scale for the 91 BHs in Fig. 1 and for GNz11 and CEERS_1019 ($M_{BH} < 1e+07$ solar masses, bottom left corner). The symbols are identical to those in Figs. 1&2.

via luminous accretion depends on its seed mass as (Exp 14.6)×Ms or $\sim 2.2 \times 10^6$ Ms, which translates into $(6.6 \pm 2.2)10^{10} M_\odot$ for the empirically determined upper limit of Ms $= (3 \pm 1) \times 10^4\, M_\odot$ in excellent agreement with a theoretical limit of $\sim 5 \times 10^{10}\, M_\odot$ that in extreme cases could reach $\sim 2.7 \times 10^{11}\, M_\odot$ proposed by [15].

6. Application to lower-z SMBHs: Seed classification and mechanisms

We applied Eq. (4B) to the 132,446 AGN with $M_{BH} \geq 10^7\, M_\odot$ at $z < 2.4$ listed by [16] to simultaneously test the universality of its applicability and derive the size distribution of the seeds. The resulting Ms are sorted into narrow bins and the number in each mass bin is shown in Table 1. The uncertainty in M_{BH} in most cases is unknown but is of little importance except when there are relatively few seeds. Of the total population of BHs, 540 BHs have $\geq 10^{10}\, M_\odot$ and none of their predicted Ms exceed the preceding empirically established upper limit of $(3 \pm 1) \times 10^4\, M_\odot$ except possibly in 5 cases (Table 1) and that too by a factor of < 1.7 in the worst case. The masses of these possible few exceptions, however, are not constrained. In particular, we note that the predicted Ms for TON 618 at $z = 2.219$ with $M_{BH} = 4.07 \times 10^{10}\, M_\odot$ (see [34]), which is often cited as the most massive BH observed to date, is identical to that of the largest high-z BH (#31). At the lower end of the Ms spectrum,

the results (Table 1) show that 88 BHs have predicted Ms between $5 - 10\,M_\odot$ and ~ 1000 between $10 - 20\,M_\odot$ in agreement with the lower limit of Ms expected from the high-z data. This striking agreement on the limits on the size of seeds deduced from 2 entirely different sets of data covering different cosmic periods cannot simply be fortuitous and testifies to the validity and universal applicability of Eq. (4).

The seed counts in Table 1 indicate that $\sim 90\%$ of the seeds have Ms $\leq 1.5 \times 10^3\,M_\odot$. The histogram in Fig. 4 shows their mass distribution, where each bin has the same size of $50\,M_\odot$ and is identified by the central value of Ms in the bin. The remaining 10%, not plotted because of their small numbers, follow the same pattern decreasing asymptotically towards zero at Ms $\sim 3 \times 10^4\,M_\odot$ the upper limit of seed mass. Table 1, however, gives the number of seeds in different bin sizes for the remaining 10% of AGN that amount to less than the number in the single bin of $50 - 100\,M_\odot$ centered at Ms $= 75\,M_\odot$ in Fig. 4. The seeds in Fig. 4 range in Ms from a low $\sim 5\,M_\odot$ to a high of $\sim 1.5 \times 10^3\,M_\odot$ and can be designated as light to intermediate-size seeds based on their size classification discussed earlier. They constitute an overwhelming majority of the seeds. In contrast, seeds $\geq 10^4\,M_\odot$ or heavy seeds constitute a minuscule number totaling ~ 210 or a fraction of ~ 0.0016 of the seed population (see Table 1).

Ms	Count	Ms	Count	Ms	Count	Ms	Count
$5-10$	88	$200-250$	8.473	$800-850$	1.963	$1400-1450$	745
$10-20$	1014	$250-300$	7.063	$850-900$	1.963	$1450-1500$	703
$20-30$	2394	$300-350$	6.063	$900-950$	1.721	$1500-1800$	3383
$30-40$	3332	$350-400$	5.241	$950-1000$	1.528	$1800-2200$	2775
$40-50$	3605	$400-450$	4.700	$1000-1050$	1.419	$2200-2700$	2217
$50-60$	3595	$450-500$	4.064	$1050-1100$	1.231	$2700-3400$	1747
$60-70$	3481	$500-550$	3.728	$1100-1150$	1.161	$3400-4200$	1051
$70-80$	3261	$550-600$	3.226	$1150-1200$	1.081	$4200-6400$	1097
$80-90$	3110	$600-650$	2.910	$1200-1250$	944	$6400-10000$	462
$90-100$	2979	$650-700$	2.672	$1250-1300$	926	$10000-14000$	144
$100-150$	12.739	$700-750$	2.385	$1300-1350$	843	$14000-30000$	61
$150-200$	10.159	$750-800$	2.217	$1350-1400$	829	>30000	5

Table 1: Ms seed mass (solar mass). The count is the number of seeds in a bin. Bin size varies.

Light seeds are thought to have formed from the collapse of massive metal-free first or Pop III stars. Our finding that the seeds formed around $z = 30$ is consistent with the notion that the first stars formed at $z \sim 30$, see e.g. [8]. Their initial stellar mass functions derived from simulations range from $< 10\,M_\odot$ to $\sim 1000\,M_\odot$, see e.g. [12], [13], [32]. These simulations have been reviewed by Latif and Ferrara (see [18]) who concluded that overall the results suggest that the typical mass of Pop III stars is $\sim 100\,M_\odot$ except for a few cases of $1000\,M_\odot$. Fig. 4 shows that the number of seeds decreases as Ms increases except at the beginning or low end of the

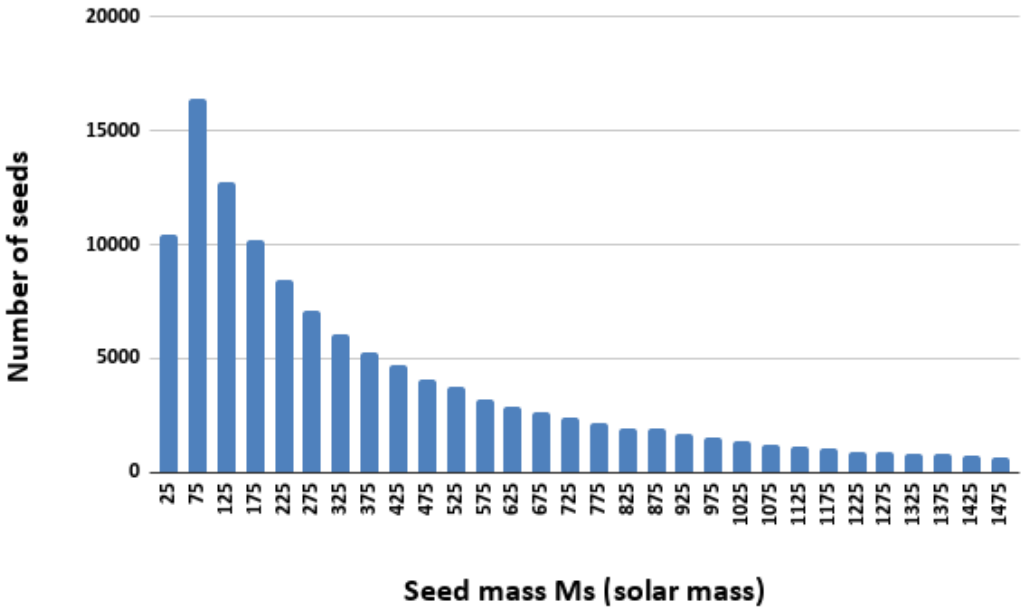

Figure 4: Histogram showing the number of seeds in bins of $50\,M_\odot$ (solar masses) for 90% of 132,446 SMBHs at $z < 2.4$ predicted by Eq. (4B). Each bar is plotted at the central mass value of the bin. The distribution of the rest at Ms $> 1500\,M_\odot$, not plotted because of their small numbers, is given in Table 1 Note the initial increase in seed counts before the monotonic decrease, the significance of which is discussed in the text.

Ms spectrum. A closer examination reveals that at the low end of the Ms spectrum, the number of seeds increases exponentially and reaches a plateau before decreasing monotonically. The counts in Table 1 show that the number of seeds increases from 88 having Ms $\leq 10\,M_\odot$ to 1014 and 2395 in the successive bins of $10-20\,M_\odot$ and $20-30\,M_\odot$ and reaches a plateau of $\sim$ 3600 in the bins of $40-50\,M_\odot$ and $50-60\,M_\odot$; after which the counts decrease slowly but monotonically. This predicted mass distribution of light seeds resembles the steller-mass distribution shown in Fig. 5 of [12] derived from hydrodynamic simulations. Their histogram of 100 first stars accreting at lower rates, identified by red and blue colors, shows that the number of stars increases $>$ 10-fold from 1 with a mass $< 10\,M_\odot$ to 11 with a mass of $\sim 40\,M_\odot$, after which the number of stars decreases almost monotonically to 1 at $\sim 1000\,M_\odot$. However, as noted by them, most stars have masses from a few tens to a few hundred solar masses, consistent with the distribution of seeds in Table 1 and Fig. 4 that show that $\sim$ 60% of the seeds with Ms $< 1000\,M_\odot$ have masses between $10\,M_\odot$ and $300\,M_\odot$ and 70% have $< 400\,M_\odot$. Thus, there is a good agreement between the mass distribution of the first stars derived from simulations and the empirically derived mass distribution of seeds that presumably formed from the collapse of the first stars

with 2 caveats. The major difference could be that the BH seeds in this study formed at $z \sim 30$, whereas in the simulations it is not evident at what redshifts between $15 - 35$ the stars formed. Second, in their simulation, there is a marked low in the number of stars immediately following the maximum, whereas in Fig. 4 there is no such hiatus. Later, we provide an explanation reconciling this dichotomy.

Most likely, there is an overlap in the sizes of light and intermediate seeds. There is, however, no decipherable change, hiatus, or break in the asymptotic decrease in the number of seeds as Ms increases in Fig. 4. Thus, it is difficult, if not impossible, to define a strict Ms boundary in Fig. 4 between the light and intermediate seeds. In contrast to light seeds, intermediate-size seeds are thought to have formed either via runaway collisions of stars in dense stellar clusters (see [28]; [11]; [23]) or by the hierarchical merger of BHs in stellar clusters, see [9]; [20]. Devecchi in [10] performed simulations simultaneously investigating the formation of Pop III remnants and BHs via runaway collisions in nuclear star clusters. The results in their Fig. 4 show that the BHs formed via runaway collisions decrease in number by a factor of ~ 5 as BH mass increases from $\sim 400\,\mathrm{M}_\odot$ to $\sim 3000\,\mathrm{M}_\odot$, qualitatively in agreement with the decrease in the number of seeds as Ms increases in Fig. 4 and Table 1 of this study. Note that $\sim 97\%$ of the seeds in Table 1 have Ms $< 3000\,\mathrm{M}_\odot$. Hence, intermediate-size seeds formed via runaway collisions of stars and light seeds formed by the collapse of the first stars could together account for the entire population of seeds in Table 1 except $\sim 3\%$. There is, however, a potential problem. The seeds in Table 1 were deduced to have formed at $z \sim 30$, whereas the intermediate-size BHs via runaway collisions of stars in the simulations formed at $z \sim 15$, a time difference of $\sim 150\,\mathrm{Myr}$.

On the other hand, Lupi et al. in [20] explored the gas-induced runaway merger of BHs dubbed the GIRM model, following the [9] prescription of hierarchical growth of BHs in dense stellar clusters. Their results in Fig. 7 also show that the number of BH seeds formed via GIRM decreases dramatically as the seed mass increases from $\sim 400\,\mathrm{M}_\odot$ to $\sim 2000\,\mathrm{M}_\odot$. Most of the BHs in their simulations also formed at $z < 20$. They, however, point out that GIRM requires some degree of metal pollution of the intergalactic medium from the explosions of the massive Pop III stars and that the "GIRM channel does not pose any constraint on the level of metallicity of the parent halo, and hence on the time of formation, provided Pop III stars have enhanced the metallicity above a threshold". If so, this mechanism and that for the formation of light seeds could together also account for at least 94% of the seed population in Table 1. This mechanism has the advantage that the Pop III remnants could provide the degree of metal pollution required in the simulations. Alternatively, the formation of intermediate-size BHs could have resulted from the merger of Pop III remnants, but whether this is a realistic possibility can be ascertained by simulations, a task beyond the scope of this paper. If possible, it would explain why there is no hiatus or break in the mass distribution of seeds in Fig. 4 and Table 1 and why intermediate-size follow the same asymptotically decreasing trend as the light seeds. Furthermore, the probability of forming larger seeds from a given population of

stellar seeds would systematically decrease as seed mass increases, consistent with the systematic decrease in seed counts as Ms increases observed in Fig. 4 and Table 1.

It is remarkable that in the preceding simulations, whether involving runaway collisions of stars or runaway mergers of BHs, the resulting mass spectrum of intermediate-size seeds is strikingly similar ranging from $\sim 400\,\mathrm{M}_\odot$ to $\sim 2000-3000\,\mathrm{M}_\odot$. Thus, based on the results of these simulations and the preceding discussion on the distribution of seeds in Fig. 4 in the context of the results of the simulations by [12], we can classify seeds $< 400\,\mathrm{M}_\odot$ as light seeds predominantly formed from the collapse of first stars and those between $400\,\mathrm{M}_\odot - 3000\,\mathrm{M}_\odot$ as predominantly intermediate-size. Based on this working classification we conclude that of the 132,446 seeds in Table 1, $\sim 58\%$ are light and $\sim 39.4\%$ are intermediate-size. The remaining $< 3\%$ or 3681 have Ms between $\sim 3\times10^3\,\mathrm{M}_\odot - 3\times10^4\,\mathrm{M}_\odot$ (dubbed heavier seeds in contrast to heavy), of which only 210 have Ms $\geq 10^4\,\mathrm{M}_\odot$ that could strictly be classified as heavy seeds. Moreover, these few heavy seeds have Ms $< 3\times10^4\,\mathrm{M}_\odot$ or at the lower end of the expected mass spectrum of $10^{4-5}\,\mathrm{M}_\odot$ for heavy seeds thought to have formed by the DCBH mechanism. The implication is that the DCBH mechanism did not play an important role in forming the seeds of SMBHs. Moreover, the 'number of "heavier" seeds decreases as Ms increases (see Table 1) following the same pattern as the light to intermediate-size seeds in Fig. 4; which suggests that the same mechanism responsible for forming intermediate-size seeds may also account for the rare formation of heavy seeds. Apropos, Davies et al. in [9] have proposed that seeds as large as $10^5\,\mathrm{M}_\odot$ can be formed by hierarchical growth of BHs in dense stellar clusters.

7. Accretion rate, Eddington ratio, and radiative efficiency

Having established the universal applicability of Eq. (4), we can use its derivative to gain insights into the growth history of SMBHs. Differentiating $\mathrm{M_{BH}}(\mathrm{dM_{BH}}/\mathrm{d}t)$ in Eq. (4A), we get Eq. (5) expressing a BH's instantaneous accretion rate $\dot{\mathrm{M}}$ (solar mass/year) as a function of $\mathrm{M_{BH}}$ and age t (Myr) or as a function of z using the approximation $1/t \propto (1+z)^{3/2}$ (see [4])

$$\dot{\mathrm{M}}(\mathrm{M}_\odot/\mathrm{yr}) = 14.6\times10^{-4}\mathrm{M_{BH}}/t^2 \cong 4.96\times10^{-12}\mathrm{M_{BH}}(1+z)^3. \qquad (5)$$

For example, Eq. (5) yields $\dot{\mathrm{M}} \sim 0.012\,\mathrm{M}_\odot/\mathrm{yr}$ for GNz11 at $z = 10.6$, $\sim 24\,\mathrm{M}_\odot/\mathrm{yr}$ for the largest high-z SMBH at $z = 6.3$ (#31), and $\sim 6.6\,\mathrm{M}_\odot/\mathrm{yr}$ for TON 618 at $z = 2.219$. Moreover, by substituting $\mathrm{M_{BH}}$ in Eq. (5) with its expression in Eq. (4B), we get Eq. (6) expressing $\dot{\mathrm{M}}$ as a function of a BH's seed mass Ms and redshift z.

$$\dot{\mathrm{M}} = 4.96\times10^{-12}\mathrm{Ms}(1+z)^3\exp 14.6[1-(1+z)^{3/2}/(1+30)^{3/2}]. \qquad (6)$$

Using Eq. (6). one can infer the history of a BH's accretion rate from its inception at $z = 30$ to any redshift z by plugging in Eq. (6) the BH's seed mass Ms inferred from Eq. (4B), Figure 5 shows the accretion rate history of a seed of unit solar mass. Initially $\dot{\mathrm{M}}$ increases exponentially and reaches a broad peak between $z = 8.5$ and 6,

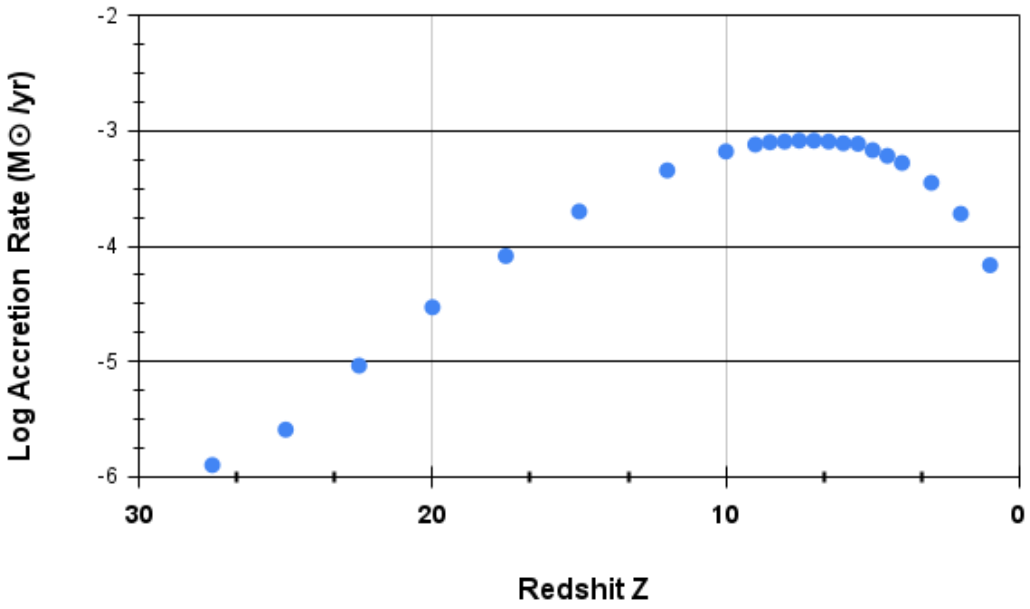

Figure 5: Log of spot accretion rate $\dot{M}$ for a BH seed of unit (solar) mass $M_\odot$ as a function of redshift z starting at $z \sim 30$ based on Eq. (6). Initially $\dot{M}$ increases exponentially, reaches a broad peak between $z \sim 8.5$ and 6 with a maximum at $z \sim 7$, and steadily decreases after that towards $z = 0$.

beyond which it decreases slowly but monotonically towards $z = 0$. In the Standard Cosmological Model, the density of matter or gases scales as $(1 + z)^3$, and hence $\dot{M}$ scales as the product of the BH's mass (gravitational reach) and the ambient gas density. Two competing factors, namely the increase in a BH's mass or gravitational reach as it ages and the decrease in the ambient gas density as z decreases, determine a BH's $\dot{M}$ at any instant of its life. Initially, the BH's mass or its gravitational reach increases faster than the decrease in the ambient gas density. The two competing factors reach a parity near $z \sim 7$, after which the decline in gas density dominates over the gradual increase in the BH's mass and $\dot{M}$ steadily decreases. For example, Eq. (4B) predicts that the seed of TON 618, one of the largest SMBHs, grew from Ms $= 3.03 \times 10^4\,M_\odot$ by ~ 5.5 orders of magnitude to $\sim 9.8 \times 10^9\,M_\odot$ by $z = 7$ and after that by a factor of ~ 4 until its present $z = 2.219$. And, Eq. (6) predicts that its accretion rate changed from $0.08\,M_\odot$/yr at $z = 25$ to $24.6\,M_\odot$/yr at $z = 7$ and $6.6\,M_\odot$/yr at $z = 2.219$.

Using Eq. (5), we can also define the Eddington ratio λ, or the ratio of a BH's bolometric luminosity $L_{\rm bol}$ to its Eddington luminosity ($L_{\rm EDD}$), as a function of z and radiative efficiency ε, $L_{\rm bol} = (\dot{M}c^2)\varepsilon/(1-\varepsilon)$ where c is the velocity of light and $\dot{M}$ the accretion rate; and $L_{\rm EDD} = 1.3 \times 10^{38} M_{\rm BH}$ in ergs/s with $M_{\rm BH}$ in solar mass. Radiative efficiency ε is conventionally defined with respect to the mass inflow rate

such as the Bondi rate and a BH's $\dot{M}$ is smaller by $(1-\varepsilon)$. Thus, by Substituting $\dot{M}$ from Eq. (5) into the definition of $L_{\rm bol}$, we get Eq. (7) expressing the Eddington ratio λ as a function of a BH's redshift and radiative efficiency

$$\lambda = 2.18 \times 10^{-3}(1+z)^3\varepsilon/(1-\varepsilon). \tag{7}$$

Equation (7) implies that λ decreases as z decreases irrespective of whether ε depends on z. This implication is validated by empirical evidence. Using Kozslowski's data for the tens of thousands of AGNs at $z < 2.4$, Aggarwal in [1] unambiguously showed that λ decreases with z. Moreover, Eq. (7) implies that of 2 BHs at similar redshifts, the BH with a higher λ is less efficient (higher ε) in accreting gases than the one with a lower λ. This implication is also consistent with the finding by [1] that larger BHs have lower λ and are more efficient than smaller BHs. And using the Bondi prescription for spherically symmetric accretion and observational data for temperature and density profiles near BHs in galaxies M87, NGC 3115, and NGC 1600, Aggarwal in [1] derived a scaling relation for λ identical in form to the above Eq. (7). Thus the substantiations of the implications of Eq. (7) and the similarity between scaling relations for λ derived from 2 different prescriptions and entirely different data sets are further evidence of the validity and universal applicability of Eq. (4) from which Eq. (7) is derived.

A BH's radiative efficiency ε can be inferred from Eq. (7) knowing its λ. Unfortunately, estimating λ is prone to multiple errors arising from uncertainties in the BH's mass, its luminosity, and the correction factor used to get its bolometric luminosity. However, by applying Eq. (7) to large groups of similarly situated BHs at markedly different redshifts, we can garner insights into the dependence of ε on z. For example, Shen et al. in [31] list 50 BHs, most of which have $1-4\times10^9\,{\rm M}_\odot$ with redshifts close to 6 and a mean $\lambda \sim 0.32$, whereas a large group of similar-size BHs at $z \sim 1$ in Kozlowski's catalog have a mean $\lambda = 0.03$. Applying Eq. (7) to the two groups, one gets $\varepsilon \sim 0.63$ for the lower and $\varepsilon \sim 0.3$ for the higher-z group; a decrease by a factor of 2 despite a $\sim$ ten-fold increase in λ from $z \sim 1$ to $z \sim 6$. The implication is that ε decreases as z increases consistent with a similar finding by [1].

The overwhelming majority of the values of λ for the BHs in Table 2 and reported by [31] and [16] are < 1, all of which are at $z < 7.7$. GNz11 is a notable exception that deserves special attention because it is the highest-z AGN observed so far and is inferred to be accreting by as much as 5 times the Eddington rate, see [22]. If so, Eq. (7) predicts a radiative efficiency ε of ~ 0.59 that ostensibly is extremely high especially since ε has been shown to decrease as z increases. And, it would imply that GNz11 is a rather poor accreter, accreting only $\sim 41\%$ of the gas inflow. Interestingly, a lower λ would make GNz11 a more efficient accreter. For example, $\lambda = 1$ would yield $\varepsilon = 0.227$, making GNz11 ~ 2.6 times more efficient than if its $\lambda = 5$ without affecting its accretion rate. Its λ is probably highly overestimated. In fact, Schneider in [29] estimated a significantly lower λ of $2-3$ for it.

Given that λ is prone to large uncertainties and hence a poor predictor of whether a BH is accreting above the Eddington limit, we propose instead the following. As noted earlier, the growth efficiency parameter $\mathcal{V}$ defined by Eq. (2) has a value of 1 for a BH accreting at the Eddington limit ($\lambda = 1$) with a radiative efficiency $\varepsilon = 0.1$ (its canonical value) and a duty cycle $\delta = 1$. For $\delta = 1$, a value of $\mathcal{V} > 1$ implies that the BH is either accreting above the Eddington limit ($\lambda > 1$) or that its $\varepsilon < 0.1$. Substituting λ from Eq. (7) into Eq. (2) (the definition of $\mathcal{V}$), one gets $\mathcal{V} \sim 2.4 \times 10^{-4}\delta(1+z)^3$. Shankar et al. (2010) found that in their sample of AGNs, the duty cycle δ increased with z reaching ~ 0.9 at $z = 6$. It is likely therefore that $\delta \sim 1$ at even higher redshifts. Hence, at very high redshifts $\mathcal{V} \sim 2.4 \times 10^{-4}(1+z)^3$ or solely a function of the gas density. The implication is that for a BH at $z > 15$, $\lambda > 1$ or $\varepsilon < 0.1$. It is likely therefore that during the first ~ 150 Myr of its life, a BH experiences super-Eddington accretion or its radiative efficiency is much < 0.1. This finding is consistent with the suggestion by [36] and [26] that super-Eddington accretion is possible when a BH is embedded in sufficiently dense gas that renders the radiation pressure less effective.

8. Conclusions

Prompted by insights derived from a deconstruction of the so-called Salpeter relation (Eqs. (1)–(3)), we analyzed the mass versus age distribution of 91 high-z SMBHs (Fig. 1) that resulted in the formulation of Eq. (4), the foundation on which the findings and conclusions of this paper are based. It describes a BH's mass $\mathrm{M_{BH}}$ as a function of its age t or redshift z, from which the BH's seed mass Ms can be determined. It was extensively tested throughout the paper by verifying its implications and predictions. It, together with its derivates (Eqs. (5)–(7), comprises a set of powerful tools to decipher the origins, growth, and properties of SMBHs.

We applied Eq. (4) to 93 high-z (> 5.6) and 132,446 AGNs at $z < 2.4$ listed by [16]. The resulting mass distributions of seeds (Figs. 2, 3, 4, and Table 1) show that the masses of the smallest to the largest actively accreting SMBHs observed to date are accounted for by seeds formed at $z \sim 30$ ranging in Ms from a low of $\sim 5\,\mathrm{M_\odot}$ to a maximum of $(3 \pm 1) \times 10^4\,\mathrm{M_\odot}$. In particular, the $\mathrm{M_{BH}}$ of GNz11, CEERS_1019, and UHZ1), the 3 highest redshift ($z = 8.7 - 10.6$) AGNs discovered recently, are accounted for by stellar-mass seeds ranging from a few tens to a few hundred solar masses. Specifically, the results exclude the possibility that the seed of UHZ1 was heavy presumably a DCBH as postulated by [24]. Equation (4A) places an upper limit of $\sim 2,2 \times 10^6$Ms on the mass a seed can accrete via luminous accretion; which translates into $(6.6 \pm 2.2) \times 10^{10}\,\mathrm{M_\odot}$ for Ms$= (3 \pm 1) \times 10^4\,\mathrm{M_\odot}$ in agreement with a theoretical limit proposed by [15] and with the size of the largest SMBHs observed to date.

The mass distribution of seeds shown in Fig. 4 and Table 1 was analyzed and compared with the simulated mass functions of first stars and intermediate-size BHs reported in the literature. Based on this comparative analysis, we classified the seed

population into 3 broad categories depending on seed size and the likely mechanism for its formation, fully recognizing that there is probably overlap between the categories. Seeds $\leq 400\,M_\odot$ were classified as light seeds predominantly formed from the collapse of massive metal-free first stars, see [21]; [14]). Their observed mass distribution in Fig. 4 and Table 1 resembles the mass function in simulations of first stars performed by [12]. Seeds ranging in mass from $400\,M_\odot - 3\times10^3\,M_\odot$ were classified as intermediate-size seeds formed either by runaway collisions of stars in dense stellar clusters (see [28]; [11]) or by the hierarchical growth of BHs via runaway mergers, see [9]; [20]. Their observed mass distribution in Fig.1 and Table 1 resembles the mass functions of BHs in simulations of runaway collisions of stars by [10] and in simulations of gas-induced runaway merger of BHs by [20]. Under this classification, light seeds constitute $\sim 58\%$ and intermediate size $\sim 39.4\%$ of the population in Table 1 The remaining $< 3\%$ raging in mass from $\sim 3\times10^3\,M_\odot$ to $\sim 3\times10^4\,M_\odot$ were dubbed heavier seeds in contrast to the classical heavy seeds ($10^{4-6}\,M_\odot$) thought to be DCBHs.

Of the 2 mechanisms for intermediate-size seeds, the hierarchical growth of BHs via runaway mergers is the more likely for the following reasons. In [10] simulations, the BHs formed at $z\sim15$ or significantly later than at $z\sim30$; whereas there is no such time restriction for the runaway merger of BHs as pointed out by [20]. Furthermore, if the hierarchical growth occurred through the merger of Pop III remnants instead of BHs formed at a later time, it would explain why light and intermediate-size seeds formed almost concurrently at $z\sim30$, why the two follow the same asymptotically declining trend as seed mass increases with no hiatus in the distribution of seed sizes observed in Fig. 4, and why light seeds outnumber intermediate-size seeds. Of the heavier seeds, only a minuscule number (210) have $> 10^4\,M_\odot$ and that too at the lower end of the presumed sizes of DCBHs; which led us to conclude that the DCBH mechanism did not play a significant role in the formation of seeds of SMBHs and propose that the heavier seeds could also have formed via the merger of light to intermediate-size seeds. Apropos, Davies et al. in [9] proposed that BHs as large as $10^5\,M_\odot$ can form via runaway merger of BHs. In summary, the entire population of seeds in Table 1 could be Pop III remnants and BHs resulting from their hierarchical growth via runaway mergers under appropriate conditions. One such condition could be the inflow of gases as in the simulations by [20].

Equation (5) gives a BH's instantaneous accretion rate as a function of its mass M_{BH} and age t or redshift z and in terms of its seed mass Ms (inferred from Eq. (4)) and z in Eq. (6). For example, Eq. (5) predicts a rate of $\sim 0.012\,M_\odot$/yr for GNz11 the smallest ($\sim 1.5\times0^6\,M_\odot$) high-$z$ (10.6) AGN; $\sim 24\,M_\odot$/yr for the largest ($\sim\ 1.24\times10^{10}\,M_\odot$) high-$z$ (6.3) SMBH; and $6,6\,M_\odot$/yr for TON 618 at $z\sim2.22$ arguably the largest ($4.07\times10^{10}\,M_\odot$) AGN observed to date. Figure 5 illustrates the change in a BH's $\dot{M}$ with z from its inception as a seed at $z\sim30$ to the present. Initially, $\dot{M}$ increases exponentially, reaches a broad plateau between $z=8.5-6$, and thereafter decreases monotonically. Two factors namely the increase in a BH's gravitational

reach as its mass increases and the decrease in gas density as z decreases modulate the accretion rate as the BH ages. A BH's mass increases by ~ 6 orders of magnitude in the first billion years and only by a factor of ~ 4 in the next ~ 12.8 billion years.

Equation (7) expresses the Eddington ratio λ as a function of a BH's z and radiative efficiency ε. It implies that λ decreases with z; an implication substantiated by unambiguous empirical evidence, see [1]. Furthermore, a BH's radiative efficiency ε can be determined using Eq. (7) from its λ. We, however, stressed that λ is prone to large errors resulting from numerous uncertainties (see text), and hence Eq. (7) should be used with caution. Nevertheless, using λ data for 2 large groups of similar-size BHs at 2 different redshifts, we showed that ε is significantly lower for the higher-z group even though its λ is substantially higher. The implication is that ε increases as z decreases or that a BH becomes less efficient in accreting gases as it ages; which suggests that ε is an inverse function of the ambient gas density consistent with Wythe et al. in [36] and Pacucci et al. in [26] suggestion that the radiation pressure is less effective when a BH is embedded in dense gas. Finally, applying Eq. (7) to Eq. (2), we inferred that at redshifts > 15 the radiative is significantly < 0.1 its canonical value or that $\lambda > 1$; which suggests that SMBH's may have experienced super-Eddington accretion for a short period of ~ 150 Myr from the inception of their seeds at $z \sim 30$.

Acknowledgements

I thank Manuel Chirouze for solving the equations using the SANN method, drafting the figures, and suggesting using density contours in Figs. 1 and 2.

Data availability

No new data were generated in this study.

References

[1] Aggarwal, Y., 224, MNRAS. 530, (2024) 1512–1515.

[2] Begeleman M. C., Volonteri M., Rees M. J., 2006, MNRAS, 370, 289.

[3] Belisle, C.J.P., 1992, J Applied Probability, 29, 885–895.

[4] Bergström L., and Goober I., 2006, Cosmology and Particle Astrophysics, Springer 77.

[5] Bondi, H., On the spherically symmetric accretion. MNRAS, 112, 195 (1952).

[6] Bromm V., Loeb A., 2003, ApJ, 596, 34.

[7] Chon, S., 2018, `http://www-utap.phys.s.u-tokyo.ac.jp/Theses/D_Chon.pdf`

[8] Couchman, H. M. P., Rees, M. J. 1986, MNRAS, 221, 53.

[9] Davies M. B., Miller M. C., Bellovary J. M., 2011, ApJ, 740, L42.

[10] Devecchi B., Volonteri M., Rossi E. M., Colpi M., Portegies Zwart S., 2012, MNRAS, 421, 1465.

[11] Freitag M., Gürkan M. A., Rasio F. A., 2006, MNRAS, 368, 141.

[12] Hirano S., et al., 2014, ApJ, 781, 60.

[13] Hosokawa T., et al., 2016 ApJ 824, 119.

[14] Johnson J. L., Bromm V., 2007, MNRAS, 374, 1557.

[15] King A. R., 2012, MNRAS, 421, 3443.

[16] Kozłowski S., 2017, ApJS, 228, 9.

[17] Larson, L.R., et al., 2023, ApJL 953, L29.

[18] Latif, M. A., Ferrara, A., 2016, PASA, 33, e051.

[19] Lodato G., Natarajan P., 2006, MNRAS, 371, 1813.

[20] Lupi A., Colpi M., Devecchi B., Galanti G., Volonteri M., 2014, MNRAS, 442, 3616.

[21] Madau, P., Rees, M. J, 2001, Astrophys. J. Lett. 551, L27–L30.

[22] Maiolino, R., et al., 2024, Nature 627, 59–63.

[23] Mapelli, M..2016, MNRAS, 459, 3432–3446.

[24] Natrajan, P., et al., 2024 ApJL 960 L1.

[25] Pacucci F., Loeb A., 2020, ApJ, 895, 95.

[26] Pacucci, F., Ferrara, A., Volonteri, M., and Dubus, G., 2015, MNRAS. 454, 3771.

[27] Planck group, 2020, A& A, 641, A6.

[28] Portegies Z., et al., 2004, Nature 428, 724–726.

[29] Schneider, R., et al., 2023, MNRAS 526, 3250–3261.

[30] Shang C., Bryan G. L., Haiman Z., 2010, MNRAS, 402, 1249.

[31] Shen Y. et al., 2019, ApJ, 873, 35.

[32] Stacy, A., Bromm, V., Lee, A. T., 2016, MNRAS 462, 1307–1328.

[33] Volonteri, M., Habouzit, M., Colpi, M., 2021, Nat Rev Phys 3, 732–743.

[34] Xue Ge, Zhao, B-X. Bian, W-H., Frederick, G.R., 2019, AJ, 157, 14.

[35] Wu, X.B., et al., 2015, Nature, 518, 512.

[36] Wythe J. S. B., Loeb A., 2012, MNRAS, 425, 28.

[37] Zubovas K., King A., 2021, MNRAS, 501, 428.

Supplementary Information

Table 2 gives the data for 59 of the 91 SMBHs in Figs. 1 and 2 with references for the sources of data. The BHs are listed in order of their redshift z from the highest to the lowest. The first reference # is for BH's discovery paper and the second # is for BH's mass estimate. The rest of the 32 SMBHs are in Table 3 of [31] in the order they appear.

J0002+2550; J0008−0626; J0810+5105; J0835+3217; J0836+0054; J0840+5624; J0841+2905; J0842+1218; J0850+3246; J1044−0125; J1137+3549; J1143+3808; J1148+5251; J1207+0630; J1243+2529; J1250+3130; J1257+6349; J1403+0902; J1425+3254; J1427+3312; J1436+5007; J1545+6028; J1602+4228; 1609+3041; J1621+5155; J1623+3112; J1630+4012; P000+26; P060+24; P210+27; P228+21; and P333+26

BH #	Black Hole Name	BH Mass MBH ($M_\odot$)($\pm1\sigma$)	z	Age (Myr)	Ref
1	J0313-1806	$1.6\times10^9(+0.4/-0.4)$	7.64	676	1
2	ULAS J1342+0928	$9.1\times10^8(+1.3/-1.4)$	7.541	688	2
3	J100758.264+211529.207	$1.5\times10^9(+0.2/-0.2)$	7.52	690	3
4	ULAS J1120+0641	$2.0\times10^9(+1.5/-0.7)$	7.085	747	4
5	J124353.93+010038.5	$3.3\times10^8(+2.0/-2.0)$	7.07	749	5
6	J0038-1527	$1.33\times10^9(+0.25/-0.25)$	7.021	756	6
7	DES J025216.64-050331.8	$1.39\times10^9(+0.16/-0.16)$	7	759	7
8	ULAS J2348-3054	$2.1\times10^9(+0.5/-0.5)$	6.886	775	8
9	VDES J0020-3653	$1.67\times10^9(0.32/-0.32)$	6.834	783	9
10	PSO J172.3556+18.7734	$2.9\times10^8(+0.7/-0.6)$	6.823	784	10
11	ULAS J0109-3047	$1.5\times10^9(+0.4/-0.4)$	6.745	796	8
12	HSC J1205-0000	$2.9\times10^9(+0.4/-0.4)$	6.73	799	11,12

BH #	Black Hole Name	BH Mass MBH ($M_\odot$)($\pm 1\sigma$)	z	Age (Myr)	Ref
13	VDES J0244-5008	$1.15 \times 10^9 (+0.39/-0.39)$	6.724	800	9
14	PSO J338.2298	$3.7 \times 10^9 (+1.3/-1.0)$	6.658	810	13
15	ULAS J0305-3150	$1.0 \times 10^9 (+0.1/-0.1)$	6.604	819	8
16	PSO J323.1382	$1.39 \times 10^9 (+0.32/-0.51)$	6.592	821	14
17	PSO J231.6575	$3.05 \times 10^9 (+0.44/-2.24)$	6.587	820	14
18	PSO J036.5078	$3 \times 10^9 (+0.92/-0.77)$	6.527	831	13,14
19	VDES J0224-4711	$2.12 \times 10^9 (+0.42/-0.42)$	6.526	831	9
20	PSO J167.6415	$3 \times 10^8 (+0.08/-0.12)$	6.508	834	13,14
21	PSO J261+19	$6.7 \times 10^8 (+0.21/-0.21)$	6.483	839	15
22	PSO J247.2970	$5.2 \times 10^8 (+0.22/-0.25)$	6.476	840	14
23	PSO J011+09	$1.20 \times 10^9 (+0.51/-0.51)$	6.458	843	15
24	CFHQS J0210-0456	$8 \times 10^7 (+5.5/-4.0)$	6.438	846	16
25	CFHQS J2329-0301	$2.5 \times 10^9 (+0.4/-0.4)$	6.417	850	16
26	SDSS J1148+5251	$2.7 \times 10^9 (+0.4/-0.4)$	6.41	851	17,18
27	HSC J0859 +0022	$3.8 \times 10^7 (+0.1/-0.18)$	6.388	855	11,19
28	HSC J1152 +0055	$6.3 \times 10^8 (+0.8/-1.2)$	6.36	860	11,19
29	SDSS J1148+0702	$1.26 \times 10^9 (+0.14/-0.14)$	6.339	863	20
30	SDSS J1030+0524	$1.0 \times 10^9 (+0.2/-0.2)$	6.3	870	21,22
31	SDSS J0100+2802	$1.24 \times 10^{10} (+0.19/-0.19)$	6.3	870	23
32	CFHQS J0050+3445	$2.6 \times 10^9 (+0.50/-0.4)$	6.253	879	16
33	HSC J2239 +0207	$1.1 \times 10^9 (+3/-2)$	6.245	880	19
34	VDES J0330-4025	$5.87 \times 10^9 (+0.89/-0.89)$	6.239	881	15
35	VDES J0323-4701	$5.5 \times 10^8 (+1.26/-1.26)$	6.238	881	15
36	SDSS J1623+3112	$1.5 \times 10^9 (+0.3/-0.3)$	6.211	886	21
37	SDSS J1048+4637	$3.9 \times 10^9 (+2.1/-2.1)$	6.198	889	24
38	PSO J359–06	$1.66 \times 10^9 (+0.21/-0.21)$ 6.164	895	15	
39	CFHQS J0221-0802	$7 \times 10^8 (+7.5/-4.7)$	6.161	896	16
40	HSC J1208-0200	$7.1 \times 10^8 (+2.4/-5.2)$	6.144	899	19
41	ULAS J1319+0950	$2.7 \times 10^9 (+0.6/-0.6)$	6.13	902	25,26
42	CFHQS J1509-1749	$3 \times 10^9 (+0.3/-0.3)$	6.121	903	16
43	PSO J239-07	$3.63 \times 10^9 (+0.20/-0.20)$	6.114	905	15
44	HSC J2216-0016	$7 \times 10^8 (+1.4/-2.3)$	6.109	906	19
45	CFHQS J2100-1715	$3.37 \times 10^9 (+0.64/-0.64)$	6.087	910	16
46	SDSS J0303-0019	$3 \times 10^8 (+2.0/-2.0)$	6.079	911	24
47	SDSS J0353+0104	$1.4 \times 10^9 (+1.0/-1.0)$	6.072	913	24
48	SDSS J0842+1218	$1.7 \times 10^9 (+1.2/-1.2)$	6.069	913	24
49	SDSS J1630+4012	$9 \times 10^8 (+0.8/-0.8)$	6.058	915	24
50	PSO J158-14	$2.15 \times 10^9 (+0.25/-0.25)$	6.057	916	15

BH #	Black Hole Name	BH Mass MBH ($M_\odot$)($\pm 1\sigma$)	z	Age (Myr)	Ref
51	CFHQS J1641+3755	$2.4 \times 10^8 (+1.0/-0.8)$	6.047	918	16
52	SDSS J1306+0356	$1.1 \times 10^9 (+0.1/-0.1)$	6.017	923	21
53	SDSS J2310+1855	$2.8 \times 10^9 (+0.6/-0.6)$	6.003	926	27, 19
54	CFHQS J0055+0146	$2.4 \times 10^8 (+0.9/-07)$	5.983	930	16
55	PSO J056-16	$7.5 \times 10^8 (+0.07/-0.07)$	5.975	932	15
56	SDSS J1411+1217	$1.1 \times 10^9 (+0.1/-01)$	5.93	941	28, 22
57	SDSS J0005-0006	$3 \times 10^8 (+0.1/-01)$	5.85	957	28,22
58	SDSS J0836+0054	$2.7 \times 10^9 (+0.6/-0.6)$	5.82	964	28, 22
59	SDSS J1044-0125	$1.05 \times 10^{10} (+0.16/-0.16)$	5.784	971	29, 21

Table 2: Parameters of SMBHs at $z > 5.7$.

Notes: BHs are listed in order of their redshift from the highest to the lowest. The first reference # is for the BH discovery paper and the second # is for the BH mass estimate.

References in Table 2

[1] Wang, F., et al., ApJL. 907, L1 (2021)

[2] Bañados, E. et al. Nature, 553, 473 (2017)

[3] Yang, J., et al. ApJL. 897, L14 (2020)

[4] Mortlock, D.J., et al. Nature, 474, 616 (2011)

[5] Matsuoka, Y., et al. ApJL 872, L2 (2019)

[6] Wang F., et al. ApJL 869, L9 (2018)

[7] Wang, F., et al. ApJ. 896, 23 (2020)

[8] Venemans, B.P., et al. ApJ. 779, 24 (2013)

[9] Reed, S.L., et al. MNRAS. 2, 1874-1885 (2019)

[10] Bañados, E. et al. ApJ. 909, 80 (2021)

[11] Matsuoka, Y., et al. ApJ. 828, 26 (2016)

[12] Kato, N., et al. ASJ. 72, (5), 84 (2020)

[13] Venemans B.P., et al. ApJL 801, L11 (2015)

[14] Mazzucchelli, C., et al. ApJ. 849, 91 (2017)

[15] Eilers, A.C., et al. ApJ. 900, 37 (2020)

[16] Willott, C.J., et al. ApJ. 140, 546 (2010)

[17] Willott, C.J., McLure, R.J., Jarvis, M.J. ApJL 587, L15 (2003)

[18] Gallerani S. et al. MNRAS. 467, 3590.(2017)

[19] Onoue, M., et al. ApJ. 880, 77 (2019)

[20] Jiang, L., et al. ApJ. 833, 222 (2016)

[21] Jiang, L., et al. ApJ. 134, 1150 (2007)

[22] Kurk, J.D., et al. ApJ. 669, 32 (2007)

[23] Wu, X.B., et al. Nature, 518, 512 (2015)

[24] De Rosa, G., et al. ApJ. 739, 56 (2011)

[25] Mortlock, D.J., et al, A&A, 505, 97 (2009)

[26] Shao, Y., et al. ApJ. 845, 138 (2017)

[27] Wang, F., et al. ApJL. 739, L34 (2011)

[28] Fan, X., et al. ApJ. 131, 1203 (2006)

[29] Fan, X., et al. ApJ. 120, 1167 (2000)

Acknowledgements. The author is indebted to Eva Ritterová for converting this article from WORD to LaTeX and to Hana Bílková for final editing of the manuscript.

Conference *Cosmology on Small Scales 2024*
Michal Křížek and Yurii Dumin (Eds.)
Institute of Mathematics CAS, Prague

CAN THE QUASI-OSCILLATORY STRUCTURE OF LOW MULTIPOLES IN THE CMB SPECTRUM BE ASSOCIATED WITH THE DOMAIN STRUCTURE OF VACUUM?

Yurii V. Dumin[1,2]

[1]Sternberg Astronomical Institute (GAISh) of Lomonosov Moscow State University,
Universitetskii prosp. 13, Moscow, 119234 Russia
[2]Space Research Institute (IKI) of Russian Academy of Sciences,
Profsoyuznaya str. 84/32, Moscow, 117997 Russia
dumin@yahoo.com, dumin@pks.mpg.de

Abstract: Anomalous behavior of low multipoles in the CMB spectrum—namely, their apparent quasi-oscillatory pattern—is a well-known problem of observational cosmology, which was clearly recognized when data by the space observatories *WMAP* and *Planck* became available. Here, we suggest to interpret this anomaly as an imprint of the domain structure of vacuum formed after a symmetry-breaking phase transition of the specific scalar field, e.g., one of Higgs fields, which are commonly postulated in the modern theories of elementary particles. Following this idea, we firstly explain why the domain structure will affect the CMB spectrum at the largest scales (i.e., the lowest multipoles). Secondly, based on the most general assumptions, we estimate the number of vacuum domains in the observable part of the Universe, which turns out to be in the range from 4 to 46.

Keywords: cosmic microwave background (CMB), low multipoles, early Universe, phase transitions

PACS: 98.65.Dx, 98.80.Cq, 98.80.Es

1. Introduction

As is known, analysis of the spectrum of spatial fluctuations of the cosmic microwave background (CMB) became in the last two decades one of the major tools for testing the cosmological models and deriving the basic cosmological parameters [8]. However, while—under appropriate choice of the fitting parameters—a perfect agreement between the theory and observations can be achieved in the region of sufficiently high multipoles ℓ (namely, above a few dozens), a much worse situation takes place at the low multipoles, $\ell \lesssim 30$, as illustrated in Figure 1. Firstly, the measured amplitudes substantially deviate from the theoretical predictions. Secondly, these amplitudes exhibit a quasi-oscillatory structure, especially at $\ell \lesssim 10$.

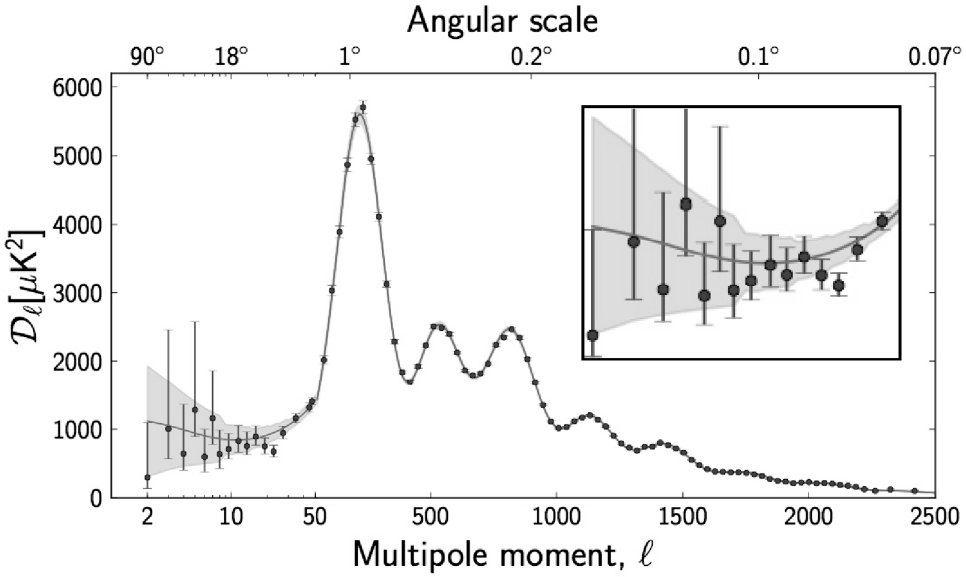

Figure 1: The spectrum of CMB fluctuations measured by *Planck* satellite; adapted from [1]. The circles with error bars are the experimental values, while the solid curve is the theoretical calculation. A quasi-oscillatory structure of low multipoles is shown in the insert in the upper right corner.

By now, the above-mentioned anomaly was clearly recognized, but its physical nature remains unknown. One point of view is that this is just a result of poor statistical significance of the low multipoles (or, the so-called "cosmic variance"). Another point of view is that this anomaly resulted from some kind of a "new physics" acting in the early Universe. In the present work, we shall follow the second approach. Namely, we believe that the anomalous behavior of the low harmonics might be an imprint of the domain structure of the physical vacuum. Such vacuum domains should be naturally expected in the early Universe described by some versions of the Grand unification theories (GUT) of the elementary particles.

2. The Symmetry-Breaking Phase Transitions and Topological Defects

Formation of the non-trivial domain structure of the physical vacuum was predicted soon after emergence of the first gauge theories of elementary particles with a spontaneous symmetry breaking of the Higgs field. N.N. Bogoliubov seems to be the first researcher who drew attention to this problem in 1964 at the conference dedicated to the 400'th anniversary of the birth of Galileo Galilei. Two years later, the corresponding report was published in the journal article [2].

The basic idea was that—since the energetically favorable ("vacuum") states of the Higgs field in the remote spatial subregions should be established independently in the course of expansion and cooling of the early Universe—their phases, in general,

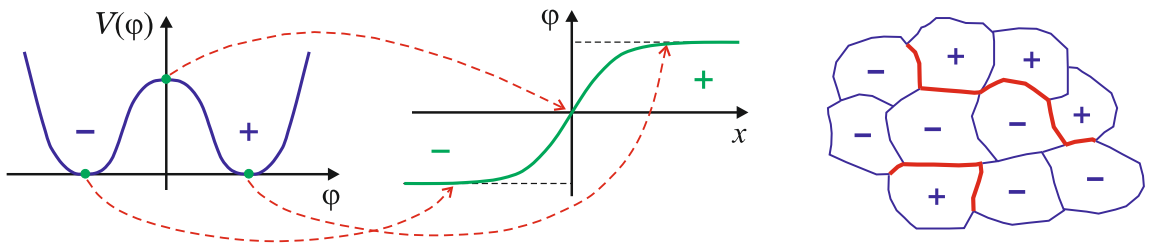

Figure 2: Sketch of formation of a domain wall ("kink") due to the relaxation of the field φ into two different states in the remote regions of space (left panel) and the domain structure of vacuum resulting from such process (right panel).

will be different. As a result, the entire space will be split into domains of different vacua, separated from each other by the domain walls (or "kinks"). For example, in the simplest case of the real Higgs field φ with the Lagrangian $\mathcal{L}$ possessing $\mathbb{Z}_2$ symmetry group,

$$\mathcal{L} = K(\varphi) - V(\varphi) = \frac{1}{2}\Big[(\partial_t\varphi)^2 - (\nabla\varphi)^2\Big] - \frac{\lambda}{4}\Big[\varphi^2 - (\mu^2/\lambda)\Big]^2, \qquad (1)$$

the process of formation of the domain walls is illustrated in Figure 2. Namely, the average value of the field φ in the high-temperature phase equals zero due to a large contribution from the kinetic term K. However, when the Universe expands and its temperature drops down, the role of the kinetic term decreases and major contribution comes from the potential term V. As a result, the field φ relaxes to one of the energetically preferable states:

$$\varphi_\pm = \pm\mu/\sqrt{\lambda}\,, \qquad (2)$$

where the Hamiltonian $\mathcal{H} = K + V$ becomes minimal. This phenomenon was predicted by D.A. Kirzhnits [4] and subsequently studied in detail by A.D. Linde [6] and other researchers.

Let us emphasize that—although both vacuum states have zero energy and, as a result, are indistinguishable from each other—the energy of the domain walls will be non-zero and, therefore, they can exhibit some observable effects.

It is interesting to mention that in the early 1960's N.N. Bogoliubov was an opponent of the gauge theories with the spontaneous symmetry breaking, and separation of vacuum into the distinct domains was used by him as one of the arguments against such models. However, when in the late 1960's and early 1970's the above-mentioned theories (and, first of all, the Glashow–Salam–Weinberg electroweak model) became commonly accepted, the possibility of the domain structure of vacuum was taken seriously, and study of the respective cosmological consequences was initiated [9].

At the same time it was realized that, in the case of Higgs field with a continuous symmetry group, the original domain structure should relax to other types of the stable topological defects, such as the cosmic strings (or vortices) and monopoles [3]. As regards, the domain walls (or kinks), they are stable and can survive up to the present time only in the theories with discrete symmetry. On the other hand, since the most perspective and experimentally verified theories of elementary particles (such as the electroweak theory, quantum chromodynamics, as well as the most popular versions of the Grand unification theories) do not involve the discrete symmetries, the interest in the domain walls sharply dropped in the subsequent two or three decades, and the main focus was on the cosmic strings and monopoles.

Particularly, a considerable effort was devoted in the late 1990's and early 2000's to searching for the non-Gaussian features in the CMB spectrum, which might be produced by evolution of the "web" of cosmic strings; much attention was paid also to the laboratory experiments on the detection of monopoles [5]. Unfortunately, all these efforts were unsuccessful and, as a result, the problem of the non-trivial structure of the physical vacuum and its cosmological consequences faded into the background.

3. Effect of the Domain Walls on the CMB Spectrum

Despite of the above-mentioned failure to find the observable manifestations of the strings and monopoles, a new hint at the domain walls could be derived from the CMB observations performed by *WMAP* and *Planck* satellites in the last two decades. Namely, this is the anomalous behavior of the low multipoles in the CMB spectrum, already mentioned in the Introduction and illustrated in Figure 1.

Unfortunately, since we do not know the exact parameters of the elementary-particle model responsible for the domain formation, we cannot trace in detail how the variations of the Higgs field φ are ultimately transformed into the observable fluctuations of the electromagnetic field:

$$\delta(\mathbf{E}, \mathbf{H}) = f(|\varphi|)\,, \tag{3}$$

where f is the unknown transformation function. Nevertheless, *we can make the most general assumption that this function is, at least, monotonic.* Therefore, although we cannot derive any relation between the amplitudes of Fourier harmonics of $\mathbf{E}$ (or $\mathbf{H}$) and φ, we should expect that the positions of their spectral maxima and minima should be interrelated, i.e., the spectra will be qualitatively similar to each other.

Next, a well-known feature of the Fourier transformation is that *sharp structures in the original function result in the oscillatory behaviour of its Fourier harmonics and vice versa.* Therefore, *the observed quasi-oscillatory structure in the CMB spectrum might be attributed just to the sharp variations of the scalar field φ in its symmetry-broken phase, i.e., to the domain walls.*

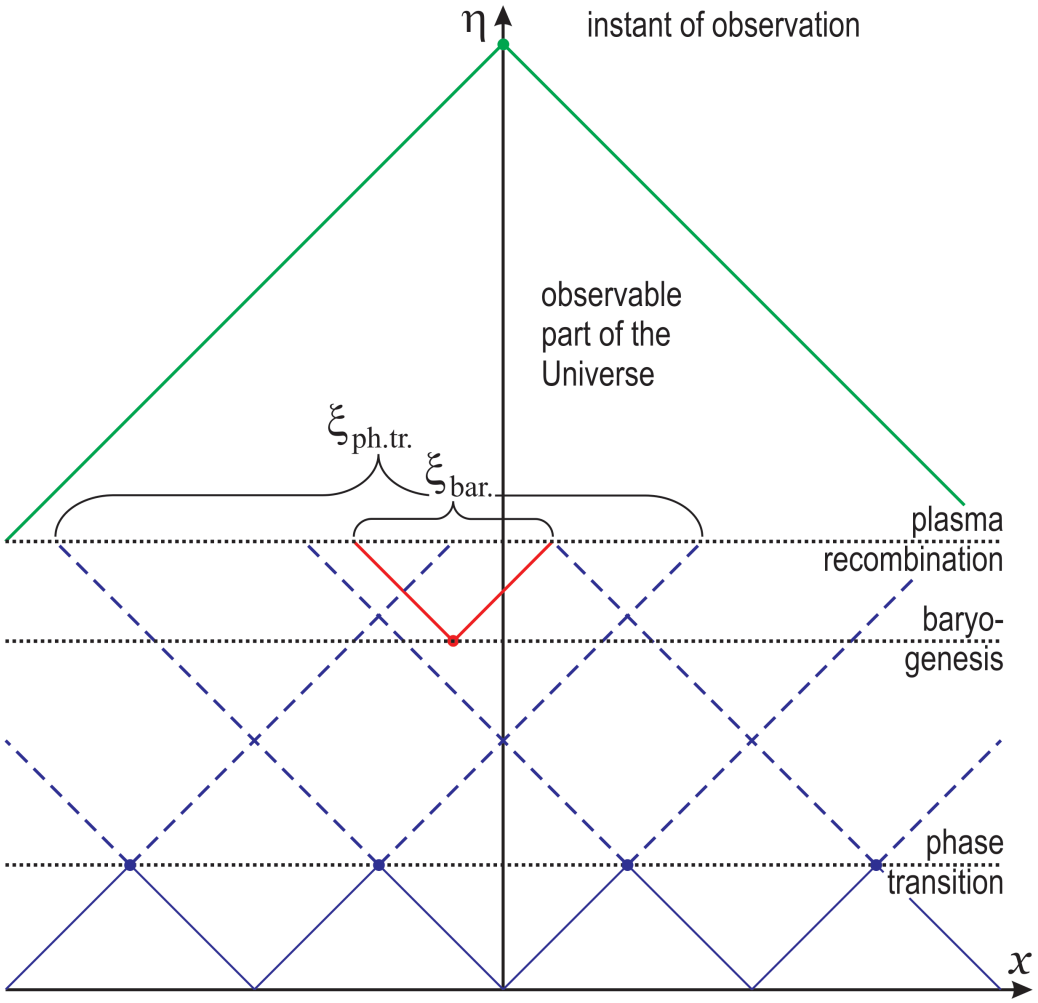

Figure 3: Conformal diagram of the space–time after the Big Bang. The light cones originating at the instant of phase transition (and, therefore, showing the development of irregularities of the field φ) are drawn by the dashed blue lines; and the light cones originating an the instant of baryogenesis (and showing the development of irregularities of the ordinary matter), by the solid red lines.

Next, *such domain walls should affect the CMB spectrum at the largest spatial scales, i.e., the lowest multipoles.* This fact can be easily illustrated by the conformal diagram of the space–time presented in Figure 3. Really, starting from the standard Friedmann–Robertson–Walker (FRW) metric,

$$ds^2 = dt^2 - a^2(t)\, dx^2 \tag{4}$$

(for simplicity, we consider here a single spatial coordinate x), and introducing the

conformal time

$$\eta = \int \frac{dt}{a(t)}\,, \tag{5}$$

we can get the conformally-flat metric [7],

$$ds^2 = a^2(t)\,[\,d\eta^2 - dx^2\,]\,, \tag{6}$$

where the light rays ($ds^2 = 0$) are represented by the straight lines inclined at $\pm\pi/4$:

$$x = \pm\,\eta + \text{const}\,. \tag{7}$$

Therefore, both the past and future causality cones can be depicted by the right triangles, whose legs are oriented either downwards or upwards.

Since the phase transition occurred much earlier than, for example, a baryogenesis, the corresponding correlation length $\xi_{\text{ph.tr.}}$ at the instant of recombination (when the CMB spectrum became observable) should be much greater than the correlation length $\xi_{\text{bar.}}$. This fact is obvious in Figure 3, where $\xi_{\text{ph.tr.}}$ and $\xi_{\text{bar.}}$ are represented by the hypotenuses of the respective triangles. On the other hand, the perturbations formed by interaction between the plasma and radiation, which are responsible for the major peaks in the CMB spectrum, evidently developed after the baryogenesis and, therefore, should possess the even smaller correlation lengths (and, correspondingly, the greater multipoles).

It is important also to note that the domain walls and, for example, the cosmic strings behave differently in the course of cosmological evolution. The grid of domain walls is approximately fixed in the co-moving coordinates and, thereby, expands with a rate of the standard Hubble flow. On the other hand, the cosmic strings tend to form closed loops, which begin to shrink under the internal tension. Therefore, just the domain walls produce perturbations at the largest scales and lowest multipoles.

4. The Number of Domains in the Observable Universe

As was already mentioned above, we cannot study in detail how the domain structure of vacuum affects the observed CMB spectrum, because we have no information on the parameters of the underlying Higgs field φ. However, using the assumption that fluctuations of the observed electromagnetic field depend monotonically on the variations of φ, it is possible to estimate some of its spatial parameters in the symmetry-broken phase, for example, the number of domains in the observable part of the Universe.

Let ξ be the characteristic size of a domain (in the co-moving coordinates); and R, the radius of the horizon (i.e., the last-scattering surface, where CMB spectrum is formed); see Figure 4. Then, the following rough estimates can be performed:

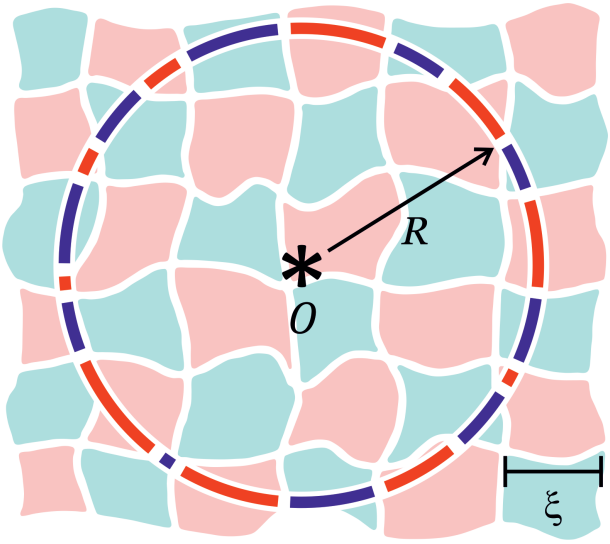

Figure 4: Sketch of the vacuum domains (represented by the irregular rectangles of different colors) within the observable horizon (a circle centered at the position of the observer O).

- The number of domains on "the circle of the last scattering" (which is a 2D cross-section of the sphere of the last scattering, as shown in the above-mentioned figure):
$$\mathcal{N}_{\rm cir} \approx 2\pi R/\xi\,. \tag{8}$$
- The number of domains on the surface of the 2D cross-section inside the sphere of the last scattering:
$$\mathcal{N}_{\rm sur} \approx \pi R^2/\xi^2\,. \tag{9}$$
- The number of domains in the volume inside the sphere of the last scattering:
$$\mathcal{N}_{\rm vol} \approx (4\pi/3)\, R^3/\xi^3\,. \tag{10}$$

Combining these formulas, we can easily get:

$$\mathcal{N}_{\rm sur} \approx \mathcal{N}_{\rm cir}^2/(4\pi)\,, \tag{11}$$
$$\mathcal{N}_{\rm vol} \approx \mathcal{N}_{\rm cir}^3/(6\pi^2)\,. \tag{12}$$

In fact, it is most interesting to find the number of domains in the observable part of the Universe $\mathcal{N}_{\rm vol}$.

As follows from the *Planck* data reproduced in Figure 1, the most pronounced low multipoles in the CMB spectrum are $\ell = 3, 5$, and 7. It is reasonable to assume that one of them might be formed just by the set of domains, while the higher multipoles

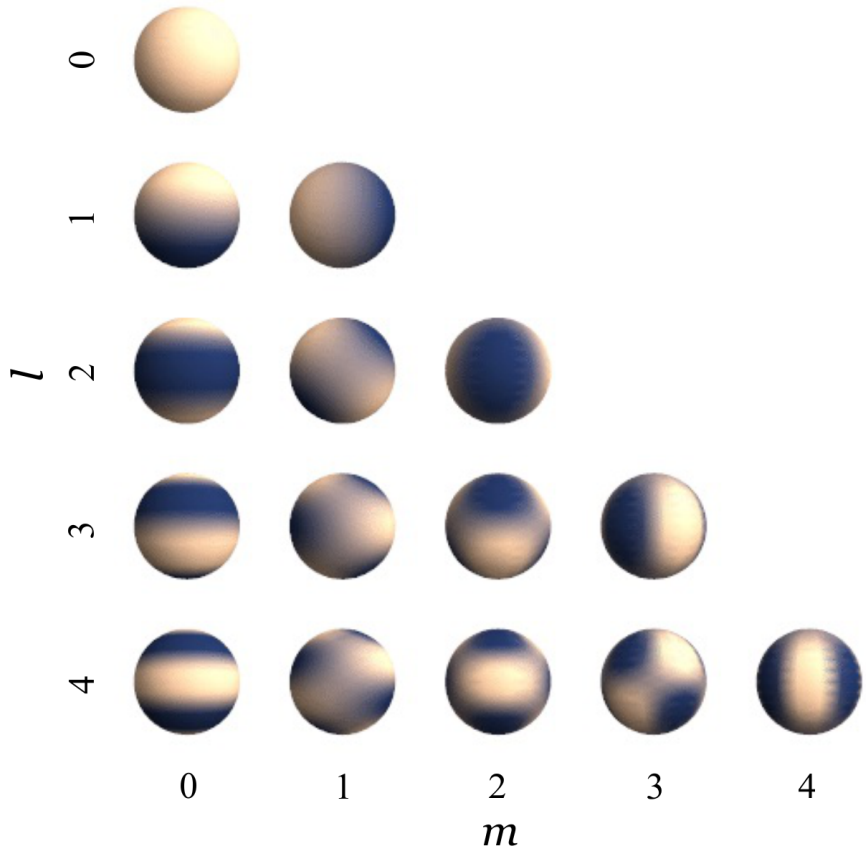

Figure 5: Basic properties of the spherical functions with the specified values of the polar and azimuthal values l and m. Their maxima and minima are shown by the light and dark areas, respectively.

appeared because of their sufficiently sharp boundaries (i.e., small thickness of the domain walls).

Recalling the basic properties of the spherical functions, illustrated in Figure 5, we see that at the above-mentioned values of ℓ the number of domains along the circle of the last scattering should be approximately

$$\mathcal{N}_{\rm cir} \approx 2l \ = 6, 10, \ \text{or} \ 14\,. \tag{13}$$

Next, using relations (11) and (12), we get the values listed in Table 1. Therefore, *the number of domains with different vacua in the observable part of the Universe is estimated to be 4 to 46.* Of course, this is a rather crude analysis, which should be considered just as the first step to the future more accurate statistical modelling.

l	3	5	7
$\mathcal{N}_{\rm cir}$	$\sim$6	$\sim$10	$\sim$14
$\mathcal{N}_{\rm sur}$	$\sim$3	$\sim$8	$\sim$16
$\mathcal{N}_{\rm vol}$	$\sim$4	$\sim$17	$\sim$46

Table 1: Estimated parameters of the domain structure in the observable part of the Universe.

5. Discussion and Conclusions

In the present paper, we (1) explained why a grid of domain walls, formed by the symmetry-breaking phase transition in the early Universe, might be a reasonable explanation of the anomalous (quasi-oscillatory) behaviour of low multipoles in the CMB spectrum and (2) roughly estimated the number of such domains in the observable part of the Universe.

Of course, the next important question is how generic is the pattern of domains that could result in the required oscillations in the CMB spectrum, i.e., what is the probability of its formation among all possible configurations? We plan to address this issue in one of the subsequent papers.

Acknowledgements

This work was substantially stimulated by the discussions with A.A. Starobinsky at the previous CSS conferences, who also paid much attention to the anomalous behavior of low multipoles in the CMB spectrum. However, he was mostly interested in the apparent depression at $\ell \approx 20$ rather than in its oscillatory structure at $\ell \lesssim 10$. I am also grateful to I.E. Bulyzhenkov, A.V. Toporensky, and Yu.S. Vladimirov for valuable discussions and comments.

References

[1] Ade P.A.R., et al. (Planck Collaboration): Planck 2013 results. I. Overview of products and scientific results. Astron. & Astrophys. **571** (2014), A1.

[2] Bogoliubov N.N.: Field-theoretical methods in physics. Suppl. Nuovo Cimento (Ser. prima) **4** (1966), 346.

[3] Kibble T.W.B.: Topology of cosmic domains and strings. J. Phys. A **9** (1976), 1387.

[4] Kirzhnits D.A.: Weinberg model and the "hot" Universe. JETP Lett. **15** (1972), 529.

[5] Klapdor-Kleingrothaus H.V. and Zuber K.: *Particle astrophysics*. Inst. Phys. Publ., Bristol, 1997.

[6] Linde A.D.: The inflationary Universe. Rep. Prog. Phys. **47** (1984), 925.

[7] Misner C.W.: Mixmaster Universe. Phys. Rev. Lett. **22** (1969), 1071.

[8] Scott D. and Smoot G.F.: Cosmic microwave background. In: C. Patrignani, et al. (Particle Data Group), *Review of particle physics*, Chin. Phys. C **40** (2016), 100001, p. 411.

[9] Zel'dovich Ya.B., Kobzarev I.Yu., and Okun' L.B.: Cosmological consequences of a spontaneous breakdown of a discrete symmetry. J. Exp. & Theor. Phys. **40** (1975), 1.

Conference *Cosmology on Small Scales 2024*
Michal Křížek and Yurii Dumin (Eds.)
Institute of Mathematics CAS, Prague

THE FAINT YOUNG SUN PARADOX

Elizaveta G. Khramova

Institute of Terrestrial Magnetism, Ionosphere
and Radio Wave Propagation RAS (IZMIRAN),
Kaluzhskoe shosse 4, Troitsk, Moscow, 108840 Russia
sinop@yandex.ru

Abstract: A new formulation of the Faint Young Sun Paradox is presented. We believe that the paradox can be solved by the action of the enhanced activity of the young Sun on the planetary atmospheres. In addition, we suggest the hypothesis of the planetary organic films, which enables us to remove restrictions on the concentration of greenhouse gases in the atmosphere and, thereby, to resolve the Faint Young Sun Paradox for the Earth.

Keywords: Faint Young Sun Paradox, solar variability, greenhouse gases

PACS: 92.30.Np, 92.70.Qr, 96.90.+c

1. The Faint Young Sun Paradox: physical background

The Faint Young Sun Paradox was formulated by the American astronomers Carl Sagan and George Mullen in 1972 [20]. It follows from the contradiction between the paleoclimatic data and the astrophysical models of evolution of the Sun. As follows from the stellar modeling, the solar luminosity 4 billion years ago was about 75% of its current value (see, for example, Figure 3 below), which should result in freezing of the planet. On the other hand, as follows from the planetological data, mean temperature on the Earth's surface in that period was 40^o to 70^o C. Just this fact is the basis of the commonly-accepted formulation of the Faint Young Sun Paradox.

Let us analyze possible solutions of this paradox. As follows from the Stefan–Boltzmann law, the equilibrium thermal radiation of the Earth is described by the formula:

$$L(1-A) = 4\sigma T_e^4\,, \tag{1}$$

where $L = 1361\,\mathrm{W/m^2}$ is the solar constant, $A = 0.367$ is the Earth's geometric albedo, $\sigma = 5.669.10^{-8}\,\mathrm{W/(m^2K^4)}$ is the Stefan-Boltzmann constant, and T_e the Earth's effective temperature, whose contemporary value is 249 K or -24° C.

Consequently, the Earth would still be frozen, if not for the property of its atmosphere, namely, a sufficient transparency in the visible range and much lower transparency in the infrared one. The atmosphere transmits better the solar radiation to

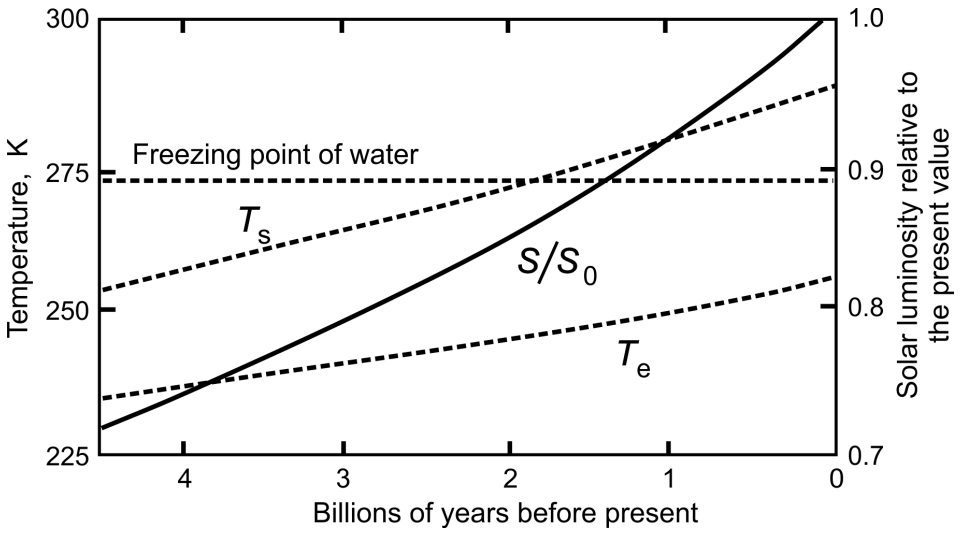

Figure 1: Kasting diagram: Dotted curves show the time dependences of the effective and surface temperatures of the Earth (with the albedo equal to its modern value) and the freezing temperature of water, while the solid curve shows variation of the solar luminosity when the Sun was at the Main sequence [8].

the Earth's surface than the infrared radiation from it. This was called the greenhouse effect, whose magnitude can be written as $\Delta T = T_s - T_e$, where T_s is the average surface temperature of the Earth. Currently, $T_s = 288\,\mathrm{K} = 15^\circ\,\mathrm{C}$, so that $\Delta T = 39\,\mathrm{K}$.

To illustrate these discrepancy, the Kasting diagram (Figure 1) [8] is commonly employed: the curves of the effective and surface temperatures of the Earth are plotted under the condition of a constant albedo (equal to the present value) and permanent properties of the Earth's atmosphere. It can be seen from the graph that the Earth's surface temperature would have reached, under the specified conditions, the freezing temperature of water about 2 billion years ago. Therefore, the paradox is often formulated as follows: In the first 2–2.5 billion years of its existence the water on the Earth, according to the solar models, should have been frozen. This contradicts the geological and paleontological data. But the fact that water on the Earth's surface in the last 2 billion years was in a liquid state is generally accepted. What is the incorrectness of this formulation?

Let us plot the same dependencies taking into account the initial albedo of the Earth's surface (70 %) in the case of a snowball Earth (Figure 2). Obviously, the increase in luminosity by 30 %, up to the present level, without involving additional factors is not enough to melt the Earth, and the planet would still remain a frozen ball. This is an additional serious argument in favor of a warm young Earth. Thus, the paradox of the faint young Sun in a commonly-accepted treatment is a purely physical paradox, and the paleoclimatic data only confirm it.

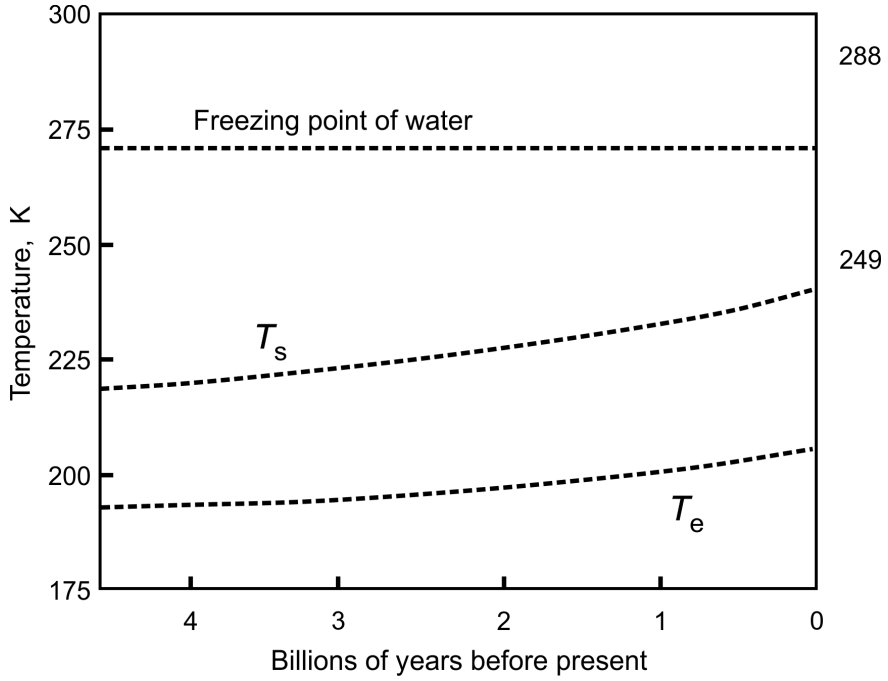

Figure 2: Time dependences of the effective and surface temperatures of the Earth calculated for the albedo 70 % and the contemporary magnitude of the greenhouse effect *versus* the freezing temperature of water [11].

2. Options for solving the Faint Young Sun Paradox

What are the possible solutions of the paradox? The following options steam from the above equations:

1. the incorrectly calculated solar constant of the young Sun;
2. a significantly smaller albedo of the young Earth;
3. the unaccounted additional energy sources;
4. a more powerful greenhouse effect;
5. reduced radii of the planetary orbits in the young Solar system due to the local Hubble expansion.

The proposed hypotheses were repeatedly discussed in the scientific community, e.g., review [5]. The additional analysis was carried out in the articles [10] and [15]. Here is a brief summary of the main findings:

1. Solving the paradox of the faint young Sun by changing the solar constant seems unlikely. However, some loss of the star mass could slightly reduce the missing 30 %.

2. The attempts to solve the problem by reducing the albedo alone are unsuccessful, as they are not able to compensate for such a significant lack of the solar energy. The albedo of the modern Earth is about 30%. To solve the paradox, it would be necessary to remove this albedo completely.

3. When geothermal flows are considered, the possibility of the convective heat transfer stimulated by the influence of the nearby young Moon is not taken into account. This mechanism could increase a contribution of the geothermal energy to heating a surface of the young planet.

4. The most likely option looks a more powerful greenhouse effect, proposed by C. Sagan and G. Mullen. But it rests against the serious counterarguments on the part of mineralogy, which imposes restrictions on the content of carbon dioxide in the atmosphere of the young Earth (no more than three times higher than the current level), which is clearly not enough to provide the necessary greenhouse effect [18, 10].

5. The possibility to compensate the increasing luminosity of the Sun by the expanding orbit of the Earth [12] looks rather interesting and attractive. Unfortunately, it remains unclear by now if the cosmological Hubble expansion can manifest itself at the planetary scales [2, 4].

It should be noted that the calculation in which the luminosity of the young Sun was 30 % lower than the modern value is based on the standard model of solar evolution, which assumes the mass of the Sun to be constant. In fact, there is some loss of the solar mass, but at this moment there is no an accurate quantitative estimate of this effect.

It was suggested that the mass increase of the young Sun by only 5 % could solve the problem [14]. For main sequence stars with a mass close to that of the Sun, the luminosity is approximately proportional to the fourth power of the mass. The planetary orbital distance is inversely proportional to the solar mass, and the flux of the solar radiation coming to the Earth is inversely proportional to the square of the orbital distance. It turns out that the sunlight flux at the orbital distance of the planet is approximately proportional to $M_{\rm Sun}^6$. So, for the flux of thermal radiation by the young Sun on the Earth's orbit (the solar constant) to be roughly as it is now, and to compensate for the effect of the faint young Sun (30 %), its mass had to be $\sim$5 % larger than the modern value. There is no justification for such a large mass loss [10]. In addition, the mass loss by the stars is uneven: a sporadic radiation intensity of the young stars is much higher than that of the mature ones. Most likely, the situation developed by the following way: at first, the lack of luminosity was partially compensated by the excessive mass, but with the expiration of this excess the compensation was no longer possible.

One of the main arguments against finding a solution of the faint young Sun paradox by compensating for the luminosity by the mass loss is the fact that this

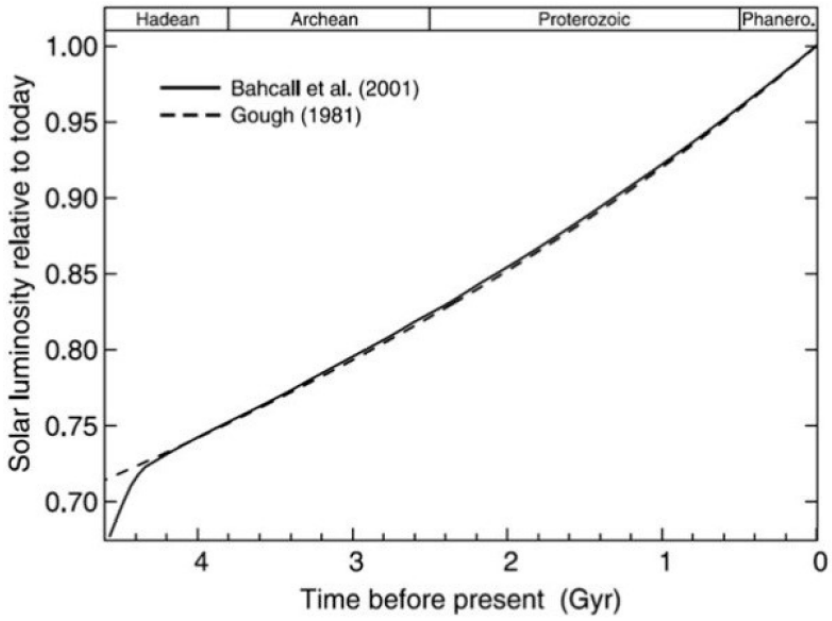

Figure 3: Evolution of the solar luminosity over the four geologic eons for the standard solar model [1] (solid curve) and according to the approximation [7] (dashed curve); reproduced from [5].

paradox is also relevant to Mars. The flux of solar radiation in its orbit is about 60 % lower than in the Earth orbit. Even if it were possible to solve the paradox for the young Earth by increasing the solar constant, the faint young Sun paradox for Mars would be more than 50 %.

3. New treatment of the Faint Young Sun Paradox

It is worth turning to the peculiarities of the faint young Sun paradox on which the attention of researchers was not usually focused. Comparing the thermal characteristics of Venus, Earth, and Mars, we get the apparently obvious result: a surface temperature of the planets decreases with distance from the Sun. However, the albedo of Venus is more than 70 %. As a result, its surface receives less heat than the Earth, and the effective temperature is 25 K lower than that of the Earth [22]. So, the high temperature on the surface of Venus is due to the powerful greenhouse effect in its atmosphere.

Let us compare now the graphs of the temporal dependences of the solar luminosity and the Earth's surface temperature (Figure 3). According to the biological and paleontological data, mean temperature on the Earth during this period was about $+70^\circ$ C [17] (or, according to the most modest estimates, not less than $+40^\circ$ C) as compared to its contemporary value $+15^\circ$ C (Figure 4). Reconstruction of the ancient protein sequences gives the optimal temperature $55^\circ - 65^\circ$ C, while the evolutionary changes suggest a gradual cooling of their environmental medium [6].

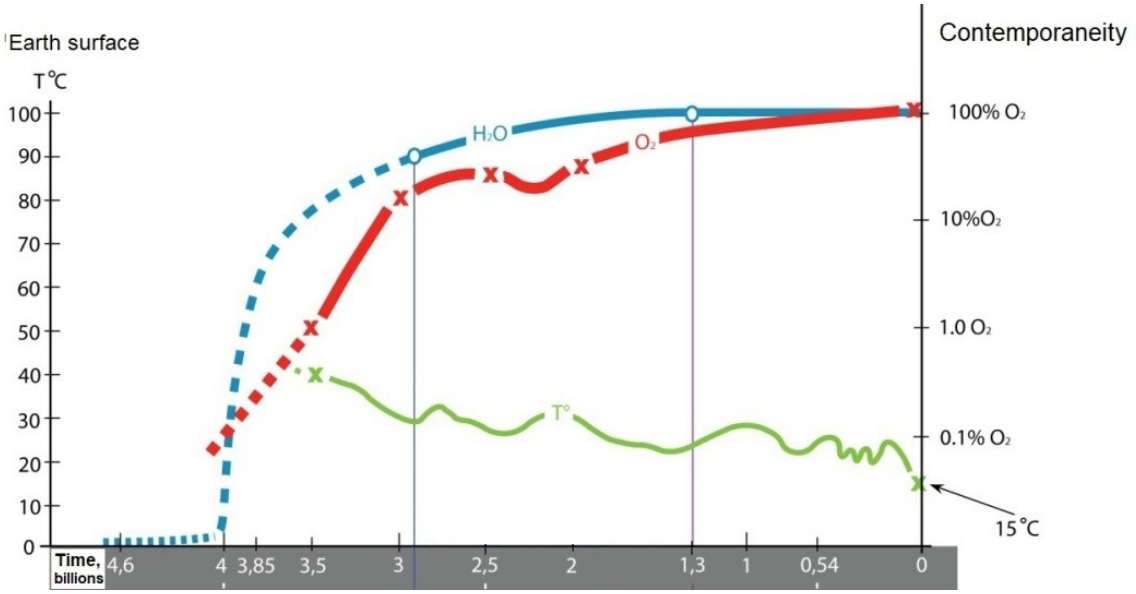

Figure 4: The geologically documented history of the Earth: surface temperature over the last 4 billon years (lower green curve), concentration of the water vapor (upper blue curve), and oxygen (middle red curve) [19].

It is surprising in the faint young Sun paradox not only that at low solar luminosity there was a high temperature on the Earth but also that with increasing the luminosity (Figure 3) the temperature of the Earth's surface (green lower curve in Figure 4) decreases steadily. The temperature on the young Mars was also higher than modern, which is confirmed by traces of liquid water left on its surface.

Starting from these facts, let us present the following new definition: *The Faint Young Sun Paradox is a gradual decrease in the surface temperatures of the Earth and Mars under the monotonically increasing solar luminosity.* The same phenomenon probably takes place also at Venus, but the available information does not allow us yet to draw a definitive conclusion.

Is it possible to find a common factor of influence on the planets, falling both with a distance from the Sun and with the lifetime of the Solar system? *A suitable candidate for this role can be the solar activity, i.e., the processes associated with strong variable magnetic fields of the Sun, resulting in various kinds of the sporadic emission.*

The young Sun was very different from the present one: it was not only considerably less luminous but also much more active. Its rotation period was 6–8 days and mass up to 103 %; while the actvity was very unstable and irregular, with the intensity of sporadic radiation processes 100–1000 times greater than its modern level. It is possible that the ordered cycles were not established immediately but only about 2–2.5 billion years ago, with a rotation period of 15 days and the magnetic field in-

tensity 5–10 times greater than the modern values [16]. The flares on the early Sun occurred much more frequently and reached the energies 3–4 orders of magnitude greater than today [15]. The short-wavelength (gamma, X-ray and ultraviolet) radiation, radio emission, coronal mass ejections, and solar cosmic rays were 2–3 orders of magnitude higher than the modern ones [9].

Influence of any of these factors (or possibly several factors at once) on the planetary atmospheres could well explain all the difficulties in the paradox. Apparently, the mechanism of influence on all the atmospheres is the same; but the reactions are probably different, depending on the chemical composition of the particular atmosphere. As a result, the greenhouse gases are formed specifically to each atmosphere. A combination of the various greenhouse gases with different absorption bands can give the maximal greenhouse effect [10].

4. The organic film hypothesis

So, among all the proposed solutions of the faint young Sun paradox, it is most likely that just the influence of the greenhouse gases is able not only to compensate for the lack of the solar luminosity but also to produce an excessive effect. However, is it possible to simulate the situation in which a sufficiently high content of the greenhouse gases in the atmosphere would not contradict the data of mineralogy?

A certain balance of carbon dioxide concentration in the atmosphere and in the ocean, depending on the temperature, is maintained. But the chemical composition of the young ocean in the presence of the oxygen-free atmosphere should have been very different from the modern one. These conditions contributed to the synthesis of the organic compounds, and we could assume that an organic film was formed on the surface of the ocean. The presence of such a film prevents a gas exchange between the ocean and the atmosphere. So, a ratio of the atmospheric and dissolved gases will vary depending on the chemical composition of the film, its thickness, and area of the coverage. This makes us to take a different look at the data of mineralogy.

Evidently, the chemical composition of the above-mentioned film could be very diverse. The film located at the phase boundary was exposed to the ultraviolet radiation, which would pass freely through the oxygen-free atmosphere. As a result of photodissociation, the various greenhouse gases should be formed. In the oxygen-free atmosphere, these were primarily methane, carbon dioxide (in smaller quantities), and also possibly nitrogen oxides. In the process of oxygen saturation, the atmospheric opacity for the ultraviolet radiation increases, and the photolysis of the organic film decreases, but its oxidation intensifies. The consist of decomposition products shifts toward carbon dioxide. Thus, the organic film could be a permanent donor of the greenhouse gases.

In addition,—due to creating a certain barrier for the gas exchange—the film changes a heat transfer. For example, a film of the modern oil significantly affects the gas exchange and reduces the water evaporation by 60 % [3]. This will reduce the heat transfer due to evaporation, thereby increasing the temperature of the ocean

surface layer. It is worth to note that the paleontological temperature data are based primarily on the characteristics of the oceans.

It can be assumed that such a thin object will not live long and will be destroyed by the waves. Of course, the film will sometimes tear, especially, in the surf zone. But this will not affect substabtially its integrity in the open ocean. Even in antiquity, the sailors watered a surface of the sea with a vegetable oil to smooth out the excitement. The theoretical basis for this phenomenon was developed by Acad. V.V. Shuleikin [21]. In addition, the film will be permanently renewed. Besides, it does not have to cover the entire surface of the ocean. The effect will depend on the percentage of the surface area it occupies.

While a modern oil film is considered disastrous for an ecosystem, the ancient analogue could be the integral and significant component. It is necessary to say that, even now, considerable areas of the ocean surface are covered with the organic film of non-anthropogenic origin; and its significance in the biological cycles has not yet been adequately studied. These natural spills do not upset the ecological balance and are a breeding ground for about a hundred different types of microorganisms. So, the ancient films became a basis for the first Earth's ecosystems. Moreover, the microorganisms in the process of oil utilization also form the greenhouse gases, such as methane, carbon dioxide, and nitrous oxide.

The mechanism of atmospheric self-regulation is laid down in the following model: There are more greenhouse gases at the higher level of ultraviolet radiation, but at the same time the abundance of the film decreases, which, in turn, inhibits the emission of greenhouse gases, and *vice versa*. When the microorganisms—which feed on the film—appear, they are included into the thermoregulation mechanism. There is already not only chemical but also the biological feedback. A possibility of existence of the hydrocarbon haze, which is also included in the self-regulation mechanism, cannot be discounted. When concentration of methane in the atmosphere is low, there is a little smog. So, intensity of the ultraviolet radiation reaching the surface of the water is high. Consequently, rising decomposition of the organic film increases a concentration of the greenhouse gases, including methane, which leads to increase in the concentration of smog and reduce the intensity of ultraviolet radiation.

Lithology and paleontology often encounter hard-to-explain sharp changes in the concentrations of many substances. The presence of the atmosphere and ocean—two relatively isolated buffer capacities, whose degree of isolation can easily change—may help us to explain these phenomena.

In view of the paradox, the moments of global glaciation (720–635 million years ago) are especially interesting in the fossil records. There is no a commonly-accepted opinion about the degree of glaciation: the viewpoints vary from the most of the surface under the ice to the complete glaciation (Earth-snowball). During these periods, the Earth's albedo increased significantly, up to 70 % in the Earth-snowball version; and even with the modern solar luminosity it is not clear how the planet can be brought out of this state. To increase the content of greenhouse gases to such an

extent seems to be an almost impossible task. This paradox of the lack of energy is twice the faint young Sun paradox.

It would be most reasonable to find a way to reduce the albedo. The glaciation periods lasted for several million years. Firstly, the volcanic dust could precipitate. At the low humidity accompanying such low temperature, it would not be covered with snow too intensively. It seems unlikely that volcanic activity was so high that it could significantly affect the albedo. However, another mechanism connected with the same film, covering a surface of the ocean, looks more promising. The oil rising to the surface of the water was accumulated under the ice. The ice protected the oil from a decomposition by ultraviolet. Bacterial flora—another factor of its decomposition—was most likely inactive at such low temperatures. The accumulated oil—due to diffusion—rose through the ice [13]. This is a long process, but the glaciation itself continued for a long time. When the oil film appeared on the ice surface, albedo was sharply reduced. Besides, the film—being located on the surface—reduced solvability of the greenhouse gases in the water covering the melting glaciers, thereby resulting in conservation of the high concentration of the gases in the atmosphere.

Here is a list of possible mechanisms of influence of the organic film on the greenhouse effect:

1. Change in the ratio of carbon dioxide concentrations in the ocean and atmosphere due to disruption of the gas exchange, which can contribute to the relatively rapid accumulation of the gases in the atmosphere.

2. Possible increase in the ocean surface temperature due to decrease in the vaporization.

3. A permanently replenished source of the greenhouse gases due to photodissociation of the organic film by ultraviolet.

4. Reduction of the high albedo at the possible surface temperature $60^\circ - 70^\circ$ C due to the limited humidity. Although albedo of the oil film (about 15 %) is higher than albedo of the clean ocean (about 8 %), decrease in the cloud cover (whose albedo is about 80 %) should lower the average albedo.

5. Existence of the effect of self-regulation of the greenhouse gases by the Earth's ecosphere.

6. A potential way for the planet to exit the global glaciation due to decrease in albedo by the organic pollution of the ice.

In addition, the organic film seems to be a key to resolve one more paradox, namely, the inconsistency between the absorption spectra of chlorophylls and the spectrum of solar radiation. In other words, the hypothesis of the planetary films can explain why the trees are green. This fact supports the possibility to resolve the Faint Young Sun Paradox by means of the hypothesis of the organic films.

5. Conclusions

1. Solving the faint young Sun paradox, it is not enough to look for a factor that compensates for the lack of solar luminosity to maintain the water on the Earth's surface in a liquid state. It is necessary to explain the cornerstone of the paradox, namely, decrease in the surface temperatures of the Earth and Mars with increase in the solar luminosity. Influence of the solar activity on the planetary atmospheres through strengthening the greenhouse effect may well be the factor explaining all the features of the paradox.

2. The organic film hypothesis outlined in this article can resolve the mismatch between the required greenhouse effect and the mineralogical data.

3. The film itself is a thermoregulating factor due to the variation in the gas exchange between the atmosphere and ocean, the decrease in the vaporization, and the ability to replenish the greenhouse gases when it is decomposed by ultraviolet radiation and later, when it is oxidized by oxygen.

4. Accounting for the presence of the organic film as a climate-forming factor can make significant adjustments to the contemporary climate models.

Acknowledgements

I am grateful to V.N. Obridko, M.V. Ragulskaya, E.A. Rudenchik, M.B. Simakov, A.Yu. Rozanov, M.Ya. Marov, L.M. Zelenyi, V.N. Snytnikov, M.M. Katsova, A.V. Belov, S.V. Starchenko, S.V. Ayukov, Yu.V. Dumin, E.S. Savinykh, A.A. Kolukshev, A.A. Fomin, V.V. Pipin, R.A. Kislov, A.U. Borisova, M.A. Nikitin, A.S. Kutsenko, I.V. Makushevich, N.E. Skoblikow, L.M. Zukakishvili, and I.A. Khramov for the discussion of various aspects of the Faint Young Sun Paradox and the hypothesis of the organic films.

This work was performed in the framework of the Institutional Research Program of the Department of Solar Physics and Solar–Terrestrial Relations of IZMIRAN.

References

[1] Bahcall J.N., Pinsonneault M.H., and Basu S.: Solar models: Current epoch and time dependences, neutrinos, and helioseismological properties. Astrophys. J. **555** (2001), 990–1012.

[2] Bonnor W.B.: Local dynamics and the expansion of the Universe. Gen. Rel. Grav. **32** (2000), 1005–1007.

[3] Bratkov V.V. and Ovdienko N.I.: *Geoecology (Geoekologiya)*, p. 109. Ileksa, Moscow, 2005 (in Russian).

[4] Dumin Yu.V.: Local Hubble expansion: Current state of the problem. In: *Proc. Int. Conf. "Cosmology on Small Scales 2016: Local Hubble Expansion and Selected Controversies in Cosmology"*, pp. 23–40. Inst. Math., Czech Acad. Sci., Prague, 2016.

[5] Feulner G.: The faint young Sun problem. Rev. Geophys. **50** (2012), 2.

[6] Gaucher E., Govindarajan S., Ganesh O.: Paleotemperature trend for Precambrian life inferred from resurrected proteins. Nature **451** (2008), 704–707.

[7] Gough D.O.: Solar interior structure and luminosity variations. Solar Phys. **74** (1981), 21–34.

[8] Kasting J.F., Toon O.B., and Pollack J.B.: How climate evolved on the terrestrial planets. Sci. Amer. **258** (1988), 2, 90–97.

[9] Katsova M.M. and Livshits M.A.: Activity of the young Sun. In: *Space factors in the evolution of biosphere and geosphere (Kosmicheskie faktory evolutsii biosfery i geosfery)*, pp. 67–81. VVM, St. Petersburg, 2014 (in Russian).

[10] Khramova E.G.: On the faint young Sun paradox. In: *Life and Universe (Zhizn' i Vselennaya)*, pp. 74–88. VVM, Moscow, 2017 (in Russian).

[11] Khramova E.G., Ragulskaya M.V., and Obridko V.N.: Physical conditions in the early Solar system and life origin: compatible models. In: *IAU-2018*, Vienna, 2018.

[12] Křížek M. and Somer L.: Manifestations of Dark energy in the solar system. Grav. Cosmol. **21** (2015), 59–72.

[13] Mansurov M.I.: Prospects for the discovery and development of the gas, condensate, and oil deposits on the Russian sea shelf. In: *Mechanisms of the oil spill behavior in the freezing seas (Mekhanismy povedeniya neftyanykh razlivov v zamerzayushchikh moryakh)*, pp. 64–69. VNIIGAS, Moscow, 1998 (in Russian).

[14] Nandy D., Martens P.C.H., Obridko V., Dash S., and Georgieva K.: Solar evolution and extrema: current state of understanding of long-term solar variability and its planetary impacts. Prog. Earth Planet. Sci. **8** (2021), 40.

[15] Obridko V.N., Ragulskaya M.V., and Khramova E.G.: Young Sun, galactic processes, and origin of life. J. Atmosph. Sol.–Terr. Phys. **208** (2020), 105395.

[16] Pipin V.V.: Dependence of magnetic cycle parameters on period of rotation in non-linear solar-type dynamos. Mon. Not. Roy. Astron. Soc. **451** (2015), 1528–1539.

[17] Ragulskaya M.V., Obridko V.N., and Khramova E.G.: Early solar system, paleomagnetic field and the biosphere: current issues. In: *11th Intern. conf. and school "Problems of geocosmos"*, pp. 167–168. St. Petersburg, 2016.

[18] Rosing M.T., Bird D.K., Sleep N.H., and Bjerrum C.J.: No climate paradox under the faint early Sun. Nature **464** (2010), 744–747.

[19] Rozanov A.Yu.: Living conditions on the early Earth after 4.0 billion years ago. In: *Problems of the life origin (Problemy proiskhozhdeniya zhizni)*, pp. 185–198. PIN RAN, Moscow, 2009 (in Russian).

[20] Sagan C. and Mullen G.: Earth and Mars: evolution of atmospheres and surface temperatures. Science **177** (1972), 52–56.

[21] Shuleikin V.V.: *Physics of the sea (Fizika morya)*. Nauka, Moscow, 1968 (in Russian).

[22] Titov D.V., Markiewicz W.J., Ignatiev N.I., et al.: Morphology of the cloud tops as observed by the Venus Express Monitoring Camera. Icarus **217** (2012), 682–701.

Conference *Cosmology on Small Scales 2024*
Michal Křížek and Yurii Dumin (Eds.)
Institute of Mathematics CAS, Prague

IN MEMORY OF PROF. ALEXEI STAROBINSKY (19.04.1948 – 21.12.2023)

Yurii V. Dumin[1,2]

[1]Sternberg Astronomical Institute (GAISh) of Lomonosov Moscow State University,
Universitetskii prosp. 13, Moscow, 119234 Russia
[2]Space Research Institute (IKI) of Russian Academy of Sciences,
Profsoyuznaya str. 84/32, Moscow, 117997 Russia
dumin@yahoo.com, dumin@pks.mpg.de

Abstract: Obituary of Prof. Alexei Starobinsky (19.04.1948 – 21.12.2023), who was a member of the Scientific Committee and active participant of the "Cosmology on Small Scales" conferences. His major scientific achievements are briefly outlined; and special attention is paid to his pedagogical, educational, and administrative activities.

Keywords: obituary, early Universe, cosmological inflation

PACS: 01.60.+q, 98.80.Cq

Unfortunately, in the upcoming conference we shall be unable to welcome our colleague Prof. Alexei Starobinsky, who suddenly passed away on December 21, 2023. He was a member of Scientific Committee of the "Cosmology on Small Scales" conferences and an active participant of our meetings since the second conference in 2018: In that year, he personally visited Prague with his wife, and afterwards he participated on-line because of the COVID epidemic and other restrictions.

Prof. A. Starobinsky was world famous as one of the founders of the theory of cosmic inflation. His first papers on this topic were published around 1980, i.e., simultaneously with the well-known works by A. Guth and A. Linde. However,—while a commonly-used approach to the driving force of inflation in that time was an evolution of the scalar field with a specific potential—the idea by Starobinsky was that the inflation is produced by the modified theory of gravity, involving the higher-order terms of curvature in the Lagrangian, which was later called the $f(R)$-gravity. Such an approach did not attract initially an appreciable attention; but starting from the 2000's it became one of mainstreams both for a description of the early Universe and for the explanation of the present-day Dark energy.

It is interesting to mention that the first time I have seen A. Starobinsky just during his report on that topic at the Zel'dovich seminar in the Sternberg Astronomical Institute. This was approximately in 1984 or 1985, when I was a graduate student

Figure 1: Prof. A. Starobinsky at the CSS 2018 conference in Prague.

in the Moscow Institute of Physics and Technology (MIPT) and occasionally visited Zel'dovich seminars. During the seminar, a conference hall of the Sternberg Institute and even its lobby were crowded. If I remember correctly, Starobinsky came there just after his visit to Cambridge University and told about some results obtained there. His speech was very impressive and enthusiastic. Prof. Ya.B. Zel'dovich, who was sitting not far from me, a few times tried to ask him something; but Starobinsky did not notice his questions at all. After that, Zel'dovich shook his head and said, "Oh, it is impossible to stop a running bison, singing Kobzon[1], and speaking Starobinsky."

Apart from his scientific achievements, A. Starobinsky is also well-known as outstanding teacher and mentor, who helped many young cosmologists at the early stage of their scientific career. As told me Prof. I. Bulyzhenkov—who worked with him in the Landau Institute of Theoretical Physics,—in 1990's Starobinsky was responsible for processing the so-called "letters", which were the papers and research proposals from the amateurs of astronomy and specialists in other branches of science interested in astronomy and astrophysics. In that time, such a position was in every institute of the Russian Academy of Sciences. In fact, the most of respective persons performed their duties rather formally. They usually quickly wrote just a standard answer that the author is not a specialist in astrophysics and his work is of no value. But this was not the case of Starobinsky. He often told, "Science has different levels of complexity, and everyone can work at his own level."

So, A. Starobinsky tried to find an appropriate reviewer for each "letter", who

[1] J.D. Kobzon (1937 – 2018) is the famous Russian singer.

Figure 2: Prof. A. Starobinsky presenting his report at the CSS 2018 conference.

could identify something reasonable in that work. As Prof. I. Bulyzhenkov recalled, Starobinsky looked for the reviewers everywhere, not only inside the Landau Institute but also in its surroundings. For example, a few times he caught Bulyzhenkov at the bus station near the institute and asked him to become a referee of the "letter".

Another interesting recollection of how Starobinsky communicated with the newcomers in cosmology I heard from Prof. V. Vargashkin, who passed away just before Starobinsky. As Vargashkin told me, in the beginning of conversation Starobinsky usually tried to determine the level of knowledge of his interlocutor and then to continue the conversation at the level accessible for that person.

As I remember, at any conference A. Starobinsky was surrounded by a lot of participants, who tried to discuss something with him and to get his advices. It is interesting that such contacts were often initiated not only by that persons but also by Starobinsky himself. For example, in 2001 I participated in the "Cosmion" conference in Moscow with a report about the efficiency of topological defect formation during the cosmological phase transitions. By that time, I was not familiar personally with Starobinsky. However, before the session with my report he came to me, shook my hand, and helped me to establish contacts with other people working on similar topics. Yet another case happened a few years later at the Marcel Grossmann Meeting on General Relativity either in Berlin or Paris (I do not remember exactly): during the conference banquet he invited me to take a seat at his table

Figure 3: Prof. A. Starobinsky (sitting at the first table) in the conference hall of the Institute of Mathematics of CAS in Prague during the CSS 2018 conference.

and introduced me to Prof. R. Sunyaev. He also introduced him a few other young people, mostly from India.

In the process of preparation of the second "Cosmology on Small Scales" conference in 2018, we invited a number of the well-known cosmologists and astrophysicists. About half of them refused or did not reply at all. However, A. Starobinsky agreed to participate instantly and then visited Prague together with his wife. A few pictures of that visit are included into the present paper.

There was a funny story during that visit. When we discussed his accommodation in Prague, he told me that he does not need any special comfort, but his room must be either on the ground floor or equipped with an elevator, because his wife has some problem with her leg and cannot walk up the stairs. I told him, "OK, don't worry, please: there is an elevator in the academic hotel," and did not pass on his request to other members of the organizing committee. Unexpectedly, they reserved for him the best penthouse on a roof of the hotel; and this was the only place inaccessible directly by the elevator...

Unfortunately, because of the COVID pandemic and political situation A. Starobinsky was unable to come again to Prague at the subsequent conferences, but he continued to participate actively on-line. Frankly speaking, as a vice-chair of the organizing committee, I was rather surprised that his was so interested in our meetings, although he received a lot of invitations from all over the world. For example, in the peak of COVID epidemic in 2020, he contacted me several times on his own initiative and asked if it would be possible to present his report remotely.

By now, almost a whole year has passed since Prof. A. Starobinsky left us. How-

Figure 4: Discussion between Prof. A. Starobinsky (sitting on the right) and Chair of the Organizing Committee of CSS 2018 Prof. M. Křížek (standing on the left).

ever, when we meet with other cosmologists, they often recall their contacts with him, as well as his outstanding contribution to cosmology and astrophysics.

Figure 5: Group photo of the participants of the second conference "Cosmology on Small Scales 2018" in Prague. Prof. A. Starobinsky is in the middle of the first raw, between the tables.

ABSTRACTS

DATA FROM TWENTY-THREE LOCALISED FRB'S CONFIRM THE PREDICTIONS OF NEW TIRED LIGHT AND THAT THE UNIVERSE IS STATIC AND NOT EXPANDING

Lyndon Errol Ashmore
460 Ashingdon Road, Rochford, Essex SS4 3ET, United Kingdom
lyndonashmore@outlook.com

Abstract: Fast radio bursts (FRB's) as extragalactic phenomena provide a tantalizing insight into the structure of the IGM. What is exciting is that there are now 23 FRB's with the redshift of the host galaxy along with the dispersion measure (DM) of the FRB. This allows us to test our cosmological ideas against actual data. Mainstream cosmologists look to the Macquart relationship – a highly complicated and processed relationship between the dispersion measure of the FRB and the redshift of the host galaxy (along with some "adjustable parameters"). Dispersion measure is produced by the interaction of the photons of emitted radiation and the "free" electrons encountered on their passage through the IGM. New Tired Light (NTL) explains redshifts in terms of a static universe and an energy loss of the photons as they traverse the IGM and interact with electrons on the way. Consequently, we would expect a direct relationship between DM and redshift, z in a static universe where both redshift and DM are caused by a photon-electron interaction. That relationship is (in SI units) $\mathrm{DM} = (m_e c/(2hr_e)) \ln(1+z)$ or $\mathrm{DM} = 7.3 \times 10^{25} \ln(1+z)$. A plot of the data with the weighting of DM removed for an assumed expansion gives a trend line of $\mathrm{DM} = 6.7 \times 10^{25} \ln(1+z)$ – a difference of just 9% from the NTL predicted value of a combination of universal constants relating to the photon and the electron – with no adjustable parameters. A far better correlation than that predicted by an expanding universe. Fast radio bursts thus provide strong evidence that the universe is static and consequently that the redshifts of distant galaxies are an optical effect and not due to "expansion".

STATIC INTERPRETATION OF FLRW METRIC

Juan De Vicente
CIEMAT, Av. Complutense 40, Madrid 28040, Spain
juan.vicente@ciemat.es

Abstract: In 1933, Etherington demonstrates from General Relativity (GR) the luminosity to angular distances relation given by $d_L = d_A(1+z)$ for a local (i.e. non expanding universe). The relation has been adapted to an expanding universe as $d_L = d_A(1+z)^2$, by defining the comoving distance (d_M) related to the observable luminosity distance by $d_L = d_M(1+z)$. In this work, we show that dropping out the ad hoc concept of comoving distance, the FLRW metric represent a static universe by interpreting the coordinates as luminosity (distance) coordinates rather that comoving ones. In such a universe, the observable luminosity distance is directly derived from FLRW metric and the redshift is still explained by the $a(t)$ factor, which would be interpreted as a time dilation factor rather than a scale factor of an expanding universe. This interpretation agrees with the relation $d_L = d_A(1+z)$ we have found experimentally.

ON THE CONSISTENCY OF THE GAIA WIDE BINARY GRAVITATIONAL ANOMALY WITH MOND

Xavier Hernandez
Instituto de Astronomía, Universidad Nacional Autónoma de México
Apartado Postal 70–264 C.P., 04510 Mexico
xavier@astro.unam.mx

Abstract: Over the past couple of years a clear gravitational anomaly has been reported and confirmed by two independent research groups carefully considering relative velocities, v and separations, s, on the plane of the sky, for wide binary star samples from the most recent GAIA catalogue. Over various studies covering a range of sample selection strategies and statistical analysis techniques, a surprising phenomenology has emerged. While the small separation samples for $s < 2000$ au accurately conform to Newtonian expectations, for separations above 3000 au, a clear and systematic departure from Newtonian predictions appears. This high separation regime shows a v proportional to $s^{-1/2}$ scaling, but corresponding to Keplerian orbits under an effective gravitational constant of $1.5G$. Given the narrow range of total masses of around $1.6M_{\odot}$ in the samples considered, the critical separation at which a change in regime appears corresponds to approaching the a_0 threshold, where a_0 is the characteristic acceleration scale of MOND, as inferred from galactic rotation curve observations. Further, the precise distribution of wide binary relative velocities measured, closely corresponds to MOND expectations for such solar neighbourhood systems under the external field effect predicted by MOND. Now that a low acceleration validity limit for Newtonian gravity has been found, precisely at the acceleration scales over which the presence of dark matter has been proposed, astrophysical inferences for such hypothetical component become suspect.

JWST SUGGESTS A POSITIVE CURVATURE OF OUR UNIVERSE DUE TO THE SPACETIME-LENS PRINCIPLE

Michal Křížek
Institute of Mathematics, Czech Academy of Sciences
Žitná 25, CZ-115 67 Prague 1, Czech Republic
krizek@math.cas.cz

Abstract: Global geometry and shape of the physical universe may be revealed by observing objects at large cosmological redshift z, since for small z the universe seems almost flat. Recent infrared measurements of the James Webb Space Telescope (JWST) indicate that there exist very luminous galaxies at distances $z \geq 13$ that should not exist according to the standard ΛCDM cosmological model for the flat universe with curvature index $k = 0$. We introduce a spacetime-lens principle that could explain why these very distant galaxies shine so much. We show that the observed large flux luminosities may be mere optical effects due to the positive curvature index $k = 1$ of an expanding 3-sphere modeling our physical universe in time. For Euclidean or hyperbolic geometries such large flux luminosities seem implausible. This suggests that the right model of a homogeneous and isotropic physical universe for each fixed time instant is a 3-sphere.

The standard cosmological model is based on the normalized Friedmann equation $\Omega_{\mathrm{M}} + \Omega_\Lambda + \Omega_k = 1$, where $\Omega_{\mathrm{M}} + \Omega_\Lambda \doteq 1$ by measurements. We show that this does not imply that $\Omega_k = 0$ and $k = 0$ as it is often claimed.

RELATIVITY PREDICTS A VARIABLE G

Frederic Lassiaille
Nice, Massena, France
lumimi2003@hotmail.com

Abstract: It is shown that relativity predicts a variable G. The proof starts by considering a dimensionless particle in an empty universe. Then two particles, three particles, and an infinite set of particles are studied. This allows to calculate formally space-time structure for any realistic energy distribution. The proof uses the interchange of limits theorem, and ad hoc sequences of energy distributions. With only one particle the result is a singularity everywhere if the universe is empty outside of the particle. Those singularities disappear completely with three particles. Then this calculation is done for any realistic energy distribution. An equation of G is given naturally in the process. This equation is a correct approximation in most of the cases. The fundamental principles building Einstein equation are still valid, but now the constant anthropocentric solar system value is shown to be weaker in strong matter density environments, and greater in low matter density environments. It means that the surrounding effect arises, it was introduced by a previous work [1, 2]. And this effect was shown to solve the gravitational mysteries of today in astrophysics and in cosmology. Under a unifying relevant assumption, a solution is also given to the Millenium Yang-Mills problem.

[1] Lassiaille, F.: Surrounding Matter Theory. In: M. Krızek, Y. Dumin (Eds.), Cosmology on small scales 2018, Dark matter problem and selected controversies in cosmology. Inst. of Math., Prague, 2018, 204–228.

[2] Lassiaille, F.: Relativity in Motion: Short Version, Nuclear Theory, Vol. 39 eds. M. Gaidarov, N. Minkov, Heron Press, Sofia (2022).

LCDM AND MOND: PREDICTION AND EXPLANATION IN COSMOLOGY

Anastasiia Lazutkina
University of Wuppertal, Alsenstrasse 29, Wuppertal, 42103 Germany
a.k.lazutkina@gmail.com

Abstract: The mainstream view in cosmology today is that the universe is best described by the standard model, lambda cold dark matter (LCDM), that predicts an inflationary period right after the Big Bang, the existence of cold dark matter particles, and dark energy, and describes spacetime as flat, homogeneous, and isotropic. The acceptance of LCDM can be traced back to the 1990s and is usually associated with a year 1995 when two papers, one by Ostriker and Steinhard (1995) and another paper by Krauss and Turner (1995), convincingly presented reasons to replace the standard cold dark matter (SCDM) due its disagreement with empirical evidence on several scales.

Today's majority view in cosmology is that since that time LCDM has passed significant tests, there have been no similar crises, and thus LCDM remains the best cosmological model (Peebles 2020, 2024). However, there exist a number of critical papers that challenge that and argue that LCDM has failed tests on all of the scales and thus should be refuted (see, for example, Banik and Zhao 2021, Haslbauer et al. 2022, Kroupa et al. 2023). The questions I raise concern the following:

1) What is meant by "significant tests"?
2) When do they lead to crises?
3) Has the way we test theories and models in cosmology changed since the 1990s?

To answer those questions I will begin with the historical reconstruction of the tests used in the transition from SCDM to LCDM to identify why the main test of current LCDM became the main evidence for the model. I will then analyze the epistemological difference between the tests used for transition from SCDM to LCDM and the tests used for establishing reliability of LCDM against its rivals like MOND after the late 1990s till now. Lastly, I will present a normative account of whether the current reliance on LCDM is justified and if alternatives like MOND are more reliable.

HUBBLE (NON-)TENSION AND HIGH-z GALAXIES OLDER THAN ΛCDM UNIVERSE

Martín López-Corredoira
Instituto de Astrofisica de Canarias, Via Lactea, s/n
E-38205 La Laguna, Tenerife, Spain
martin@lopez-corredoira.com

Abstract: 1) Using a historical compilation of Hubble-Lemaître constant (H_0) values in the standard cosmological model, we want to determine whether or not the stated error bars truly represent the dispersion of values given. For this analysis, a χ-squared test was executed on a compiled list of past measurements. It was found through statistical analyses of the data (163 data points measured between 1976 and 2019), that the χ^2 values (between 480.1 and 575.7) have an associated probability that is very low: $Q = 1.8\text{E}-33$ for a linear fit of the data vs. epoch of measurement and $Q = 1.0\text{E}-47$ for the weighted average of the data. This means that either the statistical error bars associated with the observed parameter measurements have been underestimated or the systematic errors were not properly taken into account in at least $15-20\%$ of the measurements. The fact that the underestimation of error bars for H_0 is so common might explains the apparent 4.4-σ discrepancy formally known today as the Hubble tension. Here we have carried out a recalibration of the probabilities with the present sample of measurements and we find that x-sigmas deviation is indeed equivalent in a normal distribution to the $x_{eq.}$ sigmas deviation, where $x_{eq.} = 0.83x^{0.62}$. Hence, the tension of 4.4-σ, estimated between the local Cepheid-supernova distance ladder and cosmic microwave background (CMB) data, is indeed a 2.1-σ tension in equivalent terms of a normal distribution, with an associated probability $P(> x_{eq.}) = 0.036$ (1 in 28). This can be increased to an equivalent tension of 2.5-σ in the worst cases of claimed 6-σ tension, which may in any case happen as a random statistical fluctuation.

2) We analyze JWST photometric observations of massive red galaxies at redshifts $z > 6$ by fitting a stellar population model to the optical and near-infrared photometric data. These fits include a main stellar population in addition to a residual younger population and with the same extinction for both (a lower extinction for the younger population is unphysical). Extra stellar populations or the inclusion of an AGN component do not significantly improve the fits. These galaxies are being viewed at very high redshifts, with an average $\langle z \rangle \approx 8.2$, when the ΛCDM Universe was only ≈ 600 Myr old. This result conflicts with the inferred ages of these galaxies, however, which were on average between 0.9 and 2.4 Gyr old within 95% CL. Given the sequence of star formation and galaxy assembly in the standard model, these galaxies should instead be even younger than 290 Myr on average, for which our analysis assigns a probability of only $< 3 \times 10^{-4}$ ($\gtrsim 3.6$-σ tension).

ON THE INITIAL CONDITIONS OF THE νHDM COSMOLOGICAL MODEL

Nikolaos Samaras
Astronomical Institute, Charles University
V Holešovičkách 2/747, CZ-180 00 Praha 8, Czech Republic
nicksam@sirrah.troja.mff.cuni.cz

Abstract: The νHDM is the only currently known cosmological model based on Milgromian Dynamics (MOND). While MOND accounts for galaxies, with a priori predictions for spirals and ellipticals, a light sterile neutrino can assist recovering scaling relations on the galaxy-cluster scale and the CMB power spectrum. In the latest published hydro-dynamical νHDM simulations by Wittenburg et al 2023, although the authors managed to fit the temperature CMB fluctuations as initial conditions, the match to the Planck data is not optimal. In this work, we utilize a Bayesian statistics package to re-evaluate the cosmological parameters. We achieve a much better fit with $H_0 = 55.65$ km/(s Mpc) and $\Omega_m \approx 0.5$. These values are more discordant to the locally observed H_0 and Ω_m which may either mean this model to be ruled out or that we are situated in a very large deep underdensity.

LIST OF PARTICIPANTS

Yash-Hemu Aggarwal
Lamont-Doherty Earth Observatory of Columbia University, 822 Winton Drive, Petaluma, CA 94954; Palisades, NY 10965, U.S.A.
haggarwal(at)hotmail.com

Elena Asencio
Argelander-Institut für Astronomie, University of Bonn, Auf dem Hügel 71, D-53121 Bonn, Germany
s6elena(at)uni-bonn.de

Lyndon Errol Ashmore
460 Ashingdon Road, Rochford, Essex SS4 3ET, United Kingdom
lyndonashmore(at)outlook.com

William Roger Ashworth
44 Blackfriars, Yarm, TS15 9HG, United Kingdom
roger.ashworth(at)gmx.com

Artyom Valerievich Astashenok
Immanuel Kant Baltic Federal University, st. Alexandra Nevsky 14, 236041 Kaliningrad, Russia
artyom.art(at)gmail.com

Hana Bílková
Institute of Mathematics, Czech Academy of Sciences, Žitná 25, CZ-115 67 Prague 1, Czech Republic
hbilkova(at)math.cas.cz

John C. Botke
1200 N. Mariposa Road, no. 405, Nogales, Arizona, 85621, U.S.A.
jcbotke(at)gmail.com

Ioakeim-Gerasimos Bourbah
University of Crete, Greece
ibourbah(at)physics.uoc.gr

Kyu-Hyun Chae
Department of Physics and Astronomy, Sejong University, 209 Neungdong-ro, Seoul 05006, Republic of Korea
chae(at)sejong.ac.kr, kyuhyunchae(at)gmail.com

Juan De Vicente
CIEMAT, Av. Complutense 40, Madrid 28040, Spain
juan.vicente(at)ciemat.es

Harry Desmond
University of Portsmouth, 31 Charter House, Lord Montgomery Way, Portsmouth PO1 2SG, United Kingdom
harry.desmond(at)port.ac.uk

Vyacheslav I. Dokuchaev
Institute for Nuclear Research of the Russian Academy of Sciences, prospekt 60-letiya Oktyabrya 7a, Moscow 117312, Russia
dokuchaev(at)inr.ac.ru

Yurii V. Dumin
Sternberg Astronomical Institute of Lomonosov Moscow State University, Universitetskii pr. 13, R-119 234 Moscow, Russia
dumin(at)yahoo.com, dumin(at)pks.mpg.de

Antonín Dvořák
Kovoprojekta Brno a.s., Voroněžská 10, CZ-616 00 Brno, Czech Republic
antonin.dvorak(at)centrum.cz

Jan Fikáček
Avenue Prekelinden 32, box 6, 1200 Bruxelles, Belgium
jfikacek(at)gmail.com

Itzhak Goldman
Physics Department, Afeka Engineering College and Tel Aviv University, Mivtza Kadesh 38, Tel Aviv, Israel
goldman(at)afeka.ac.il

Ivan Gudoshnikov
Institute of Mathematics, Czech Academy of Sciences, Žitná 25, CZ-115 67 Prague 1, Czech Republic
gudoshnikov(at)math.cas.cz

Xavier Hernandez
Instituto de Astronomía, Universidad Nacional Autónoma de México, Apartado Postal 70–264 C.P., 04510 Mexico
xavier(at)astro.unam.mx

Čestmír Hradečný
IQS Group, s.r.o., Hlavní 130, 250 68 Řež, Czech Republic
cestmir.hradecny(at)iqstructures.cz, hradecnyc(at)seznam.cz

David Kaftan
Nad Soutokem 1418/9, CZ-143 00 Prague 4, Czech Republic
david.kaftan(at)post.cz

Elizaveta Khramova
IZMIRAN, Institute of Terrestrial Magnetism, Ionosphere, and Radio Wave Propagation, Russian Academy of Sciences, Kaluzhskoe Hwy 4, Troitsk, Moscow, 108840, Russia
sinop(at)yandex.ru

Roman Knobloch
Department of Mathematics, Technical University of Liberec, Studentská 2, Liberec, Czech Republic
Roman.Knobloch(at)tul.cz

Michal Křížek
Institute of Mathematics, Czech Academy of Sciences, Žitná 25, CZ-115 67 Prague 1, Czech Republic
krizek(at)cesnet.cz, krizek(at)math.cas.cz

Pavel Kroupa
Astronomical Institute, Faculty of Mathematics and Physics, Charles University, V Holešovičkách 2, CZ-180 00 Praha, Czech Republic; University of Bonn, Helmholtz-Institut für Strahlen- und Kemphysik, Nussallee 14–16, D-53115 Bonn, Germany
pavel(at)astro.uni-bonn.de, pkroupa(at)uni-bonn.de,

Frederic Lassiaille
Nice, Massena, France
lumimi2003(at)hotmail.com

Anastasiia Lazutkina
University of Wuppertal, Glanzstoffhaus Kasinostrasse 19–21, 42103 Wuppertal, Germany
a.k.lazutkina(at)gmail.com

Namhyung Lee
Columbia Southern University, 761 Blue Moon Lane, Westminster, MD 21157, U.S.A.
namhyung.lee(at)columbiasouthern.edu

Petri Lievonen
Physics Foundations Society, Helsinki, Finland
petrilievonen(at)gmail.com

František Lomoz
Sedlčany Astronomical Observatory, CZ-115 67 Sedlčany, Czech Republic
F.Lomoz(at)seznam.cz

Martín López-Corredoira
Instituto de Astrofisica de Canarias, Via Lactea, s/n, E-38205 La Laguna, Tenerife, Spain martin(at)lopez-corredoira.com

Jan Maršák
Pedagogical Institute, Prague, Czech Republic
jmarsak(at)seznam.cz

Jaroslav Mlýnek
Department of Mathematics, Technical University of Liberec, Studentská 2, Liberec, Czech Republic
Jaroslav.Mlynek(at)tul.cz

Klaus Morawetz
FH Münster University of Applied Sciences, Department of Physical Engineering, Stegerwaldstrasse 39, D-48565 Steinfurt, Germany
International Institute of Physics-UFRN, Campus Universitário Lagoa nova, 59078-970 Natal, Brazil
morawetz(at)fh-muenster.de, morawetz(at)physik.tu-chemnitz.de

Mustafa Moumni
Department of Physics, Faculty of Matter Sciences, University of Batna 1, Allées 19 mai, Route de Biskra 0500 Batna, Algeria
m.moumni(at)univ-batna.dz

Vladimír Novotný
Cosmological Section of the Czech Astronomical Society, Jašíkova 1533/4,
CZ-149 00 Prague 4, Czech Republic
nasa(at)seznam.cz

Tomáš Ondro
Department of Technology and Automobile Transport, Faculty of AgriSciences, Mendel University in Brno, Zemědělská 1665/1, Brno, CZ-613 00 Czech Republic
tomas.ondro(at)mendelu.cz

Veronika E. Řezníková
44 Blackfriars, Yarm, TS15 9HG, United Kingdom
veronikareznikova67(at)gmail.com

Petr Sadílek
Cosmological Section of the Czech Astronomical Society, Prague, Czech Republic
petr.sadilek(at)post.cz

Nikolaos Samaras
Astronomical Institute, Faculty of Mathematics and Physics, Charles University, V Holešovičkách 2/747, CZ-180 00 Praha 8, Czech Republic
nicksam(at)sirrah.troja.mff.cuni.cz

Eugen Stanislavovich Savinykh
Sternberg State Astronomical Institute of Moscow State University, Garibaldi street, building 12, apartment 92, Moscow, 117393 Russia
z-0000001(at)hotmail.com

Atinc Cagan Sengul
University of Pittsburgh, 414 S Evaline St., Apt. B, Pittsburgh, PA, U.S.A.
aa2(at)pitt.edu

Dominic Siedhoff
TU Dortmund University, Am Alten Garten 12, 44357 Dortmund, Germany
dominic.siedhoff(at)tu-dortmund.de

Varun Sohanda
University of Bonn, Am Jesuitenhof 1, Room number-116, Bonn-53117, Germany
varunsohanda.physics(at)gmail.com

Lawrence Somer
Department of Mathematics, Catholic University of America, Washington, D.C., 20064, U.S.A.
somer(at)cua.edu

Avril E. R. Styrman
University of Helsinki, PL 24, Unioninkatu 40, 00014 Helsinki, Finland
avril.styrman(at)helsinki.fi

Tuomo Suntola
Physics Foundations Society, Vasamatie 25, 02630 Espoo, Finland
tuomo.suntola(at)gmail.com

Aleksandr Sergeevich Tepliakov
Immanuel Kant Baltic Federal University, st. Alexandra Nevsky 14, 236041 Kaliningrad, Russia
teplyakow.7(at)yandex.ru

Václav Vavryčuk
Faculty of Science, Charles University, Prague 2, Czech Republic
vv(at)ig.cas.cz

Youngsub Yoon
Department of Physics and Astronomy, Sejong University, 209 Neungdong-ro Gwangjin-gu, Seoul 05006, Republic of Korea
youngsuby(at)gmail.com

Ivan L. Zhogin
Institute of Solid State Chemistry and Mechanochemistry of the Siberian Branch of the Russian Academy of Sciences, Novosibirsk, Russia
zhogin(at)mail.ru

PROGRAM OF THE CONFERENCE
COSMOLOGY ON SMALL SCALES 2024

Thursday, September 19

8:00–9:00 Registration

9:00–9:10 **Michal Křížek**, Opening

Chair: Pavel Kroupa

9:10–10:00 **Xavier Hernandez**, On the consistency of the GAIA Wide Binary Gravitational Anomaly with MOND

10:00–10:30 Coffee Break

10:30–11:15 **Tuomo Suntola**, The Dynamic Universe (DU)

11:15–12:00 **Avril Styrman**, Evaluation of theories and methodologies: Relativistic Physics vs. the Dynamic Universe

12:00–14:00 Lunch Break

Chair: Xavier Hernandez

14:00–14:30 **Elena Asencio**, The distribution and morphologies of Fornax Cluster dwarf galaxies suggest they lack dark matter

14:30–15:00 **Pavel Kroupa**, Observational data rule out dark-matter based models

15:00–15:30 **Nikolaos Samaras**, On the initial conditions of the νHDM cosmological model

15:30–16:00 **Klaus Morawetz**, Cosmology with torsion – time dependent Hubble constant

16:00–16:30 Conference photo – Coffee Break

Chair: Klaus Morawetz

16:30–17:15 **Václav Vavryčuk**, On the existence of the event horizon around black holes

17:15–17:35 **Atinc Cagan Sengul**, Finding and measuring low mass dark matter halos with strong gravitational lensing

17:35–18:00 **Michal Křížek**, A few critical remarks on the special theory of relativity

Friday, September 20

Chair: Tuomo Suntola

9:00–9:30 **Petri Lievonen**, Hyperspherical models of the universe: supernova observations, pulsar timescales, and concise mathematical ideas of Suntola

9:30–10:00 **Juan De Vicente**, Static interpretation of FLRW metric

10:00–10:30 **Harry Desmond**, Tests of gravity within and beyond the Galaxy (ZOOM presentation)

10:30–11:00 Coffee Break

Chair: Petri Lievonen

11:00–11:20 **Anastasiia Lazutkina**, LCDM and MOND: prediction and explanation in cosmology

11:20–11:40 **Tomáš Ondro**, Lognormal seminumerical simulations of the Lyman α forest

11:40–12:00 **Michal Křížek**, JWST suggests a positive curvature of our universe due to the Spacetime-Lens Principle

12:00–13:45 Lunch Break

Chair: Ivan Gudoshnikov

13:45–14:30 **Martín López-Corredoira**, Hubble (non-)tension and high-z galaxies older than ΛCDM Universe (ZOOM presentation)

14:30–15:00 **Yurii V. Dumin, Elizaveta G. Khramova**, Solution of the faint young Sun paradox: Greenhouse effect vs. the local Hubble expansion
(ZOOM presentation)

15:00–15:30 **Vyacheslav I. Dokuchaev**, Searching indications for dark energy in the images of black holes (ZOOM presentation)

15:30–16:00 **Ivan L. Zhogin**, Cosmology with one extra dimension (ZOOM presentation)

16:00–16:30 Coffee Break

Chair: Avril Styrman

16:30–16:50 **Artyom Valerievich Astashenok**, Some scalar dark energy models in light of DESY-2024 and other observational data (ZOOM presentation)

16:50–17:10 **Yurii V. Dumin**, Can the quasi-oscillatory structure of low multipoles in the CMB spectrum be associated with the domain structure of vacuum? (ZOOM presentation)

17:10–17:30 **Aleksandr Sergeevich Tepliakov**, Holographic dark energy: models and observational data (ZOOM presentation)

17:30–17:50 **Yash-Hemu Aggarwal**, Solving the enigma of the origins and growth of supermassive black holes (ZOOM presentation)

17:50–18:20 **Itzhak Goldman**, Gas accretion onto galaxies and Kelvin-Helmholtz turbulence (ZOOM presentation)

18:20–18:40 **Lyndon Errol Ashmore**, Data from twenty-three localised FRB's confirm the predictions of New Tired Light and that the universe is static and not expanding (ZOOM presentation)

Saturday, September 21

9:00–12:00 Excursion through astronomical and cosmological sites of Prague guided by **Michal Křížek** (total length about 6 km):

In the footsteps of Johannes Kepler and Albert Einstein in Prague

We will meet at 9:00 in front of the main gate of the Institute of Mathematics at Žitná 25. From there we will take a short walk to the Faculty of Science of Charles University at Viničná Street no. 7/1594. A memorial plaque dedicated to **Albert Einstein** is located in the lobby at the ground floor. It was unveiled on the 10th anniversary of his death in 1965 and recalls that Einstein worked in this building in 1911–1912. Einstein had his office there, where he found the calm necessary to formulate basic ideas of his General Theory of Relativity. In this building, Einstein also taught his seminar on theoretical physics for students and met the famous Professor of mathematics Georg Pick (1859–1942) with whom he became friends soon after arriving in Prague. Pick worked on non-Euclidean geometries and taught Einstein mainly foundations of tensor calculus. In Prague, Einstein got his first full professorship and was at the beginning of his fame. Another memorial plaque with Einstein's bust can be found in Lesnická Street no. 7/1215 in Smíchov (in 1911 this street was called Třebízského). In this house, Einstein lived with his family, in particular, his wife Mileva (born Marić) and two sons Hans Albert and Eduard. This bronze memorial plaque was unveiled in 1979 on the 100th anniversary of Einstein's birth.

A memorial plaque on Charles Square no. 20 marks the place, where **Christian Doppler** (1803–1853), professor of mathematics at the Czech Technical University in Prague and the founder of the Institute of Physics in Vienna, lived before 1840. The date of his death on the plaque is incorrect and an unusual first name in the form of Kristian is presented.

The third memorial plaque dedicated to **Albert Einstein** (see [4]) was unveiled on the 14th March 1999 on the occasion of the 120th Einstein's anniversary in the Old Town Square (Staroměstské náměstí) no. 17/551. The plaque contains the following English (and also Czech) text :

"Here, in the salon of Mrs. Berta Fanta, Albert Einstein, Professor at Prague University in 1911 to 1912, founder of the Theory of Relativity, Nobel Prize Winner, played the violin and met his friends, famous writers Max Brod and Franz Kafka."

After his arrival in Prague in 1911, Einstein often visited this house and met there the Jewish intellectuals Max Brod, Hugo Bergmann, Felix Weltsch, and also Franz Kafka, see [1, pp. 153, 186], [6, p. 402], [7, p. 7]. He took part in Tuesday's evening lectures and philosophical debates on diverse topics.

It was the above-mentioned Georg Pick who introduced Einstein into this company. In particular, two topics brought Pick and Einstein together. The first of them was discussion about mathematical methods that later Einstein used to formulate his General Theory of Relativity. Their second common interest was music. Max Brod

recalls that in the Salon of Berta Fantová[1] he played on piano and was accompanied by Einstein on violin performing together the Mozart violin sonata (see [1, p. 153]). They also took part in philosophical discussions in that Salon. According to [3, p. 21] (see also references therein), Einstein gave a lecture on the theory of relativity in this salon on May 24, 1911, and here he also met Kafka. By [1, p. 152] Kafka stopped going there in 1913, when Einstein was no longer in Prague,

The painting on the next Storch House no. 16/552 recalls the half-a-year long visit paid to Prague by **Giordano Bruno** in 1588. A memorial plaque placed at the Planetum in Prague recognizes his work.

Professor of physics **Ernst Mach** had lived for some time in the house no. 19/549 situated on the right part of the Einstein memorial plaque. A bust honoring Mach is located at Ovocný trh no. 7/562. There is also a memorial plaque, see Figure 1.

Figure 1: Memorial plaque dedicated to Ernst Mach.

The most admired and sought-after monument there is obviously the Astronomical Clock on the Old-Town Hall, also known as the Prague Horologe. Its astronomical dial represents a geocentric cosmological model of our universe, see [5] for details.

The Old Town Square and its surrounding streets also commemorate a number of outstanding scientists and artists who lived in Prague. For example, the Church of Our Lady (Týnský chrám) is the final resting place of the great Danish astronomer **Tycho Brahe** (1546–1601). He was probably the best observer of the heavens before the invention of telescope. He is buried in front and to the right of the altar. The nearest pillar holds a tombstone made of rose marble from nearby Slivenec, portraying Tycho Brahe in relief and accompanied with the following inscriptions in Latin:

[1]Berta Fantová (1865–1918), the mother of Professor Otto Fanta, see the letter of Max Brod to Franz Kafka from the 20th December 1918 in [6, p. 212].

"Esse potius, quam haberi" [Rather to be somebody than only to give such an impression] and *" Nec fasces, nec opes, sola artis sceptra perennant"* [Neither power, nor riches, only the scepter of knowledge persists.]

Figure 2: A plaque commemorates that Tycho Brahe lived in this house from 1599 and died here in 1601. Here he also carried out his observations with Johannes Kepler.

In Figure 2, we see a memorial plaque dedicated to Tycho Brahe which is located at the entrance to the Kepler's gymnasium at Parléřova street no. 2/118. To more plaques can be found in Nový svět no. 1/76.

Johannes Kepler (1571–1630) lived in Karlova street no. 4/177 (see Figure 3) from 1607 to 1612 which is indicated there on two commemorative plaques and the monument in the courtyard (see Figure 4). During this period he discovered the first two of his three laws about elliptic orbits of planets around the Sun. They were published in *Astronomia nova* (1609). J. Kepler was living in the Prague city since 1600. A sculpture of Tycho Brahe and Johannes Kepler is also located at the intersection of Keplerova and Parléřova streets near Prague Castle.

The Charles University campus in Celetná Street includes Carolinum which is also accessible from Železná Street. It is the main historic building of Charles University, founded by the Czech King and Roman Emperor Charles IV in 1348 and was the first university in Central Europe. Although Carolinum is a national historic landmark, it continues to serve as an important university facility. Graduation ceremonies and other important events are held in its Great Hall. In another hall of Carolinum –

Figure 3: Johannes Kepler lived in this house from 1607 to 1612.

its Vlastenecký sál [Hall of Patriots] – a famous lecture *"Über das farbige Licht der Doppelsterne"* [On the color light of binary stars] was given by **Christian Doppler** (1804–1853) in 1842. He presented there his concept of the phenomenon that was later given his name – the Doppler effect, see [2]. In 2006, a memorial plaque honoring Doppler was placed on the house at U Obecního dvora no. 7/799, where he lived from 1843 to 1847.

Figure 4: The monument commemorating Kepler's discoveries is located in the courtyard of Karlova Street no. 4 in front of the former Kepler Museum.

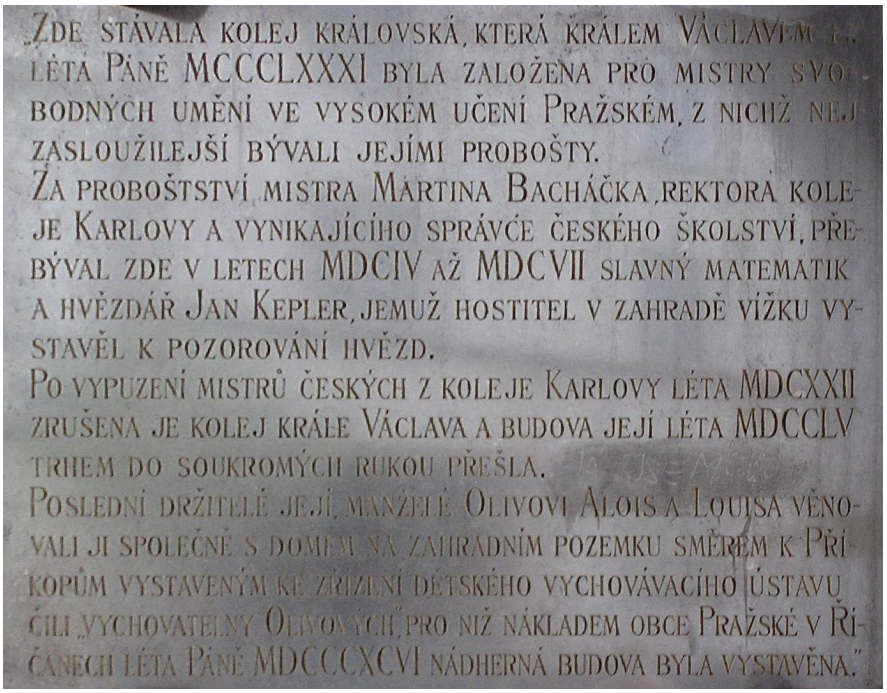
„Zde stávala kolej královská, která králem Václavem [illegible]
léta Páně MCCCLXXXI byla založena pro mistry svo-
bodných umění ve vysokém učení Pražském, z nichž nej-
zasloužilejší bývali jejími probošty.
Za proboštství mistra Martina Bacháčka, rektora kole-
je Karlovy a vynikajícího správce českého školství, pře-
býval zde v letech MDCIV až MDCVII slavný matematik
a hvězdář Jan Kepler, jemuž hostitel v zahradě vížku vy-
stavěl k pozorování hvězd.
Po vypuzení mistrů českých z koleje Karlovy léta MDCXXII
zrušena je kolej krále Václava a budova její léta MDCCLV
trhem do soukromých rukou přešla.
Poslední držitelé její, manželé Olivovi Alois a Louisa věno-
vali ji společně s domem na zahradním pozemku směrem k Pří-
kopům vystaveným ke zřízení dětského vychovávacího ústavu
čili „vychovatelny Olivových", pro niž nákladem obce Pražské v Ří-
čanech léta Páně MDCCCXCVI nádherná budova byla vystavěna."

Figure 5: The famous mathematician and astronomer Johannes Kepler had an observation tower in this former university dormitory.

The former university dormitory at 12/573 Ovocn'y Market was the site. **Johannes Kepler** lived from 1604 to 1607. There he found out that the orbit of Mars is elliptical. In 1604, he observed a supernova (bearing his name at present) in the constellation Ophiuchus from a wooden observation tower in the garden of this house university buildings. A memorial plaque (see Figure 5) is placed on the left side of the passage.

References

[1] M. Brod: *Život plný bojů*, Nakl. Franze Kafky, Praha, 1966.

[2] Ch. Doppler: *Ueber das farbige Licht der Doppelsterne und einiger anderer Gestirne des Himmels*, Abh. böhm. Ges. Wiss. 2 (1842), 466–482.

[3] M. D. Gordin: *Einstein v Čechách*, ARGO, 2022; Einstein in Bohemia, Princeton Univ. Press, 2020.

[4] M. Křížek, A. Šolcová, M. Toepell: *Neues Einstein-Denkmal in Prag 1999*, MNU (Der mathematische und naturwissenschaftliche Unterricht) 53 (2000), H4, 252–253; see also Pokroky Mat. Fyz. Astronom. 44 (1999), 258–261.

[5] M. Křížek, L. Somer, A. Šolcová: *From Great Discoveries in Number Theory to Applications*, Springer, Cham, 2021.

[6] M Pasley: *Franz Kafka & Max Brod, přátelství, korespondence*, Hynek, Praha, 1998.

[7] S. Strohs: *Josef Winternitz a teorie relativity*, Filosofia, Praha, 1995.